UNIVERSIDAD CARLOS III DE MADRID

TESIS DOCTORAL

Self-powered and low mass autonomous platform for planetary surface exploration

Autor:
Francisco Javier Álvarez Fernández
Director:
Luis Enrique Moreno Lorente
Codirector:
Diego Fernández Infante

DEPARTAMENTO DE INGENIERÍA DE SISTEMAS Y AUTOMÁTICA

Leganés, Febrero 2016

TESIS DOCTORAL (THESIS)

Self-powered and low mass autonomous platform for planetary surface exploration

Autor (Candidate): Francisco Javier Álvarez Fernández

Director (Adviser): Luis Enrique Moreno Lorente
Codirector (Co-Adviser): Diego Fernández Infante

Tribunal (Review Committee)

Javier Gómez-Elvira Rodríguez. Presidente (Chair): _____

Ernesto Gambao Galan. Vocal (Member): _____

María Dolores Blanco Rojas. Secretario (Secretary): _____

Calificación (Qualification): _____

Título (Grade): Doctorado en Ingeniería Eléctrica, Electrónica y Automática

Leganés, ____ de Febrero de 2016

Abstract

Nowadays and during the following decades, planetary surface exploration of rocky bodies in our Solar System (especially the Moon, Mars and some asteroids), will be one of the main strategic goals for the different space agencies around the world. This thesis stablishes the technological basis for the implementation of a fixed scientific monitoring infrastructure over a planet surface. The concept proposed is aimed to provide a reliable and cost effective system for the continuous surface monitoring of the inner rocky planets of our Solar System.

Traditionally these surface exploration missions have been led by progressively more and more complex and expensive systems with challenging scientific and technological objectives (i.e. NASA Mars rovers, ESA ExoMars program or the Chinese Chang'e 3 mission). This space exploration paradigm benefits from deploying highly ambitious and expensive platforms able to perform complex scientific experiments, but it is exposed to the risk of a complete mission loss in the case of a platform failure.

Beyond the traditional rovers or landers, the concept proposed is based on an ad-hoc Wireless Sensor Network composed of small fixed platforms aimed to sense, process, share between them and finally transmit scientific data to a satellite orbiter for further transmission to Earth. The conceived system is able to operate autonomously during years, harvesting the required energy from the planet surface environment. Such a concept deployed over a planet surface would represent the first fixed infrastructure over an extraterrestrial rocky body.

This work is focused in the platform overall design, including the ad-hoc scientific payload, and provides reliable technological solutions for the different critical aspects of the concept proposed.

The platform conceived is a low mass dual body: (i) a tetrahedron body highly optimized both in mass (2000g) and volume (tetrahedron envelope of 200x200 mm of base and 200 mm of height) that will remain over the planet surface; (ii) a penetrator body (3260 g) of 300 mm in height, 100 mm in diameter and with the shape of a ballistic missile aimed to go between 0.3 and 1.2 meters below the subsurface of

the planet. The deployment method selected is penetration (hard-landing). This method drastically simplifies the descent system required, thus reducing the related costs. Specific solutions for the conceived platform are proposed with the objective of ensuring the platform operability after the landing impact.

The scientific payload conceived is highly integrated with low power consumption requirements. The payload presented in this work comprises a dust deposition sensor, three surface temperature sensors, a radiation sensor and three multiespectral irradiance sensors.

Day and night energy harvesting systems are proposed, which represents an innovation in this kind of platforms.

Finally, a specific control architecture is presented aimed to provide the required autonomous behavior to the platform. This autonomous behavior in combination with a dynamic thermal regulation and the day and night energy harvesting systems allow the platform conceived to drastically increase its science return and life time.

Resumen

En la actualidad y durante las próximas décadas, la exploración de las superficies planetarias de los cuerpos rocosos de nuestro Sistema Solar (especialmente de la Luna, Marte y la de algunos asteroides), será uno de los objetivos estratégicos de las diferentes agencias espaciales de todo el mundo. Esta tesis establece las bases tecnológicas para la implantación de una infraestructura de monitorización científica sobre la superficie de un planeta. El concepto propuesto está orientado a obtener un sistema fiable y económico para la monitorización continua de la superficie planetaria de los cuerpos rocosos internos de nuestro Sistema Solar.

Tradicionalmente este tipo de exploración de superficies planetarias ha sido llevada a cabo por sistemas cada vez más y más complejos y costosos (por ejemplo los vehículos exploradores para Marte de la NASA, el programa ExoMars de la Agencia Espacial Europea o la misión china Chang'e 3). Este paradigma de exploración espacial aprovecha la oportunidad de desplegar plataformas muy complejas y ambiciosas capaces de realizar complejos experimentos científicos, pero expuestas al riesgo de la pérdida completa de la misión en caso de un fallo en la plataforma de exploración.

Más allá de los tradicionales vehículos exploradores o sondas, el concepto propuesto se basa en pequeñas plataformas capaces de medir, procesar, compartir entre ellas y finalmente enviar los datos medidos a un satélite en órbita para una posterior transmisión a la Tierra, mediante el uso de redes de sensores inalámbricos a medida. El sistema ideado es capaz de operar autónomamente durante años, recolectando la energía requerida en el propio ambiente de la superficie del planeta. Este tipo de concepto, desplegado sobre la superficie de un planeta, representaría la primera infraestructura fija sobre la superficie de un cuerpo rocoso extraterrestre.

El trabajo presentado se enfoca en el diseño global de la plataforma, incluyendo la instrumentación científica y aporta soluciones técnicas para los aspectos más críticos del concepto propuesto.

La plataforma ideada está basada en dos cuerpos: (i) un cuerpo con forma tetraédrica muy optimizado en peso (2000 gr) y en volumen (envolvente del tetraedro

de 200x200 mm de base y 200 mm de altura) que permanecerá en la superficie del planeta; (ii) el cuerpo del penetrador (3260 gr) de 300 mm de altura, 100 mm de diámetro y con la forma de un misil balístico enfocado a enterrarse entre 0.3 y 1.2 metros por debajo de la superficie del planeta. El sistema de despliegue seleccionado es la inserción (‟aterrizaje duro″del inglés ‟hard-landing″), simplificando drásticamente de esta forma el sistema de descenso requerido, y por lo tanto reduciendo los costes asociados. Se proponen igualmente soluciones específicas para la plataforma ideada de forma que se asegure su integridad operacional después del impacto durante el aterrizaje.

Se ha definido una instrumentación científica altamente integrada y con unos requisitos de consumo muy bajos. La instrumentación desarrollada consta de un sensor de polvo depositado, tres sensores de temperatura superficial, un sensor de radiación y tres sensores de irradiación multiespectral.

Se proponen asimismo sistemas de obtención de energía durante el día y la noche, lo que representa una innovación en este tipo de plataformas. Finalmente, se presenta una arquitectura de control específica enfocada a proporcionar a la plataforma el comportamiento autónomo que se requiere. Este comportamiento autónomo en combinación con un sistema dinámico de regulación térmica y de los sistemas de obtención de energía durante el día y la noche permite a la plataforma concebida incrementar en gran medida la información científica obtenida y la vida útil de la misión en su conjunto.

A mis padres.

Agradecimientos

Es difícil incluir en una pocas líneas la gran ayuda recibida, tanto personal como profesional, para la consecución de este trabajo. Por ello, y sabiendo que inevitablemente no podré mencionar a todos, haceros llegar mi gratitud más sincera por vuestra ayuda.

En primer lugar me gustaría agradecer a mis tutores, Luis y Diego, que me apoyaron y acompañaron desde los inicios, y no me refiero sólo a este trabajo, sino desde hace ya más de 10 años en los diferentes proyectos fin de carrera y tesinas que he ido realizando. Gracias por vuestra confianza.

Quiero agradecer al equipo del Grupo Arquimea Ingeniería, desde el primero hasta el último, su gran ayuda en estos años en los que hemos ido creciendo juntos profesionalmente en el mundo del I+D. Especialmente me gustaría agradecer a Cayetano sus inestimables aportaciones a este trabajo, no sólo en el ámbito de los mecanismos diseñados, sino también por todo su apoyo. No quiero olvidarme de Carlos y Jesús, diseñadores del ASIC de radiación y que perdieron algún que otro fin de semana por llegar a tiempo para la fabricación de los mismos. Gracias Naiara, Marcelo, Paco y Dani por vuestras correcciones y comentarios en las diferentes publicaciones y en este mismo trabajo. Agradecer igualmente a David sus indicaciones para la electrónica del sensor de polvo. Aunque ya no está entre nosotros porque pasó a una mejor vida (en las soleadas costas de Florida), agradecer a Lorenzo su ayuda y confianza durante los inicios de esta tesis.

No puedo dejar de incluir aquí mis agradecimientos al grupo de trabajo del proyecto europeo SWIPE: "My most sincere gratitude to the SWIPE Project team: thank you for your great collaboration ".

Gracias a mi hermano, a mi sobrino por arrancarme sonrisas y a mis padres por llevarme hasta aqui. Finalmente, quiero agradecer a Stephy no sólo toda su ayuda, apoyo y cariño durante estos años, sino también por haberme aguantado, lo cual es mucho más complejo que cualquiera de los conceptos aquí propuestos.

A todos, gracias.

Abbreviations

AI - Artificial Intelligence
ASIC - Application-Specific Integrated Circuit
AU - Astronomical Unit
CAD - Computer-Aided Design
COSPAR - Committee on Space Research
DDS - Dust Deposition Sensor
DHMR - Dry Heat Microbial Reduction
DLR - German Aerospace Centre
DM - Descent Module
DS2 - Deep Space 2
EM - Engineering Model
EoL- End of Life
FPGA - Field-Programmable Gate Array
FM - Flight Model
GS - Ground Segment
GSP - General Studies Programme
IR - Infra-Red
ISAS - Institute of Space and Astronautical Science
ITAR - International Traffic in Arms Regulations
LED - Laser Emitting Diode
LEO - Low Earth Orbit
LoS - Line-of-Sight
MANET - Mobile wireless Ad hoc NETworks
MIT - Massachusetts Institute of Technology
MLI - Multi-Layer Insulation
MMRTG - Multi-Mission Radioisotope Thermoelectric Generator
MNL - Met-Net Lander
MPL - Mars Polar Lander
PCB - Printed Circuit Board
PDS - Penetrator Delivery System

PEM - Proton Exchange Membrane
PSRR -Power Supply Rejection Ratio
QM - Qualification Model
REACT - REsettable Hold-Down and Release ACTuatorn
R&D - Research and Development
RTG - Radioisotope Thermoelectric Generator
SEB - Single-Event Burnout
SEGR - Single-Event Gate Rupture
SEL - Single-Event Latch-up
SEFI - Single Event Functional Interrupt
SET - Single Event Transients
SEUs - Single Effect Upsets
SMA - Shape Memory Alloy
SOC - State of Charge
SPOF - Single Point of Failure
SS- Space Segment
SWIPE - Space WIreless sensor networks for Planetary Exploration
TEG - Thermoelectric Generator
TID - Total Ionizing Dose
TMM - Thermal Mathematical Model
TRL - Technology Readiness Level
UC3M - Carlos III University of Madrid
UV - Ultra-Violet
VIS - Visible

Contents

Abstract i

Resumen iii

Agradecimientos vii

Abbreviations ix

1 Motivation 1
- 1.1 Space research motivation general outline . . . 3
- 1.2 Cost . . . 4
- 1.3 Planetary surface environmental constrains . . . 8
- 1.4 Motivation summary . . . 15

2 Objectives 17
- 2.1 Objectives description . . . 19
- 2.2 Objectives considerations . . . 22

3 Research approach 23
- 3.1 Research framework . . . 25
  - 3.1.1 SWIPE: FP–7 project . . . 25
- 3.2 General outline of the proposed solution . . . 26
  - 3.2.1 The Moon: selection as target scenario for technologies demonstration . . . 31

4 State of the Art 33
- 4.1 State of the art in small platforms for planetary exploration . . . 35
  - 4.1.1 The Lunar-A mission . . . 35
  - 4.1.2 UK Penetrator Consortium (MoonLITE mission) . . . 36
  - 4.1.3 Deep Space 2 . . . 37
  - 4.1.4 Luna-Glob . . . 40

4.1.5 Met-Net . . . 41
4.1.6 RF-WIPE . . . 43
4.1.7 Hopping robots . . . 43
4.2 State of the art analysis . . . 48

5 Self–powered and low mass fixed platform 53
5.1 Platform configuration . . . 55
5.2 Surface tetrahedral platform description . . . 58
5.2.1 Tetrahedron shape selection . . . 58
5.2.2 Inner electronics bay . . . 61
5.2.3 Scientific payload distribution . . . 62
5.2.4 Solar panels deployment subsystem . . . 63
5.3 Penetrator body description . . . 64
5.4 Harnessing . . . 65
5.5 Redundancy considerations . . . 67
5.6 Main and redundant On Board Computer architecture overview . . . 71
5.7 Platform mass budget . . . 73

6 Scientific low mass and low power consumption payload 77
6.1 Scientific payload conceived . . . 79
6.2 Dust Deposition Sensor . . . 80
6.2.1 Introduction and requirements definition . . . 80
6.2.2 Proposed Dust Deposition Sensor design . . . 80
6.3 Radiation sensor . . . 85
6.3.1 Introduction and requirements definition . . . 85
6.3.2 Proposed radiation sensor design . . . 87
6.4 Multispectral Irradiance sensor . . . 90
6.4.1 Introduction and requirements definition . . . 90
6.4.2 Mathematical model for Moon's surface solar irradiance estimation . . . 92
6.4.3 Proposed Multispectral Irradiance Sensor design . . . 96
6.5 Surface temperature sensor . . . 99
6.5.1 Introduction and requirements definition . . . 99
6.5.2 Mathematical model for lunar Surface temperature estimation 99
6.5.3 Proposed lunar surface temperature sensor . . . 103
6.5.4 Scientific payload acquisition electronics . . . 106

7 Solutions for the deployment of a large number of robotic platforms over the planet surface 113
7.1 Trade-off of platform deployment methods . . . 115
7.2 Platform deployment: solution conceived . . . 117

7.2.1 General overview . . . 117
7.2.2 The descent phase and descent module . . . 119
7.2.3 The surface impact: configuration and high impact survival techniques proposed. . . . 122

8 Thermal design: conceived technologies for thermal regulation of the exploration platform 129
8.1 Thermal design introduction and objectives . . . 131
8.2 Thermal Mathematical Model . . . 132
8.2.1 The energy balance . . . 132
8.2.2 Platform multi-node discretization . . . 135
8.3 Thermal design solutions and model results . . . 139

9 Energy management and innovative concepts for energy harvesting. 147
9.1 Energy harvesting for space exploration . . . 149
9.2 Energy management and energy consumption mathematical model . . 150
9.3 Solutions proposed for energy harvesting . . . 153
9.3.1 Energy harvesting for space exploration . . . 155
9.3.2 Thermoelectric generator . . . 156
9.3.3 Solar energy harvesting . . . 166

10 High level control architecture 173
10.1 Control architecture introduction . . . 175
10.2 The sequencer . . . 178
10.3 World model estimator . . . 182
10.4 The planning layer: Automated planning and checker . . . 184
10.5 The control layer . . . 187

11 Platform prototyping and laboratory test results 189
11.1 Platform prototyping introduction . . . 191
11.2 Tetrahedral platform structure . . . 192
11.3 Solar panels deployment system, functional tests and results . . . 194
11.4 Scientific payload prototype functional tests and results . . . 195
11.4.1 Dust Deposition Sensor prototype and laboratory tests results 195
11.4.2 Irradiance sensor prototype and laboratory test results . . . 200
11.4.3 Surface temperature sensor prototype and laboratory test results 202
11.4.4 Acquisition electronics prototype . . . 204
11.5 Thermal switch prototype functional tests and results . . . 204

12 Conclusions and future research **209**
12.1 Conclusions 211
12.2 Future research 213

Bibliography **215**

List of Tables

1.1 Temperature, gravity and atmospheric pressure characteristics of main solar system rocky bodies (data obtained from [WB4] and [Heiken et al., 1991]) . . . 12
1.2 Dust main effects over planetary surface systems . . . 13

4.1 State of the art comparative table . . . 50

5.1 Platform redundancy summary . . . 72
5.2 Platform mass budget . . . 75

6.1 List of commands for the acquisition electronics . . . 111

8.1 Platform thermal coupling node matrix . . . 137
8.2 Parameters used in the Thermal Mathematical Model . . . 138

9.1 Platform subsystems power consumption estimation . . . 152
9.2 Energy consumption mathematical model equations . . . 153
9.3 TEG for the lunar platform exploration characteristics . . . 164
9.4 TEG designed output characteristics for steady state condition ($T_h = 250,15K$ and $T_c = 100K$ and $R_L = R_{TEG}$) . . . 165
9.5 Solar panels parameters construction . . . 169

10.1 Control layer hardware operations. . . . 188

11.1 Power consumption DDS actuator test results. . . . 196
11.2 Summary of results obtained during the two DDS laboratory test campaigns. . . . 199

List of Figures

2.1 hayabusa 20

4.1 Lunar A mission 36
4.2 MoonLITE 37
4.3 DS2 39
4.4 LunaGlob 41
4.5 METNET 43
4.6 Canadian Space Agency hopping mechanism (extracted from [Montminy et al., 2008] 44
4.7 hayabusa 47

5.1 closedplatform 56
5.2 openplatform 57
5.3 25 N pin puller based on SMA 63
5.4 Harness 66
5.5 umbilical 67
5.6 OBC 73

6.1 dust Moon 81
6.2 esquema DDS 82
6.3 DDS and auxiliary electronics. Functional prototype. 84
6.4 radiation moon 86
6.5 rad scheme 89
6.6 radfet 90
6.7 Radiation sensor functional prototype (RADFET not included) . . . 90
6.8 Solar Irradiance spectra for a total integrated irradiance of 1367.28±0.02 W/m^2 (Extracted from [Tobiska et al., 2000]) 91
6.9 geome 94
6.10 irr 96

6.11 Solar Irradiance at 90° latitude (top) and −90° latitude (center) obtained with the model developed for year 1994. Solar irradiance results for year 1994 extracted from [Badescu, 2012], chapter 15. North Pole (solid line, bottom figure) and South Pole (dotted line, bottom figure) 97
6.12 Disposition of the irradiance sensors on the platform structure (top view). 97
6.13 Photodiodes selected for the multispectral irradiance sensor ([Pacific-Silicon-Sensor, 2010], and [GmbH, 2013] [Optoelectronics, 2015]) 98
6.14 Front end electronics (Photovoltaic mode). 99
6.15 Thermal balance sketch 101
6.16 Lunar surface temperature at equator (bottom left) and 80°N (top left) in one year extracted from [Li et al.,] compared with results obtained for year 2015 with the model developed at the equator (bottom right) and at 80°N (top right). 103
6.17 Model calculations of lunar surface temperature variations as a function of local time and latitude extracted from [Paige et al., 2010] after [Vasavada et al., 1999]. Local time is expressed in lunar hours which correspond to 1/24 of a lunar month. At 89° latitude, diurnal temperature variations are shown at summer and winter solstices (bottom). Results obtained using the model herein developed (top). . 104
6.18 Temperature probes for lunar surface temperature monitoring (left) and selected thermistor P1K0.232.6w.A.010 ([IST, 2014]) (right) . . 105
6.19 Temperature sensors front end electronics and Voltage output range in function of the PTC resistance values 105
6.20 Low power/low mass acquisition electronics block diagram 108

7.1 Highly schematic cross-section illustrating the idealized effects of large-scale cratering on the structure of the upper lunar crust. (Extracted from [Heiken et al., 1991] 117
7.2 Section of the pressurized compartment and the clamp band system conceived for docking the tetrahedral platform to the Descent Module (Descent Module based in the concept proposed by the UK Penetrator Consortium, [Gowen et al., 2011] and used as example of Descent Module in the figure) 121
7.3 Schematic section of the tetrahedral platform illustrating the different cohesion materials used for shock protection 126
7.4 Compression curve for metal foam (schematic extracted from [Ashby et al., 2000]) 128

8.1 Isothermal nodes selection for the platform thermal model 135

8.2 Thermal switch model . . . 139
8.3 SMA based thermal switch (7mm in height and 111 mm in diameter). 140
8.4 Thermal nodes temperature evolution during approximately 1 lunar day considering 0W dissipation. . . . 142
8.5 Thermal nodes temperature evolution during approximately 1 lunar day considering 0.2 W continuous power dissipation in the inner electronics bay. . . . 143
8.6 Thermal nodes temperature evolution during approximately 1 lunar day considering 2 W power dissipation during 10 hours in the inner electronics bay for a punctual measurement during the lunar night. . 145

9.1 Overview of the harvesting techniques conceived for the platform . . . 154
9.2 Mean substrate temperature at the four probes from the Apollo missions in function of depth (extracted from [Langseth et al., 1976]). 155
9.3 Commercial thermoelectric generator system from Marlow Industries ([Marlow Industries, 2015], model XLT6-4-01LS) (left) and schematic section of a TEG (right), extracted from [LeBlanc, 2014]. . . . 157
9.4 Proposed metal wires bundle sketch . . . 159
9.5 First and second derivative Seebeck coefficients for type J thermocouples in function of the temperature (extracted from [Powell et al., 1974]) . . . 161
9.6 TEG performance during one lunar cycle . . . 166
9.7 Solar power generated per solar panel (top), total power generated by all the solar panels (centre) and solar incident angle (bottom). Data obtained for January 2016, 0°latitude,0°longitude and solar panel 1 facing the lunar equator. . . . 170
9.8 Maximum solar power harvested for January 2006 in function of the increasing latitude towards North Pole (top); and maximum solar angle of the Sun in function of the latitude (bottom) . . . 171

10.1 Traditional remote control and proposed control scheme. . . . 176
10.2 High level control architecture proposal. . . . 178
10.3 Proposed sequencer flowchart. . . . 179
10.4 OBC status checking subroutines between the redundant OBC and main OBC. . . . 182
10.5 Planning algorithm scheme overview. . . . 186

11.2 Node structure assembled (left). Upper structure with PP assembled (center). Lower structure with electronics rack integrated (right). . . 192

11.1 SWIPE node platform without solar panels (top); SWIPE node with solar panels closed and power cable (bottom left) and open with power cable removed (bottom right). 193
11.3 Solar panels deployment sequence. 194
11.4 Low temperature tests. 195
11.5 DDS actuator activation sequence at ambient temperature. 196
11.6 $5\mu m$ samples with a different dust particles distribution over the optical window (top); $100\mu m$ Corundum sample (bottom right); and $100\mu m$ glass microspheres sample (bottom left). 197
11.7 $100\mu m$ Corundum dust particles suspension and samples prepared for dry in the oven at 85°C. 198
11.8 Assembled irradiance sensor. 200
11.9 Optical test bench (left and center) and measurements at ambient light (right). 201
11.10Temperature probe prototype details 202
11.11Calibration of temperature sensor. 0°C top and 100°C bottom. 203
11.12Acquisition electronics PCB (left) and acquisition electronics integrated in the SWIPE structure (right). 205
11.13Thermal switch test set-up. 205
11.14Thermal vacuum test results. 206

Chapter 1

Motivation

Planetary surface exploration using robotic systems became a reality in the last century; nevertheless we have just scratched the surface of a vast field of the science and engineering.

In this chapter a general overview of the main drivers of space exploration is given, focusing on the reasons that motivate the development of new technologies able to reduce the overall cost mission for planetary surface exploration. Particularly, the analysis is focused on the necessity of developing new technologies with low mass and low power consumption with the objective of reducing the costs of future planetary exploration missions using robotic systems.

1.1 Space research motivation general outline

Space exploration and more specifically planetary surface exploration represents nowadays one of the most challenging and effort demanding dares for the humanity. Space exploration is usually followed by controversy due to the high cost and efforts required to perform advances in our knowledge of the outer space, when in our own world there are innumerable scientific and engineering challenges to face. Besides the high cost and high demanding efforts required it is important to consider the following main significant returns that the space exploration generates:

- Development of new technologies and science reinforcement that used in terrestrial applications enhances our quality of life. Space environmental constrains represents an extraordinary experimental platform for technological innovation.
- Increase human understanding of the Earth origin, evolution and its place in the Universe.
- Enable the exploitation of space natural resources, as telecommunication capabilities, by means of communication satellites or new possibilities of energy and material harvesting.
- Generation of links and cooperation between different nations worldwide by means of a common objective, that promote peaceful relations between governments.

From centuries, astronomical observations from the Earth have provided important information about the bodies of our Solar System and beyond. Nowadays this exploration from our world is providing invaluable information year by year obtaining fascinating findings. During the past fifty years different orbiter or fly-by missions have been used in order to provide fundamental information from

the different elements of our Solar System. The data gather by these means includes information that cannot been obtained from the observations from the Earth (imaging, magnetic, gravity and other remote sensing instruments operating in gamma rays, X-rays, ultraviolet, visible, infrared or radio waves giving global and synoptic data of the explored bodies ([Bhandari, 2008], p.190).

The following step, previous to direct exploration by humans, is the surface exploration by robotic systems. Robotic systems are used as reliable environmental monitoring systems for planetary surface exploration. During the past decades, several landing missions (including fix platforms as landers or mobile platforms as rovers) have performed experiments over the surface of different Solar System bodies that gathered information about the body environment as precise surface temperature, pressure, mineralogical and chemical soil composition, solar irradiance conditions, atmosphere characterization ...

Planetary surface exploration by robotic means is a challenging and costly activity due to multiple hard constrains as explained in detail afterwards. Although, robotic exploration is indispensable for future manned missions.

This thesis is focused in the development of a new autonomous, SMA-actuated, low mass and self-powered platform for planetary surface exploration with the objective of reducing the overall cost of planetary surface exploration. The cost reduction of the overall mission is a prior objective in order to be able to afford the space exploration.

Nowadays, and during the following decades, missions to explore the planetary surface of the rocky bodies in our Solar System (especially Moon, Mars and asteroids) will be one of the main strategic goals for the space agencies ([Hufenbach et al., 2014]). This thesis is motivated due to the necessity to incorporate new low power consumption and low mass technologies able to work reliably in the harsh environment of outer bodies exploration.

1.2 Cost

General space access costs

During the cold war, the space race (1955–1972) endorsed the investment of enormous quantities of money in space research, been the technology the limiting factor. The Soviet Union (USSR) and the United States (US) were the main players in this investment. Nowadays, the cost has become the main driven factor for space exploration and the number and complexity of players in the space access have grown drastically, including private companies, conglomerate of different nations and even research institutions as private Universities.

The transport cost to space depends on the launcher used and on the capacity of the launcher's rocket (biggest rockets are more expensive). US dollars per pound to Low Earth Orbit ($/pound-LEO) is the main key parameter used to quantify the costs related to transport mass to space. This cost is changing year by year due to the different private and public organizations that provide transport capabilities to space. Therefore, reducing the mass of the space systems is a straightforward way of reducing the mission costs. Transport cost just represents a part of the total costs required to develop space systems, other relevant actors that determinate the space mission costs are:

- ***Reliability***. Reliability is a main driver of aerospace designs. A high reliability design implies that all the systems and subsystems developed shall consider high safety factors and procedures to comply with the mission constrains. Moreover, the systems (and all the elements, materials or parts that conforms them) shall be subjected to a complex qualification and validation tests campaigns that imply a huge cost in manufacturing prototypes, models for testing, facilities of tests, personnel, etc.

- ***Limited producers, reduced market and inability to large production.*** The availability of space qualified components is highly limited. The space sector generates a reduced market in terms of units per year and usually the production techniques and the product itself is not compatible directly with non-space applications. For these reasons the cost of recurrent components for space application are between tens to hundreds times larger than their commercial equivalents. Obviously this represents an important cost factor to be considered. Additionally we have to be aware that the delivery lead times could be as large as 1 year or even more for certain components, what clearly implies a great impact for the mission scheduling.

  Finally, it is important to note that the environmental conditions differ drastically from one planet to other and moreover are usually different from the outer space conditions. Most of the developed space technologies are focused on the satellite market (operational phase is perform in outer space conditions), thus there is a lack of technologies or components available for planetary surface exploration missions as the proposed in this work. A great part of the components used for planetary surface exploration missions have to be qualified specifically for the mission with the consequent expenses.

- ***ITAR and other export restrictions.*** Components used in space market are subjected also to ITAR (International Traffic in Arms Regulations) because of their potential use in military applications. Availability in Europe of some

space components developed in USA are occasionally limited, or the lead time is increased due to the complex burocrazy in order to apply for an export license.

- ***Ground segment.*** During the lunch phase and mission phase, Earth facilities (control rooms, computers, high gain antennas for space signal tracking, etc.) and personnel shall be able to follow and command the space segment. Moreover it is required to receive, gather and record the data during the mission exploitation phase. In most of the cases, analysis of the data gathered during the mission could take years after the mission ending.
- ***Additional infrastructure for planetary surface exploration.*** Infrastructure required for surface planetary exploration does not end with the launchers and the ground segment. The communications infrastructure between the robotic system over the planet surface and the ground segment is accomplished using communication satellites. An orbiter shall receive the data from the surface exploration systems and transmit this data to Earth's ground segment network. Obviously this infrastructure represents a huge cost and complexity and the deployment of orbiter satellites around the planet under study are considered missions on their own.

Primary energy source selection, power consumption and mass reduction as strategies for mission cost decrease.

Mass reduction strategy implies a direct cost reduction of the mission, reducing the cost of space access as explained previously. Consequently innovative systems and subsystems, as the proposed in this document, that could perform their functionalities reducing their mass with respect to traditional systems would decrease the mission overheads. A main factor related to the system mass is the power consumption. Technologies that decrease their power consumption increase the system efficiency and consequently reduce the power demand of the primary energy source, that can be smaller, thus saving mass. Following this approach it is possible to go further: low power consumption could reach to the possibility of changing the primary energy source from one expensive with high performance to other with less capabilities and cheaper, reducing drastically the mission costs.

The primary energy source is known as the technology that converts from the energy form found in the nature to electrical power by a transformation process. In a satellite "primary energy source converts a fuel into electrical power", [Fortescue et al., 2011], p.326.

Current technologies for planetary exploration are mainly based on Radioisotope Thermoelectric Generators (RTGs) as primary energy source. RTGs use the heat

generated from the natural decay of radioisotope materials (in USA systems mainly Plutonium 238) and transform this heat into electricity thanks to the principle of thermoelectric generation. Not only the electricity generated by the RTG is used, also the heat continuously generated in the RTG permits to heat the systems during extreme cold conditions. As described in [Furlong and Wahlquist, 1999], there are mainly four reasons why RTGs have been used in several space exploration missions since 1961:

- ***Long life.*** New developments at NASA (Multi-Mission Radioisotope Thermoelectric Generator or MMRTG) obtains lifetimes for this technology as a minimum of 14 years.
- ***Environment.*** Nuclear power sources can operate in extreme environmental conditions, even during night at very low temperatures (solar panels are just operative with incident radiation). They are not affected by dust (e.g. solar panels covered by dust reduce its efficiency depending on the quantity of dust deposited over their surface).
- ***Operational independence.*** Apart from a temperature difference between the surrounding environment and the RTG it does not require any external element to generate electricity.
- ***Reliability.*** Missions working up to three decades have proven the reliability of these power generators.

Europe is currently developing its own RTGs. As described in [Williams et al., 2012], Europe is focused on developing ^{241}Am (Americium–241) as an alternative isotope for future European RTGs.

However, besides the great advantages of RTGs, we have to consider two main disadvantages in relation to the use of RTGs as primary energy source: cost and radiation contamination risk. RTGs are very expensive elements with low availability. The necessity of using radioisotope materials directly implies hard restrictions related to their procurement and final use that shall be managed by governments. Also we have to consider that these materials are only available at long term (e.g. reduced availability worldwide of Plutonium 238).

Additionally we have to consider the environmental impact of using radioisotope materials not only just in the Earth, also in the environment of the planet under study. Potential accidents that could result in the release of radioactive material in the environment shall be also considered. In [Dahl, 2006], we can find an environmental impact study as an example of the environmental impact of using RTGs in Earth and Mars. The development of new technologies with a low power consumption that could be powered using energy harvested over the planet surface could permit to

reduce drastically the cost of the mission and also would reduce the risk of potential accidents with radiative materials involved.

1.3 Planetary surface environmental constrains

Right after transportation, environmental conditions are the responsible of a great part of the elevated costs related to outer planets surface exploration. The reason is because those environmental conditions are incompatible with the commercial, industrial or even military technologies developed for Earth operation. This means that specific technologies shall be developed to withstand the specific environmental conditions of each individual mission. Furthermore the space systems shall complete almost three different environmental conditions or phases: pre-launch, launch and space operation. In [Fortescue et al., 2011], p. 11 and following, it is possible to find a general description of the pre-launch and launch phases environmental constrains. Herein the environmental constrains of the operation phase are described specifically for the planetary surface exploration case.

Pending on each individual mission, the following environmental conditions will vary. In most of the cases the specific environmental conditions will imply a design constraint that will require custom and innovative developments.

In the following paragraphs, the more important environmental factors involved in space exploration that will play an important role in this thesis are presented, as main drivers for design decision making or as scientific measurement objectives by themselves. During the dissertation of this thesis, the environmental parameters presented below are described in detail for the lunar surface exploration environment case in order to determine boundary conditions for the technologies proposed. Below a general overview of each parameter is described.

Radiation

We can briefly overview the natural space radiation environment differentiating two main groups:

- Particles trapped by planetary magnetospheres including protons, electrons, and heavier ions of all of the elements of the periodic table.
- Transient radiation consisting of galactic cosmic rays (GCR mainly originating outside the Solar System are composed primarily of high-energy protons and atomic nuclei) and particles from solar events, such as coronal mass ejections and flares.

The harmful radiation effects over the space exploration subsystems and crews have been studied from the origin of the space exploration and nowadays are currently under further analysis in numerous knowledge areas as physics, medics or engineering.

The effects of the radiation over the astronauts depend mainly on the type and amount of radiation exposure. We can consider two main categories of effects: short and long term effects. Between the short term effects the astronauts can experiment nausea, vomiting, central nervous system damage and even death. The main concern related to the long terms effects is the increase of cancer risk for astronaut radiation exposure to space radiation.

The radiation effects over the robotic exploration subsystems are diverse. Important effects are the material degradation of textiles, optic elements as lens or windows, solar cells or even dielectric materials that could result in punctual harmful arc discharges.

Radiation effects are specially challenging for the electronics and microelectronic elements of the space systems. For a general overview we can consider two different radiation effects over the electronics subsystems:

- ***Cumulative effects.*** Usually defined as the cumulative damage caused by ionizing radiation over the exposition time. These effects are responsible of the gradual degradation of the electronic devices. Total Ionizing Dose (TID) parameter is used to characterize these effects and it is measured in rads ($1rad = 0.01Gy = 0.01J\backslash kg$). In semiconductors (as CMOS devices) the effects could go from a total failure of the device to important drifts of several parameters as threshold voltage modifications or increase of leakage currents thru transistors.

- ***Single Event Effects (SEE).*** The main organization for microelectronics standards, JEDEC, defines the SEE as "any measurable or observable change in state or performance of a microelectronic device, component, subsystem, or system (digital or analog) resulting from a single energetic-particle strike". For simplicity we can divide in two big groups of SEE:

  - Soft errors: nondestructive functional errors induced by energetic ion strikes. The main characteristic of this group is that the effect itself is momentary, thus introducing a temporary malfunction (more or less critical depending in the outcome of the malfunction and the functionality affected). Two of their most known effects are the Single Event Transients (SET) and Single Event Upset (SEU). The main difference is if these effects are affecting an analogue circuit parameter (SET) or a digital circuit output (SEU). The SET is a modification of the voltage or current in a circuit causing a non-permanent effect. A SEU is the temporal modification of a digital circuit output momentarily.

  - Destructive SEE. The most common are the single-event latch-up (SEL), single-event burnout (SEB) and single-event gate rupture (SEGR).
    * Single Event Gate Rupture. Affects the gate oxide of a MOSFET generating a permanent malfunction of the MOSFET.
    * Single Event Burnout. Generation of high current state in the device due to the strike of a high energy particle that generates a permanent failure of the device functionality.
    * Single Event Latchup, SEL. A SEL is an abnormal high-current state in a device caused by the strike of a single energetic particle (heavy ion or high energy proton) creating a parasitic bipolar (p-n-p-n) that connects with a very low impedance the power supply to ground. If the device is not powered off the effect could cause the permanent loss of device functionality.

Temperature

The environmental temperature drastically depends on the specific planet under study, however all of them share extreme temperature conditions: large temperature ranges due to night and day cycle and maximum/minimum temperatures which represent a real engineering challenge (table 1.1). As it can be appreciated in figure 6.16, the Moon´s surface temperature can vary from 390K to 100K at mid latitudes. The robotic subsystems must be capable of surviving cryogenic temperatures during extended night periods, and at the same time, be able to tolerate high temperatures during the day. These extreme variations make the temperature a major environmental constrain for space exploration. All the robotic subsystems have two main defined temperature ranges:

- Survival temperature range: The system/subsystem shall be preserved within this temperature range (even unpowered) to avoid partial or total failure.
- Operational temperature range: Within this range the system/subsystem is able to operate under its nominal specification.

The extreme temperatures generate the following major problems:

- Electrical and electronics critical subsystems (OBC, batteries, sensors, etc.) have operational and survival temperature ranges considerably reduced compared to the environmental temperature variation over the planet surface. As a consequence, thermal regulation is required. This implies elevated costs, risks and reduced performance of the subsystems.

- The temperature rate of change is another important parameter that generates thermal stresses and could potentially damage permanently the equipment.
- Thermal expansions and contractions generate structural deformations that affect all the robotic subsystems.

Traditionally RTGs have been used to heat up the robotics subsystems during space exploration; however, as commented in section 1.2, one of the objectives of this thesis is to substitute these costly, risky and controversial devices using alternative approaches. In this way, the temperature is a major environmental constrain that drives most of the design decisions contemplated in this document.

Atmospheric pressure

From the high density atmosphere of Venus to the nearly vacuum of the Moon or Mercury (table 1.1), the robotic systems design has to consider the implications of the atmospheric pressure:

- The atmospheric pressure of the planet influences directly the mission outline (possibility of using the atmosphere to reduce the entrance velocity).
- The thermal design of the systems changes drastically between planets with a significant atmosphere or planets with nearly vacuum conditions without heat losses by convection.
- Influences the planetary surface temperatures. Planets with near vacuum conditions experiment drastic temperature changes during the day and night cycles, whereas planets with a medium dense atmosphere mitigates the day-night temperature variations.

Vibration and shock

Vibration and shock cannot be considered formal planetary environmental constrains as the main vibration and shock effects are generated during the transport of the systems to the planet surface. However, as the robotic systems shall survive the vibration and shock effects during the whole mission, they have to be considered.

Mainly, we can consider three different phases during the robotic system transport from Earth to the planet surface, where high vibration and shock effects has to be analyzed:

Planet	**g** $[m \cdot s^{-2}]$	**Mean Temperature [K]**	**Atm. press (x Earth´s)**	**Atmospheric composition**
Mercury	0.378	100 night 590–725 day	$1 \cdot 10^{-15}$	$42\%O_2$, $29\%Na, 22\%H_2, 6\%He, 0.5\%K$
Venus	0.905	737	92	$96.5\%CO_2, 3.5\%N_2 0.015\%SO_2$, $0.007\%Ar, 0.002\%H_2O$, $0.002\%CO, 0.001\%He, 0.001\%Ne$
Earth	1	283 night 293 day	1	$78.08\%N_2, 20.95\%O_2$, $0.934\%Ar, 0.038\%CO_2$, $H_2O highly\ variable(< 1\%)$
Mars	0.379	184 night 242 day	0.004–0.009	$95.32\%CO_2, 2.7\%N_2$, $1.6\%Ar, 0.13\%O_2, 0.08\%CO$, $0.021\%H_2O, 0.01\%NO$
Pluto	0.059	~ 50	$3 \cdot 10^{-6}$	CH_4, N_2
Moon	0.1654	100 night 390 day (at equator)		Traces of Ar, He, Ne, Na, K and H

Table 1.1: Temperature, gravity and atmospheric pressure characteristics of main solar system rocky bodies (data obtained from [WB4] and [Heiken et al., 1991])

During the launch phase:
As described in [Fortescue et al., 2011], the launch sequence entails high levels of vibration, associated both with the noise field and structural vibration, modest–to–high levels of acceleration during ascent and mechanical shock due to pyrotechnique device operation. The severe acoustic/vibration environment during launch is due to both the operation of the launch vehicle´s main engines, and also the aerodynamic buffeting as the vehicle rises through the lower region of the Earth's atmosphere.

Separation from launcher, spacecraft or lander:
During the separation of the robotic systems from a vehicle (launcher, spacecraft or lander) the systems are subjected to medium/high shock levels. These instantaneous events can provide extremely high–acceleration levels lasting only a few milliseconds. Their frequency spectrum is characterized by high–frequency components. In the case of Ariane 5, during payload separation the peak excitation that the satellite must survive is some 1000g at frequencies above 35kHz ([Fortescue et al., 2011]).

Landing over the planet surface:
Depending on the considered landing approach, the shock and vibration levels perceived by the robotic systems during this phase differ drastically. In section 7.1, a brief trade-off between the different landing approaches is presented. Two main approaches can be considered: soft and hard landing. The first considers

auxiliary systems that reduce or mitigates significantly the shock perceived by the subsystems during the landing. The second considers the robotic system is robust enough to support elevated g–forces and the landing occurs by impact of the robotic system over the planet surface. Obviously this generates tremendous levels of shock ($1 \cdot 10^4$ *to* $3 \cdot 10^4 g$).

Therefore the shock and vibration effects shall be considered as a critical parameter for the robotic systems design as they could potentially destroy the systems in seconds.

Dust

The dust over the upper surface of outer rocky space bodies as planets, moons or comets is a problem of main importance for the space subsystems. Usually, this environmental parameter is not as known or characterized as the previously presented, however it is critical for the mission success.

Some of the most relevant effects of the dust are listed in the table below:

Effect	Cause
Reduction of solar panels efficiency	By dust accumulation over the solar panel and scattering of light if the dust is suspended or levitating.
Material premature end of life due to adhesion and abrasion	Adhesion of particles by surface energy related forces as van der Waals or electrostatic charges. Once the particles are adhered to the material, due to the abrasive nature of the fine dust could cause the material end of life reduction by degradation.
Damage to seals and mechanisms	Adhesion of particles by surface energy related forces as van der Waals or electrostatic charges. Once the particles are adhered to the surface of the mechanism tribology effects could cause severe damage to mechanism and seals.
Astronaut health hazards	The size of the dust and chemical reactivity are two of the main factors that make the dust especially harmful for astronauts. The sealing mechanism to avoid dust to be in contact with the astronaut could not work properly due to the sub-micro size of the dust of some planetary surfaces as the Moon.
Optical depth reduction	The dust levitating or suspended in the atmosphere will scatter the light reducing the optical depth of optical systems.
Thermal regulation problems	Dust adhesion to thermal control surfaces (as radiators) changes the absorptivity (α) and the emissivity (ϵ) thus reducing the thermal regulation efficiency of those surfaces.
Electrical disturbances in electronic systems	If the dust is charged it could induce disturbances due to charging of the surface in contact with the dust.

Table 1.2: Dust main effects over planetary surface systems

Apollo missions to the Moon that landed several man crews to the lunar surface

(Apollo 11, 12, 14, 15 16 and 17) are the main source of data related to the harmful effects of the dust. In [Gaier, 2005] we can find several examples of these harmful effects during the Apollo missions: ‟Lunar dust was identified by the astronauts as an unforeseen problem that affected all exposed surfaces, movable parts or mechanisms and spatial suits, by adhesion and subsequent abrasion, besides posing other problems related to electrostatic charges, vision, airlocks, or even health issues″.

The dust transportation over the planetary surface can be generated by natural means (dust electrostatic levitation or dust transport by the wind) or by man-made or man-induced disturbances. It will be important to reduce as much as possible the second cause with the objective of reducing the harmful effects of the dust.

Planetary protection considerations

Other important restrictions related with the environment, which must be considered for planetary surface exploration missions, are the planetary protection considerations. These, usually less known restrictions, are imposed by the human law and not by the natural environment of the planet under study. Planetary surface operations imply a potential danger to contaminate the planet under study with terrestrial microorganisms (or vice versa in return missions). Planetary protection considerations are aimed to mitigate the potential contamination risks.

The Committee on Space Research (COSPAR) meets every two years and one of its tasks is to develop recommendations for avoiding interplanetary contamination, specifying regulations for space systems cleanliness. Planetary Protection requirements are applied according to the mission category considering the severity of the possible contamination (restrictions more severe are applied in the case of missions to planets where conditions are favorable for life as Mars). Landing on the Moon requires the implementation of planetary protection requirements of category II as specified by COSPAR in [Rummel et al., 2009]. Landing on Mars requires the implementation of a more severe Planetary Protection plan ([Margheritis et al., 2015]).

The planetary protection requirements depends on the category of the specific mission, and contemplate measurements as clean room assembly with different cleanness levels, clean procedures using alcohol wiping or procedures as Dry Heat Microbial Reduction (DHMR) to reduce the number of bacterial spores. Planetary protection requirements shall be stablished and studied at the beginning of the mission to ensure compatibility of the robotic systems used with these requirements.

1.4 Motivation summary

During the next decades missions to explore the planetary surface of the rocky bodies in our Solar System will be one of the main objectives for the different space agencies. Traditionally these missions have been led by complex systems with a wide range of science objectives, with high cost and long development timelines.

With the objective to be able to fund these missions, new technologies capable of reliably withstand the harsh environment conditions with a reasonable cost will be of major interest.

Innovative approaches that reduce the mass of the robotic platforms for surface exploration imply directly an important cost reduction and therefore are of great interest. Similarly, technologies that could reduce their power consumption would permit increase the efficiency of the system, therefore reducing the power requirements of the primary energy source that could potentially be smaller, thus saving mass.

With the reduction of mass and power consumption of the different platform subsystems and considering the availability of energy resources over the planet surface it would be possible to think about replacing the costly and low available RTGs as primary power source and use energy harvesting techniques, consequently reducing drastically the cost of the mission.

Motivated by these reasons this thesis presents an innovative self-powered platform including low mass and low power consumption technologies to be used for environmental planetary surface monitoring. The need of developing such technologies is founded on the lack of technologies that could permit, with reduced costs, address the challenging constrains of planetary surface exploration. Specifically the technologies proposed are particularly interesting for Wireless Sensor Networks consisting in a large number of small nodes that collaborate to acquire scientific data over the planet surface.

Chapter 2

Objectives

2.1 Objectives description

Traditionally, surface exploration missions have been led by progressively more and more complex and expensive systems with challenging scientific and technological objectives (i.e. NASA Mars rovers, ESA ExoMars program or the Chinese Chang´e 3 mission). This space exploration paradigm benefits from deploying highly ambitious and expensive platforms able to perform complex scientific experiments, but it is exposed to the risk of a complete mission loss in the case of a platform failure. Besides, current technologies for planetary exploration are mainly based on Radioisotope Thermoelectric Generators (RTGs) as main source of power. The use of RTGs implies elevated costs and risk, environmental impact and uncertainty due to the reduced availability of these systems. With the aim of reducing the dependency on Radioisotope-based nuclear power systems for planetary exploration where other source of power could be exploited (e.g. solar power), it is required the development of new technologies that could face the planetary exploration constrains with a reduced power consumption, mass and volume.

The main objective of this thesis is to propose new solutions that could permit to reduce the cost, the power consumption and the total mass of planetary surface exploration systems. The technologies proposed herein shall permit to improve the energy consumption of the robotic systems, thus opening the possibilities of using harvested energy instead of RTGs. Moreover, the proposed technologies shall be low mass, reliable and compatible with the thermal environment of application. With these characteristics the overall cost of the mission will be reduced in relation to conventional technologies.

The specific objectives and the expected achievements associated to this thesis are listed and described in detail below.

Specific objective 1: Conception of a self-powered and low mass fixed platform for planetary surface exploration.

A low mass and low volume fixed platform for planetary surface space exploration shall be proposed. This platform shall be shelf-powered using energy harvesting technologies over the planet surface and additionally be compatible with the planet environment. The platform proposed shall be autonomous and shall permit to monitor the environmental surface characteristics.

The expected achievement of this specific objective is to obtain a new platform out of the state of the art for space exploration. The platform proposed shall also be able to support the other technologies proposed in this thesis.

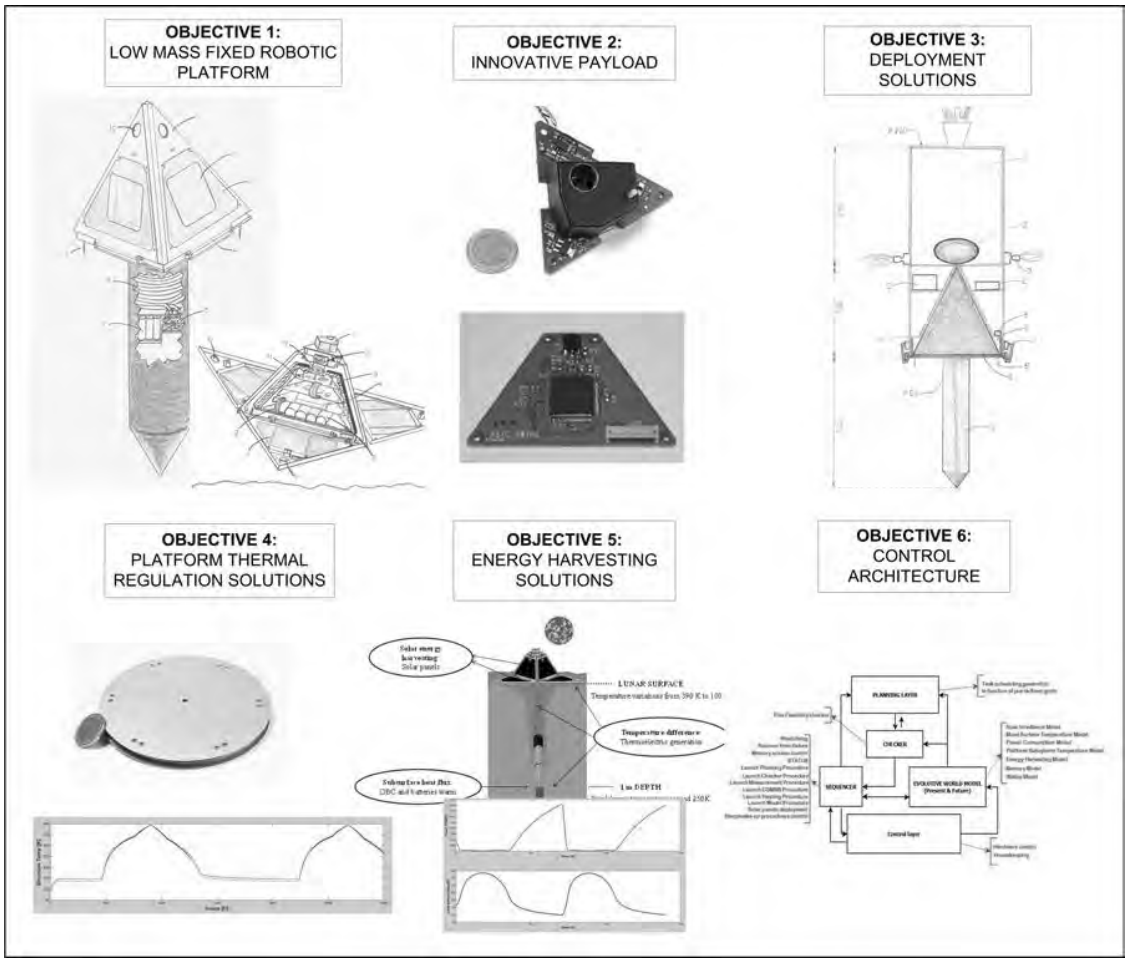

Figure 2.1: Thesis main objectives overview.

Specific objective 2: Definition of a low mass and low power consumption scientific payload for planetary exploration.

New sensors for planetary surface environmental characterization shall be proposed. The conceived sensors shall be low mass, low power consumption and be compatible with the robotic platform proposed in the specific objective 1.

The expected achievement of this particular objective is to obtain a new low power and low mass payload for planetary surface exploration that could be used in different exploration missions for environmental characterization.

Specific objective 3: Solutions for the deployment of a large number of robotic platforms over the planet surface.

The deployment of a large number of small platforms over the surface of an outer space body is a complex challenge. The system shall permit to deploy the small platforms undamaged, and what is more complex, use a low mass system to do it. If it is required to deploy a large number of platforms, the landing system has to be light in order to allow affordable missions that could deploy tens of platforms per mission.

The expected achievement of this objective is to propose a valid solution that could permit a feasible method for the deployment of a large number of the platforms obtained in the specific objective 1.

Specific objective 4: Solve the thermal regulation problem of the proposed fixed robotic platform.

Innovative technologies for thermal regulation of the node shall be proposed. Night/day cycles over the planetary surface will require advanced thermal regulation techniques. Solutions for this thermal regulation shall be proposed. A good thermal regulation will imply directly a more efficient use of the energy harvested from the planet surface.

The expected achievement of this objective is to obtain efficient approaches for thermal regulation of robotic systems subjected to a wide operational temperature range.

Specific objective 5: Innovative concepts for harvesting energy over the planet surface.

If it is desired to reduce the dependency of Radioisotope-based nuclear power for exploration systems, then it is required to propose new energy harvesting techniques. Innovative concepts for energy harvesting shall be proposed.

The expected achievement of this specific objective is to propose new energy harvesting techniques for future missions that could potentially substitute directly the use of RTGs as primary power source.

Specific objective 6: Definition of a high level control architecture for the autonomous robotic platform.

A specific control architecture shall be defined. The platform proposed in specific objective 1 shall be autonomous (impossibility of communicate with the Ground Segment during large periods of time pending on the orbiter satellite field of view and distance between Earth and the planetary surface explored). The expected achievement of this specific objective is to define a high level architecture compatible with the new platform proposed that could demonstrate the autonomy of the robotic system.

2.2 Objectives considerations

The objectives proposed for this thesis are highly ambitious, extensive and cover a large different number of fields of knowledge (thermal design, control design, aerospace design, electronics design, systems design, etc.). In order to propose realistic objectives for this work the following elements will be considered out of the scope of this thesis.

- Communication systems, algorithms and methods of communication between the different platforms or with the orbiter satellite.
- Specific mechanical designs.
- ASICs (Application-Specific Integrated Circuit) and FPGA (Field-Programmable Gate Array) design.

When a specific development would require any of the fields listed above and with the purpose of achieve the research objectives stated, the following procedure will apply:

1. The required element will be completely specified including interface requirements, functionality requirements and performance requirements.
2. The design of the specific element will be done by an expert designer or an external organization in the specific field and the solution proposed will be studied and re-defined if necessary.
3. Once the proposed design is agreed, it will be manufactured and included as other subsystem in the platform/technology proposed in this thesis.

Chapter 3

Research approach

3.1 Research framework

The research work presented in this thesis is the result of the collaboration between the University Carlos III of Madrid and the research company Arquimea Ingeniería S.L.U during the last 8 years in the area of space robotics.

This thesis presents a dissertation of the proposed solutions to the technological problem of planetary surface exploration using low mass and self-powered platforms. The University Carlos III of Madrid through its Robotics Lab group guides this thesis with the objective of stablish the proper research methodologies and procedures.

3.1.1 SWIPE: FP–7 project

SWIPE (Space WIreless sensor networks for Planetary Exploration) project intends to bring Mobile wireless Ad hoc NETworks (MANET) to space. In order to prepare for manned missions to other planets, it is necessary to monitor permanently the surface environment and have a clear notion of its conditions. Dozens and up to hundreds of autonomous sensors would create their own ad hoc network.

The author of this thesis is involved in this project as the responsible for the development of the platform concept and structure, solar panels deployment system and scientific payload of the SWIPE node for technological demonstration of the SWIPE project. The synergies of the work developed by the author of this thesis under the FP–7 program and the thesis development itself are of great interest and permitted the manufacturing and the test of some of the technologies herein described.

It is important to remark that SWIPE project includes only some of the concepts proposed in this thesis: scientific payload, solar panels deployment system, thermal switch and tetrahedral platform structure. However, the following technologies and concepts proposed in this thesis are not covered, included or considered within the SWIPE project:

- Platform deployment system over the planet surface: the penetrator concept and auxiliary shock absorption subsystems.
- Thermal design.
- Thermoelectric and thermal energy harvesting techniques.
- Redundant techniques herein proposed.
- OBC high level architecture and related mathematical modelling.

On the other hand, SWIPE project is focused on the development and demonstration of WSN communications systems (including radio antenna interface, communication software, WSN smart algorithms and data fusion techniques) that are not covered

in any form in this thesis. The communication technologies developed and the results obtained under SWIPE project are an important input for this thesis, as they demonstrate the feasibility of implementing a WSN using the hardware platforms herein conceived.

SWIPE project received funding from the European Union´s Seventh Framework Programme for research, technological development and demonstration under grant agreement no 312826. SWIPE consortium members are Tekever, Arquimea Ingeniería S.L.U, University of Leicester, CRAT and Airbus Defence and Space.

As part of the activities dedicated to the project results and knowledge diffusion throughout the scientific and technological community, industrial and service providers and the public in general this thesis is contemplated within the dissemination plan of SWIPE project.

3.2 General outline of the proposed solution

With the objective of creating an overall picture of the proposed solutions, before to introduce them in detail, in this section a general outline depicts the approach followed to solve the objectives stated in chapter 2.

The approach proposed in this thesis for planetary surface exploration is the deployment of a large number of small fixed platforms over the planetary surface to be explored. These platforms are completely autonomous system units that are able to obtain and gather the atmospheric data of the planetary surface, share this information between the different platforms, store it and send this data to a satellite orbiting the planet, moon or asteroid under study. The proposed fixed robotics platforms are able to harvest energy to operate from the planetary surface, using solar power and thermal energy. Low mass, low power consumption and smart thermal regulation are three of the main objectives to be achieved when using energy harvesting as the main power source instead of RTGs conventionally used for planetary exploration as analysed in chapter 1 . Solar energy instead RTGs significantly reduces the cost of each single node.

This approximation matches the requirements of technology needs described in chapter 1. A trade-off study of the solution proposed is presented below.

Main advantages of this approach are the following:

- The overall mission risk is significantly reduced because the failure of a single platform does not represent the mission failure as could be the case of landers and rovers approach.

- It is possible to obtain data simultaneously from many different locations over the planet surface under study. This is of main importance for some scientific

measurement, as radiation monitoring, and it is a procedure that is impossible to be implemented using single or a reduced number of landers or rovers.

- The communication scheme changes drastically. With this approximation it will be possible to generate a WSN as the proposed in SWIPE and described in [Rodrigues et al., 2014] and [Rodrigues et al., 2015], using smart data gathering and fusion algorithms as described in [Oddi et al., 2014a] and in [Zhai et al., 2014].

- The increase in the number of exploration platforms will permit to reduce the cost of each individual platform with respect to conventional large landers traditionally used (recurring manufacturing costs).

- Each node platform can be configured with different sets of instruments, thus increasing significantly the scientific objectives of the whole mission.

- Hard-landing (penetrator) approach can be used for low mass platforms as the one herein proposed (refer to section 7.1 for hard and soft landing definition), thus reducing considerably the cost of each platform deployment.

- The reduced size, mass and power consumption permit to use energy harvesting, extending the mission life without increasing its costs.

- The small platforms can be developed using a modular approach, enabling to swap subsystems easily, without losing or significantly redesigning their functionality and in this way be able to re-use the platform concept for different missions targeting different planets, moons or asteroids.

In the other hand we have to consider the following disadvantages:

- The limitation in the available mass and energy imply restrictions in the complexity of the sensors included in the node platforms. Thus, complex instrumentation packages demanding high power or mass/volume cannot been included in the platform proposed.

- Solar energy as primary source of power is just a solution for inner solar system rocky bodies (Mercury, Venus, Mars their respective moons and asteroids as Ceres or other big asteroids of the asteroid belt).

Obviously, the proposed solution will be only adequate for a certain type of missions, although a very interesting solution for those missions compatible.

Following, a more specific overview of each of the main technological solutions proposed in this thesis are presented in relation with the corresponding objective

stated in chapter 2.

Specific objective 1. Conception of a low mass and volume fixed platform for planetary surface exploration.

The solution proposed is a dual body fixed platform. The platform can be subdivided in two different bodies: (i) a tetrahedron body (also referred as aftbody following the nomenclature commonly used in the literature) highly optimized both in mass (2000g) and volume (tetrahedron envelope of 200x200 mm of base and 200 mm of height); (ii) a penetrator body of 300 mm in height, 60 mm in diameter and with the shape of a ballistic missile. The penetrator is attached to the baseplate of the tetrahedral platform and its total mass is below 3300 grams. The tetrahedral body remains over the planet surface while the penetrator body is introduced in the lunar subsurface using the kinetic energy generated during the platform deployment from the orbit. Both bodies are interconnected using umbilical cables. The tetrahedral platform will contain all the scientific payload, solar panels, communication systems, power modules and auxiliary batteries while the penetrator body will contain the On Board Computer with the principal batteries and related electronics.

The system proposed can be considered as a fixed micro-meteorological platform due to its dimensions, volume and because it is aimed to monitor the atmospheric characteristics of the rocky body surface where it is deployed. Each of the platforms deployed are considered a node of the Wireless Sensor Network approach described previously.

Figure 5.1 and figure 5.2 illustrate a general overview of the platform proposed. The robotic platform configuration foresees deployable solar panels installed in the surface platform. When closed, the deployable walls in form of petals protect the node from environment during transportation and deployment (avoiding dust contamination of the sensors and solar panels). A light aluminum structure that forms the tetrahedron and provides stiffness to the node keeps all the elements together. The inner part of the tetrahedron includes a dust sealed electronics bay thermally regulated.

Specific objective 2. Definition of a low mass and low power consumption scientific payload for planetary exploration.

The scientific payload is the ultimate objective of the complete system and its definition is of main importance in order to obtain scientific valuable data to fulfill the scientific mission objectives. Scientific payload definition shall be consequent

with the mission objectives, the specific planetary surface to be explored and with the platform to be used to support this payload. As previously stated, one of the main drawbacks of a small low power consumption platform is the complexity limitation of the scientific payload associated. For this reason, in this thesis an ultra-low power and mass scientific package of sensors is proposed to demonstrate the potential of these platforms. The payload proposed is conceived for the Moon surface scenario; nevertheless the scientific package shall be re-defined in function of possible new targets or scientific objectives.

Four different scientific sensors compatible with the platform concept proposed in this thesis have been defined:

- A novel Dust Deposition Sensor (DDS) that will measure the dust deposited by natural means during a certain exposition period over a flat surface and that will determine the dust deposition rate as a function of both the solar incidence and soil temperature. The DDS is an ultra-low mass sensor/actuator system of 40g. This kind of sensor represents an innovative scientific instrument with a very challenging mass and power consumption characteristics.

- Three temperature probes (located in the base of the surface platform will enter in contact with the lunar soil during the landing), will be responsible for temperature characterization of the top layer of the planetary soil.

- Radiation over the Moon surface is an environmental parameter of major importance for a future stable human presence on the Moon surface. In order to reduce at a minimum the mass of this sensor and optimize the power consumption, a radiation sensor based on a mixed signal ASIC has been specified and manufactured. The detailed design of this ASIC was completed by the Microelectronics Group of Arquimea Ingeniería S.L.U. The design of the ASIC is outside the scope of this thesis, although herein the ASIC overall specification and integration in the platform are introduced. This sensor is able to provide Total Ionizing Dose (TID) and Single Effect Upsets (SEUs) radiation monitoring over the planetary surface.

- Three multispectral irradiance sensors (each one including three sensors at Visible, IR and UV) have been conceived for irradiance characterization of the planetary surface under study. The robotic platform shape proposed is fundamental for this sensor. Three of these multispectral sensors are aimed to be placed with a separation of 180° for a total field of view of 360° (in each face of the tetrahedron).

Specific objective 3. Solutions for the deployment of a large number of

autonomous platforms over the planet surface.

In section 7.1 an analysis of different deployment strategies is presented. A hard-landing approach using a penetrator and a combination of different shock absorption technologies is herein proposed. Moreover, the deployment strategy suggested will permit to use the energy of the deployment from the orbit to bury a penetrator body in the subsurface of the Moon with the objective of using the heat of the subsurface to maintain the principal battery and On Board Computer of the system warm during the Moon nights. A Descent Module (DM) is considered to properly orientate the platform before the impact with the planet surface.

Specific objective 4. Solve the thermal regulation problem of the proposed fixed platform

As previously described, smart thermal regulation is one of the main and more challenging objectives for the small robotic platform proposed. A dynamic regulation strategy for the platform is proposed. This strategy is based in the following ideas (a complete thermal model and analysis of the platform is presented in section 8.2):

- The electronics bay (inner bay within the tetrahedral platform), is thermally regulated using heaters and an ultra-low volume and low mass passive thermal switch aimed to protect the electronics from the hard environment of the lunar surface. This thermal switch is based on SMA material. This automatic reconfigurable hardware will regulate the temperature of the electronics bay in function of the external temperature of the planetary surface. The thermal switch will isolate the electronics bay during the cold nights and will put it in thermal contact with the planet surface during the hot days. The thermal switch is completely passive (0 W) and its total mass is below 120g.

- The sub-surface planet heat flow (in this case the Moon), is used to maintain the principal batteries and the OBC subsystems (located in the penetrator body) in a stable temperature range (around –23°C). In this way it will be possible to store in the principal battery the energy harvested during the day and use it during the cold nights, keeping the system operative for punctual scientific measurements.

- If the temperature reaches extremely low or high values, that could damage the node, the node has the capability of switch off and stay in an "hibernation" mode until the temperature would reach a secure range.

- The structure of the node has the capability of work as a radiator during the day in order to reduce its temperature increase due to the incident solar radiation.

Specific objective 5. Innovative concepts for energy harvesting over the planetary surface

Energy harvesting from the planet surface is mandatory for long term missions if RTGs are not used. Photovoltaic, thermal and thermoelectric energy harvesting techniques are proposed. The solar energy will be harvested using solar panels.

The platforms, released from the Descent Module at a certain altitude of the planet surface, will penetrate in the sub-surface of the planet using the missile shaped penetrator proposed in chapter 7. It is important to highlight the advantages of this strategy, that does not use the energy stored in the batteries to dig into the planet surface, and uses the kinetic energy of the robotic platform during the deployment. As explained in detail in chapter 9, the temperature difference between the planet surface and the subsurface will be used to:

- Harvest thermal energy to maintain the penetrator body above $-25°C$, ensuring in this way the operability of the OBC and principal batteries continuously (even during the cold nights).
- Use the temperature difference between the surface and the subsurface to generate electrical power using a new and innovative Thermoelectric Generator (TEG).

Specific objective 6. Definition of a high level control architecture for the autonomous robotic platform.

A complete custom control architecture is proposed for the robotic platform. Chapter 10 introduces the control architecture conceived, based in an hybrid architecture. Thermal, irradiance, power consumption and power generation mathematical models are also developed as required inputs for the platform control.

3.2.1 The Moon: selection as target scenario for technologies demonstration

Although the platform concept proposed can be potentially used in different outer space rocky bodies, it is required the selection of a specific target with the objective

of stablish the boundary conditions that shall be used during the calculations for the design and the definition of the demonstration tests and simulations.

The selected scenario is the Moon. Lunar surface exploration has been selected as target scenario due to its excellent conditions for the demonstration of the technologies developed under this thesis. The main considerations that justify this selection are the following:

- Environmental conditions. The environmental conditions of the Moon generate a representative scenario where it is possible to find most of the environmental conditions that could be found in other extraterrestrial bodies:
  - Radiation. Without a magnetosphere or an atmosphere to protect the Moon, the lunar surface is exposed to the space radiation including Cosmic Galactic Rays, solar events and space radiation as described in section 6.3.
  - Temperature. The Moon presents a wide range of extreme thermal conditions as described in section 6.5.
  - Illumination. At mid latitudes the Moon has a long diurnal cycle (approximately 28 days long, been 14 days of day and 14 days of night at mid latitudes). This cycle varies in function of the latitude (refer to section 6.4 for details of illumination conditions over the lunar surface).
  - Atmospheric pressure. The Moon surface presents near vacuum conditions.
  - Gravity. Low gravity conditions are of great interest for scientific experiments.
  - Dust. The dust, as explained in section 1.4, is a harmful environmental phenomenon that can be found in most of the outer space bodies.
- Knowledge, proximity and infrastructure ([Marshall et al., 2001]). The Moon is the closest and most accessible extraterrestrial body with launch opportunities available during all the yearlong. It provides options for low cost missions of high scientific and technological value. As the Moon is only a few days away by spacecraft, missions can be sent to the Moon, operated from either the Earth or the Moon, and completed within a week. Additionally we have to consider that orbiting spacecrafts for space link between the surface platforms and the Earth are already available or can be deployed at a low cost compared with other extraterrestrial objectives as Mars.
- SWIPE project opportunity for demonstration technologies. As described in section 3.1.1, SWIPE project targets the Moon as main objective. As this thesis takes the opportunity to test several of the technologies herein proposed and developed under the SWIPE project, the selection of the Moon as scenario mission is of critical importance.

Chapter 4

State of the Art

In this chapter a state of the art focused on planetary surface exploration platforms and concepts that are similar or in somehow related with the platform proposed in this thesis is presented. Therefore the literature study is focused on small volume and reduced mass platforms. As a threshold, platforms below 40 kg will be included in this state of the art (it is important to remember that the surface platform proposed in this thesis is below 2 kg and the penetrator body is below 3.3 kg). This implies that big landers as the Lunar Lander proposed by ESA, the Chinese Chang'e 3 or rovers as those sent by NASA to Mars surface are out of this study.

After a brief presentation of the different missions or concepts found in the literature (section 4.1), a comparative analysis with the platform herein proposed is presented in section 4.2.

4.1 State of the art in small platforms for planetary exploration

4.1.1 The Lunar-A mission

The Lunar-A mission ([Mizutani et al., 2005] and [Mizutani et al., 2003]), was conceived by the Institute of Space and Astronautical Science (ISAS) in collaboration with the Japanese Space Agency (JAXA) as a Japanese penetrator mission to the Moon. Several times re-scheduled, was finally cancelled in January 2007. The scientific objective was to explore the lunar interior by seismic and heat-flow experiments.

The mission contemplated the deployment of two penetrators from an orbiter satellite using deorbit rocket engines. These engines will be fired, after satellite separation, with the objective of cancelling completely the spacecraft orbital velocity, and make it fall freely from about 25 km altitude onto the lunar surface. The final impact velocity of the penetrator will be about 285m/sec; it will encounter a shock loading of about 8000 g at impact on the lunar surface. The penetrators are missile-shaped cylinders with a mass of 13.5 Kg (excluding retro-motor and attitude control system) and a total mass of the whole system of approximately 45 Kg.

Each penetrometer contains a two-component seismometer, a heat flow probe, a tilt-meter, an accelerometer, a radio transmitter and an antenna. The system does not contemplate a primary source of energy, only several $Li - SOCl_2$ batteries with an EoL of approximately 1 year. The main scientific objectives were seismological observation of deep moonquakes, heat flow and temperature gradient measurement of the Moon regolith.

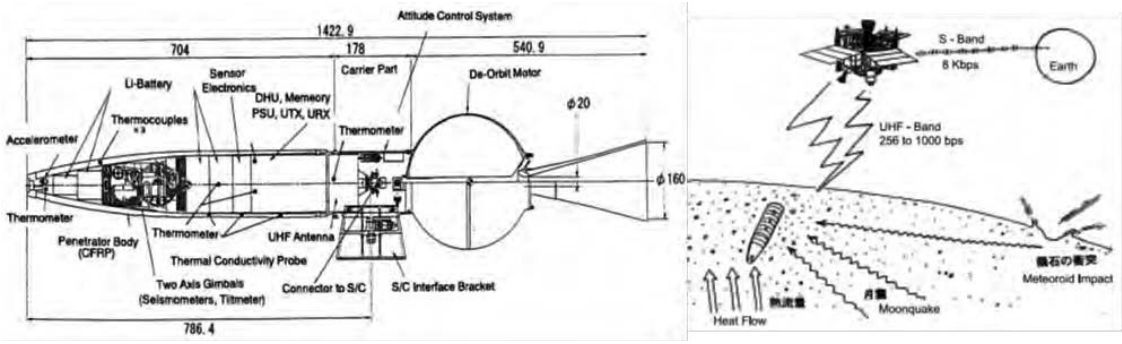

Figure 4.1: Internal structure and size of the Lunar-A penetrator (left) and schematic diagram of the Lunar-A penetrator operation (right). Extracted from [Mizutani et al., 2005] and [Mizutani et al., 2003].

4.1.2 UK Penetrator Consortium (MoonLITE mission)

The UK Penetrator Consortium is a consortium of UK organizations beginning in 2002. The consortium objective is to develop low weigh penetrators (below 15 Kg) aimed to bury themselves a few meters into different planetary surfaces for scientific exploration ([Collinson et al., 2008], [Gowen et al., 2007]). Between the possible missions of the consortium (Mars, Europa, Titan or Enceladus) the most promising proposal was the MoonLITE (Moon Lightweight Interior and Telecom Experiment) mission aimed to deploy 4 penetrators from the lunar orbit to its surface. The penetrator technology proposed by the UK Penetrator Consortium generated interest in ESA and also NASA and presents a very interesting approach for low cost exploration with several similarities to the Lunar-A mission concepts.

"The MoonLITE mission concept comprises a small orbiter and four penetrators ... The orbiter will demonstrate communications and navigation technologies aimed at supporting future exploration missions, whilst the primary scientific goal is to investigate the seismic environment and deep structure of the Moon"([Gao et al., 2008]).

A Descent Module (DM) comprising a penetrator and a Penetrator Delivery System (PDS) was conceived to be ejected from the host orbiter. The PDS provides de-orbit thrust and attitude control manoeuvres to slow down its penetrator for near normal incident angle impact at 300m/s into the lunar surface, embedding themselves around 2-5m under the surface. Each DM is essentially a complete miniature spacecraft ([Gowen et al., 2008]).

The penetrator itself contains power, data handling, communication subsystems

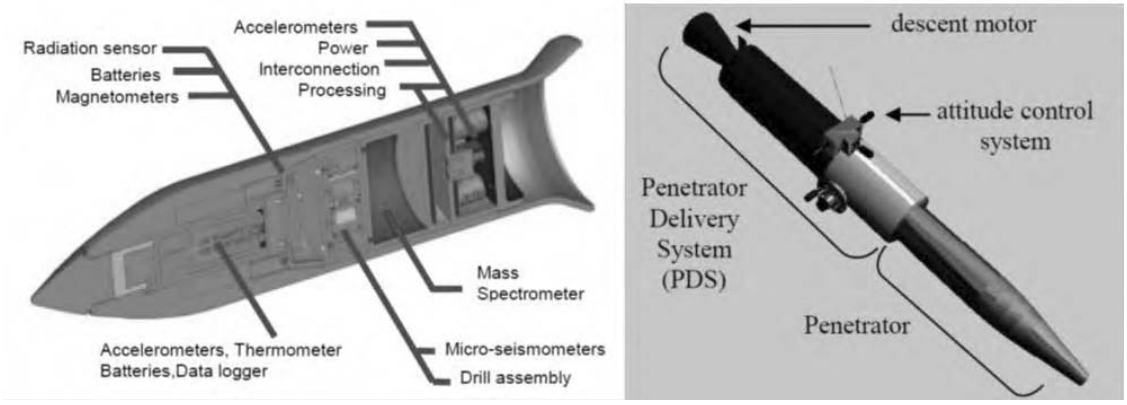

Figure 4.2: MoonLITE Penetrator internal bay structure and contents locations (left) and Concept Of Penetrator Descent Module (right). Extracted from [Gowen et al., 2008]

and a scientific payload. The Mass of each penetrator will be around 13Kg and its length is approximately 0.5 m. The payload (2Kg) is composed by micro-seismometers, a heat flux package, chemistry package, an accelerometer and a descent camera. The penetrators are aimed to be deployed over different Moon locations (in permanently shadowed craters in the poles, near existing Apollo sites or in the far side of the Moon). These sites are globally distributed to create a seismic network thanks to the orbiter used for the deployment as link in the network. Important test trials were performed demonstrating that the penetrator subsystems and instruments are able to survive to the expected impact. Moon LITE mission does not proposed energy harvesting systems to recharge the batteries. The mission EoL is estimated to be near 1 year.

4.1.3 Deep Space 2

The Deep Space 2 mission was the second of the NASA's New Millennium Program aimed to flight and test new technologies for future planetary surface exploration missions. The DS2 mission is the only small volume and reduced mass platform in cluding a penetrator for space exploration successfully lunched (although as described hereafter lost after landing). For this reason this platform shall be considered as an important reference and source of lessons learned for other similar platforms aimed to planetary surface exploration as the one herein proposed.

The mission (launched on 3 January 1999 and with a total cost of $28.2 \cdot 10^6$\$)

comprised two penetrators that weigh 2.4 kg each and are being carried as a piggyback payload on the Mars Polar Lander cruise ring. The spacecraft arrived at Mars on December 3, 1999. The two identical penetrators should have impacted the surface at 190 m/s and penetrate up to 0.6 m. They should have landed within 1 to 10 km of each other and about 50 km from the Polar Lander on a sector at approximately 76°S, 195°W on the edge of the Martian south polar layered terrain ([Albee et al., 2000] and [Smrekar et al., 1999]).

MPL approached Mars on 3 December 1999, in apparent good health. It was expected that the first data from the DS2 probes would be received on 4 December at 7:25 p.m. PST, about 7 hours after MPL touchdown. However, no communications from MPL or the probes were received ([Albee et al., 2000]).

The main mission objective was to demonstrate technologies for future network science missions as the one proposed in this Thesis. Even though, it must be remark that the two probes had not capabilities of communication between each other, only with the Mars Global Surveyor orbiter. An additional mission objective was to obtain scientific data: measure the water content and thermal properties of the regolith, atmospheric density, pressure and atmospheric temperature derived from the descent deceleration data. Also the impact accelerometer data would be used to determine the depth of penetration, the hardness of the regolith, and the presence or absence of 10 cm scale layers.

The mission considered two penetrators, referred as "microprobes"(figure 4.3). About 5 minutes before MPL entered the upper atmosphere, the lander entry body and cruise stage were to have separated using pyro devices. The DS2 aeroshell was designed to passively align itself even if it is tumbling when it enters Mars Atmosphere.

The probes would then penetrate the surface by as much as a meter, first separating into two parts at surface impact. An aftbody (which would stay at the surface) and a penetrator (which would come to rest below the surface) connected with a cable. The probes were expected to strike the surface with an impact velocity of about 200 m/s. The aftbody was designed to withstand a peak rigid body shock of about 60000 g´s and the penetrator a shock of about 30000 g´s. Approaching the shape of the aftbody to a cylindrical shape, the outer diameter was around 140mm and a height of 120 mm. The penetrator had a hemispherical nose with a total length of 100mm long and 39 mm in diameter. The technologies proposed for the surface body could operate up to $-80°C$ while the penetrator could survive up to $-120°C$.

Micro-instruments in the penetrator were designed to perform sample collection with a miniature drill, move about 100 milligrams of soil into a cup, heat the sample, and attempt to detect water vapour using a tuneable diode laser assembly. Also encased in the penetrator were a power micro-electronics unit, an advanced micro-controller, and sensors to measure soil conductivity. A mixed signal ASIC was designed for power control, and a Spartan computer system integrated in a

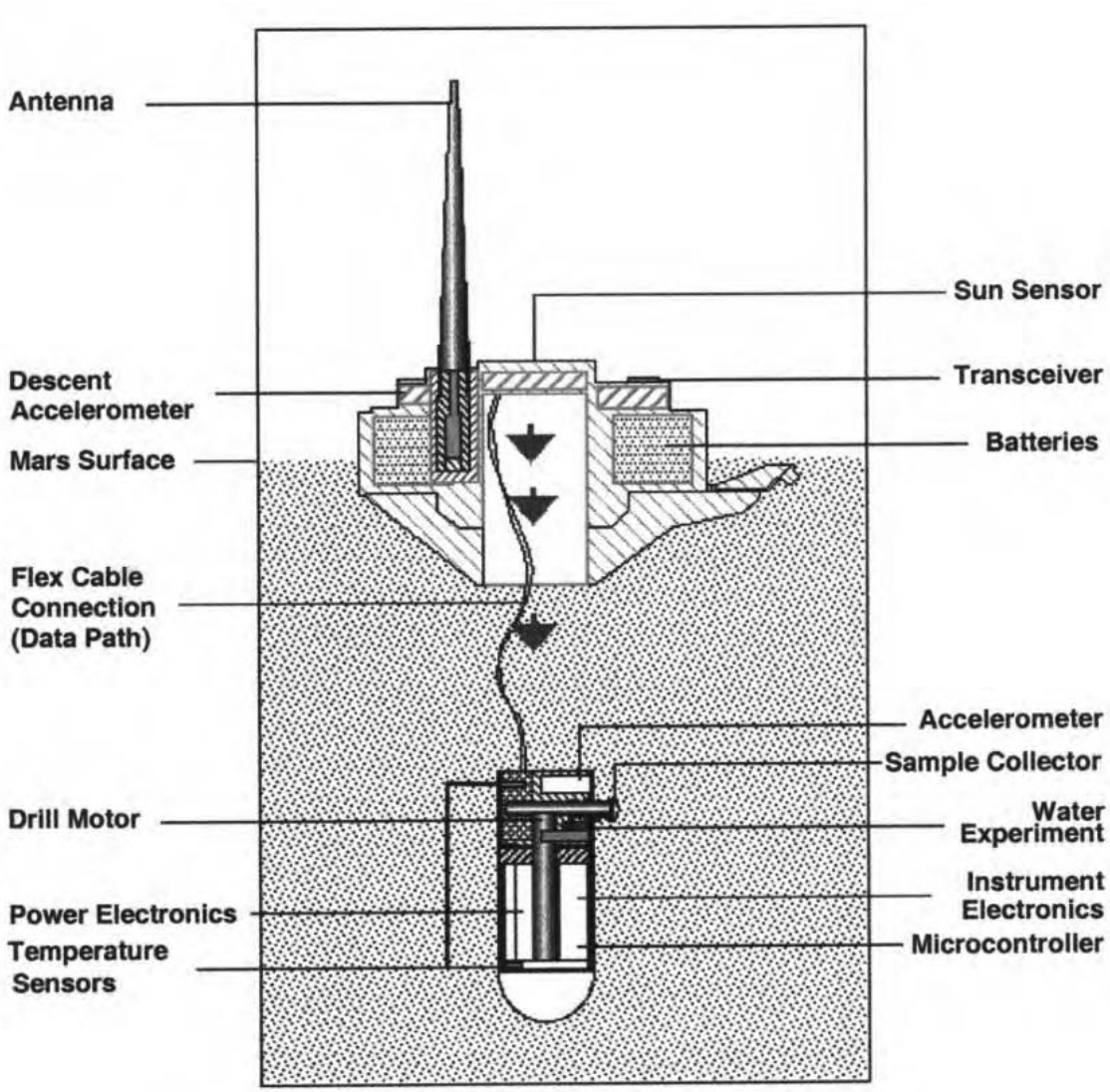

Figure 4.3: DS2 schematic overview ([Smrekar et al., 1999])

80C51 microprocessor was used as control unit. Data from the penetrator were to be transmitted via the flexible connecting cable to a micro-telecommunications system in the aft-body and then transmitted to MGS.

Special mention must be focus in the specifically developed low-temperature lithium-thionyl chloride batteries (located in the surface module) able to work at

temperatures as low as $-80°C$. The probes used 2 batteries with a total mass of 80 grams (40 g per battery). Batteries were the unique source of power, for this reason once the batteries were depleted the mission would end, approximately after one or two Martian days (no harvesting technologies were proposed in this mission).

Despite the low mass and volume of the DS2 probes, a complex experiment was included for soil water content measurement. A micromotor would drive a small drill at the side of the penetrator. The soil sample would be deposited into a heater cup (sealed with a pyro system). The soil would be then heated, driving any water vapour into the analysis chamber. If water was present, it would be detected by measuring the difference in light intensity of a laser shining through the vapour. The tuneable diode laser was set so that its light is at the point in the spectrum where water absorbs light.

The penetrator system development required a complex test program ([Lorenz et al., 2000]). The probe´s bullet-like forebody is designed with a half circle nose (tungsten) to ensure penetration over a wide range of entry conditions.

4.1.4 Luna-Glob

The Russian Luna-Glob mission was conceived during the 90s with the objective of studying the origin of the Earth-Moon system and the investigation of the chemical composition and physical characteristics of the lunar materials at the landing site including the detection of water traces. The mission was cancelled and rebirth several times due to funding problems mainly, also it was redefined several times. From the beginning, high-speed penetrators were considered. Around 2010 it was decided to abandon the development of penetrators for the Luna-Glob mission. Between the reasons to abandon the penetrator technology were that hard-landing and semi-hard landing approach considered were found too risky for the mission (first lunar Russian mission to the Moon in decades) and there were problems developing the thrusters initially considered for the semi-hard landing (Russian Space Web, [WB1]).

For the analysis of the state of the art herein presented it is considered the original mission scenario as described in [Galimov, 2005] and [Surkov et al., 1999], and specifically the high speed small penetrators initially proposed. The original Lunar-Glob mission contemplated four different systems:

- 10 small high-speed penetrators (hard-landing).
- 2 penetrators-landers (semi-hard-landing). Focused in complex scientific experiments including broadband seismometery.
- Polar station consisting in a landing module, braking engine and inflated shock absorber powered by a RTG.

- Orbiter. The remaining orbiter of the spacecraft (after separation of the landers) would be used as communication link between the landers and the Earth and also it would be used for global cartography of the Moon.

The 10 small high-speed penetrators would be deployed in two circles (refer to figure 4.4), creating a virtual seismic antenna on the surface of the Moon. This experiment based on the concept of small aperture seismic array was proposed by Khavroshkin and other seismologists at the Institute of the Earth Physics in Moscow, with the objective of studying the internal composition and history of the Earth's natural satellite. The high speed penetrators are assembled into a ring cassette. The penetrator cassette is provided with a battery, solid-fuel engines and a control unit. The seismic array is best deployed in an area having low seismicity and thick regolith layer.

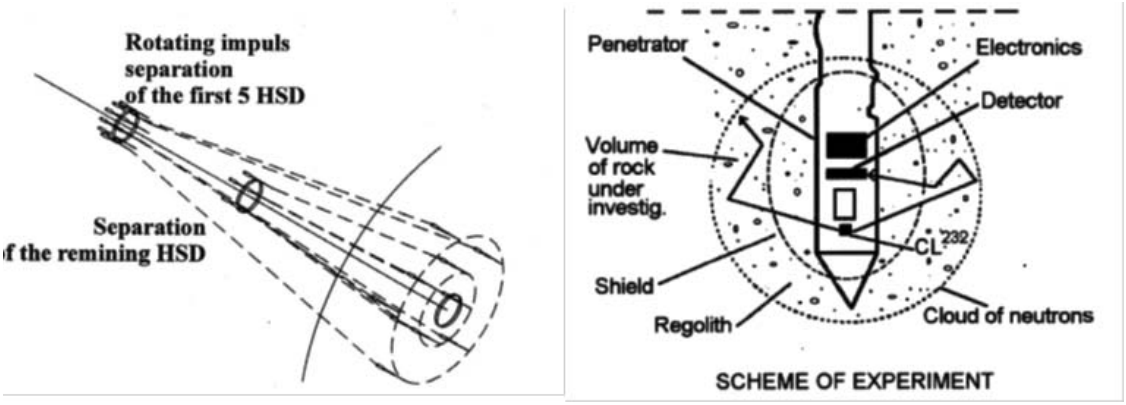

Figure 4.4: Schematic of the deployment of high speed penetrator extracted from [Galimov, 2005] (left) and scheme of the high speed penetrator buried under the Moon surface extracted from [Surkov et al., 1999]

The information available in the literature about the small penetrators is very confusing and with important gaps as the small penetrator dimensions, mass and detail description.

4.1.5 Met-Net

MetNet Mars Mission ([Harri et al., 2007]), is a mission proposal aimed to deploy an in situ observational network and orbital platform to investigate the Martian environment.

The scope of the MetNet Mission is to deploy MetNet Landers on the Martian surface by using inflatable descent system structures accompanied by an atmospheric sounder and data relay onboard the MetNet Orbiter, which is based on ESA Mars Express satellite platform. The MetNet Landers are attached on the three sides of the satellite and are deployed to Mars separately, a few weeks prior to the arrival to Mars. The MetNet Orbiter will perform continuous atmospheric soundings thus complementing the accurate in situ observations at the Martian ground produced by the MetNet observation network, as well as the orbiter will serve as the primary data relay between the MetNet Landers and the Earth.

The MNLs are equipped with a science payload focused on the atmospheric science of Mars. Detailed characterization of the Martian atmospheric circulation patterns, boundary layer phenomena, and climatological cycles, as well as interior investigations, require simultaneous in-situ meteorological, seismic and magnetic measurements from networks of stations on the Martian surface.

The MetNet Mars Mission proposal was implemented in collaboration with ESA, FMI, LA, IKI and the payload providing science teams (INTA, UC3M and UPM among others).

The payload of the two MNL precursor models includes the following instruments ([Harri et al., 2015]):

- Atmospheric instruments: MetBaro Pressure device, MetHumi Humidity device and MetTemp Temperature sensors.
- Optical devices: PanCam Panoramic, MetSIS Solar irradiance sensor with OWLS optical wireless system for data transfer and DS Dust sensor.

Among the science teams that developed the payload for the MetNet Landers, the author of this thesis participated in the Arquimea´s team that subcontracted by the University Carlos III de Madrid developed a Dust Sensor (Figure 4.5 right), aimed to characterize the suspended dust in the Martian atmosphere, Alvarez 2011.

The initial landing sites are selected in a latitude range of ± 30 degrees and at low altitudes, thereby allowing the use of only solar panels as energy source and avoiding the political problems of including radioactive generators into the Lander. For high-latitude missions radioactive heaters will be necessary to make the systems survive the Martian winter ([Harri et al., 2012]). MNL flexible solar panels provides a total of approximately 0.7-0.8 W of electric power during the daylight time. As the provided power output is insufficient to operate all instruments simultaneously, they are activated sequentially according to a specially designed cyclogram table which adapts itself to the different environmental constraints.

The total mass of the entry vehicle is 22.2 Kg (4Kg of payload). Currently one complete flight unit has been manufactured and tested to acceptance levels at Lavochkin and the mission is waiting for a flight opportunity.

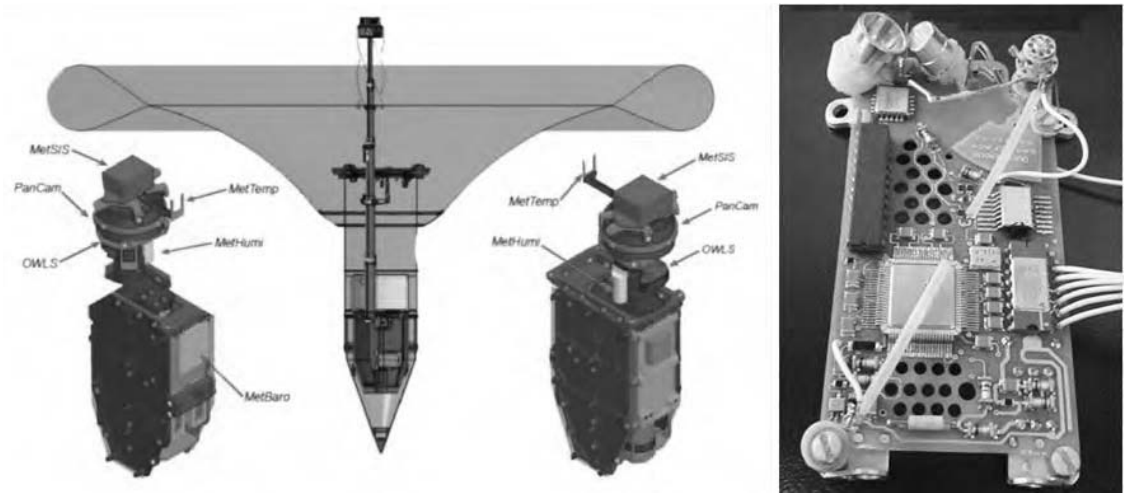

Figure 4.5: MetNet Lander section view extracted from WB5 (left). Dust Sensor Flight Model (right) courtesy of Arquimea Ingeniería S.L.U and University Carlos III of Madrid.

4.1.6 RF-WIPE

The RF-WIPE ([Sanz et al., 2013]), was a study supported by ESA under GSP contract and developed by GMV acting as prime contractor in partnership with SUPSI, (Scuola Universitaria Professionale della Svizzera Italiana) and UPM, (Universidad Politécnica de Madrid). This study was focused on analysing the sensor networks for planetary exploration to identify and characterize all possible exploration scenarios suitable to exploit the capabilities of sensors network technologies based in the 802.15.4 protocol standard. Although the study does not specify hardware details of the space compatible systems to be used for the proposed WSN, the study presents a robotic launcher device ([Sanz et al., 2010]), developed using commercial components and implemented to deploy the nodes that compound the WSN. The study analyses different deployment techniques and network configurations. Even though this study is not focused in the planetary exploration platform itself, it provides a detail study of the feasibility of use WSN for space exploration and also demonstrate the interest of the Space Agencies (in this case ESA), in WSN as an alternative for space exploration.

4.1.7 Hopping robots

The term "hopping robots"refers to robotic systems with the capability of move using different jumping methods that permits them to avoid obstacles and move through

the terrain. Several of these hopping robots have been proposed for planetary surface exploration. Currently, Hayabusa 2 mission shipped two jumping robots that are in their way to meet an asteroid in the following two years.

These hopping robots are miniature mobile robots (few kg or even below the kg), with scientific payload used for distributing sensing. Most of the proposed concepts make use of WSN. Although the proposed platform in this thesis is a fixed platform, these hopping robots are presented and analysed in this state of the art since they share several attributes similar to the technologies herein proposed: low mass, low power consumption and distributing sensing using WSN. In the literature can be found several proposals of hopping robots for planetary surface exploration, below some of the most similar to the concept proposed in this thesis are presented for comparative purposes with the technologies herein studied.

Canadian Space Agency hopping robot

The Canadian Space Agency ([Montminy et al., 2008]) developed a hopping robot prototype for Mars surface exploration based on regular tetrahedron geometry and a SMA actuator for jumping. The tetrahedron provides robustness to recover from the landing after the jump in any possible configuration.

Figure 4.6: Canadian Space Agency hopping mechanism (extracted from [Montminy et al., 2008]

One of the main technologies proposed in this platform, that makes the concept a very promising alternative for space exploration, is the SMA actuator. This actuator uses the variations of temperature on the Martian surface as a source of energy, thus

reducing the dependence of stored energy for locomotion. After the jump the robot deploys its petals that roll the robot to its vertical configuration. The petals are covered with solar panels in order to provide energy to the on-board subsystems. A single SMA based actuator is used for the jumping, petals deployment and retracting of the mechanism to perform the following jump. This locomotion mechanism is low power (0W actually), low mass and permits to jump (inaccurately) 3 meters per sol over the Mars surface. The total lander mass was conceived to be less than 2 Kg with 250 g of mass for the payload.

MIT hopping micro-robots

The Massachusetts Institute of Technology (MIT) supported by the NASA Institute for Advanced Concepts ([Dubowsky et al., 2006]), proposed a mission concept based on the deployment of a large number of small jumping spherical mobile robots. The robots would be deployed from orbit using, one or several, soft landing modules with the capability of deploy tens to hundreds of these units. The proposed spherical robots (10 cm in diameter and about 100 grams) could be able of generate mobile WSN and collaborate with surrounding nodes. These robots would be equipped with a suite of miniaturized sensors as imagers, spectrometers and chemical analysis sensors. The locomotion system is based on a "foot"composed of a dielectric elastomer actuator powered by hydrogen/oxygen fuel cells. The slow rate of power generation charges slowly the dielectric elastomer actuator and releases the energy during the jump. A very efficient fuel storage concept based on Proton Exchange Membrane (PEM) fuel cells powered by stored, on-demand hydrogen in the form of metal hydrides is proposed as main source of power ([Thangavelautham et al., 2012]). This robot does not include harvesting energy concepts. A passive thermal control based on radiators and intelligent power control is proposed for thermal regulation. The concept is based on several technologies not available at the moment of the proposal that were expected to be developed in the near future. Thus a prototype of the complete platform was not developed. Even the concept is very interesting, the mass estimation is really optimistic and based on technologies developments which feasibility have to been proven (e.g. space compatible miniaturized sensors and subsystems, fuel cells of low mass and volume and high power output).

CalTech hopping robot

The California Institute of Technology in collaboration with the Universitá di

Verona, developed several prototypes of small jumping robots ([Burdick and Fiorini, 2003]). The authors define the mobile platform proposed as ˝minimalist jumping robots˝with the capability of exploring planetary surface large areas, coordinating their motions to collectively gather distributed scientific data. The work was focused in the locomotion system including mechanical methods for locomotion, attitude control ([Tammepõld et al., 2011]) and localization. The 1^{st} generation prototype was a football shaped device capable of short jumps, but stimulated much of the results of successive developments. The 2^{nd} prototype was a minimalistic device powered by a single motor, capable of about 3 m jumps and equipped with self-righting capabilities. The 3^{rd} generation prototype is equipped with wheels and is capable of long, but coarse, jumps using the hopping mechanism, and short, precise motion using wheels. The proposed work does not detail the mission concept or the overall platform design, although it is an important step onwards the demonstration of feasible jumping systems for space exploration.

HAYABUSA2 (mission)

Japan (JAXA) launched the second sample return spacecraft ˝Hayabusa2˝to the Near-Earth asteroid ˝1999JU3˝in December 2014. Hayabusa2 is a scientific-driven mission to retrieve some fragments from a C-type asteroid ([Yoshimitsu et al., 1999]). The predecessor spacecraft ˝Hayabusa˝made a great success when it returned to the Earth in June 2010 with a capsule containing some particles obtained from the S-type asteroid ˝Itokawa˝([Kawaguchi et al., 2010]).

Hayabusa2 mission contemplates the inclusion of three hopping robots to explore the asteroid surface:

- Two twin hopping robots developed by JAXA: MINERVAII
- Hopping robot developed by the German Aerospace Centre (DLR) and the Centre National d'Etudes Spatiales (CNES): MASCOT

Both hopping robots are described in the following paragraphs.

MINERVAII

Minerva II payload consists of two rover containers, a relay module and an antenna to communicate with the rovers. Three rovers are included in the two containers (figure 4.7). Two of the three rovers look like a cylinder and have a mass of approximately 1.1 kg each one ([Kubota and Tomiki, 0015]). Each rover has installed a different set of sensors. The rovers are simultaneously ejected when the spacecraft

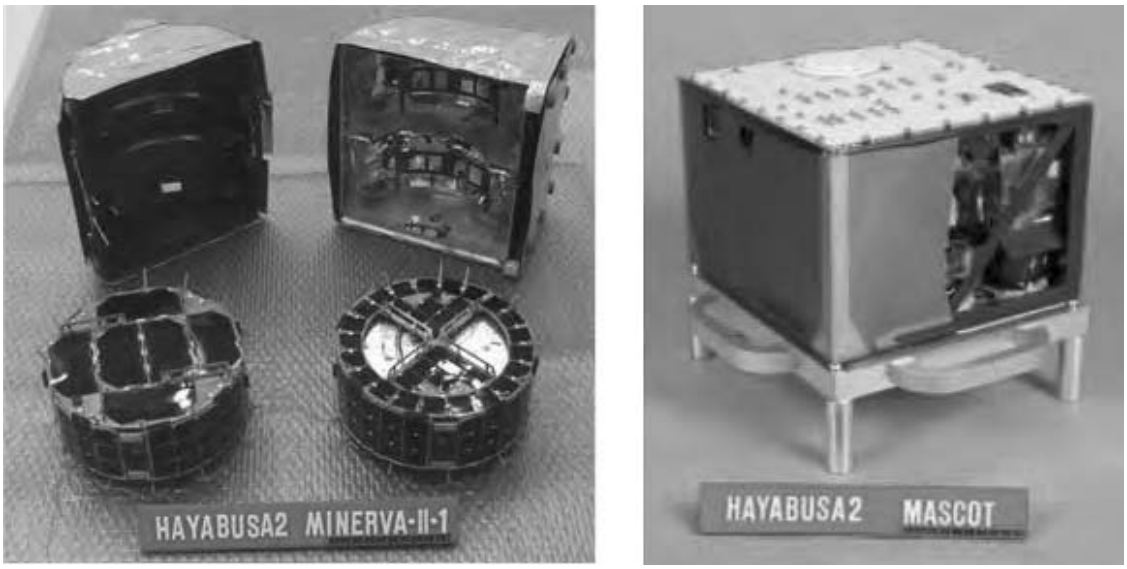

Figure 4.7: MINERVA II twin rovers (extracted from [Yoshimitsu et al., 1999] and [Ziach, 2015]

descends to the surface after the arrival at the asteroid. They fall into the asteroid surface by a weak gravity and then start an autonomous exploration. The obtained data are transmitted to the relay module on the mother spacecraft. There is a torquer inside the rover´s body and rotating the torquer makes the rover hop into the free space by a repulsive force against the surface of the asteroid (more details about the hopping system can be found in [Yoshimitsu et al., 1999]).

The payload of the rovers includes cameras, thermometers, potentiometers accelerometer, gyro and photodiodes. Solar cells generating 2W at approximately 1.4 AU from the Sun feed ultra-capacitors of 100 F working at 2.5 V.

MASCOT

MASCOT (Mobile Asteroid surface SCOuT) is a small hopping rover included in the Hayabusa2 mission. MASCOT will be ejected via a spring mechanism from Hayabusa2. The lander measures 0.275 x 0.290 x 0.195 m^3, has a mass of 9.6 kg ([Ziach, 2015]). The platform is divided into two segments: a warm compartment containing the electronics-box with the majority of MASCOT´s electronics, the battery package and the mobility mechanism, and a cold compartment housing

the payload. The payload includes a spectrometer, a camera, a radiometer and a magnetometer. MASCOT´s telemetry will be relayed to ground via Hayabusa2. A mobility mechanism allows MASCOT to hop across the surface at a distance of up to 220 m.

The platform contains only a primary battery (9 LSH-20 cells in a 3s3p configuration). The expected lifetime of MASCOT is limited by the energy stored in its battery, in the order of 10 hours.

4.2 State of the art analysis

The following table presents a brief comparative of the different missions and concepts of the literature including the platform proposed in this thesis.

Mission/ Concept	Mass	Deployment	Scientific Payload	Area coverage	Energy source
Lunar-A (mission)	45 Kg (13.5 Kg excluding deployment system)	Penetration/ hard landing	-Seismometer -Heat flow	Low coverage Few square meters per penetrator (without communication capabilities between penetrators)	Li-SOCl2 batteries (1 year EoL) No harvesting
MoonLITE (mission)	36 kg: 23 kg propulsion 13 kg penetrator (science payload 2 kg)	Penetration/ hard landing	-Micro-seismometer -Heat flow package -Accelerometer -Thermal sensors -Descent camera -Chemistry package -Radiation sensor	Low coverage Few square meters per penetrator (4 penetrators without communication capabilities between them directly)	Batteries (1 year EoL) No harvesting
Deep Space 2 (mission)	3,107 Kg (0,7Kg aeroshell, 1,737Kg surface platform and 0,67Kg penetrator)	Penetration/ hard landing	- Subsurface soil sampling/water -Soil conductivity -Temperature -Sun sensor -atmospheric pressure -accelerometer	Low coverage Few square meters per penetrator (without communication capabilities between penetrators)	Ultra-low temperature lithium battery Lifetime 1/2 Martian days No harvesting
Luna-Glob (mission)	Not specified	High-speed penetration (hard landing)	-Small aperture seismic array	Low-medium coverage	Battery and solid-fuel engines
MetNet (mission)	22.2 Kg (4Kg payload)	Penetration/ Semi-hard landing	-Pressure sensor -Humidity sensor -Temperature sensors -Panoramic camera -Solar irradiance -DS Dust sensor	Large-medium coverage Coverage depending on the number of MNLs deployed	Flexible solar panels at mid latitudes RTG for polar regions

Mission/ Concept	Mass	Deployment	Scientific Payload	Area coverage	Energy source
RF-WIPE (concept)	No specified	Rover deployment	-Temperature -Relative Humidity -Pressure -"Ambient light"	Large coverage Max. area 100x100 m per device	No specified No harvesting
Canadian Hopping robot (concept)	1-2 Kg (excluding deployment system)	No specified	250 grams for non-specified scientific payload	Large coverage.	Energy harvesting: -Temperature for SMA actuator -Solar panels
MINERVA II mission	1.6 Kg (excluding deployment system)	Semi-soft landing	-Cameras -thermometers -potentiometers -accelerometer -gyro -photodiodes	Low coverage Few hundred meters	Solar cells and ultra-capacitors
MASCOT	9.6 Kg (excluding deployment system)	Semi-soft landing	-Spectrometer -Camera -Radiometer -Magnetometer	Low coverage Few hundred meters	9 LSH-20 cells 10 hours EoL No harvesting
Conceived in this THESIS	5.25 Kg (2Kg surface platform, 3.25 Kg penetrator body)	Penetration/ hard landing	-Dust Depostion -Multiespectral Irradiance Sensor -Radiation sensor -Temperature Sensor	Large coverage (20 nodes 5Km^2)	Day and night Energy harvesting >3 years EoL

Table 4.1: State of the art comparative table

The state of the art presents a large variety of very interesting concepts and missions which represent a starting point with vast information of lessons learned and different ways of solve similar problems. However, none of the developments found in the literature solve certain key points presented in previous sections that motivates this thesis:

- Large mission life (years) using several energy harvesting systems (without RTGs), including energy harvesting during the cold planet nights.
- Effective solutions to the deployment system (even in vacuum conditions) in order to obtain a low mass entry system that could survive hard landing deceleration forces.
- Low cost development of several low mass platforms using available technologies in the state of the art.
- High reliable platforms relaying in redundant or complement systems without increase the total mission mass.

Analysing in detail the different concepts and missions we could directly distinguish some of them that are in a low TRL stage (Call Tech hopping robots), present incomplete studies of the exploration platform conceived (RF WIPE or Luna Glob) or even are based in concepts which are not technologically available currently (MIT hopping robot).

In the other hand we can find mature concepts and missions based on technologies with a large heritage or with high TRL:

- Even though the Lunar-A mission was cancelled, the knowledge and information obtained during the years of research provide an important input for future development of penetrators for space exploration. Particularly interesting is the knowledge acquired by the development team during the penetrator tests. As drawbacks of the concept proposed, it can be outlined the lack of energy harvesting systems and the reduced payload considering the large mass of each penetrator.
- Certainly the MoonLITE mission presents a very valuable heritage including interesting approaches that shall be considered in future proposals or developments. In this thesis, the Descent Module (DM) designed by the MoonLite team has been used as a reference for the DM proposed. The field tests campaigns realized, demonstrating the penetrator concept and high shock survival techniques, are of special interest. The lack of energy harvesting technologies and the elevated mass of the penetrator that reduce the number of penetrators to be deployed are specific drawbacks of this concept.

- The Deep Space 2 mission is of main importance, in the state of the art presented, as it is the only mission based on a similar concept of the one herein proposed that has been launched. Even designed and launched in the latest 90s, the developed technologies as the ultra-low temperature batteries are currently very interesting. The lessons learned and compiled in [Albee et al., 2000], shall be carefully studied and considered for future missions. The lack of harvesting energy systems with a very limited life (only 2 Martian days) and the need of including reliable shock protection systems are two important drawbacks of this concept.

- MetNet mission is other mature concept developed and currently searching for a mission opportunity that demonstrates the potential of penetrator technologies for planetary exploration. The concept, that initially contemplated the use of RTGs, changed to solar harvesting as primary source of power certainly improving in this way the mission concept. Its payload and platform distribution make it a very interesting approach for the meteorological characterization of a planet with atmosphere. Its large mass and the impossibility of harvesting energy during de night are drawbacks of the concept proposed. Also it must be considered that the deployment concept requires an atmosphere in order to reduce the entry velocity of the platform.

- The Canadian hopping robot concept presents a smart locomotion system based on thermal energy harvesting. Even though the concept does not define a mission or subsystems detail description (communications between nodes or robots deployment over the planet surface) it introduces an innovative system of locomotion for future developments.

- Hayabusa 2 jumping robots demonstrate that small platforms with a reduced payload are very valuable for surface exploration of rocky bodies. Of particular interest is the Minerva II robot, with capabilities of harvesting solar energy and store it in ultra-capacitors for a limited time operation over the body surface. These systems are designed for semi-hard landing on a low gravity body, similar concepts could not be used on larger planets with a higher gravity without incorporate shock protection systems. Also, the thermal design based on a short day/night cycle is incompatible with the large day/night cycles of larger bodies.

Chapter 5

Self–powered and low mass fixed platform

5.1 Platform configuration

Reviewing the state of the art (chapter 4), we can distinguish two different platforms concepts: (i) subsurface platforms (penetrators as those proposed by Moon-LITE or Lunar–A missions) or (ii) surface platforms (as the RF–WIPE, Canadian or MIT hopping robots). A more flexible approach is the one followed by the DeepSpace2 or MetNet missions in which part of the platform is beneath the surface and the other part remains over the surface. In line with this mixed configuration, this thesis introduces a new platform that exploits all the advantages of having a dual body platform that were not fully exploited in previous concepts proposed: as a dynamic thermal regulation (chapter 8), energy harvesting (chapter 9), redundancy (section 5.5), shock absorption (section 7.2.3) and cost reduction for the deployment of a large number of platforms (chapter 7).

As introduced, the conceived configuration is based in a two-body system as depicted in figure 5.1 and 5.2:

- A tetrahedral platform that will remain over the planet surface, also referred in the literature as aftbody. The design, development and testing of this platform are described in detail in this thesis. The tetrahedral platform contains all the scientific payload and acquisition electronics, solar panels, communication systems, power module and auxiliary batteries. Section 5.2 describes in detail the conceived configuration of this part of the proposed platform.

- A penetrator body that will enter into the planet subsurface. The penetrator is situated in the baseplate of the tetrahedral platform and it will separate from the surface body during the penetration in the planet sub-surface as described in section 7.2. The penetrator body will contain the On Board Computer (OBC), the principal batteries including the related power electronics and the umbilical cable that interconects both bodies of the platform. Section 5.3 describes the penetrator body concept.

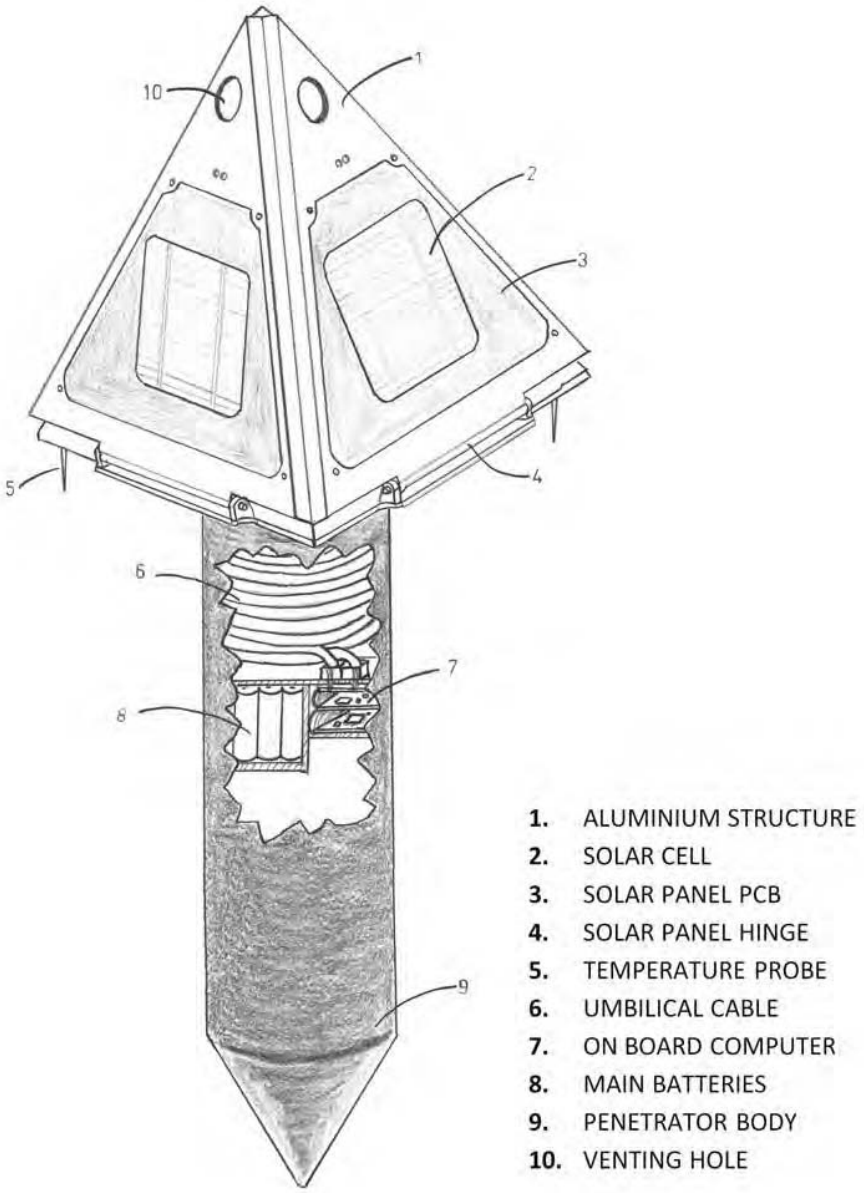

Figure 5.1: Two-body platform prior to landing impact (external solar cell shock protection material not shown)

Figure 5.2: Platform deployed, tetrahedral body over the surface and penetrator body underground (frontal solar panel and protective resin removed for inner subsystems view)

5.2 Surface tetrahedral platform description

The surface platform designed is a regular tetrahedron with an envelope of 200x200 mm of base and 200 mm of height (figure 5.2), with a total mass below 2000g. The proposed system configuration considers deployable solar panels. When closed, the deployable walls in form of petals protect the node from the environment during transportation and deployment (shock and dust contamination during deployment by penetrator, refer to chapter 7). Once the platform is over the planet surface a release mechanism based on a shape memory alloy pin-puller device ([Nava et al., 2012]) is activated and the solar panels are deployed, allowing the exposure of the payload sensors and inner solar panels to the lunar surface.

A light aluminum structure, forming the tetrahedron and providing stiffness to the node, holds all the elements together. The structural material selected for the tetrahedral platform is aluminum. Aluminum and its alloys are non-magnetic materials with a good combination of high stiffness to density ratio, high ductility, high corrosion-resistance, excellent workability and availability at a low cost. Specifically, due to the high stress that the structure shall support during the platform deployment, a 7075 aluminum alloy is selected.

The inner part of the tetrahedron includes a dust sealed electronics bay dynamically regulated by an ultra-low volume and weight passive thermal switch to protect the electronics from the hard environment of the lunar surface. The inner bay includes the following elements: power subsystem, communication subsystem, auxiliary batteries and payload acquisition electronics (that includes a redundant On Board Computer as described in section 5.5).

5.2.1 Tetrahedron shape selection

The tetrahedron shape selection of the platform impacts directly in the node performance and capabilities. The selected shape introduces specific and significant advantages for the proposed concept of mission with minor drawbacks. Other solutions were considered, as the pyramidal shape (four faces) or dice shape (cube). A comparative analysis between the different alternatives considered is presented below. The spherical solution was discarded due to its incompatibility with the mission concept: higher manufacturing costs and interface complexity with other subsystems.

Mass and volume considerations.

Mass is one of the main design drivers. The tetrahedron shape permits to reduce considerably the mass and volume of the node maintaining its performance. The

three faces of the tetrahedron can be used to place sensors or antennas maintaining approximately a 360° coverage. Pyramidal configuration (four faces) or dice shape (five faces) will imply the addition of a fourth, and even a fifth face, involving more mass and volume and not providing an important advantage. Another faces will increase the solid angle resolution of the sensors or antennas, although with a proper design a fourth or a fifth face will not be necessary to maintain a nearly 360° coverage.

Mechanical and structural considerations.

With the objective of being compatible with a penetrator technology deployment, the structure of the platform shall be structurally robust. The most stable structure shall be considered, due to the high shock levels expected during the landing. Considering a basic structural analysis of the platform, with the objective to select the most stable structure shape, we can consider to analyze the number of external reactions. The number of external reactions must be greater than the number of equations available for the structure to remain in a static equilibrium. Thus, for the structure to be stable, the following equation shall be satisfied:

$$m \geq 2j - D \tag{5.1}$$

Where parameter m represents the number of elements of the considered structure, j is the number of joints and D is the number of equations available for the structure to remain in a static equilibrium. D value is three for two-dimensional (planar) structures and it is six for three–dimensional (non-coplanar) structures. Considering this, the most stable and resistant structure in 2–D is the one composed by triangles. The triangle shape, under an external force applied, will deform with resistance; the force will be distributed between the joints and beams of the triangle that shall be designed to support the expected loads. Considering this basic analysis, the selection of a tetrahedron shape (composed of regular triangles) ensures the most simple and resistant structure. The pyramidal shape also satisfies equation 5.1. Although a pyramidal shape will reduce drastically the resistance of the structure compared with the tetrahedron. The reasons are that the number of joints increases as the number of beams connected to the upper node. And considering that joints will be the points that will most suffer during the shock they are the most probable points of failure. Reduce the number of joints will reduce the probability of structural failure during the shock. Also it could be possible to use stronger and heavier joints if its number is reduced, thus maintaining a low total mass of the structure.

Performance considerations.

The advantages of a platform with pyramidal or dice shapes with respect to a tetrahedron shape are mainly of performance:

- Available area for solar panels. With up to six faces the available space for solar panels is drastically enhance.
- Increase the solid angle resolution of the different elements. In this case, the pyramidal shape would have a better performance. Using an additional sensor or antenna it is possible to cover with major resolution a virtual field of view of 360°.
- The effective available volume inside the platform is highly increased in the pyramidal shape and the dice shape.

Node integration considerations

The low volume and mass obtained with the tetrahedral shape is directly in conflict with the integration complexity of the node. Because of the reduced space, integration complexity is increased (including mounting and harnessing connection).

Cost considerations

The inner space of the tetrahedron node and the faces are triangular shaped. This is an important drawback for the use of commercial PCBs, solar panels or batteries while they are usually available with a square form. The project philosophy foresees the deployment of hundreds of nodes, then it would be possible to manufacture custom solar panels being a cost effective solution due to the large number of units to be produced.

Concluding, the tetrahedron shape of the platform will imply a more advantageous mass/volume relation maintaining the mechanical structure stability with an adequate performance. From a performance point of view, without consider the structural stability of the platform, the dice shape would be the best choice because this shape would increase the effective available space inside the node and the area for solar energy harvesting. This is one of the main reasons why the dice shape has been selected for the majority of satellites lunched.

Because the main directive is the mass and structure stability (a heavier node would be incompatible with the deployment of an important number of nodes and a less robust structure will be destroyed during the hard landing) the tetrahedron has been selected as the optimum shape for the proposed platform.

5.2.2 Inner electronics bay

The inner electronics bay is one of the key elements of the proposed two-body platform. The electronics bay contents the following critical subsystems:

- Scientific payload acquisition electronics. Described in section 6.5.4, controls the entire payload and performs an acquisition procedure when commanded by the OBC. Also this subsystem includes an enhanced FPGA capable of work as redundant OBC in case of malfunction of the nominal OBC (section 5.5).

- Communication subsystem. This subsystem allows the platform to communicate with the rest of the nodes of the WSN and includes the ad-hoc, energy-efficient network protocols required for an efficient, reliable and low-power consumption WSN. This subsystem is out of the scope of this thesis. A description of this subsystem developed under the SWIPE project and compatible for the platform herein proposed can be found in [Rodrigues et al., 2014], [Rodrigues et al., 2015] and [Oddi et al., 2014a].

- Power subsystem. This subsystem performs the node power regulation and individually supplies power to the different subsystems of the platform. A high reliability design using high reliability components is required for this critical subsystem. A power regulation block is also included in the penetrator body aimed to control the charging and discharging of the principal batteries when the main power regulation block is not operative (lunar nights or failure).

- Auxiliary batteries. The auxiliary batteries permit to extend the node operational time drastically. Even more, in case of a malfunction of the principal batteries (located in the penetrator body) the auxiliary batteries will be able to maintain the operation of the node. The batteries considered are rechargeable lithium-ion battery model VL 34570 ([Saft, 2009]).

All these subsystems within the inner electronics bay are integrated in a light aluminium rack and embedded in a special resin (refer to section 7.2.3). The only relevant area in thermal contact between the inner bay and the external structure is located in its base, where a thermal switch is located to control the heat flux interchange between the inner electronics bay and the external structure.

The electronics bay will protect the electronics from the environmental constrains:

- Temperature: Thermally regulated by a thermal switch and active heaters, as explained in chapter 8, the inner bay will increase the operational time of the electronics subsystems. The resin that embedded all the subsystems helps to maintain a uniform temperature between the subsystems included in the inner bay.

- Vibration and shock. The embedded elements inside the inner bay are protected from the high shock and vibration during the deployment of the platform over the planet surface as described in section 7.2.3.

- Dust: The dust could not affect the inner electronics bay subsystems. The external structure including the solar panels and the resin avoid the dust to enter in contact with the electronics components.

5.2.3 Scientific payload distribution

The customized conceived low power consumption and low mass payload for Moon surface exploration is summarized below. The detail design description of each sensor is described in chapter 6. It is important to remark that the scientific payload included in each node can be customized. Each node platform can be configured with different sets of instruments, thus increasing drastically the scientific objectives of the whole mission. Likewise, sensors in the penetrator body could be included if required.

- Three temperature probes. These probes are sharpening aluminum probes that are located in the base of the surface platform near triangle corners (section 6.5).

- Three multispectral irradiance sensors (each one including three sensors at visible, IR and UV) placed with a separation of 120° for a total field of view of 360° at the three faces of the tetrahedral platform (section 6.4).

- A radiation sensor based on a mixed signal ASIC that provides Total Ionizing Dose (TID) and Single Effect Upsets (SEUs) radiation monitoring. This ASIC has been designed using radiation-hardening techniques and it is located in one of the deployable solar petals. Its location in the external corner permits to reduce the influence of the platform in the radiation measurement (section 6.3).

- A Dust Deposition Sensor (DDS) for measuring the Moon dust deposited by natural means over its optical surface. This sensor is located on the top of the platform to reduce the influence of the rest of the platform elements in its measurments (section 6.3).

The acquisition electronics for all the sensors is located in the thermal regulated inner bay. A dedicated FPGA commanded by the OBC will be in charge of controlling all the platform sensors obtaining the different measurement when requested by the OBC.

5.2.4 Solar panels deployment subsystem

The release mechanism used for the deployment of the solar panels is based on a pin puller from the family of actuators based on SMA (Shape Memory Alloy) from Arquimea Ingeniería S.L.U.

Pin Puller non-explosive release actuators are mechanical devices which function is to retract a pin that is used to lock a system that has to be released or deployed for operation. These release mechanisms are high reliability devices enhanced for space environment and commonly used in spacecraft for solar panels, antennas or payloads deployment. These release mechanisms incorporate redundant SMA trigger capable of independently activate the actuator. Pin Puller release mechanism is a low shock non-explosive actuator; it is reusable and can be reset by hand with the help of a tool. The mechanism is reset by simply retract the pin. The selected pin puller model pulls down its pin when actuated with a force not lower than 25N (figure 5.3). The total mass of the pin puller is 60 grams.

Figure 5.3: 25 N pin puller based on SMA

Considering that there are three panels to deploy, an auxiliary three–arm mechanism releases the three panels using one pin puller. The three–arm auxiliary piece locks the solar panels while it is engaged to the mechanical fixation pieces of the solar panels. Once the pin puller is actuated the three–arm piece releases the solar panels and permits their deployment. A spring placed in the hinge of the solar panels provides the required force for the deployment. An external end of stroke sensor is used to control the pin puller activation.

During the solar panels deployment some dust will be ejected as consequence of the impact of the solar panels over the non–compacted upper layer of dust of the Moon surface. With the objective of reducing the quantity of this ejected dust, that afterwards could be deposited over the solar panels or over the optical subsystems, the solar panels hinge is situated 20 millimeters above the tetrahedron base. With this disposition, the area of the solar panels that will enter in contact with the planet surface is reduced. This height of the hinge w.r.t the platform base is also of main importance to ensure an acceptable solar panels deployment. The base of the platform could be introduced some centimeters in the lunar soil during the landing. The height

of the solar panels hinge could be increased or reduced in function of the soil conditions of the landing target.

5.3 Penetrator body description

The penetrator body part is 300 mm in height, 100 mm in diameter with the shape of a ballistic missile. The penetrator is attached to the baseplate of the tetrahedral platform and its total mass is below 3450 grams. The mechanical attachment is done using a weak mechanical connection that is broken during the penetration of the two–body platform in the planet surface as described in section 7.2. The penetrator body is estimated to enter between 0.3 to 1.2 meters in the planet subsurface leaving the tetrahedral platform over the surface.

As depicted in figure 5.1 the penetrator body contains the principal batteries and the OBC. These two elements are connected with the tetrahedral platform using a hardened and redundant bundle of cables (detail description in section 5.4). The cables are wound inside the upper part of the penetrator body and are unrolled during the penetration phase. The main objective of the penetrator structural design is to permit the OBC, batteries and cabling to be introduced in the planet subsurface. Besides the OBC, the main batteries and the cabling located in the top part of the penetrator, the rest of the penetrator body is empty to host the structure aimed to absorb as much as possible the elevated shock energy levels generated during the penetration phase. The internal structure in the lower part of the panetrator can be deformed during the penetration, thus reducing the shock energy level at which the rest of elements are exposed.

The deployment of the conceived platform using the penetration approach requires a specific design of the complete platform to support the high shock forces at which the platform is subjected, especially the penetrator body. Chapter 7.2 presents the solution proposed to minimize the harmful effects of the shock during the deployment phase. Additionally, as described in section 5.5, the considered redundant design permits to maintain operative (with a reduced performance) the tetrahedral surface platform, even in the case of malfunction or complete failure of the penetrator body. This approach increases drastically the reliability of the whole mission.

The penetrator body is of main importance in the platform concept herein proposed for the following reasons:

- During the penetration in the lunar surface, the penetrator body absorbs a great part of the shock energy, reducing the destructive effects of this shock in the surface platform (refer to section 7.2).

- The temperature range beneath planet´s surfaces is usually warmer (during the night) than in the case of the surface (e.g. the Moon). For this reason

the platform could make use of this thermal heat to maintain the OBC and the batteries operative during the cold nights. Moreover the penetrator body will permit to obtain energy from the planet subsurface using thermoelectric harvesting techniques as explained in section 9.3.

- The penetrator approach solves the deployment problem efficiently with a reduced mass and cost, thus making feasible the deployment of several WSN nodes in one mission.

5.4 Harnessing

The distribution of the different subsystems and sensors within the two–body platform proposed requires the subsequent harnessing to interconnect all of them. Figure 5.4 presents the required interconnections between all the platform subsystems.

Therefore, the elevated number of cables and connectors required within the compact conceived platform would increase the mass and cost of the overall system. Moreover, we have to consider that any connector included in the design introduces a risk of malfunction that could potentially mean the failure of the related subsystem or the complete node failure.

In the conceived platform the vast majority of connectors have been removed and the cables reduced to a minimum. The following approach has being implemented:

- Use of flexible PCB technology to interconnect the different PCB´s within the inner bay, thus removing the cables and associated connectors.

- As later described in section 7.2, the complete inner bay of the tetrahedral body, the OBC and main batteries of the penetrator and other subsystems are embedded in a special epoxy resin that reduces the shock effect in the electronics and homogenize the temperature. Thus, it is possible to remove all the connectors in the subsystems embedded in this resin. The cables can be directly soldered to the PCBs and the epoxy resin will provide the required mechanical stiffness avoiding the cable to be cut away due to relative movement of the cable and the PCB (the embedded resulting system would completely avoid the relative movement of the cable w.r.t the PCB). Obviously this radical approach of removing the great majority of the connectors in the platform shall be supported by a well–defined and qualified manufacturing and integrating procedure. Because the objective is to manufacture and integrate tents to hundred of this platforms, the efforts required to define and qualify this procedures are completely justified and the overall result is cost effective.

- The antennas harnessing are special reduced size coaxial cables and connectors. These coaxial connectors are also embedded in the protective resin.

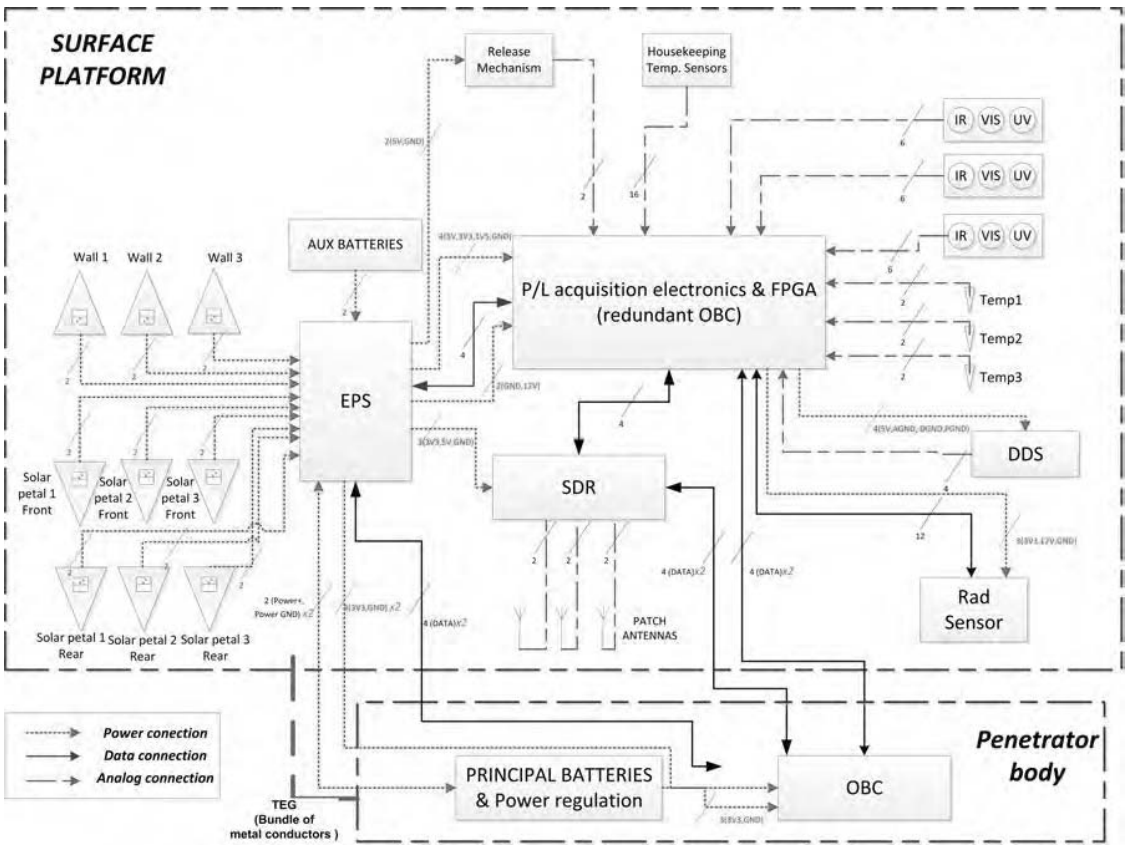

Figure 5.4: Harnessing overview

The harnessing that connects the surface tetrahedral platform and the penetrator will suffer from extraordinary efforts due to the tensions generated during the penetration phase. Additionally the cables rolled in the upper part of the penetrator shall be able to be deployed at a velocity near the initial impact velocity of the penetrator. The deployment of very similar umbilical cables has been studied, tested, reported in the literature and even patented ([Canning et al., 1981], [Murphy et al., 1981]). The deployment method described in [Canning et al., 1981] was successfully tested as described in [Murphy et al., 1981] for an arrangement compatible to the one herein proposed. Therefore a similar deployment method is proposed based in those successful experiences.

Three different bundles of cables shall be deployed between the surface platform and the penetrator body:

- Two umbilical cables for power and data connection between the surface platform and the penetrator (refer to figure 5.4). A special umbilical cable design is proposed (refer to figure 5.5). The different PTFE cables are rolled around a common inner core made with very thin iron wire. The complete assemble is covered with a protective PTFE cover leaving the possibility of movement of the rolled cables around the iron wire. The iron wire is coated using solid lubricant to avoid erosion of the PTFE cover of the cables surrounding the inner metal wire. In this way the iron wire will absorb the tensile efforts during the penetration phase leaving the cables the flexibility to adapt its position around the iron wire. Additionally, as described in section 5.5, this bundle is duplicated to provide hard redundancy to the connection. The umbilical cables are 1.5m long and have 17 inner conductors. The total diameter of each bundle of cables is 8 mm.
- A bundle of conductors for thermoelectric power generation. This bundle of cables is actually a new design concept proposed in this thesis for a Thermoelectric Generator (TEG) and it is described in detail in section 9.3.2.

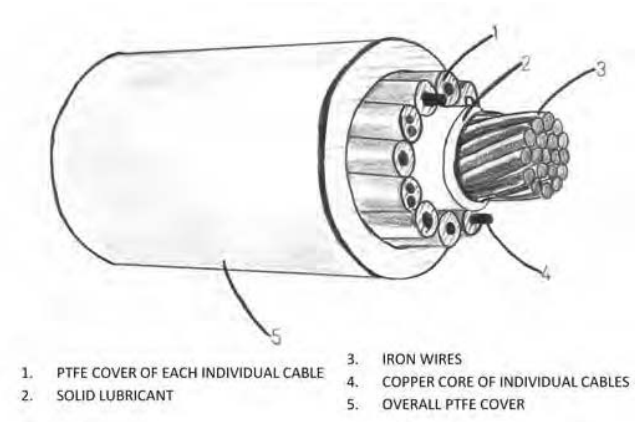

Figure 5.5: Umbilical cable descriptive section

5.5 Redundancy considerations

One way to improve the reliability of a space system is using redundancy (hardware, software, information or time redundancy can be considered). Herein we propose hardware redundancy, duplicating critical components of the platform with the

intention of increasing the reliability of the whole system. Hardware redundancy implies higher costs, mass and complexity, however the harsh environment and constrains of space exploration missions justify the use of hardware redundancy in those critical systems that are more vulnerable to a previously known possible mode of failure. The conceived two–body platform could present the following most critical modes of failure:

- Main OBC failure.
- Principal battery failure or power subsystem failure.
- Radio interface sub-system failure.
- Loss of power and/or data connection between the surface tetrahedral platform and the penetrator body.

In each case a hot or cold standby hardware redundancy technique is proposed as described below. It must be considered that the redundancy techniques herein proposed are compatible with the low mass and power consumption overall design objectives of the platform. The approach followed is to use, whenever possible, multiple functionality of the redundant system, thus reducing the impact in the overall mass.

Main OBC failure.

The main OBC is located in the penetrator body. As previously commented, place the OBC in the penetrator permits to harvest the thermal energy of the planetary subsurface with the objective of maintain the OBC and main batteries always operative. However, during the lander phase the penetrator will be subjected to extremely high shock energy levels. Even considering the design techniques described in chapter 7, we have to contemplate that the penetrator body is more susceptible to partial or total failures. This does not mean that the tetrahedral platform would not be subjected to high shock energy levels, although the penetrator will absorb the major shock levels during the penetration, as it is the first element to impact with the planet surface as later explained in chapter 7. Consequently it is proposed a hardware architecture where the OBC is duplicated using cold standby redundancy.

The concept proposed is to use the acquisition electronics control FPGA to implement a redundant OBC with the same functions that the main OBC. A control unit is, in any case, required to manage all the payload acquisition procedures, therefore the mass impact is limited to the addition of some external elements as later described in section 5.6.

The acquisition electronics FPGA is powered from the main and auxiliary batteries and will be in an ultralow power consumption state most of the operational time. The FPGA will wake-up when required from the OBC to perform a scientific data acquisition procedure. Additionally, every 20 minutes, the acquisition electronics will wake-up during some milliseconds to submit a pulling message to the main OBC. In a normal operation mode, the main OBC will immediately answer to the FPGA acquisition electronics and the latter will enter again in its hibernation low power consumption state. If the main OBC fails to answer the acquisition electronics FPGA in three consecutive attempts (in both nominal and redundant lines), the acquisition electronics will assume the failure of the OBC and will work as main OBC hereafter. Every 20 minutes the attempt to communicate with the OBC in the penetrator body will be repeated to try to restore the nominal operation.

Obviously in the redundant mode, where the acquisition electronics FPGA has assumed the OBC activities, the performance of the complete system is reduced, while the FPGA will switch off when the temperature of the surface platform descent below the operational temperature range of the FPGA, thus stopping the node operations until the temperature is again within the operational limits. After the wake-up, the node operated by the redundant OBC, shall resynchronize with the WSN and re-stablish the normal operational mode re-planning its tasks as explained in chapter 10.

It is possible that the OBC remains operative but the nominal and redundant lines connecting the main OBC and the acquisition electronics are damaged. In this case, the OBC would continue commanding other subsystems of the platform as the radio interface antenna. If this is the case, data collision could occur between the commands send by the OBC and the acquisition electronics FPGA working as redundant OBC. To avoid this, once the acquisition electronics enters in the redundant mode, the rest of the subsystems, as the power module or the radio interface subsystem, would ignore any command received from the main OBC.

In the case the acquisition electronics FPGA would fail, the OBC would remain operative implementing the WSN protocols and data distribution within the WSN, however without providing new payload measurements to the WSN.

Principal battery failure or power subsystem failure.

A common power bus (+12V, +5V and +3.3V) is shared by the surface platform and the penetrator body. This power bus is supplied by two sets of batteries: (i) auxiliary batteries in the surface platform (that will be operative when the temperature of the inner bay is within the operational temperature range of the batteries) and (ii) principal batteries located in the penetrator body and virtually

always operative.

Both sets of batteries are in a hot standby redundancy fashion. Obviously, if the principal battery set fails the complete platform only would be operative during the time the auxiliary batteries are operative.

An efficient power subsystem is placed in the tetrahedral platform within the inner electronics bay. A partial duplication of the power electronics is placed in the penetrator in order to maintain the OBC operative during the cold nights when the power electronics of the aftbody is out of its temperature range. The power subsystem is able to independently switch on and off the different subsystems. In this way, any malfunction of a subsystem that could lead in a short-circuit condition will not affect the overall platform.

Radio interface sub-system failure.

The radio interface subsystem is a critical element of the platform that cannot be duplicated because of its high mass and complexity. In case of malfunction the platform will remain inoperative because it will be unable to communicate with the rest of the nodes in the WSN. For this reason the radio interface subsystem shall be design using high reliability techniques and components. An important element of the communication subsystem is the antenna. A partial external obstruction or malfunction of this element would imply the complete loss of the platform, unable to communicate with the WSN. Three antennas will be used in the platform. Each antenna will be covering 120° for a total coverage of 360°. This approach would permit the node to communicate with the surrounding nodes. In the case of a failure of one or two antennas, the node would be able to communicate if the remaining antenna or antennas are in line with any other surrounding node.

Loss of power and/or data connection between the two-body platform elements.

The cables connecting the surface tetrahedral platform and the penetrator body are critical to maintain the overall platform performance. Even though the cables connecting both parts of the platform are specially designed to be mechanically robust (refer to section 5.4) this umbilical bundle of cables is duplicated. Two identical bundles of cables are provided to increase the reliability of this connection.

Cold standby redundancy is used for the data cables: in a normal operation mode the OBC will try to communicate using the nominal line, if not reply is received in three consecutive attempts the OBC will use the redundant line. This procedure

will be used to switch between redundant and nominal until obtain a successful communication. In the case of the power cables a hot standby redundant approach is followed. Both cables are connected to the power bus in a nominal operation.

Redundancy in the platform overview.

As a result of applying all the previous redundancy techniques it is possible to conclude that the node could maintain its functionality even in the case of major failures, as it is the case of the complete failure of the penetrator body and its related subsystems.

Table 5.5 summarizes the redundancy elements interrelation conceived for the platform.

5.6 Main and redundant On Board Computer architecture overview

As described in the previous section, the platform proposed conceives two different OBC (nominal and redundant) distributed in each of the platform bodies. A main OBC located in the penetrator body and a redundant OBC located in the surface platform (used additionally as control unit for the payload acquisition electronics).

In this section the OBC architecture is presented. This architecture is shared for both OBC (nominal and redundant), just differing in the firmware loaded in each subsystem.

The architecture block diagram is shown in figure 5.6. As it can be seen in the figure, the OBC is based on a RTAX–S radiation-tolerant FPGA from Microsemi. Specifically the RTAX2000SL model is considered due to its highly reliable, nonvolatile antifuse technology and heritage in space systems [Microsemi, 2015]. This FPGA is specially suitable for the platform proposed as it includes a low power grade option that half the standby current of standard product at worst case conditions. The RTAX–S/SL family has hot–swap and cold–sparing capabilities, which enable turn off the device for minimal power consumption during long periods as required for the platform proposed. The 1.5 V core voltage permits to increase the usage of the batteries even when those are with a low output voltage, increasing in this way the operational time.

A processor embedded in the FPGA is considered as main processing unit. The 32–bit processor LEON–FT is herein considered. The LEON3–FT processor is designed for embedded applications, combining high performance with low complexity and low power consumption ([Gaisler, 2008]). The fault–tolerant version of the

System failure	Redundancy	Operational performance
Main OBC	Cold standby redundancy Acquisition electronic´s FPGA would work as OBC.	Reduced. The electronic´s FPGA would maintain the node performance just when the inner electronics bay is within its operational temperature range. Therefore during a great part of the lunar nights the node would enter in a hibernation mode.
Acquisition electronics	Cold standby redundancy. The main OBC will maintain its operability.	Highly reduced. The node will maintain its performance as part of the WSN but without providing new scientific data to the WSN.
Auxiliary batteries	Hot standby redundancy. Both set of batteries work in parallel.	Slightly reduced. The work cycle of the node would be reduced.
Main batteries	Hot standby redundancy. Both set of batteries works in parallel.	Reduced. The auxiliary batteries would maintain the node performance just when the inner electronics bay is within the operational temperature range of the auxiliary batteries. Therefore during a great part of the lunar nights the node would enter in a hibernation mode.
One umbilical bundle of cables	Hot standby redundancy. Two different bundles of cables maintain the connection between the two platforms.	Complete. The redundant bundle would maintain a normal operation.
Penetrator body or the two umbilical cables	Cold standby redundancy. The surface platform would work independently.	Reduced. The electronic´s FPGA would maintain the node performance just when the inner electronics bay is within its operational temperature range. Therefore during a great part of the lunar nights the node would enter in a hibernation mode.
One or two temperature probes	Hot standby redundancy. There are three temperature probes measuring the soil temperature in parallel.	Complete. The remaining operative temperature probes would obtain the required soil temperature..

Table 5.1: Platform redundancy summary

LEON3 processor in combination with the radiation tolerant Microsemi RTAX FPGA gives a total immunity to radiation effects.

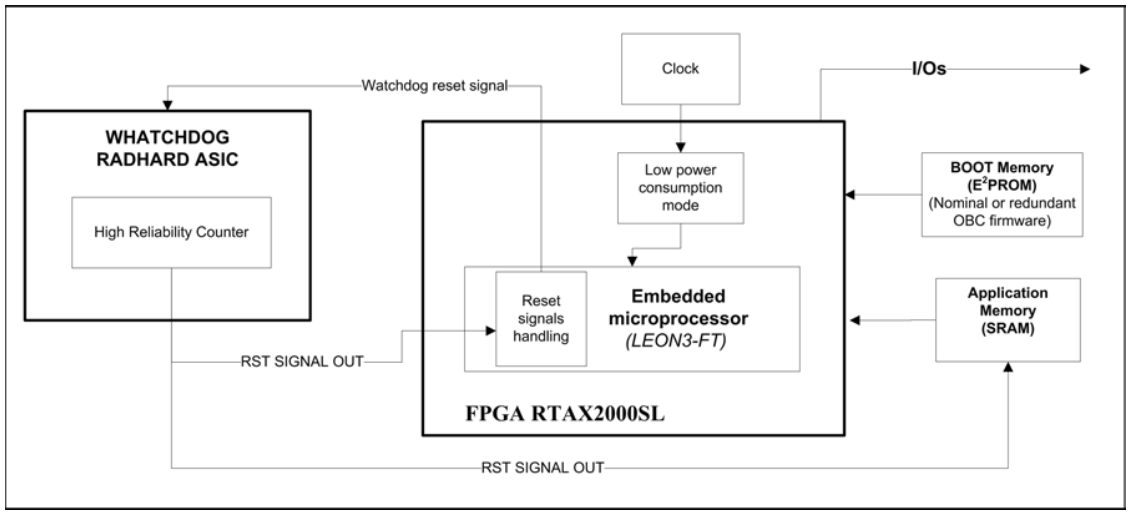

Figure 5.6: Nominal and redundant OBC architecture block diagram

The system requires a boot sequence as in SRAM-based FPGAs there is need to download their configuration code from an external storage device (Boot memory in the figure). An external memory will expand the internal memory of the LEON3–FT processor. In this way it is possible to store the data obtained from the scientific payload (from the platform itself and from other platforms of the WSN) until the conditions of energy, temperature and satellite link are adequate for a data upload procedure.

The OBC could enter into an infinite loop due to malfunction (radiation or unexpected behavior of the software program). The use of an external watchdog is herein proposed as safeguard to restore the OBC functionality. External ultra-low power digital ASIC implements a counter designed to rollover after 5 seconds. The OBC is programmed to reset the watchdog timer before 5 seconds. If the OBC enters in a malfunction mode the watchdog timer will not be reset and the watchdog device will reset the FPGA and the application memory. The firmware will be reloaded in the FPGA to re–start the OBC nominal operation. The digital ASIC implementing the watchdog shall be rad–hard and implement high reliability design techniques.

5.7 Platform mass budget

Table 5.2 presents the complete platform mass budget. This budget includes the mass estimations for each subsystem, either work–out theoretically from the design

or experimentally based on the prototype subsystems developed. It is possible to see that the mass budget is very tight and challenging to accomplish. A safety margin of 10% has been considered given the uncertainty of the estimations.

	Subsystem	Mass (grams)	Notes
Surface platform	Tetrahedral aluminium structure	520	Obtained from prototype
	Inner electronics bay (with epoxy and MLI)	545	Estimation
	DDS	40	Obtained from prototype
	Surface temperature sensors (x3)	9	Obtained from prototype
	Radiation sensor	10	Obtained from prototype
	Irradiance sensor (x3)	25.5	Obtained from prototype
	Harnessing	120	Estimation
	Solar panels	275	Estimation
	Thermal switch	117	Obtained from prototype
	Release mechanism	60	Obtained from prototype
	Antennas (x3)	30	Estimation
	External structure shock protection materials	65	Estimation. Not including epoxy resin considered in the mass of the inner electronics bay.
	Safety margin	10%	Margin considering uncertainties in the estimations
	TOTAL surface platform	**1998,15**	
Penetrator	Penetrator structure	1250	Estimation. Including shock reduction structures.
	OBC	75	Estimation
	Harnessing (umbilical cables + deployment system)	435	Estimation.
	Thermoelectric Generator	800	Estimation.
	Power electronics	120	Estimation.
	Main batteries	205	Estimation. Based on [RD8]
	Shock protection materials	75	Estimation. Aluminium foam.
	Safety margin	10%	Margin considering uncertainties in the estimations
	TOTAL penetrator body	**3256**	
Two–body platform TOTAL		**5254.15**	

Chapter 6

Scientific low mass and low power consumption payload

6.1 Scientific payload conceived

The ultimate objective of the exploration platform proposed is to obtain scientific measurements of the planetary surface aimed to achieve a better understanding of the planet, moon or asteroid.

The selection of the scientific payload, in the frame of an exploration mission, is always a decision of high responsibility shared among the different mission sponsors. Depending on the mission, the scientific payload has to adapt to the technological solutions proposed for the mission itself, or in other cases, are the scientific objectives the drivers that stablish the requirements for the technical solutions proposed.

In the frame of this thesis the main objective of the technologies proposed is to obtain a new low power and low mass payload set of planetary surface exploration sensors that could be used in different exploration missions for environmental characterization. The main requirements for the scientific payload proposed are the following:

- Complexity. The sensors shall be compatible with the platform conceived. Low mass and low power consumption sensors shall be proposed.

- Environmental characterization. As described in section 1.4, the hard environmental constrains are a limiting factor for the planetary space exploration. The set of sensors selected shall be able to characterize as many as possible relevant environmental parameters to increase our knowledge about the planetary surface under exploration.

- Valid for different targets. The reutilizations of the same sensors for different planetary surface targets would increase the number of missions were the proposed platform could be useful, also reducing the cost of reutilization. The sensors herein proposed are dimensioned for a Moon scenario (refer to section 3.2.1), although all of them are compatible with other objectives as Mars or different asteroids.

In the scope of this thesis a fixed set of sensors has been selected. Although we have to consider that this would not be the case for a mission using the concept of platform envisaged. Since the concept proposed is to deploy a large number of platforms that would generate an ad hoc Wireless Sensor Network, it would be possible to modify the scientific payload in each platform. Thus covering a large number of different scientific measurements, without increase the mass or the volume of each platform individually or the mission as a whole. Some other sensors compatible with the platform proposed are: seismic sensors (as introduced in the state of the art previously proposed in Lunar-A or MoonLITE missions), atmospheric pressure (just for missions in planets

with gaseous atmospheres), magnetometers, soil thermal and electrical conductivity, water presence sensors, camera or microphone.

The set of sensors selected was found the most advantageous solution that satisfies the requirements described above and better exploits the synergies with the platform configuration proposed. In the following subsections the design solutions proposed for the different sensors are described in detail. The science payload selected is focused on the atmospheric science of the Moon.

6.2 Dust Deposition Sensor

6.2.1 Introduction and requirements definition

As described in section 1.4, the dust is one of the main environmental constrains for space exploration. Its characterization is of main importance with the objective of design space exploration subsystems tolerant to this environmental phenomenon.

The Dust Deposition Sensor (DDS) herein presented is designed to characterize the rate of lunar dust deposition over a horizontal planar surface by natural means in function of time ([Alvarez et al., 2014]. The dust characterization shall be done excluding man-made disturbances such as during the Apollo missions. This data will be very valuable in understanding the dynamics and hazards of dust over the Moon surface, at the moment being only barely theorized ([Stubbs et al., 2006] and [Grün and Horányi, 2013]). The dust deposition rate over the Moon surface has not been experimentally characterized.

6.2.2 Proposed Dust Deposition Sensor design

From the know-how obtained in previous experiences ([Alvarez et al., 2011]), an ultra-low mass, reduced volume and low power consumption DDS has been designed and manufactured. This sensor is based on optical Mie scattering and fulfils the requirements for lunar surface operation.

The sensor is located on the top part of the tetrahedron, at approximately 133 mm of the lunar surface. This location is of main importance for the following reasons:

- The distance to the soil is enough to avoid dust to be attracted directly from the moon surface to the sensor surface due to electrostatic charge.

- Considering the ballistic trajectory theorized in [Stubbs et al., 2006] (refer to figure 6.1) the dust particles, in their descent trajectory, will be deposited over the sensor surface by natural means. Considering the model results (refer to figure 6.1 right) of Stubbs' dynamic fountain model, the great majority of

levitating particles will reach 133 mm of height. Particles as large as $1\mu m$ in radius could be deposited over the optical window of the sensor.

- At the top of the tetrahedron there is no other element of the platform that could disturb the dust particle descending trajectory.

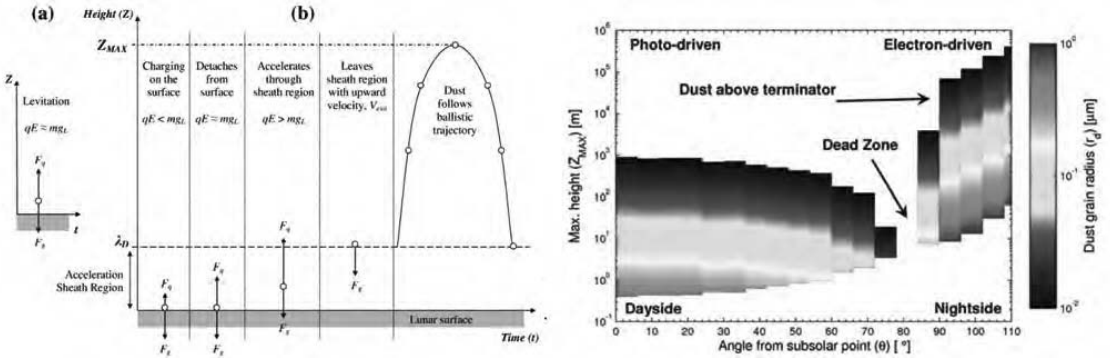

Figure 6.1: Dust ballistic trajectory (left) and dust grain maximum height reached in function of the dust grain radius and subsolar point location (right) following Stubbs' dynamic fountain model (extracted from [Stubbs et al., 2006]).

The working principle is as follows ([Alvarez et al., 2015]): Infra-Red (IR) pulses of light are emitted directly towards a high IR transmittance optical window. This window, which is positioned horizontally to the Moon surface, will accumulate the dust on it by natural deposition means. An IR detector is situated geometrically out of the path followed by nominal IR ray-pulses. The dust particles deposited over the optical window will scatter the IR rays changing their nominal paths and letting them to hit the detector, thus obtaining a measure at the IR detector as a function of the quantity of the dust (refer Figure 6.2).

In order to comply with all the challenging environmental constrains and propose a sensor compatible with the platform herein proposed, the following design approaches have been considered:

- Laser technology could not be used, as it was considered costly, heavy and power consuming for the platform conceived in this thesis. As an alternative, Laser Emitting Diode (LED) technology employing smart pulsing techniques was selected. IR pulses of quite short duration (below $1\mu s$) but with a very high optical output energy were used. The duty cycle was defined in order to permit optical energy outputs above 1W without damaging the emitter.

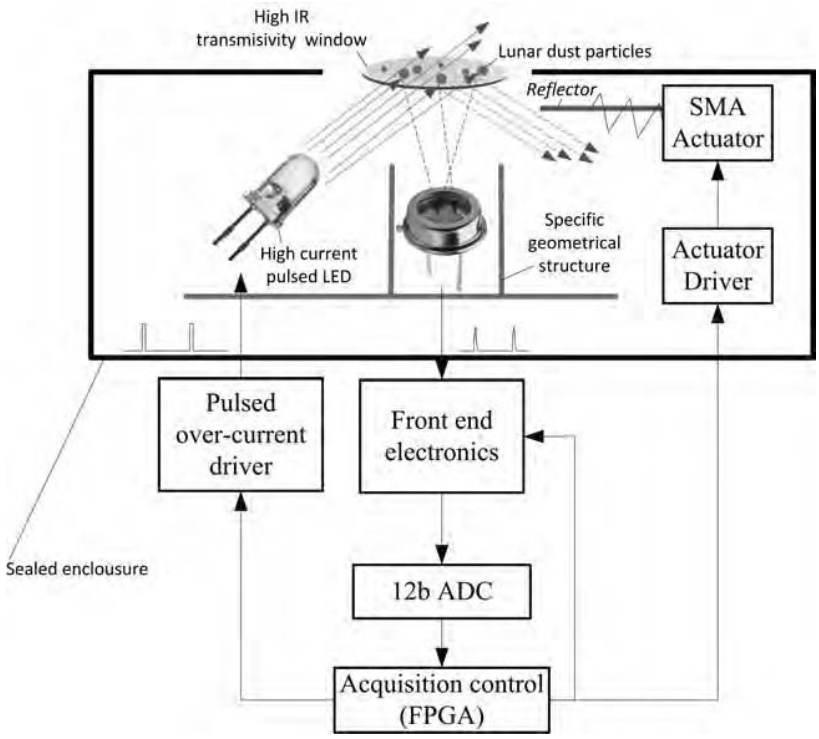

Figure 6.2: Dust Deposition Sensor working principle

- The wavelength of the emitter has been selected in the range of the expected particles size (850nm) to increase the scattering iterations with particles (Mie scattering).
- The sealed housing of the sensor has been specifically designed to enclose all the optical and electromechanical elements to avoid any external dust contamination that could disturb the measurements.
- The geometrical design of the sensor has been studied in detail in order to optimize the scattering return: (i) the IR sensor is surrounded by an optical barrier that matches the field of view of the IR detector to the optical window. (ii) the light reflected in the optical window, and not scattered by the dust particles, following the law of reflection end in an optical labyrinth that reduces by multiple reflection the probability of reach the optical surface of the sensor.
- The selection of the optical window is of paramount relevance. Two possible alternatives have been identified: Sapphire and Magnesium Fluoride (MgF_2). MgF_2 windows are manufactured for a high transmission ($\backsim$ 95%) at NIR and

they do not loss its properties after long radiation exposure as experimentally demonstrated in [Finckenor, 2006]. Sapphire transmission coefficient at NIR is lower ($\backsim 85-90\%$), although it has been traditionally used due to its stable and robust behavior in temperature and its mechanical stress. MgF_2 was selected finally due to its better transmittance and radiation tolerance.

The sensor includes an in-flight calibration system using a diffuse reflector which reflects the light emitted directly to the detector when the actuator system is commanded to do so. This will permit to use a known pattern for in-flight calibration to correct aging or other deviations of the entire measurement chain (detector, emitter and related electronics). A specific ultra-light actuator (10 g) based in SMA technology has been specified and designed by the mechanical department of Arquimea Ingeniería. Results obtained are presented in chapter 10.5. In contrast, against the simplicity of this actuator, and its low mass and volume characteristics it is important to consider the power consumption for each actuation. The total energy consumed by the actuator per each calibration procedure (in vacuum at $20°C$) will be around 150 J. This kind of actuator fits very well applications where there is need of an ultra-low mass/volume actuator that will be used occasionally (as it is the DDS calibration actuator).

The acquisition front end electronics is of main importance and very challenging for this sensor. It shall be able to measure fast pulses of current with the higher possible dynamic range. An energy integration technique, proposed by the electronics department of Arquimea Ingeniería and based on the use of a low offset amplifier, has been selected for the DDS front-end acquisition electronics. This technique permits to acquire the DC output as a function of the total energy obtained in the detector. Additionally the technique allows an increase of the dynamic range by modifying dynamically the light emission time (possibility to adapt the integration time in function of the return signal). This measurement technique prevents the dust measurements during the Moon day because the ambient light will disturb the quantification of the scattered light pulses measurement. For this reason, the DDS shall be operated right after the moon Sunset, providing a high accuracy measurement of the dust deposited over the last Moon day.

The acquisition control FPGA will be responsible for sequencing all the sensing procedures: (i) firstly ten optical measurements of the IR ambient light are performed (non-activated emitter) (ii) secondly the actuator will be commanded to move the IR reflector reference in the light path, the emitter is activated and a value obtained. This will be used as calibration measurements. (iii) Finally the measurement of the dust is performed.

The total mass of the DDS (including the actuator, PCB, screws and harnessing) is 40 grams. The DDS functional prototype is shown in figure 6.3.

The sensor proposed is aimed to measure dust deposited over its surface by natural

Figure 6.3: DDS and auxiliary electronics. Functional prototype.

means. Therefore, it is of major importance reduce to a minimum the robotic system disturbances during the measurement. This is challenging task while the deployment technology considered for the platform is by hard landing (penetrator). Additionally we have to consider the solar panels deployment once the platform is over the lunar surface. The strategy followed to avoid these two problems is following described.

During the landing, the impact of the platform and the penetrator will eject a huge amount of dust at a height of kilometers ([Gaier, 2005]). It is of main importance that this ejected dust will not reach the sensor surface. This goal is achieved due to the configuration of the platform. The platform will be closed during the landing and around 1.5 or 2 months after the landing (this time will depend on the landing time to synchronize the opening with the lunar day). During the time the platform remains closed over the Moon surface, the dust ejected will be slowly deposited over the Moon surface and the external walls of the platform. Additionally, during this time the sublimation of the protective material within the platform will take place (this is detail described in chapter 6). Thus, the sensor (inside the platform) will not be contaminated during this process.

After the first stage is completed (sublimation process concludes and the subsolar point is favorable to harvest solar energy to charge the batteries), the platform is ready to deploy the solar panels. Once the solar panels are deployed the DDS will be exposed to the dust. For this reason the solar panels deployment has been designed to reduce at a minimum the dust ejection:

- It is important to note that the Moon surface can be considered to have nearly vacuum conditions (refer to table 1.1), consequently the absence of gas flowing during the deployment of the petals will not imply dust ejection.

- An important difference in the total electric net charge of the solar panels and the lunar soil could cause dust ejection, and consequently contamination of the dust sensor. For this reason the metal frame of the solar panels and the whole structure shall ensure a good electrical connection (below $10m\Omega$). During the

time the closed structure is exposed to the lunar surface, before the solar panels deployment, and considering the direct contact of the platform with the lunar dust, it is considered that the solar panels deployed are at the same electrical net charge that the surrounding dust.

- It is unavoidable in any case that the sensor will be contaminated as a result of dust ejected from the solar panels deployment. For this reason the first measurement of the DDS shall be performed several days after the platform initiates its scientific mission: once the amount of dust ejected during the deployment procedure is settle down the first measurement will be considered as the reference. The dust deposition rate, during the lunar day/night cycle, can be obtained as the incremental measurements from this initial value.

6.3 Radiation sensor

6.3.1 Introduction and requirements definition

Radiation is an environmental parameter of major importance. As described in section 1.4, the radiation effects are certainly harmful, not only for the astronaut's health, also for the robotic subsystems (specifically for the electronics).

The main objective of the radiation sensor herein proposed is to obtain long-term information about the radiation over the Moon surface. This long term data obtained simultaneously by the different nodes of the WSN concept herein proposed will be of great help in order to eventually enable future human long term presence in the Moon surface. The SWIPE concept mission contemplates the Moon surface exploration using a WSN of tents of nodes spatially distributed over an area with a specific scientific interest. As described in [Rodrigues et al., 2014], one of the most interesting local features on the Moon's surface are swirls. Swirls have a high albedo such as the Reiner Gamma swirl ([Hood et al., 2001]) and tend to be associated with magnetic anomalies ([Halekas et al., 2001]). These anomalies have not been studied in detail yet and there is not much information available about them. There are several different swirl locations on the Moon surface, divided between nearside and farside. By analyzing different locations against several features of interest of the Moon, Mare Ingenii is the site that gathers the highest number of interesting elements, from a scientific perspective.

The SWIPE mission concept considers the deployment of around 10 to 20 nodes to monitor a region of 5 km^2 to include the curling shape of a swirl in the Mare Ingenii. As described in figure 6.4 the radiation environment over the Moon surface is rather complex and requires a challenging sensor in order to characterize the complete radiation scenario. The requirements for the radiation sensor are listed below:

Type	Solar Wind	Solar Cosmic Rays	Galactic Cosmic Rays
Nuclei energies	~0.3–3 keV/u*	~1 to >100 MeV/u	~0.1 to >10 GeV/u
Electron energies	~1–100 eV	<0.1 to 1 MeV	~0.1 to >10 GeV/u
Fluxes (protons/cm^{2}sec)	~3×10^8	~0–10^{6}†	2–4
Particle ratios‡			
electron/proton	~1	~1	~0.02
proton/alpha	~22	~60	~7
L ($3 \le Z \le 5$)/alpha	n.d.	<0.0001	~0.015
M ($6 \le Z \le 9$)/alpha	~0.03	~0.03	~0.06
LH ($10 \le Z \le 14$)/alpha	~0.005	~0.009	~0.014
MH ($15 \le Z \le 19$)/alpha	~0.0005	~0.0006	~0.002
VH ($20 \le Z \le 29$)/alpha	~0.0012	~0.0014	~0.004
VVH ($30 \le Z$)/alpha	n.d.	n.d.	~3×10^{-6}
Lunar Penetration Depths			
protons and alphas	<micrometers	centimeters	meters
heavier nuclei	<micrometers	millimeters	centimeters

** eV/u = electron volts per nucleon.*
† Short-term SCR fluxes above 10 MeV; maximum is for the peak of the August 4, 1972 event. Flux above 10 MeV as averaged over ~1 m.y. is ~100 protons/cm²sec.
‡ Ratios often vary considerably with time for the solar wind and SCR particles and with energy for SCR and GCR. The symbols L (light), M (medium), H (heavy), VH (very heavy), etc., are historical terms for nuclei charge (Z) groups greater than 2 in the cosmic rays. n.d. = not determined (usually because the ratio is too low to measure). Composition data from Feldman et al. (1977) and Bame et al. (1983) for the solar wind, McGuire et al. (1986) for the SCR, and Simpson (1983) for the GCR.

Figure 6.4: Summary of the three major types of radiation in the lunar environment collected by instruments on spacecraft beyond the Earth's magnetosphere (extracted from [Heiken et al., 1991])

- Capability of measuring long term radiation over the Moon surface and at the same time be able to monitor punctual radiation events.

- Large dynamic range. As shown in figure 6.4 the radiation that are expected to reach the Moon surface have a very large energy range, from KeV to GeV, what represents 6 orders of magnitude.

- Low power consumption and reduced mass and volume.

- Tolerant to dust exposure.

6.3.2 Proposed radiation sensor design

The previously listed requirements for the radiation sensor represent a real engineering challenge. The solution proposed is to use the known effects of the radiation over the electronics for radiation monitoring. This solution is based in the measurement of the effects generated by the radiation in some parameters of certain electronic devices. The electronics devices would be completed characterized in the laboratory, using radiation sources in order to obtain the behavior under certain radiation conditions. If the response of the electronic devices is repeatable it would be possible to calibrate the device response and use it as a radiation sensor.

Obviously the auxiliary electronics used for the polarization of the sensor and data acquisition has to be tolerant to the radiation environment in which the sensor is working. Application-Specific Integrated Circuits (ASICs) are custom devices that permit to integrate specific circuits in a single device. This reduces significantly the mass and power consumption increasing the reliability.

Hence, the sensor initially conceived is based in the use of a radiation hardened mixed signal ASIC that will integrate some elements susceptible to modify their properties due to iteration with the ionizing radiation received.

The Microelectronics Group of the Arquimea Ingeniería Company is a group expert in the development of radiation hardened mixed signal ASIC using European commercial technologies ([López-Soto et al., 2014]). This group analyzed the sensor requirements and proposed two different techniques for radiation measurement:

- A SEUs sensor design based on digital Shift Registers (SRs). This sensor would be based in four digital SRs (128b) with different susceptibility to SEUs. Because each SR is susceptible at different Linear Energy Transfer (LET) levels it will be possible to estimate a statistical occurrence of SEUs at different LET levels. The 4 LET levels stablished by design for the sensor are 0.90, 9.75, 30 and 60 $MeV \cdot cm^2/mg$.

- TID sensor monitoring the leakage current of integrated MOSFETs with different layout characteristics for different dose rates.

These LET levels cover a great part of the energy level of SEUs expected over the lunar surface (figure 6.4). However it was found that the MOSFETs integrated would have a much elevated tolerance to the radiation (>50 Krads) that the TID expected over the lunar surface ([Mazur et al., 2015]).

For this reason a search on external compatible transducers with the requirements above stated was accomplished. The RADFET model RFT300-CC10G1 from REM

Oxford Ltd. was selected ([REM, 2009]). This device is a low dose rate transducer able to work with 0V bias during the expose mode, thus increasing the TID value without requiring power consumption. The auxiliary electronics for measuring the radfet device was also included in the ASIC.

The technology selected for the design and manufacturing of this ASIC by Arquimea's Microelectronics Group was a European commercial high voltage technology with proven radiation heritage. The ASIC has been made tolerant to radiation using different radiation hardening techniques: Enclose Layout Transistors (ELTs), systematic guard rings to avoid latch-up between nMos and pMos transistors or Triple Modular Redundancy (TMR) among others. The ASIC also includes the auxiliary front-end electronics; a multiplexing and switching system to measure all the integrated sensors and a configurable charge amplifier to provide a normalized output signal as described in Figure 6.5.

The TID sensor is composed of internal and external transducers as previously introduced. The internal transducers consist on 8 integrated nMOS transistors with different sizes and different layout. The leakage current (drain to source current when the gate is grounded) is measured using an integrated charge amplifier. An analog eight channel multiplexer is used to select the output of each integrated MOSFET using the external ADC of the acquisition electronics (refer to section 6.5.4). The minimum expected response of this transducers is above 50Krads. The resolution, accuracy and range of these TID transducers shall be characterized during a radiation campaign (out of the scope of this thesis).

The external TID transducer model RFT300-CC10G1 has a responsivity in the range of 0.2 mV/rad at source to drain voltage in a zero-bias mode for low doses rates. This TID transducer has the following characteristics:

- Resolution: ±6 rad.
- Accuracy:±12rad.
- Range: 20 to 50000 rad.

The precise transfer function shall be revised after experimental calibration procedure (radiation campaign). Considering a +12V voltage input from the power module to the ASIC the transfer function would be as following:

$$V_0[V] = 1.243 \cdot \triangle V_t \tag{6.1}$$

Where $\triangle V_t$ can be obtained from the calibration curve provided by the manufacturer Figure 6.6 (red line of the Bias 0V curves).

The ASIC includes a precise current source in order to bias the RADFET. A precise bandgap allows to obtain a voltage reference for this current source.

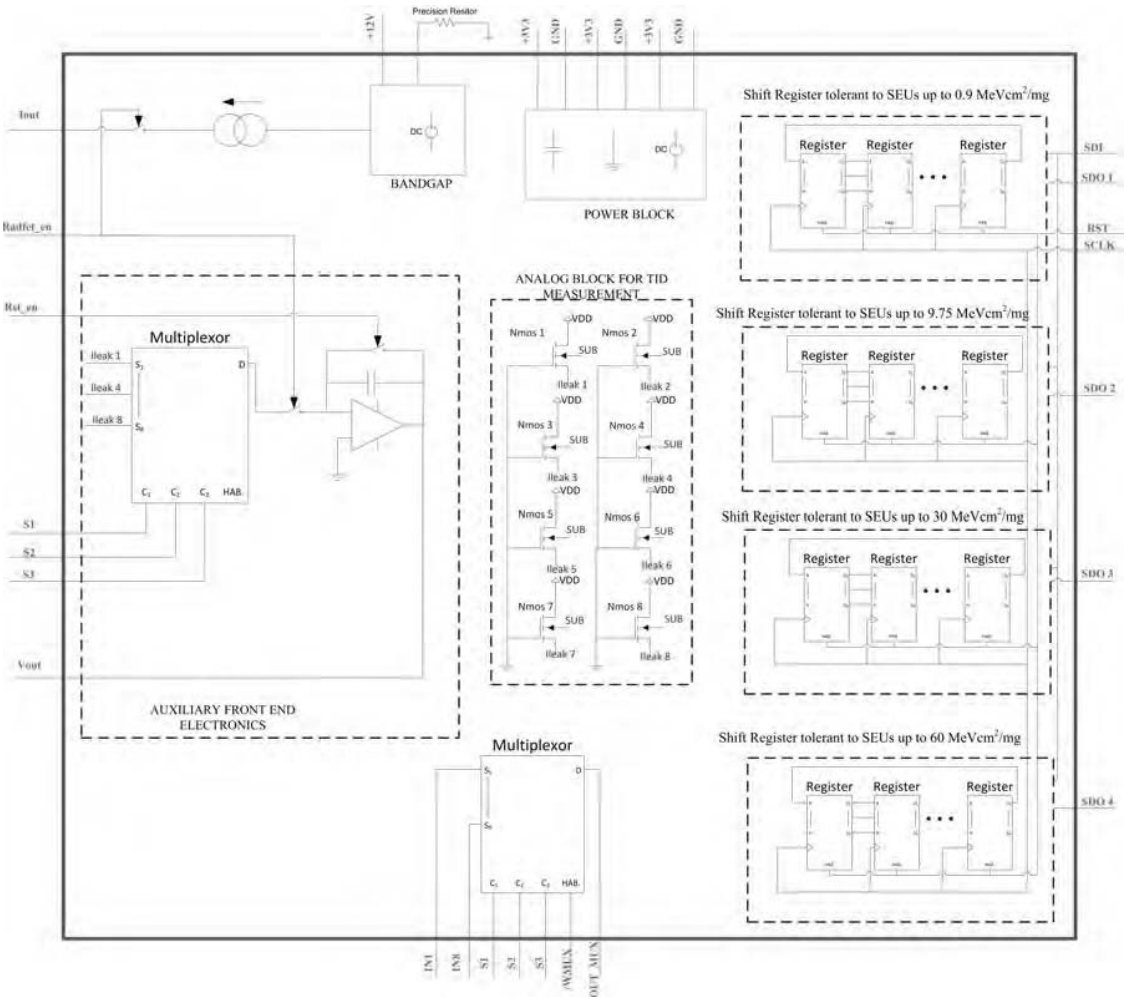

Figure 6.5: Block diagram of the rad-hard mixed signal ASIC designed by the microelectronics group of Arquimea Ingeniería for the radiation sensor aimed to monitor radiation over the Moon surface

A shown in Figure 6.7, the ASIC is encapsulated in a CQFP-64 package. A specific PCB has been designed for mechanical fixing to the node platform using four M3 screws. A PCB will be used to integrate the ASIC and auxiliary electronics (RadFet, connector, decoupling capacitors and external resistors). This PCB is located at the end corner of one of the petals as it can be seen in figure 5.2. The total mass of the radiation sensor (including the ASIC, PCB, auxiliary components and harnessing) is 10 grams.

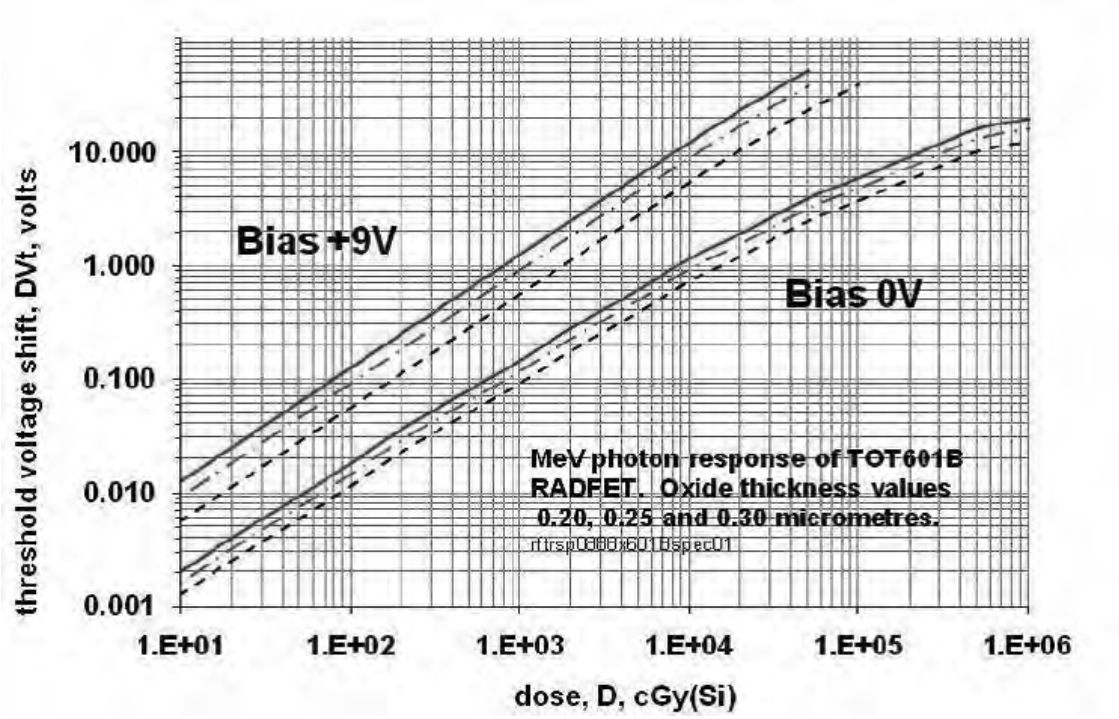

Figure 6.6: Calibration curves of the RADFET used (extracted from [REM, 2009]

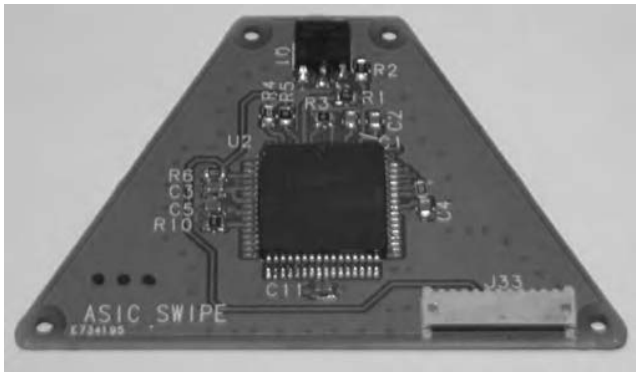

Figure 6.7: Radiation sensor functional prototype (RADFET not included)

6.4 Multispectral Irradiance sensor

6.4.1 Introduction and requirements definition

Solar radiation is the main energy source available over the Moon surface. Furthermore, the Sun irradiation rules the lunar surface temperature variation as

modeled in chapter 8. The solar radiation monitoring over the Moon surface is a key parameter for manned and unmanned lunar surface exploration missions. For these reasons a low power consumption and low mass multispectral irradiance sensor has been conceived as part of the scientific payload proposed.

The objective of the Multispectral Irradiance sensor is to monitor the spectral solar irradiance conditions over the Moon surface. As primary energy source, the characterization over the Moon surface of the radiation received in function of the spectral range, time of the lunar day and levitating dust will be very useful in order to design the best solar panels for the maximum efficiency over the Moon surface (design of filters, coatings, peak of frequency response, etc.).

The Irradiance of the Sun at 1 Astronomical Unit ($1AU = 1,49597890 \cdot 10^{11} m$) is designated as the solar constant. Figure 6.8 presents the irradiance spectra of the Sun at 1 AU.

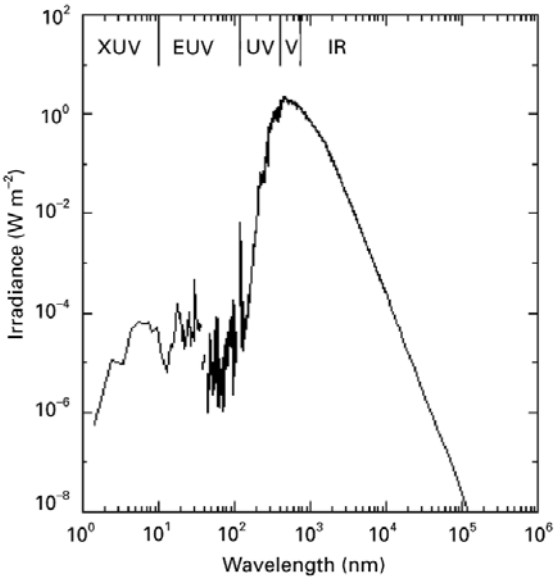

Figure 6.8: Solar Irradiance spectra for a total integrated irradiance of $1367.28 \pm 0.02\ W/m^2$ (Extracted from [Tobiska et al., 2000])

The requirements for the multispectral irradiance sensor are the following:

- Low mass and low power consumption sensor compatible with the platform conceived.
- Able to measure the irradiance in the ultraviolet, infrared and visible spectral ranges.
- Large dynamic range able to cover the maximum irradiance levels at each frequency as expected over the Moon surface.

- Omnidirectional. The node disposition w.r.t the Sun is not known. The sensor shall be able to monitor the Sun irradiance independently of the node position and the Sun angular elevation w.r.t the lunar surface.

6.4.2 Mathematical model for Moon's surface solar irradiance estimation

As commented previously, the solar irradiance rules most of the dynamic changes over the Moon's surface as the temperature or the energy available. A mathematical model that provides the solar irradiance in function of the date (year, month, day and hour) and the selenographic altitude and latitude has been developed and implemented using Matlab software. This model has been used for the following purposes in this thesis:

- To dimension and validate the design of the Multispectral Irradiance Sensor.
- As input for the lunar surface temperature model (section 6.5.2).
- As input for the Thermal Mathematical model and thermal design stablished in chapter 8.
- For the autonomous control of the platform described in chapter 10. The platform could autonomously estimate the near upcoming irradiance conditions over the lunar surface and plan in this way its activities.

If the mathematical model developed has to be useful for all the above stated objectives, then it has to comply with the following requirements:

- The processing effort shall be reduced to the minimum possible. The OBC shall compute the algorithm proposed for the tasks planning during the mission. Low power consumption is directly related with the processing effort required by the mathematical model.
- The time resolution shall be compatible with the planning requirements of the node and the thermal variation change over the lunar surface. It has been stablished a resolution of 1 hour for the mathematical model. The irradiance illumination variance during 1 hour is approximately around $9W/m^2$ (in the worst case during the Sunrise). This value represents nearly the 0.65% of the total irradiance change. Therefore 1 hour is considered an adequate time resolution for the planning and design objectives of the mathematical model. Additionally it has to be considered that a higher time resolution would imply a much higher processing effort, thus resulting in elevated power consumption during the tasks planning.

- An adequate spatial resolution has to be considered. The coordination system selected to stablish the position of the platform over the Moon surface is the selenographic coordinates of the Moon, as described in the he report of the IAU/IAG Working Group on Cartographic Coordinates and Rotational elements: 2006 ([Seidelmann et al., 2007]). The selenographic system is very similar to the one used in the Earth: latitude measures the distance north or south of an equator defined to be approximately 90°from the rotation axis, while longitude is measured east and west from an arbitrarily chosen central meridian. The origin of the coordinate system passes through the point that is most nearly, on average, pointed towards the centre of the Earth.

The main assumptions and simplifications considered for the development of this mathematical model are the following:

- The Moon is considered a perfect sphere of 1737.4 km in radius, as referenced in the report of the IAU/IAG Working Group on Cartographic Coordinates and Rotational elements: 2006 ([Seidelmann et al., 2007]).

- It has not been considered the dust absorption distortion. The dust absorption distortion is considered to be negligible for the objectives of the algorithm herein developed.

- No surface irregularities influences. Mountains and craters influence directly the solar irradiance received by the platform. This assumption will not affect the use of this mathematical model for the design objectives herein contemplated, although for the planning of the platform will involve an important factor. Geographical irregularities are not contemplated in this thesis for the mathematical modeling, future works could use the irradiance sensor data obtained during the first lunar day in order to correct the mathematical model automatically over the Moon surface to consider the shadowing effects.

- No Earth eclipses considered. The Earth eclipses could be included in the model including a third body (the Earth) in the Sun-Moon equations herein used. This would change drastically the model complexity increasing the power required for the processing. This phenomenon can be obviated considering the total eclipses would not be a frequent phenomenon (total or partial eclipses over the Moon surface in the period 2001- 2005 were 7, [Racca, 1995]). Additionally we have to consider that the platform is designed to be able to operate correctly during the approximately 4 hours that the solar irradiance is below the 60% of the solar irradiance without eclipse.

The mathematical model elaborated is based on the work of [Li et al., 2008] and adapted to the requirements of the model described above. Solar irradiance of the

lunar surface can be obtained from the total solar irradiance at moon distance and the angle of incidence over the lunar surface a:

$$I = S_0 \cdot (R_{sun-moon}(t, \lambda_A))^2 \cdot \sin(a(t, \lambda_A, \varphi_A)) \tag{6.2}$$

Where: S_0 is the constant solar irradiance for 1 AU with a value of 1367.28 W/m^2.λ_A and φ_A are the selenographic coordinates (longitude and latitude) of the point where the platform is situated. $R_{Sun-moon}(t, \lambda_A, \varphi_A)$ is the dimensionless Sun-Moon distance relative to 1AU, that varies in function of the selenographic latitude and longitude and in function of time. Finally $a(t, \lambda_A, \varphi_A)$ is the solar incidence angle as depicted in figure 6.9 and varies in function of the time and the selenographic coordinates. The solar incidence angle has been selected in this work as an angle increasing with the Sun elevation from 0 to 90° unlike the common convection used in the literature where the angle of incidence is selected as a decreasing angle with the Sun elevation from 90° to 0°. The convention followed in this thesis is a better approximation for a later use of this angle value in the thermal mathematical model developed.

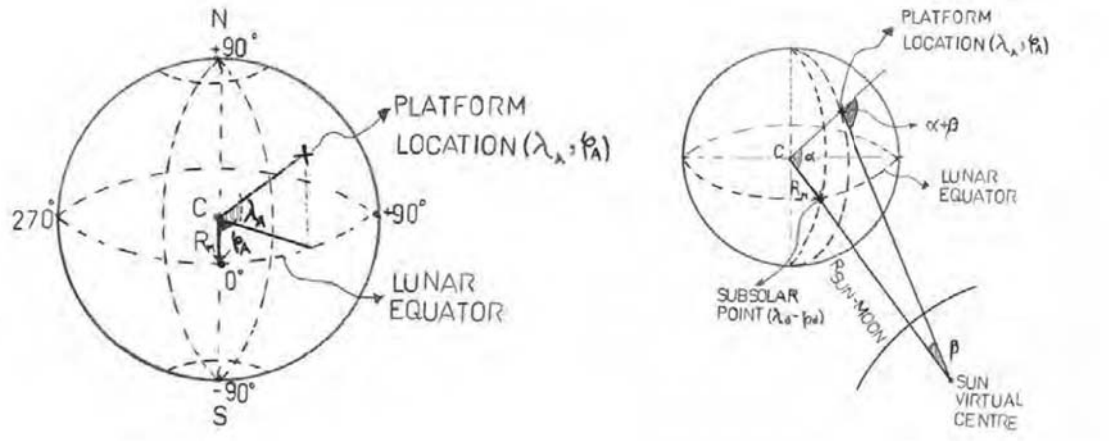

Figure 6.9: Geometrical parameters used in the mathematical model developed

As described in the figure 6.9 the angle a can be calculated as:

$$a = \frac{\pi}{2} - (\alpha + \beta) \tag{6.3}$$

Where:

$$\alpha = \arccos(\sin\varphi_A \cdot \varphi_d) - \cos\varphi_A \cdot \cos\varphi_d \cdot \cos(\lambda_A - \lambda_d) \tag{6.4}$$

$$\beta = \arcsin\left(\frac{R_{Moon}\cdot \sin\alpha}{\sqrt{(R^2_{sun-Moon} + R^2_{Moon}\cdot R_{Sun-Moon}\cdot R_{Moon}\cdot \cos\alpha)}}\right) \tag{6.5}$$

Where λ_d and φ_d are the selenographic latitude and longitude of the subsolar point and varies in function of the time. The subsolar point coordinates and the Sun-Moon distance are function of time and follow the astronomical relations between the solar system bodies. These parameters can be calculated precisely using the NASA's almanac (DE430 released in 2013). Although, the use of this almanac implies the use of hundreds of periodic terms and a data base that are not compatible with a limited data storage and low power consumption processing of the platform proposed over the Moon surface. For this reason, the subsolar point coordinates and the Sun-Moon distance are calculated using the equations proposed by [Meeus, 1991]. Meeus used the most important periodic terms obtaining an accuracy of approximately 10″in the selenographic longitude of the Moon and 4″in the latitude. This approximation is completely adequate for our purposes and simplifies drastically the processing requirements of the OBC. The 56 equations that relates the Sun position with the Moon position and the latter with the position of the platform in the Moon surface are not herein presented for simplicity, although the procedure for obtain these equations can be found in chapter 45 of [Meeus, 1991]. For simplicity the model developed accepts the date information in the following format: yyyy,mm,dd,hh where yyyy are the year, mm the month, dd the day and hh the hour from 1 to 24. The astronomical calculations used in the algorithm follow the Gregorian calendar, consequently it is necessary to include in the model the appropriate translation algorithm.

With the objective of verifying the results obtained by the algorithm developed, results published in the literature have been used as reference. The results obtained from the mathematical model match closely the results obtained by other researches, as shown in figures 6.10 and 6.11.

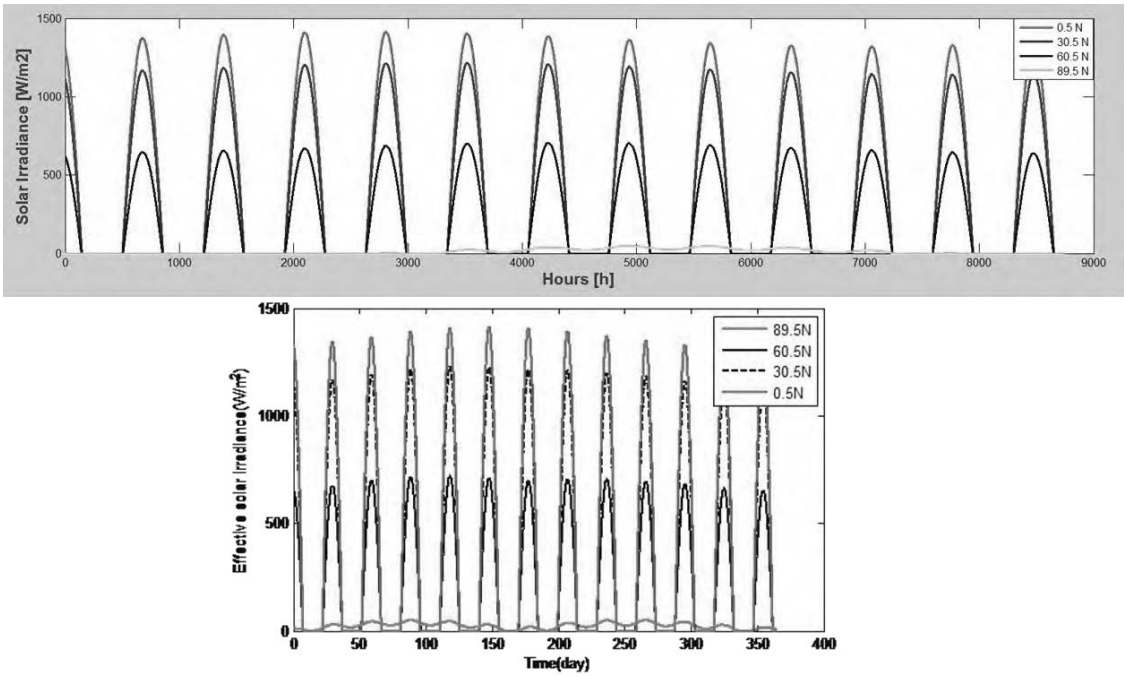

Figure 6.10: Irradiance values for year 1971 at different latitudes. Results obtained using the model developed (top). Results extracted from [Li et al.,] for different latitudes (bottom)

The selected selenographic longitude for the results presented in figure 6.10 is 60°E. As it can be seen, except for the polar region, the results obtained matched below the %5 error with respect to the results presented in [Li et al.,].

A specific analysis of the polar region is shown in figure 6.11. As it can be seen, the results obtained match very precisely the results presented in [Badescu, 2012].

6.4.3 Proposed Multispectral Irradiance Sensor design

Three identical irradiance sensors (able to measure the incident irradiance at UV, IR and VIS) are placed at each face of the tetrahedron. This configuration allows to obtain the irradiance independently of the orientation in which the platform has been positioned over the moon surface (figure 6.12). Each group of three photodiodes will be mounted with a separation of 120° for a total field of view of 360° as depicted in figure 6.12.

The irradiance sensor will be able to measure the incident irradiance at three different spectral intervals, one at IR, a second one at UV and a third one at the

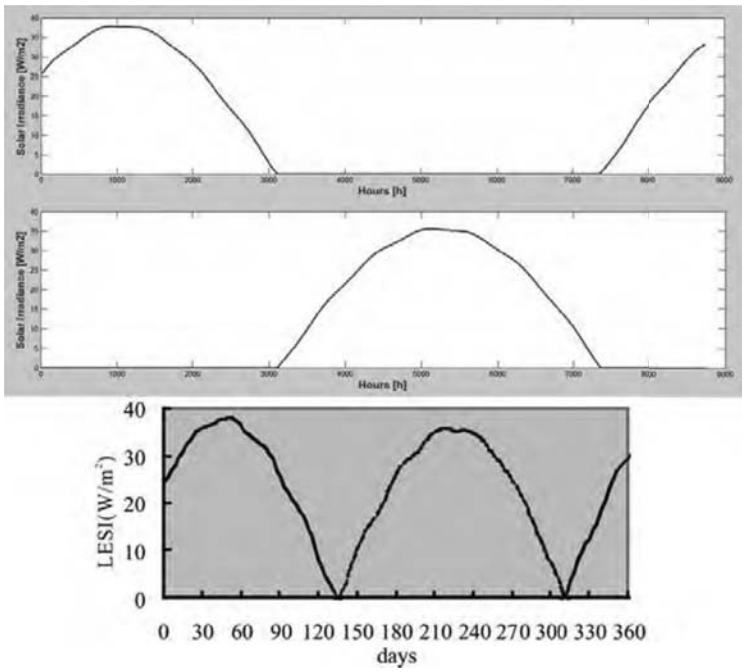

Figure 6.11: Solar Irradiance at 90° latitude (top) and −90° latitude (center) obtained with the model developed for year 1994. Solar irradiance results for year 1994 extracted from [Badescu, 2012], chapter 15. North Pole (solid line, bottom figure) and South Pole (dotted line, bottom figure)

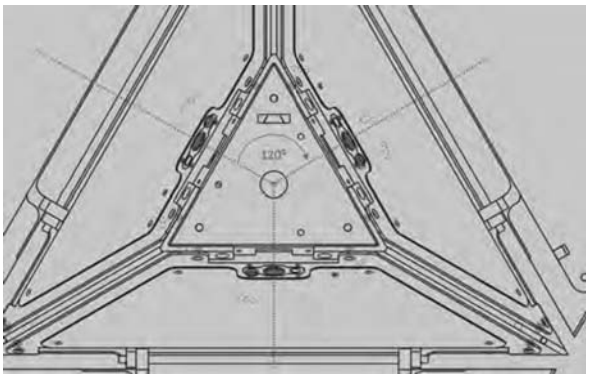

Figure 6.12: Disposition of the irradiance sensors on the platform structure (top view).

visible range. The photodiodes selected and their respective spectral responses are presented in figure 6.13:

The frontend electronics designed is shown in figure 6.14. The photodiodes operates in a photovoltaic mode with a 0V bias. The low offset operational amplifier

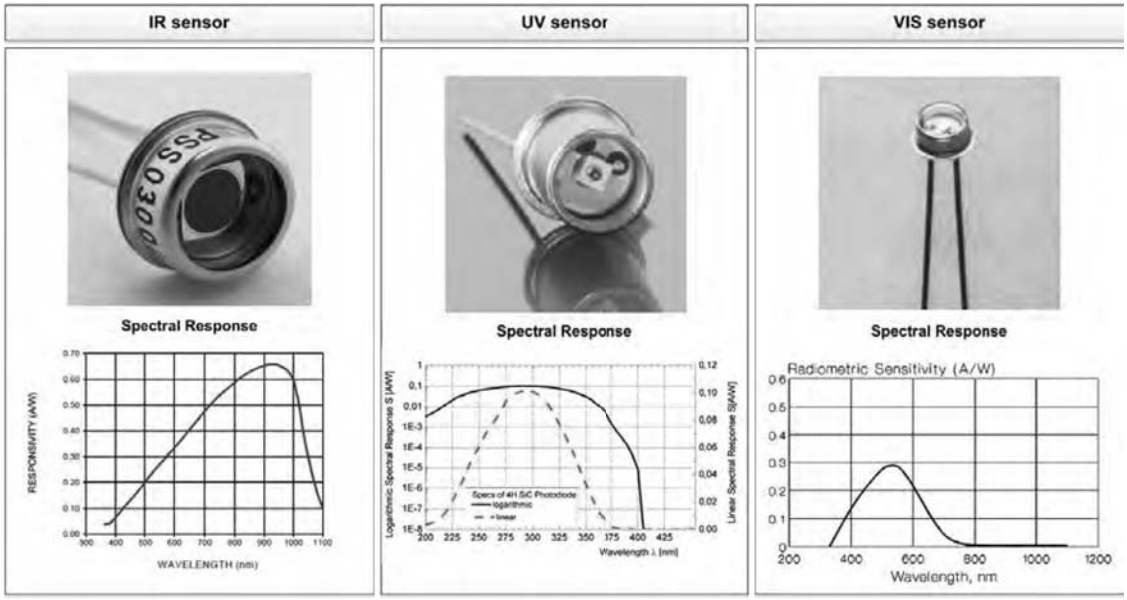

Figure 6.13: Photodiodes selected for the multispectral irradiance sensor ([Pacific-Silicon-Sensor, 2010], and [GmbH, 2013] [Optoelectronics, 2015])

used transforms the current generated by the photodiodes into a voltage level. This configuration provides an input resistance of Rf/A where A is the open-loop gain of the op amp. Even though Rf is generally very large, the resulting input resistance remains negligible in comparison to the output resistance of the photodiodes. The Operational Amplifiers selected (AD8628 for SWIPE prototype and LMP2012QML space equivalent component) are dual low offset and low input bias current operational amplifiers, specifically suitable for this application. This configuration allows to obtain the required resolution while maintaing a very low power consumption with very few components (low mass and low power consumption objectives).

The cable connection between the photodiodes modules and the P/L acquisition board will be susceptible to induced electromagnetic noise. For this reason the length of these cables is reduced locating the acquisition electronics near the irradiance sensors. The cables are twisted and additionally a first order passive low pass frequency filter is used before the ADC in order to reduce any high frequency noise induced in the circuit (e.g. clock of the FPGA).

The photodiodes are soldered to a PCB that will be fixed to the surface of the wall of the tetrahedron with 4 M3 screws. Each sensor has a total envelope dimension of 15x25x9 mm.

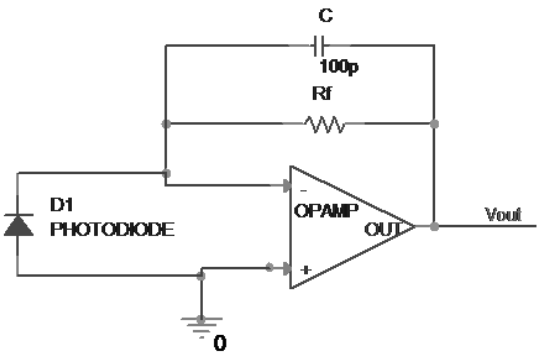

Figure 6.14: Front end electronics (Photovoltaic mode).

The total mass of each group of three photodiodes, the mechanical structure and fixing screws is 8.5 grams.

6.5 Surface temperature sensor

6.5.1 Introduction and requirements definition

Another important parameter is the lunar surface temperature variation during the synodic period. The Moon has a very large surface temperature variation with temperatures during the lunar night that can be as low as 100 K at mid latitudes. During the day the temperatures can increase up to 390 K at mid latitudes. As a consequence the temperature variation is near 300 K. This large surface temperature variation entails a challenging problem for future robotic or manned missions.

In order to obtain a complete characterization of the temperature variation during the lunar day and night cycle, the surface temperature sensors shall be designed in order to obtain the following performance.

- Resolution:$\pm 0.5°C$
- Accuracy:$\pm 1°C$
- Range:$-180°C$ to $130°C$

6.5.2 Mathematical model for lunar Surface temperature estimation

A mathematical model, able to predict the lunar surface temperature in function of the date (year, month, day and hour) and the selenographic longitude and latitude, has been developed and implemented using Matlab software. This mathematical model is aimed to fulfil the following objectives:

- To dimension and to validate the design of the surface temperature sensor.
- As input for the Thermal Mathematical model and thermal design stablished in chapter 8.
- For the autonomous control of the platform described in chapter 10.

If the mathematical model developed has to be useful for all the objectives above stated, then it has to comply with the following requirements:

- Reduce as much as possible the processing effort to be used in the OBC in order to reduce the power consumption during the mission.
- Select a time resolution compatible with the planning requirements of the node and the thermal variation change over the lunar surface.

Numerous works can be found in the literature related with the estimation of the lunar surface temperature ([Bauch et al., 2009], [Li et al.,], [Hayne, 2011], [Ran and Wang, 2014], [Bastin, 1973], [Christie et al., 2008], [Racca, 1995] or [Vasavada et al., 1999]). These works are funded in slightly different physical models, where different parameters and numerical methods are used. Departing from these works, herein a mathematical model based in a thermal equilibrium analysis over the Moon surface is presented. The following assumptions have been considered for the development of the mathematical model:

- The thermal equilibrium is based on the Irradiance Mathematical Model developed under this thesis and presented in section 6.4.2.
- The equilibrium temperature is considered to be reached at 0.2m of depth and its value is 250K based on ([Langseth et al., 1976]) as described in section 9.1.
- Differences in thermal conduction, density and heat capacity between the non-compacted regolith, compacted-regolith and rocks cause large temperature variations. In this analysis it is supposed that upper lunar regolith is composed of a non-compacted dust with low thermal inertia. The results obtained for other scenarios are quite different (for example if basalt rock is considered), although the model can be easily adapted to the scenario under study just varying the corresponding parameters of the model.

Figure 6.15 presents a sketch of the thermal balance considered at the moon surface:

As it can be seen in figure 6.15 the thermal balance can be expressed as:

$$\varphi \cdot C_p \frac{\partial T}{\partial t} = \dot{Q}_{rad,in} - \dot{Q}_{rad,out} + \dot{Q}_{planet} \tag{6.6}$$

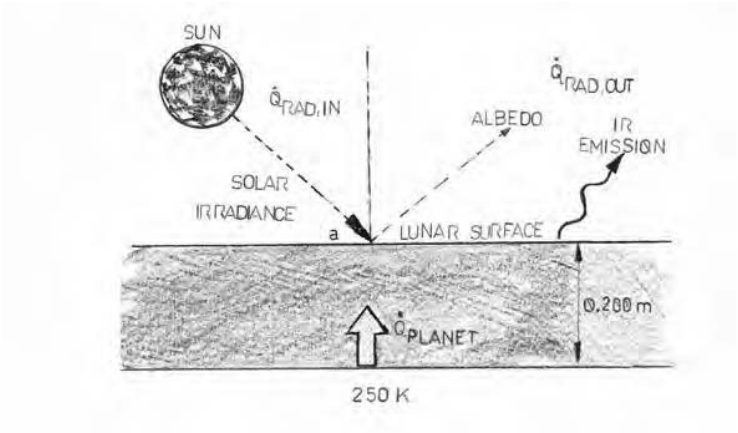

Figure 6.15: Thermal balance sketch

Where $\dot{Q}_{rad,out}$ is the total heat loss due to the IR radiation from the lunar surface, $\dot{Q}_{rad,in}$ is the heat flux absorbed from the solar irradiation and $\dot{Q}_{planet}$ is the geothermal heat flux to the surface. In this thermal analysis, the Moon is considered as a two layer structure: an inner layer at 0.2m with an equilibrium temperature of 250K and an external layer (the surface) where the temperature is variant in function of the solar irradiance. The heat diffusion equation between the upper and bottom layer can be expressed as following:

$$\varphi \cdot C_p \frac{\partial T}{\partial t} = \frac{\partial}{\partial z}\left[k \frac{\partial T}{\partial z}\right] \tag{6.7}$$

Where the right term is known as the spatial gradient of the heat flux. From here, initial thermal balance equation is evolved obtaining the thermal equation that will rule the mathematical model developed:

$$\varphi \cdot C_p \frac{\partial T}{\partial t} - \frac{\partial}{\partial z}\left[k \frac{\partial T}{\partial z}\right] = -\epsilon \cdot \sigma \cdot (T_{z=0}^4 - T_{space}^4) + (1-r) \cdot I(t, \lambda_A, \varphi_A) \tag{6.8}$$

This differential equation is solved numerically discretizing in time (1 hour time step) and in depth (from 0.2m to 0m). It is important to note that the equation is independent of the surface area considered. A brief description of each term is presented below:

ϵ is the IR emissivity of the lunar surface (a mean value of 0.97 is used, [Racca, 1995]) and $\sigma = 5.669 \cdot 10^{-8}$ $[W/(m^2 \cdot K^4)]$ is the Stefan-Botzmann constant. The temperature of the space (Tspace) is considered 2,7K. r is the reflectivity and, as previously commented, I(t,λ_A,φ_A) is the solar irradiance in function of the time and

the selenographic coordinates. I can be obtained using the Irradiance Mathematical Model developed under this thesis and presented in section 6.4.3.

The thermal conductivity k is dependent of the temperature and the inter-grain distance. Compact regolith has a better thermal conductivity due to its low inter-grain distance. The non-compacted first 20cm of the lunar regolith is a really good thermal insulator because is composed of fluff dust. The conductivity increases in function of the depth as the dust is more compacted. The following equation is used for the thermal conductivity ([Hayne, 2011] or [Li et al.,]):

$$k(T) = K_c \cdot \left(1 + \chi \cdot \left(\frac{T_{(n)}}{350}\right)^3\right) \tag{6.9}$$

K_c and χ are parameters in function of the depth. Herein the most restrictive values corresponding to the non-compacted top layer of the regolith are used: $K_c = 9.22 \cdot 10^{-4}$,$\chi = 9.228$ (Li 2010). The thermal inertia is the thermophysical parameter that represents the ability of the surface to adapt to temperature changes:

$$I = (k(T) \cdot \rho \cdot c)^{1/2} \tag{6.10}$$

The thermal inertia can be obtained from the bulk density ρ, conductivity k and heat capacity c of the material. The mean surface density is considered with a value of 1300 kg/m^3 ([Racca, 1995]). As previously commented herein it is supposed a non-compacted layer of regolith, thus the selected value for thermal inertia is 40 $J \cdot m^{-2} \cdot K^{-1} \cdot s^{-1/2}$ ([Bastin, 1973], [Christie et al., 2008] and [Hayne, 2011]). Using the inertia relation, the bulk density and the conductivity relation we can obtain the heat capacity of the terrain considered. For the values considered the heat capacity used herein is c=784.15 $J/Kg \cdot K$ what is very similar to the used by other researchers (e.g. [Racca, 1995]).

We have to consider that in this analysis we have used mean values for the density and the heat capacity. Actually, both parameters vary in function of the depth and the temperature. Some researchers, as [Li et al.,] or [Hayne, 2011] take into consideration this phenomenon. The variation can be neglectable for the objectives of the model and in this way the computational effort of the OBC is optimized.

Finally the left term represents the geothermal heat flux and it can be approximated at the lunar surface (z=0) as:

$$\frac{\partial}{\partial z}\left(k\frac{\partial T}{\partial z}\right)\bigg|_{z=0} \simeq \left(\frac{T_{(0,2)} - T_{(0)}}{l}\right) \cdot k(T) \tag{6.11}$$

The mathematical model is numerically solved using Matlab. The detail comparison of the data obtained with the data published is complex, while the surface temperature depends on the date, the selenographic coordinates and parameters of the regolith

considered. Although, below we can verify the good matching between the data obtained using the algorithm herein developed and the data published by different researches.

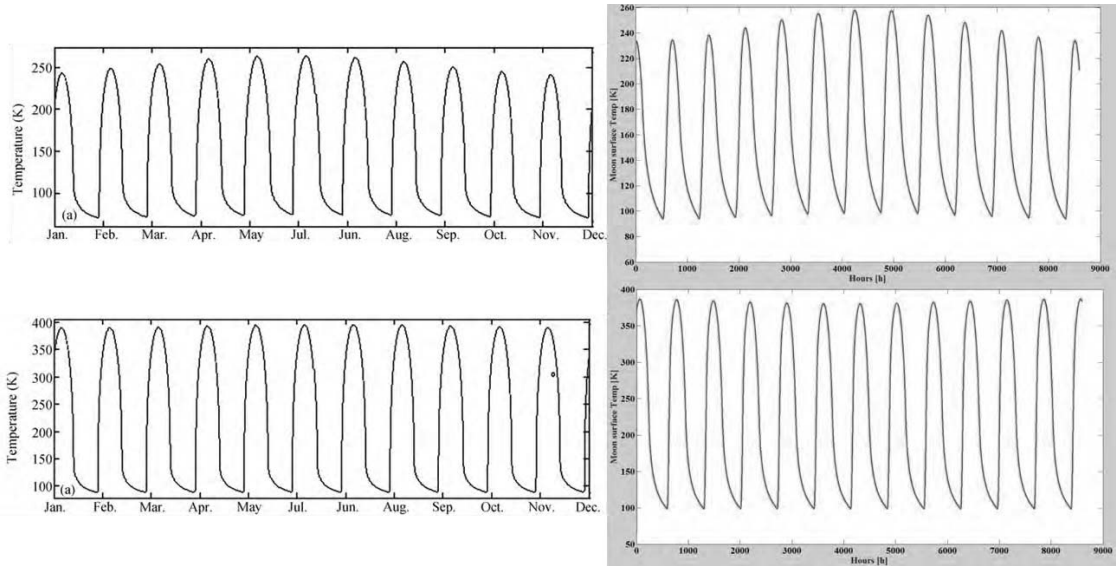

Figure 6.16: Lunar surface temperature at equator (bottom left) and 80°N (top left) in one year extracted from [Li et al.,] compared with results obtained for year 2015 with the model developed at the equator (bottom right) and at 80°N (top right).

As it can be clearly appreciated in figure 6.17, the heat capacity used in both models are different and therefore the day/night transition temperature is more abrupt in the data obtained from Paige and Vasavada than the one obtained in the model developed (smother). This can be easily corrected modifying the expected heat capacity of the expected landing once known the target objective.

6.5.3 Proposed lunar surface temperature sensor

Three temperature sensors are included in the payload. These sensors measure the temperature by conducting means. The temperature sensor is attached to a high thermal conductivity and low thermal inertia material (aluminum) that will be used as a probe to measure the upper surface temperature of the Moon (figure 6.18).

During the penetration phase of the deployment (refer to chapter 7) the sharpen probes will be introduced with force in the lunar soil. Some deformation of the probes is expected during the platform deployment. These probes are thermally isolated

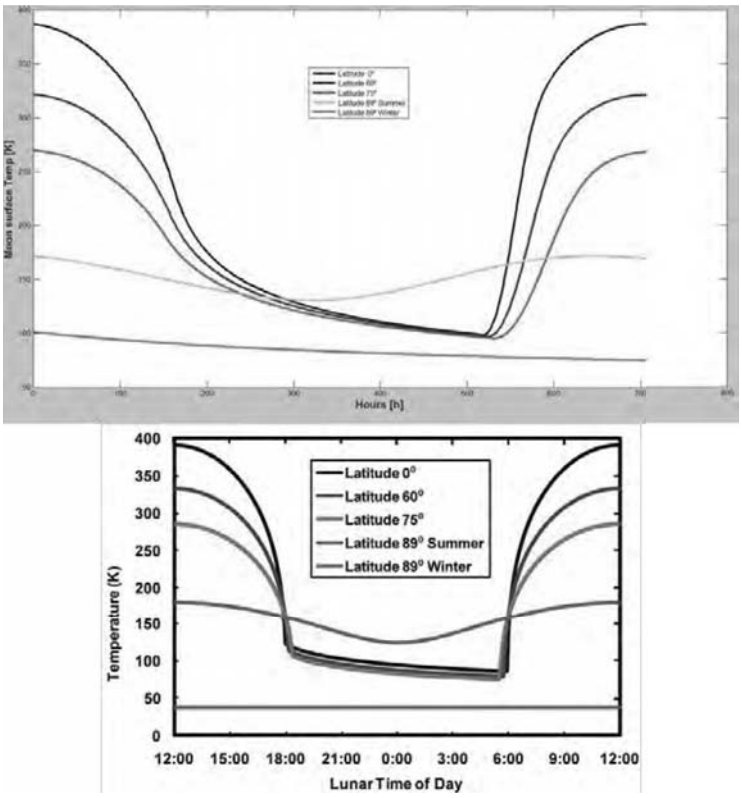

Figure 6.17: Model calculations of lunar surface temperature variations as a function of local time and latitude extracted from [Paige et al., 2010] after [Vasavada et al., 1999]. Local time is expressed in lunar hours which correspond to 1/24 of a lunar month. At 89° latitude, diurnal temperature variations are shown at summer and winter solstices (bottom). Results obtained using the model herein developed (top).

from the rest of the structure. In the base of the probes a thermistor measures the temperature of the lunar soil.

The temperature probes are located at the base of the tetrahedral platform (near to the corners).

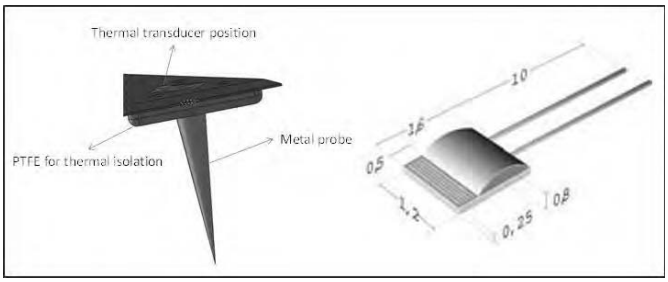

Figure 6.18: Temperature probes for lunar surface temperature monitoring (left) and selected thermistor P1K0.232.6w.A.010 ([IST, 2014]) (right)

The reduced size and the limited number of the components make the mass of each sensor as low as 3 grams. The three sensors have a total mass of 9 grams (excluding front end electronics and harnessing).

The selected thermistor P1K0.232.6w.A.010 ([IST, 2014]) is a very low size and mass Positive Temperature Coefficient (PTC) with a high temperature range (-200 to +600°C). With the objective to comply with the performance requirements stablished in 6.5.1 the following front end electronics has been design.

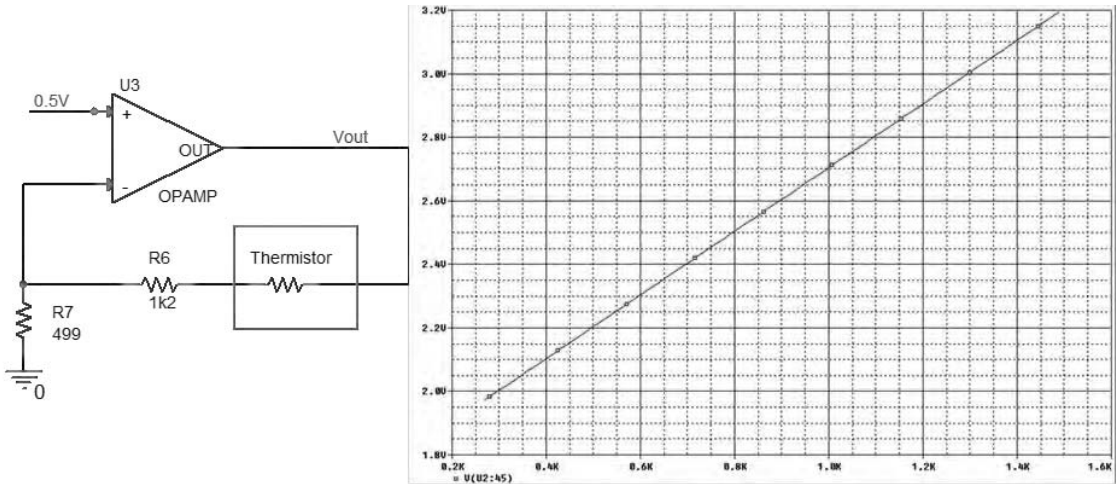

Figure 6.19: Temperature sensors front end electronics and Voltage output range in function of the PTC resistance values

This configuration has the advantage of obtaining a high linear dynamic range with very few components (low mass). The power consumption is maintained low

by switching off the 0.5V voltage reference when temperature measurement is not required. Also the self-heating of the thermistor has to be considered. For this reason the 1k2 resistors in series with the thermistor will limit the current through the thermistor to low values in order to minimize the self-heating problem. The associated theoretical transfer function is:

$$V_0[V] = 0.5 + \frac{0.5 \cdot (R_T + 1200)}{499} \tag{6.12}$$

Where R_T can be obtained from the following theoretical relations ([IST, 2014]):
From -200 to 0°C:

$$R_T(T) = R_0 \cdot (1 + A \cdot T + B \cdot T^2 + C \cdot (T - 100) \cdot T^3) \tag{6.13}$$

From 0 to 850°C:

$$R_T(T) = R_0 \cdot (1 + A \cdot T + B \cdot T^2) \tag{6.14}$$

Where: $A = 3.9083 \cdot 10^{-3}[^\circ C^{-1}]$; B $= -5.775 \cdot 10^{-7}[^\circ C^{-2}]$; C $= -4.183 \cdot 10^{-12}[^\circ C^{-4}]$

6.5.4 Scientific payload acquisition electronics

A low mass and power consumption acquisition electronics, located in the inner thermal bay of the platform, is aimed to gather the different analog signals from the different transducers and digitize them. Additionally the acquisition electronics defined is able to receive, interpret and execute the different commands from the OBC of the platform. The data obtained shall be transmitted to the OBC for further processing and transmission.

The requirements of the acquisition electronics are quite demanding:

- Low mass (below 40 grams) and low power consumption (main requirement to achieve the objectives of this thesis).
- The electronics for space application must cope with the extremely hard space environment (in section 1.4 these environmental constrains are defined). For this reason conventional electronics cannot be used. Space qualified electronics shall be considered. A common practice for the development of preliminary prototypes in the space industry is herein applied: equivalent commercial components to those of high reliability have been considered in the electronic design. In this way, it is possible to manufacture an equivalent of the final electronics and evaluate its performance. Afterwards it will be possible to introduce the high-reliability components and manufacture a Qualification Model that will be used for qualification test of the electronics, once the performance of the electronic design has been verified. Although

this approach introduces an important limitation to the design because the high reliability electronics components for space application is a very limited market where there are available a reduced number of components. Additionally the performance of those components is far from the obtained using common commercial grade electronics components.

- Reduction of the number of components used. Reducing the number of components it is possible to reduce the number of possible points of failure increasing the reliability of the complete electronics system and also it is possible to reduce the total mass.

- The electronics design has to implement high reliability design techniques (worst case design considerations, components derating following ESA standards ([ECSS, 2011]), Single Point of Failure (SPOF) analysis,etc.). The failure of the acquisition electronics would avoid the node to obtain scientific measurements, therefore the reliability of the system shall be enhanced.

Following, design solutions adopted to cope with the above defined requirements are presented.

Physically, the acquisition electronics is located in the inner bay of the tetrahedron. In this position the connection of the different sensors to this acquisition electronics is eased. Moreover, in the inner electronics bay the electronics components are protected from the light and dust and also thermally regulated thanks to the thermal switch integrated in the base of the node (refer to chapter 8 for thermal regulation solutions). Due to the reduced space of the inner bay the acquisition electronics was divided in two different PCBs. Both PCBs are connected using flex PCB technology in order to avoid connectors (mass, volume and noise reduction).

The acquisition electronics is able to monitor the temperature of the different subsystems within the platform: auxiliary batteries, node metal structure, communication module, power module, dust deposition sensor and the acquisition electronics itself. Temperature housekeeping data will be of main importance for the control unit to determinate the best planning (refer to chapter 10). Figure 6.20 depicts the main blocks involved in the acquisition electronics design:

- An ADC with an integrated 8 channel multiplexor has been selected. Three different ADC will be used as depicted in the figure. Just one of them will be enabled at a time in order to save power. The ADC selected (ADC128S102) has a direct space equivalent (ADC128S102QML-SP) with a large heritage in space applications. This device (16-TSSOP or 16-SOIC) uses a serial communication and permits to have a variable power management. Both characteristics will reduce volume and power of the acquisition electronics.

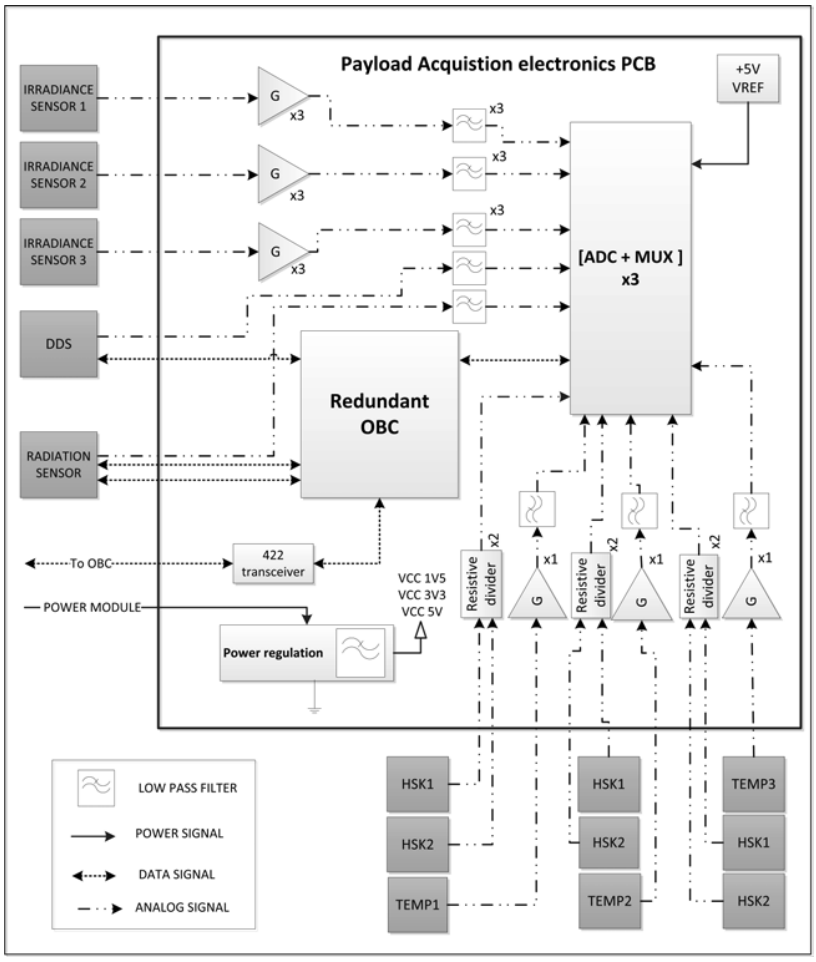

Figure 6.20: Low power/low mass acquisition electronics block diagram

- A high resolution Vref (+5V) properly decoupled is used for all the ADCs in order to provide a precise voltage reference. The space qualified part number selected is the REF02S.

- Low offset and low frequency precision operational amplifiers are used to adjust the dynamic range of the analog signals from the sensors to the ADC input voltage dynamic range (0 to +5V). Therefore, the operational amplifiers selected shall permit a rail to rail single supply operation. The commercial model used for the electronics prototype is the AD8628 dual operational amplifier. The qualified space part number with similar characteristics selected is the LMP2012QML.

- Low pass passive filters are used to reduce the spurious noise coupled to the signal (e.g. FPGA's clock signal).

- With the objective to increase the PSRR of the ADCs, voltage references and operational amplifiers, it is used a low pass filter composed of an inductance and a capacitor in all the supplies of these components. Additionally, digital components are decoupled using 100 nF capacitors.

- The redundant OBC will be used as control unit. A FPGA with space compatible solution has been used as main component of this redundant OBC as described in section 5.5. The FPGA voltage required will be 3v3 (obtained from the power module) and 1V5 obtained using a voltage regulator integrated in the acquisition electronics PCB. The part number of the commercial component used is LT1764-1.5 with space qualified equivalent LM117QML. The FPGA, as control unit of the acquisition electronics, is able to work in two different modes:

  - Nominal mode. The FPGA is in an ultra-low power consumption state waiting for a command from the OBC to wake up and perform a measurement following the commands stablished in table 6.1. Additionally, every 20 minutes the acquisition electronics will wake-up during some milliseconds to submit a pulling message to the main OBC. If during three consecutive attempts, in redundant and nominal communication lines, the FPGA is unable to obtain an answer from the OBC, the acquisition electronics will enter in the redundant mode.
  - Redundant mode. In case of an OBC failure the acquisition FPGA will enter in a continuous operation mode working as OBC, substituting the main OBC failed as described in section 5.5. Every 20 minutes the attempt to communicate with the OBC in the penetrator body will be repeated to try to restore the nominal operation.

The acquisition electronics is defined in such a way that just a scientific measurement can be obtain at the same time. In this way the sensors that are not used are not powered, reducing the power consumption of the electronics significantly.

In a nominal operation mode, the acquisition FPGA works following a pre-defined protocol. This protocol is command-oriented. The OBC commands the payload to accomplish a specific task and the payload's FPGA perform all the required actions to complete the operation commanded. This protocol uses an EIA-422 standard physical layer using space qualified transceivers (HS-26CT31RH and HS-26CT32RH). The link type is half duplex no flow control link using 8 data bits, parity bit and a date rate of 115.200 bits per second. There are 2 types of packets: command and data. There are no handshaking packets except for an acknowledge package.

A list of commands has been defined and presented in the table below. With this set of commands it is possible to operate the acquisition electronics completely from single measurement of individual sensors to a complete or partial measurement procedures. Also commands for monitoring the status of the acquisition electronics have been defined.

Command mnemonic	CMD_ID	Explanation	Data (bits)
CMD_TEST	0x01	Sent by the OBC to the P/L to ask the latter to perform a self-test routine.	12
CMD_TEMP	0x02	Sent by the OBC to the P/L to perform temperature measurement. Measurement of the three thermal sensors.	36
CMD_IRRADIANCE	0x03	Sent by the OBC to the P/L to perform Irradiance measurement. Measurement of the three irradiance sensors.	108
CMD_DDS_MEASURE	0x04	Sent by the OBC to the P/L to perform Dust Deposition Measurement.	12
CMD_DDS_CAL	0x05	Sent by the OBC to the P/L to perform DDS calibration.	12
CMD_TID	0x07	Sent by the OBC to the P/L to perform TID measurement.	12
CMD_SEU	0x08	Sent by the OBC to the P/L to perform SEU measurement.	28
CMD_FULL_PL	0x09	Sent by the OBC to the P/L to perform a complete payload measurement (including temperature, SEU,TID, DDS and irradiance).	208
CMD_HOUSEKEEPING	0x0A	Sent by the OBC to the P/L to perform the measurement of the 8 housekeeping temperature sensors.	96
CMD_STATUS	0x0B	Sent by the OBC to the P/L's FPGA to ask for the measurement status.	32
CMD_GETDATA	0x0C	Sent by the OBC to the P/L to ask for the memory dump of the P/L's internal memory, if the STATUS register indicates that there is data available.	Depends on the operation mode
CMD_RAD	0x0D	Sent by the OBC to the P/L to perform a SEU and TID measurement.	40
CMD_IRRADIANCE_1	0x0E	Sent by the OBC to the P/L to perform Irradiance measurement of the irradiance sensor 1 (face 1).	36
CMD_IRRADIANCE_2	0x0F	Sent by the OBC to the P/L to perform Irradiance measurement of the irradiance sensor 1 (face 2).	36
CMD_IRRADIANCE_3	0x10	Sent by the OBC to the P/L to perform Irradiance measurement of the irradiance sensor 3 (face 3)	36

Table 6.1: List of commands for the acquisition electronics

Chapter 7

Solutions for the deployment of a large number of robotic platforms over the planet surface

In planetary surface exploration missions, the most risky and critical phase of the mission is the landing of the robotic systems over the planet surface. During this phase the robotic systems are subjected to high g-forces and extreme environmental conditions that could potentially destroy the exploration platform in seconds. Additionally we have to consider that usually some conditions during the landing, as the surface conditions or environmental conditions, are usually barely identified or just unknown, what introduce an important risky factor to this mission phase. Several exploration missions failed during the landing phase, including missions with similar characteristics of the one herein proposed (e.g. Deep Space 2 mission).

The mission concept proposed is the deployment, over the planet surface, of a large number of small autonomous robotic platforms with the objective of generate a WSN for atmospheric conditions monitoring. Therefore there is need to conceive a realistic (and cost effective) way to deploy a large number (tents) of WSN nodes over the planet surface. In this chapter a brief review of different deployment methodologies is presented, afterwards an innovative solution for the deployment of the platform is described and analysed.

7.1 Trade-off of platform deployment methods

Essentially we can difference two type of landing systems in function of the g-forces applied to the robotic subsystems during the landing:

- Soft-landing. In soft landing missions the robotic platform includes auxiliary subsystems to reduce drastically the entry velocity from the orbit to the planet surface. These auxiliary systems could also include positioning or even image processing for landing area selection (e.g. European Lunar Lander). Even though this approximation reduces drastically the g-forces at which the robotic systems are subjected, and therefore reducing the risks of the landing operation. However, this approach also requires an important extra mass and power budgets. Most of the planetary surface exploration missions, launched or projected to be lunched in the near future, use this approximation (e.g. NASA's rovers for Mars exploration).

- Hard-landing. This type of landing approach is based on designing the platform for surface exploration robust enough to support elevated g-forces. Two subgroups can be stablished: semi-hard landing approach where an important partial reduction of the impact velocity of the lander is provided; or hard-landing where the platform shall support extremely high g-forces and there is not velocity reduction or this is minimum.

Different approaches have been considered for the deployment of the tetrahedral platform. [Crosnier et al., 2013b], presents a very detailed and complete analysis of the deployment strategies for SWIPE project. It is important to remember (section 3.1.1), that the SWIPE platform does not include the penetrator body herein described and that the auxiliary subsystems conceived in this thesis and afterwards described were not considered in SWIPE project. Briefly, the deployment strategies analysed in [Crosnier et al., 2013b] are the following:

- *Option 1.* Use of penetrators dropped from an orbiter spacecraft (hard-landing). Up to 36 nodes per spacecraft (this estimation was directly based on MoonLITE mission considering a total mass of 36 Kgs per node including the penetrator).

- *Option 2.* Each platform is precisely dropt by a rover. This implies a soft landing of the rover that would carry the nodes (soft-landing). 10-20 nodes of 2 Kgs per rover deployed over the planet surface.

- *Option 3.* Each platform is thrown by a rover. The rover, instead of depositing precisely the nodes, would drop them by some dropping mechanism (semi-hard landing). 10-20 nodes of 2 Kgs per lander.

- *Option 4.* Each platform is thrown by a lander. A traditional landing approach of a big lander would be used to, once the lander is over the planet surface, deploy the nodes using some dropping mechanism (semi-hard landing).

- *Option 5.* Each platform is thrown thanks to a quasi-lander. During the descent phase of the lander, this would drop the nodes (semi-hard landing).

- *Option 6.* Each platform is equipped with its own lander (soft-landing). 2 nodes maximum.

Options 2 to option 6 are in direct conflict with the motivation of this thesis: even feasible they would imply a high cost and they would not provide reliability increase (if the landing of the platform or the rover fails the whole mission fails). [Crosnier et al., 2013b] concludes that for SWIPE mission the option 2 is the more optimum solution while it provides an accurate deployment of 10 to 20 nodes. In this same study, option 1 was discarded because the following reasons:

- It is not possible to easily ensure an accurate positioning of the nodes.

- The nodes could be buried during the shock with the planet surface.

- Complex shock requirements would require complex platforms.

In the following subsection an innovative approach using penetrator technology for the deployment of a large number of the tetrahedral platforms is described. The solutions proposed solve the problems detected in [Crosnier et al., 2013b], and additionally permits to use the deployment energy to harvest the thermal energy present at the subsurface of most of the planets as afterwards described in chapter 9.

7.2 Platform deployment: solution conceived

7.2.1 General overview

Figure 7.1 presents a rough schematic cross section of the Moon surface extracted from [Heiken et al., 1991]: "The depth scale in the figure is highly uncertain, because the total number of large craters and basins remains unknown. Highly variable depth effects must exist in different regions, depending on the degree to which an area has been affected by basin-sized impacts."

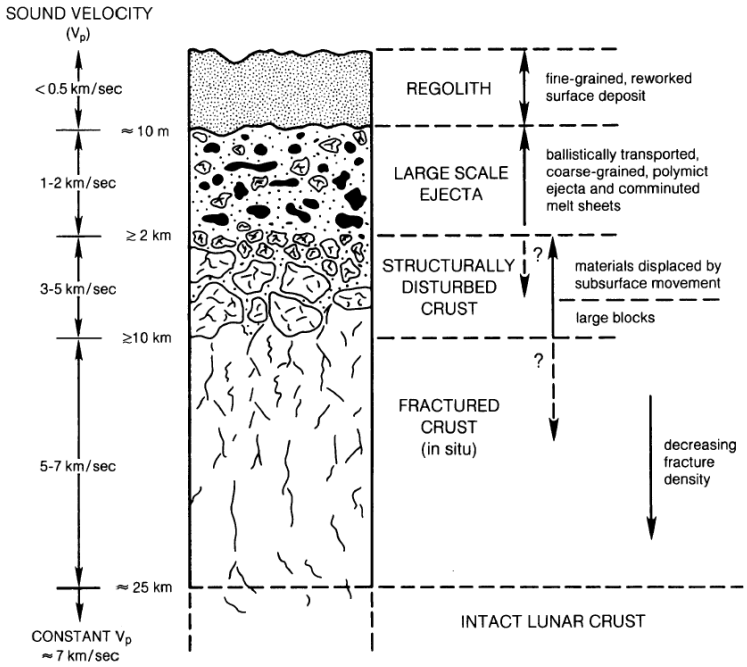

Figure 7.1: Highly schematic cross-section illustrating the idealized effects of large-scale cratering on the structure of the upper lunar crust. (Extracted from [Heiken et al., 1991]

The upper 10 m part of the surface is of interest for the proposed deployment approach. It is composed of fine-grained material that nearly everywhere forms the surface of land and overlies or covers the bedrock ([Heiken et al., 1991]). A bullet shaped penetrator could use the impact with the surface to enter into the regolith subsurface of the planet. In the case of the Moon the depth of the regolith varies drastically depending in the region from 10 to 20 meters in average to just a few meters on the maria regions. This has been experimentally verified in the Apollo missions ([McKay et al., 1974]). Therefore the depth reached by the penetrator could vary from one region to the other, depending in the regolith characteristics.

The state of the art presents a complete analysis, design and tests results of various types of penetrators: [Gowen et al., 2011], [Gowen et al., 2007], [Doengi et al., 1998], 2008 [Gao et al., 2008], 2007 [Gao et al., 2007], [Skulinova et al., 2011], [Lorenz et al., 2000] or [Surkov et al., 1999] between others. It is not the aim of this thesis propose a new penetrator design, considering that an adaptation in size and mass of one of the designs proposed in the literature would solve the problem. Nevertheless, this thesis proposes innovative solutions for the subsystems integrated in the penetrator itself and in the surface platform to survive to the penetration shock.

The general deployment strategy proposed can be summarized in the following steps:

1. An orbiter satellite, carrying several nodes, would release the platforms as commanded from Earth in function of the surface objectives and the WSN pattern configured. This satellite will be used afterwards as communication link between the WSN and the Earth.

2. Once the platform is released from the orbiting satellite, a Descent Module (DM) described in section 7.2.2 would permit to control the descending phase.

3. The DM will separate from the platform before the impact with the lunar soil.

4. The two body platform will impact with the lunar surface. As following described in section 7.2.3, the upper part (tetrahedral platform) will remain at the surface while the penetrator will go buried into the lunar subsurface. In section 7.2.3 the high shock survival approach conceived for the platform is also presented.

5. Once the platform is deployed over the moon surface, the platform will remain closed during the following two lunar cycles (approximately 2 months) waiting for the dust ejected during the landing to settle down and also for the shock protection materials to be partially evaporated from the platform as later described. Finally the OBC will check the power availability (solar illumination) and will command the deployment of the solar panels, thus starting the surface scientific measurements.

7.2.2 The descent phase and descent module

A DM (Descent Module) system is required to ensure an efficient transfer of the platform once the carrier satellite has released it. The objectives of the DM are:

- Correct the free fall trajectory of the platform. The DM shall provide the trajectory correction: from the orbital trajectory of the carrier satellite to an impact velocity perpendicular to the planet surface. In principle, with just one thruster the platform could align the trajectory perpendicular to the planet surface: if the thruster propulsion force is aligned against the horizontal velocity of the circular orbital trajectory, constant propulsion (or constant brake if a dense atmosphere can be used) could compensate the initial horizontal force to near zero. At the same time the gravity will make the system fall vertically downwards. This approach only considers horizontal surfaces, where the vertical force added by the planet gravity is perpendicular to the surface. In order to compensate topography effects additional thrusters are needed to dynamically adequate the system trajectory for a perpendicular impact to the surface.

- Release the platform at a determinate altitude. The DM shall release the platform, before the surface impact, with enough time to ensure itself impacts far enough from the scientific platform to avoid measurement disturbances.

- Evaluate the topography of the target body and, following ballistic relations, calculate the release angle w.r.t the planet surface to ensure a surface perpendicular impact of the platform.

It is important to remark that between the previous objectives a vertical velocity deceleration is not considered. This is of main importance to reduce the mass and volume of the DM, just providing the enough fuel to ensure a vertical impact of the platform. The concept proposed in this thesis uses the penetrator body and additional shock reduction techniques to handle the high shocks generated during the surface impact of the platform.

To perform the objectives previously listed, the DM shall be provided with computational capabilities, fuel, thrusters, instrumentation to dynamically measure the trajectory and altimeters. Usually, the DM is equipped with an OBC that controls the descent phase, gyroscopes and radar altimeters (Doppler effect). Additionally a reliable release mechanism shall be provided to release the platform before the surface impact.

The DM (including the solid motors, guidance and navigation control) is not under the scope of this thesis. For this reason a state of the art analysis was performed and the preliminary solution provided by the UK Penetrator Consortium, ([Gowen et al., 2011]) has been selected to be used as reference for the Moon case. This DM has been

selected just for reference purposes as an example of DM where the platform herein could be adapted. In a future implementation, a specific DM able to perform all the objectives listed above in an efficient way shall be designed. Also it is important to note that the DM with a mass of 23Kg, as described in [Gowen et al., 2011], is designed to carry a payload of 13Kg. Considering that the platform proposed in this thesis is just 5.45 Kg the total mass of the DM would be drastically reduced.

Figure 7.2 presents the configuration proposed for the DM adapted to the two body platform conceived. The interface with the DM is specially conceived to the platform herein proposed and is composed of the following elements:

- A pressurized compartment where the platform is docked inside the DM. The compartment shall be pressurized in order to avoid evaporation of the protective resin used to ensure the platform is able to survive the high shock levels at which is subjected during the landing as later explained in section 7.2.3.

- The docking separation system proposed is a Marman Clamp-band. The Marman Clamp-Band or simply Clamp Band is a well-known release mechanism system used in launchers and other space craft subsystems ([Lazansky, 2012]). Currently, these subsystems are provided from different manufactures around the world as SAAB or EADS CASA Espacio. The clamp band permits to create a reliable and stiff attachment between the DM and the tetrahedral platform base plate (note the base plate of the platform can be considered circular instead triangular without any variation of the platform design or performance). In this way, the union between the platform and the DM can be easily made hermetic to include a pressurized compartment as described in figure 7.2.

- A preloaded spring will be pulling out the platform from the DM with enough force to ensure a proper separation of both systems when commanded by the OBC of the DM.

- The release actuator considered for the Clamp Band release is a SMA (Shape Memory Alloy) based actuator from the Arquimea company family of REACT (REsettable Hold-Down and Release ACTuator) devices. The function of the SMA actuator in the REACT mechanism is to perform triggering for the device operation. In this way, it is possible to re-arm the device without requiring a substitution of any element of the release mechanism, what is cheaper and a more reliable approximation than the offered by the standard pyrotechnic devices that has to be partially substituted after its utilization.

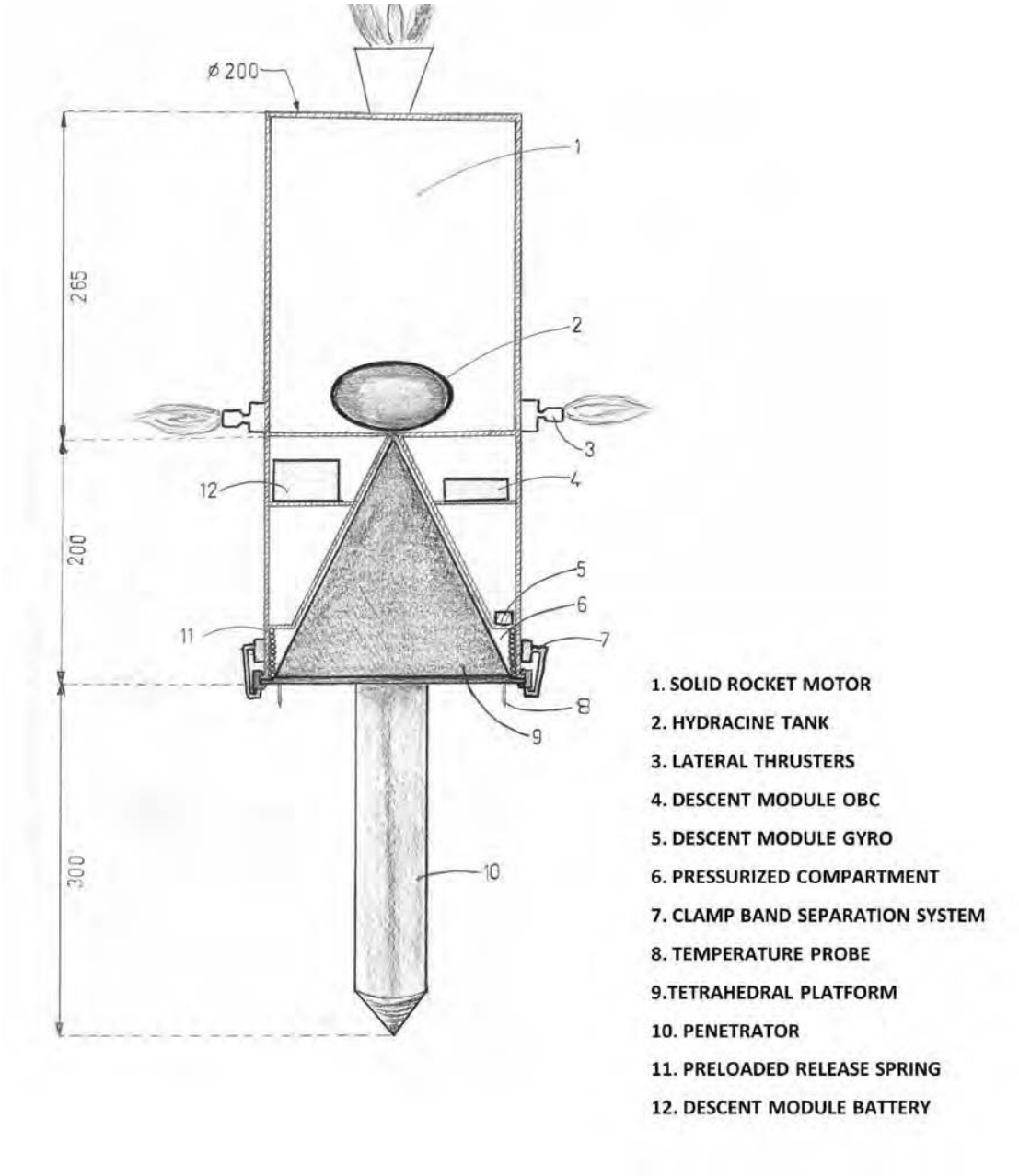

Figure 7.2: Section of the pressurized compartment and the clamp band system conceived for docking the tetrahedral platform to the Descent Module (Descent Module based in the concept proposed by the UK Penetrator Consortium, [Gowen et al., 2011] and used as example of Descent Module in the figure)

7.2.3 The surface impact: configuration and high impact survival techniques proposed.

As described in section 5.1 the platform proposed is divided in two different bodies: the upper body herein referred as the surface platform or tetrahedral platform and the penetrator body (bullet shaped), attached at the baseplate to the tetrahedral platform (refer to figure 5.1). The two different bodies will remain together up to the moment of iteration with the planet surface.

Based on previous studies ([Skulinova et al., 2011], [Doengi et al., 1998], [Hopf et al., 2010] and [Gowen et al., 2011]) the platform will impact the Moon surface at a velocity around 60 to 300 m/s (depending in factors as the planet gravity and atmosphere (table 1.1), DM design and the mass and geometry of the penetrator). A peak deceleration axial shock in the order of 10.000 g to 50.000 g is expected depending on mainly the substrate hardness. As previously described, the first meters of a great part of the Moon surface are composed of fine-grained material (figure 7.1) that will help in smoothing the shock impact (e.g. Lunar-A mission estimated an impact about 8000g [Mizutani et al., 2005], while the MoonLITE mission estimated 10000g, [Gowen et al., 2011]).

For the platform proposed, the desired depth of the penetration into the regolith has been stablished between 0.3 m to 1.2 m. In order to control the penetrator depth it is proposed to use the penetration deformation in the following way:

- The penetrator is missile shaped to ease its penetration into the Moon subsurface.

- After the initial impact and during the penetration, the penetrator body will be deformed as a consequence of the impact and contact forces with the lunar regolith. It is important to remember that the lower part of the penetrator does not contain any subsystem and it is designed to permit a structural deformation.

- The deformation of the penetrator as it enters in the subsurface will lead to the two following beneficial effects:

  - Energy is dissipated during the plastic deformation of the penetrator lower structure. This shock alleviation technique is well known in the automotive sector to reduce g-force at which the passengers are subjected in an accident. In the same way, shock-alleviation devices based on irreversible deformation are used for landers because they offer the highest specific energy absorption capability. Crushable aluminum honeycombs, foams as well as deformable tubes are commonly used for shock alleviation ([Doengi et al., 1998]).

– The deformation of the missile shape will imply a major entrance resistance in the lunar regolith, thus reducing the penetrator depth. As the deformation is higher, the entrance resistance will be higher, thus reducing the penetration depth and increasing the applied contact force to the penetrator deformed area. A trade-off between the structure deformability and penetration depth desired will permit to adjust the range of the penetration depth in function of the expected characteristics of the lunar soil.

The tetrahedral platform, with a flat surface would be retained at the surface. Both subsystems will be connected using umbilical wires for energy and data sharing between the two bodies.

This two-body concept differs from the unique body penetrator proposed in several missions (e.g. Lunar A, MoonLITE or MetNet). Similar schemes, composed of two bodies have been previously proposed (e.g. Deep Space 2 mission or the planetary micro-penetrator proposed in [Gao et al., 2007]). However, there are several peculiarities in the two-body system proposed in this thesis:

- The size relation of the penetrator body and the tetrahedral platform. In the Deep Space 2 mission and in the penetrator concept proposed in [Gao et al., 2007], the penetrator body is much smaller than the surface platform. In the approach herein proposed the penetrator body will absorb a great part of the shock and its volume is similar to the surface platform.

- As described in [Skulinova et al., 2011], the two body approach is considered less reliable than the one body approach. In the platform proposed herein the surface platform could work (with reduced performance) even in the case of the complete destruction or inoperability of the penetrator body (refer to the redundant analysis present in section 5.5). This increase drastically the two bodies approach reliability and also takes the advantages of the two body scheme.

- The synergies between the two bodies, one at the surface and other beneath the surface are exploited: thermal regulation and energy harvesting, deployment of a surface platform using a penetration concept and simultaneous access to the surface and subsurface environments between others.

The landing approach using penetrators herein proposed permits to deploy several WSN nodes using a single orbiting space craft due to its reduced mass and volume dimensions. Even though it is required to prepare the two-body platform subsystems to the high shock levels associated to the hard landing.

Different shock alleviation techniques and an innovative way of combine them in the platform conceived are following described.

In a general overview, we can consider three different approaches to protect a subsystem from a high shock impact of the platform that contains it:

- Absorbing the energy shock, as much as possible, using the structure deformation that contains the subsystem.
- Merging the different elements of the subsystem to be protected in such a way that the wave energy can travel thru it without generating relative movement between the elements that conforms the subsystem.
- Using a rigid structure to permit the shock wave to travel thru the structure without generating damage to the subsystem contained within it.

Bellow, an innovative way of combine the previous three different techniques in the platform conceived is explained. The synergies between the three different techniques permit to obtain an efficient low mass and high shock tolerant platform compatible with hard landing deployment:

Absorption of energy shock using the penetrator body

As it can be seen in figure 5.1, just approximately half of the volume available in the penetrator's body is used by the OBC, batteries and harnessing. The bottom part of the penetrator's cone does not contain any subsystem. The reason is because this volume is conceived to include a structure able to absorb shock energy deforming itself during the high velocity impact with the planet surface. The first part of the platform that enters in contact with the planet surface is the penetrator cone head, deforming itself, as explained previously, in order to absorb energy (refer to figure 7.4) and control the penetration depth.

Rigid structure

Two different rigid structures will help to protect the sensitive subsystem of the platform during the landing shock:

- A tetrahedral aluminum structure that, as explain in section 5.2.1, is designed considering the structural stability to protect the inner subsystems.
- A cylindrical structure made of aluminum located in upper part of the penetrator. This structure will content the principal batteries, power regulation and the OBC.

Both structures are designed to transfer thru them the energy shock wave, reducing the shock energy at which the sensitive subsystems are exposed.

Subsystem elements cohesion in a protective matrix.

A protective matrix is proposed to embedded the sensitive elements of the platform. The matrix used shall be able to embed the entire elements to be protected, providing adequate mechanical stiffness to permit the shock wave travel thru the assembly avoiding any damage to the subsystems. A different combination of cohesion techniques have been considered for the different subsystems of the platform.

The surface platform is embedded in two different elements that provide a complete cohesion of the whole tetrahedron.

The electronics bay is completely embedded in a high performance epoxy compound. This compound shall present a high thermal conductivity, excellent electrical insulation properties, good physical strength and a high degree of flexibility. In this way the epoxy compound not only would help to protect the electronics bay subsystems to the landing shock, additionally will provide an excellent medium to homogenize the heat within the electronics bay as explained in section 8.3. The compound selected is the EP37-3FLFAO from Masterbond ([Master-Bond-Inc., 2015]). This polymer system is certified by NASA for space application (low outgassing), its operation temperature range is from just 4 K to 394K and comply with the high thermal conductivity and electrical insulation required. The electronics bay block is externally covered with a MLI blanket to reduce the radiation heat losses (refer to figure 7.3).

The solar panels, Dust Deposition Sensor, Irradiance sensors and other subsystems not located within the electronics bay are especially sensible to suffer important damage due to the landing shock (fragile optics elements including glass). The same approach followed with the electronics bay is not valid with these subsystems, which shall be exposed to the environment directly. This is a challenging problem that requires to be solved in order to ensure the survival of key elements as the solar panels.

The solution proposed is to use a material that remains solid under Earth pressure but sublimate (passing directly from a solid to vapor) under high vacuum conditions. In this way this material can be heated up to its melting point under Earth pressure and applied to the platform covering all the empty spaces and shock sensitive elements (indicated in blue in figure 7.3). The material will solidify under Earth pressure conditions protecting the rest of subsystems of the surface platform. The pressurized compartment described in section 7.2.2 (index 6 in figure 7.2) will help to avoid sublimation of the material during the travel from Earth to the planet surface. The platform will be exposed to vacuum conditions only when the platform separates from the Descent Module, seconds before the surface impact, thus maintaining the material solid to protect the platform. Another approach considered to ensure that the sublimating material is only exposed to the vacuum conditions over the Moon surface is the following: the tetrahedron platform is covered with a hermetic

ceramic vessel that will maintain the surface platform pressurized until the moment of the surface impact, when the vessel will break exposing the protective material to vacuum conditions for sublimation. This approach will avoid the use of a pressurized compartment in the DM, although the vessel's broken parts will contaminate the area surrounding the platform. For this reason the pressurized compartment in the DM is preferred.

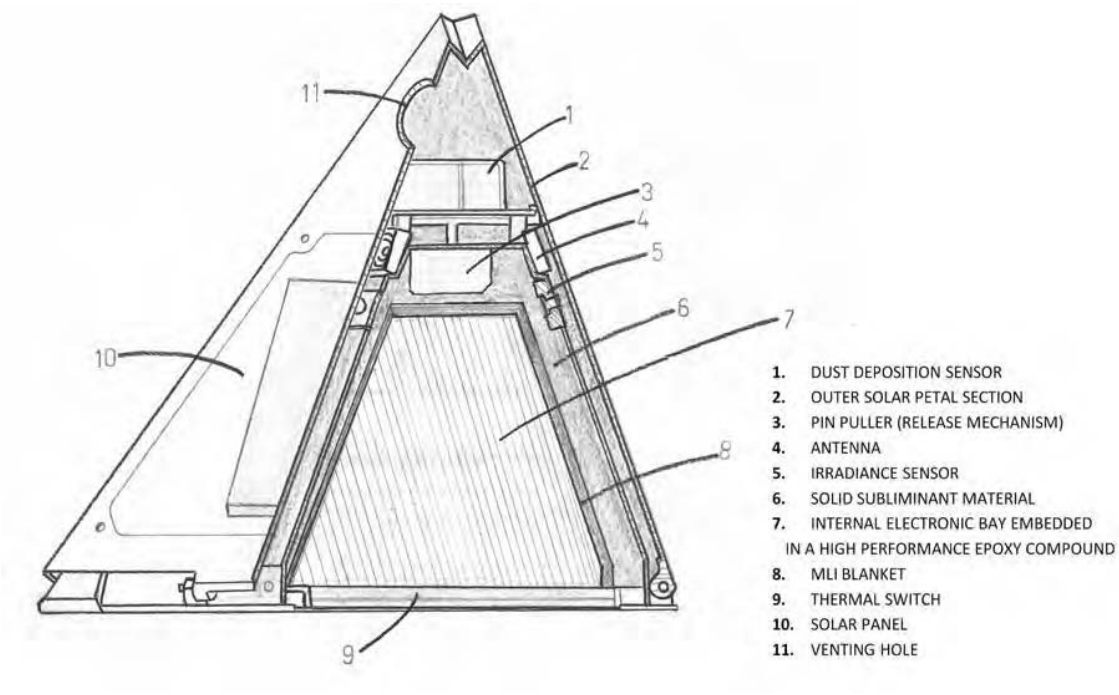

Figure 7.3: Schematic section of the tetrahedral platform illustrating the different cohesion materials used for shock protection

The shock protection by means of embedding the entire sensitive elements with a material capable of sublimating, melting, or dissolving after arrival of the instrument, at the intended site of use, was proposed in 1964 ([O'SULLIVAN JR, 1964]). Later this technique was used specifically for the protection of a MEMS device to be used in the MoonLITE mission ([Hopf et al., 2010]). A similar approach is also used during fossils transportation using Cyclododecane as described in [Brown and Davidson, 2010].

As described in [Hopf et al., 2010] materials as naphthalene, paradichlorobenzene or camphor can be considered as candidates for its use. Additional research is required

to select or chemically synthetize the optimum material for its use in the platform proposed, although once developed it could be used in several space missions.

The tetrahedral platform has to be adapted to the use of these materials providing venting holes (refer to index 11 in figure 7.3) to facilitate the vapor removal from the platform. Herein the protective material is aimed to cover a larger volume than in the case proposed by [Hopf et al., 2010], thus a larger time for complete sublimation of the material shall be considered. Almost nearly two months (2 complete lunar days) has to be considered for a partial evaporation prior to open the solar panels. This would not be a problem as the platform could remain in a low hibernation state waiting for the settlement of the dust ejected during the landing and the removal of the protective material (the impact of the platform and the penetrator will eject a huge amount of dust at a height of kilometers ([Gaier, 2005]). The thin protective material layer that protecs the external solar panels will be the first in sublimate, thus alowing to generate the energy required to maintain the node in a hibernation state up to the moment of solar panels deployment.

It is important to consider the residue that the protective material could leave over the optics of the sensors after sublimation. To avoid any residue, the sensitive optics surfaces will be covered with a thin layer of kapton prior to deposit the protective material. During the solar panels deployment, the thin kapton films will be removed using the descent movement of the solar panels connected with small wires to the kapton films. In this way the optics will be exposed to the environmental surface free from contamination.

The combination of the epoxy compound and the material that sublimates at low pressure conditions permit a complete cohesion of the surface platform (the whole surface platform will behave as a solid block). The proposed approach does not reduce the system operational capabilities and safeguard the integrity of the subsystems during the landing shock.

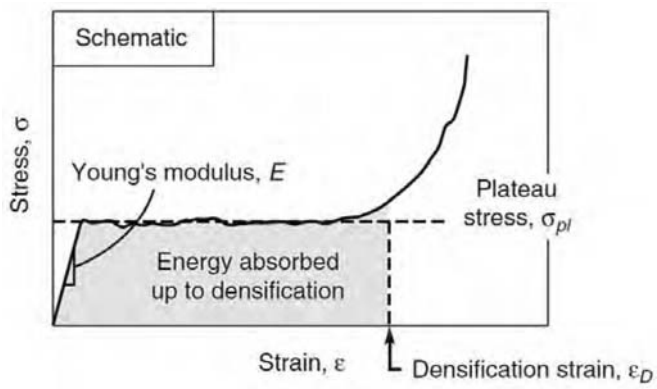

Figure 7.4: Compression curve for metal foam (schematic extracted from [Ashby et al., 2000])

The subsystems located within the penetrator shall be also protected by cohesion. In this case the approach selected is different. The batteries, power regulation and OBC are embedded in the EP37-3FLFAO epoxy. Additionally the complete epoxy block will be surrounded by a metal foam (Duocel, ERG Aerospace, [WB3]) and the whole assembly supported by a rigid structure.

Metal foams are low density absorbing materials that will permit to reduce the shock perceived by the penetrator's subsystems. As described in [Ashby et al., 2000], the work required to compress the metal foam is equivalent to the energy absorbed, and just after densification of the foam (complete compression) the foam will transfer the energy of the impact (figure 7.4).

Chapter 8

Thermal design: conceived technologies for thermal regulation of the exploration platform

8.1 Thermal design introduction and objectives

At mid latitudes, the surface temperature of the Moon varies from around -180 °C to +110°C (refer to section 6.5.2). Therefore, the surface platform should be able to survive a thermal cycle of nearly 300 degrees of change approximately every 28 Earth days (at mid latitudes, 1 lunar day is near 28 Earth days). This poses a real design challenge due to the difficulty of regulating thermally a small node having a low energy stored in extreme thermal conditions. For this reason a detailed thermal control analysis and a custom thermal design is required to guarantee the node and its subsystems are maintained within safe temperature margins.

Therefore, the objective of the thermal control design is to prevent that the different subsystems of the platform could go over their operational and non-operational temperature ranges during the different mission phases. During the on-ground activities, lunch and space travel phases the platform is in a non-operational mode and its temperature is regulated by the carrier spacecraft. Once the node is deployed over the Moon surface, the platform shall be designed to withstand the thermal environment of the Moon. As described in chapter 7 , during the platform deployment, the two bodies platform conceived are disjointed: the tetrahedron body reminds over the Moon surface, while the penetrator goes into de subsurface around 1 meter.

In section 9.1 it is described how the penetrator body will take the advantage of the lunar subsurface heat flux to maintain itself in a comfortable uniform temperature around -23 °C. Considering the good thermal contact between the penetrator and the lunar subsurface regolith it is possible to ensure that the penetrator will maintain the mean temperature of the lunar regolith. The heat generated by the OBC during its normal operation (220 mW, refer to table 9.1) will be conducted thru the penetrator body to the lunar regolith without a significant temperature growth. Consequently, the thermal control design shall be focused in the part of the platform that remains over the surface of the Moon, as the aftbody of the platform will be subjected to the lunar surface temperature environment.

An additional objective is that the thermal mathematical model (or a simplified version) could be used in the OBC of the platform operations over the planet surface. In this way, the planning algorithm could work out the near future expected temperatures of the platform and schedule the tasks correspondingly, thus improving the efficiency of the system.

In section 8.3 the thermal design solutions proposed for this low mass and low power consumption platform are described. Although to validate the thermal solutions proposed it is necessary to use a thermal model. The thermal model generated is presented in section 8.2.

8.2 Thermal Mathematical Model

8.2.1 The energy balance

As described previously, the TMM (Thermal Mathematical Model) shall verify that the platform subsystems are within the thermal limits of their operational and non-operational temperature ranges, validating the thermal design. The common approach followed in spacecraft thermal design is to use a CAD model and a thermal analysis software. The CAD model is discretised in nodes, the analysis parameters and constants introduced and the software tool performs the radiative and conductive heat transfer calculations to obtain the temperature profiles of the different nodes. In an iterative procedure of re-design and modelling is possible to optimise the thermal design of the spacecraft. Some commonly used software tools for this purpose are Esatan, Thermica Suite or Ansys thermal suite, between others. An example of this thermal analysis can be found in [Nouvellon et al., 2012].

This procedure is not valid to accomplish the objectives of the TMM presented in the previous section because the model cannot be exported to the OBC for its use in the planning algorithm. For this reason a custom TMM has been developed for the thermal design of the platform. Additionally, this model directly, or a simplified version, could be used in the OBC for planning purposes.

The Thermal Mathematical Model is based in the analysis of the total energy balance of the system under study and can be defined as:

$$\frac{dE}{dt} = \dot{W}_{elect,net} + \dot{Q}_{cond,net} + \dot{Q}_{conv,net} + \dot{Q}_{rad,net} \tag{8.1}$$

Where $\dot{W}_{elect,net}$ represents the electrical work flow, $\dot{Q}_{cond,net}$, $\dot{Q}_{conv,net}$ and $\dot{Q}_{rad,net}$ represent the conductive, convective and radiative net heat fluxes respectively.

Several assumptions will be considered for the TMM. How representative are these assumptions with the real scenario will determinate the fidelity of the TMM. The assumptions herein considered are necessary for generate a TMM representative of the system and that could be used by the OBC with a reasonable process effort.

- Complete vacuum conditions. No convective phenomena are considered in the study. This approximation fits very well with the actual conditions over the Moon's surface where just small traces of gases are present (table 1.1). The term $Q_{conv,net}$ in the total energy balance can be neglected.

- The mass of the system under study is invariant. This assumption matches correctly with the actual platform behaviour, where there are not significant mass variations during the platform operation (there is not propellant flows as in spacecraft's). It is not considered for the mathematical model the sublimation

of the shock protection material explained in chapter 7.2.3, as the sublimation process occurs before the operational phase of the platform.

- Any energy variation in the system can be related just with a temperature change or electrical energy variations, as the store of energy in the batteries, electrical work flow in the solar cells or electrical work dissipation in the platform subsystems. Other energy variations as microwave electromagnetic inputs or outputs related with the communication antennas or thermal energy stored in phase change of materials are neglected as their influence in the system under study is marginal.

- Each isothermal node considered in the TMM is uniform in temperature (there is not mass exchange between isothermal nodes but there is heat exchange between them).

- The field of view between the different isothermal nodes considered of the platform is neglected. The platform isothermal nodes have been selected in such a way the field of view between them is minimum.

- The thermal node considers radiation phenomena, for this reason the Kelvin degrees unit is used in the TMM (non-linear relations involve in the TMM).

Therefore, considering these assumptions the total energy balance equation can be split into an electrical energy balance and a thermal energy balance as following:

$$V\frac{dQ_{elect}}{dt} = \dot{W}_{elect,in} - \dot{W}_{elect,out} - \dot{W}_{elect,dis} \tag{8.2}$$

$$C\frac{dT}{dt} = \dot{Q}_{cond,net} + \dot{Q}_{rad,net} + \dot{W}_{elect,dis} \tag{8.3}$$

Where $\dot{W}_{elect,in}$ is the work flow generated by the solar panels and thermoelectric generator, $\dot{W}_{elect,out}$ is the electrical work flow within the electrical subsystems and $\dot{W}_{elect,dis}$ is the dissipated electrical power. The Electrical balance is studied in chapter 9 as part of the energy balance. The thermal energy balance is the balance that will rule the TMM.

The radiative net heat flux ($\dot{Q}_{cond,net}$) can be expressed as the difference between the radiative heat flux that enters in the platform and the radiative heat flux that is radiated from the platform:

$$\dot{Q}_{rad,net} = \dot{Q}_{rad,in} - \dot{Q}_{rad,out} \tag{8.4}$$

$$\dot{Q}_{rad,in} = \alpha \cdot I \cdot A + \dot{Q}_{planet,in} \tag{8.5}$$

$$\dot{Q}_{planet,in} = \alpha_b \cdot A_b \cdot F_{b,p} \cdot \epsilon_p \cdot \sigma \cdot T_p^4 \tag{8.6}$$

$$\dot{Q}_{rad,out} = \epsilon \cdot A \cdot \sigma \cdot (T_{hot}^4 - T_{cold}^4) \tag{8.7}$$

Where α is the dimensionless absorptance defined as the fraction of incident electromagnetic power that is absorbed at an interface. I represents the solar irradiance ($\frac{W}{m^2}$) received at the surface area (A) of interest. I value can be obtained using the algorithm developed and described in section 6.4.2. ϵ is the emissivity, a dimensionless quantity dependent of the material properties and represents the effectiveness of the surface under study in emitting energy as thermal radiation. σ is the Stefan-Boltzmann constant $5.670373 \cdot 10^{-8} \frac{W}{m^{-2}} \cdot K^{-4}$ and T_{hot} and T_{cold} are the temperature (in K) of the radiant surface and cold body respectively. The last term contemplated in the thermal balance is the thermal radiation emission from the moon surface.This term relates the energy received by the platform from the planet surface due to the IR emission of the planet. α_b A_b are the area and absorptance of the platform while ϵ_p and T_p are the emissivity and temperature of the planet surface. The term $F_{b,p}$ is the field of view factor from body surface to planet surface. In the nominal configuration of the platform (planar Moon surface) this factor can be considered as near cero, neglecting the influence of the planet emission. Nevertheless the planet thermal radiation shall be considered if the platform is deployed in an inclined plane, in a crater or near mountains.

The conductive net flux for a two isothermal nodes, considering an ideal thermal contact by an area (A) and a material of thermal conductivity $K_{1,2}$ separated a distance $d_{1,2}$ can be expressed as:

$$\dot{Q}_{cond,net} = \dot{Q}_{cond1,2} = k_{12} \cdot \frac{A \cdot (T_1 - T_2)}{d_{1-2}} = -\dot{Q}_{cond2,1} = -k_{12} \cdot \frac{A \cdot (T_2 - T_1)}{d_{1-2}} \tag{8.8}$$

The radiative net heat flux in a solar cell is slightly different from the standard terms previously presented. For a solar cell:

$$\dot{Q}_{rad,out} = \epsilon \cdot A \cdot \sigma \cdot T_{solar_cell}^4 \tag{8.9}$$

$$\dot{Q}_{rad,in} = (\alpha \cdot \eta \cdot F_{pg}) \cdot I \cdot A \tag{8.10}$$

Where $\dot{Q}_{rad,out}$ is the same as the previous terms presented but the $\dot{Q}_{rad,in}$ term takes into consideration the energy absorbed by the solar cell that is transformed in electrical work and not in heat (WB2). η is a dimensionless term representing the solar cell efficiency, defined as the ratio between the maximum electrical power

produced by the solar cell at 25°C with respect to the input irradiance of the area. F_{pg} is a dimensionless packaging factor considering the non-active area of a solar panel due to the packaging of the different solar cells that conforms the solar panel.

8.2.2 Platform multi-node discretization

The node has been discretized in isothermal nodes as described in figure 8.1.

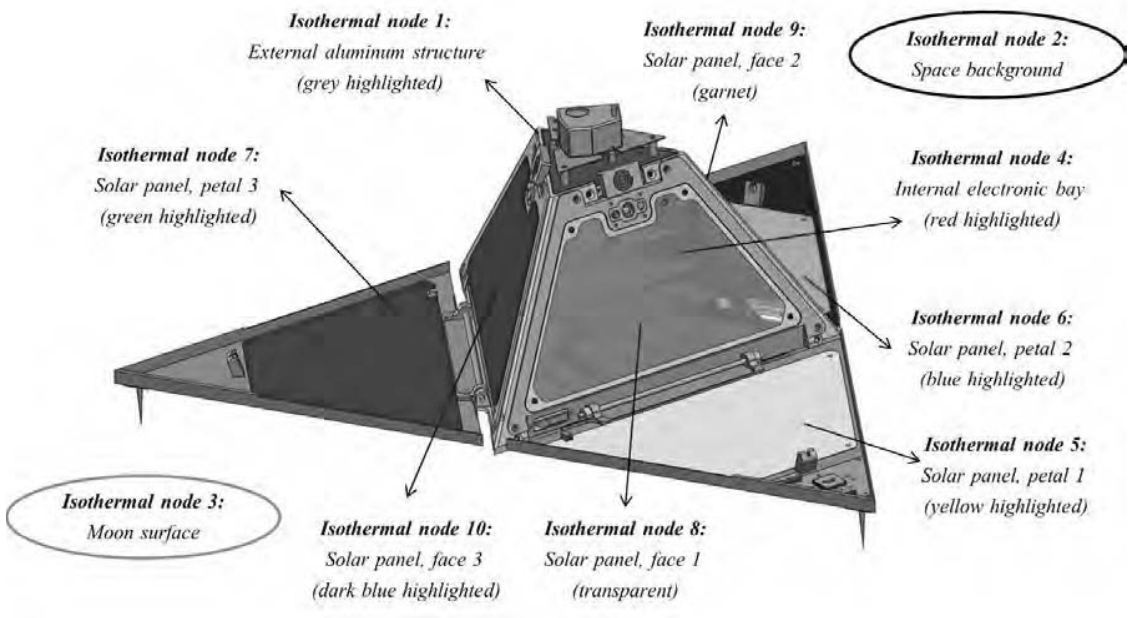

Figure 8.1: Isothermal nodes selection for the platform thermal model

During the node discretization of the platform the following considerations have been applied.

- Minimum number of nodes. Increase the number of nodes will increase the thermal accuracy of the TMM, although it will also increase the processing effort to resolve by analytical methods the TMM.

- The field of view between isothermal nodes shall be highly reduced. In this way it would be possible to simplify the TMM because radiation relations between nodes can be neglected.

- The temperatures obtained in each node shall be enough for the objectives of the TMM.

The isothermal node 2 represents the deep space temperature (2,7 K) and the isothermal node 3 is the Moon's surface temperature that can be obtained using the mathematical model developed and described in section 6.5.2.

The nodal equations for each node of the platform can be obtained from the different terms presented previously as:

$$C_i \cdot \frac{T_i^+ - T_i}{\Delta t} = \sum_{j=0}^{N} \dot{Q}_{ij} = \dot{Q}_{elect,dis_i} + \dot{Q}_{planet,in_i} + \dot{Q}_{radsolar,in_i} - \dot{Q}_{radspace,out_i} + \sum_{\substack{j=1 \\ j \neq i}} \dot{Q}_{cond,ij} + \sum_{\substack{j=1 \\ j \neq i}} \dot{Q}_{rad,ij} \tag{8.11}$$

Euler discretization of time (Δt) has been applied with the objective of solve the model using numerical solution methods. The overall thermal capacity C_i is the sum of the mass and heat capacity product of each of the elements that compose the isothermal node i:

$$C_i = \sum_{i=1}^{n} m_i \cdot c_i \tag{8.12}$$

With the objective of summarize the thermal couplings between the different isothermal nodes presented in figure 39, a thermal coupling node matrix has been developed and is presented in table 8.1. In this matrix the radiative couplings between nodes are situated in the upper triangular part of the matrix, the conductive couplings in the lower triangular part and the thermal capacities of each node in the diagonal.

Several parameters related to the different materials used in the platform are involved in the TMM developed. These parameters usually vary considerably depending on the source consulted, the specific material used, manufacturer or temperature of operation. A search has been performed in the literature to use the parameters values that better fit the materials to be used in the platform. Table 8.2 describes the parameters and the values used.

The thermal coupling between node 1 and node 4 (C_{14} in Table 7) correspond to the conductive flux thru the thermal switch. This element has been included in the thermal model as two thermal contacts in parallel dependent of the temperature. The thermal contacts have been modeled as two thermal resistors in parallel (figure 8.2). The thermal resistance denominated as $R_{support}$ models the thermal contact between

Node i/j	1	2	3	4	5	6	7	8	9	10
1	C_1	R_{12}	-	-	-	-	-	-	-	-
2	-	-	-	-	R_{25}	R_{26}	R_{27}	R_{28}	R_{29}	R_{210}
3	C_{13}	-	-	-	-	-	-	-	-	-
4	C_{14}	-		C_4	-	-	-	-	-	-
5	C_{15}	-	-	-	C_5	-	-	-	-	-
6	C_{16}	-	-	-	–	C_6	-	-	-	-
7	C_{17}	-	-	-	-	-	C_7	-	-	-
8	C_{18}	-	-	-	-	-	-	C_8	-	-
9	C_{19}	-	-	-	-	-	-	-	C_9	-
10	C_{110}	-	-	-	-	-	-	-	-	C_{10}

Table 8.1: Platform thermal coupling node matrix

node 1 and 4 corresponding to the auxiliary pieces that supports the thermal switch between the inner electronics bay and the external structure. These elements have been manufactured in PTFE to reduce their thermal conductance. This thermal resistance is always present, independent of the temperature or if the switch is closed or open. The thermal resistance denominated as $R_{contact}$ models the thermal contact of the thermal switch when it is closed and when it is open. This thermal contact (aluminum) varies the contact area in function of the temperature. The transition temperature of the thermal switch from hot to cold is 10 °C; correspondingly the temperature transition from cold to hot is 20°C. This typical hysteresis of the SMA materials is very useful in this application because avoids any possible mechanical oscillation during the hot-cold and cold-hot transitions.

Parameter	Symbol	Value	Units	Source
Stefan-Boltzmann constant	σ	$5.670373 \cdot 10^{-8}$	$\frac{W}{m^{-2} \cdot K^{-4}}$	N/A
7075 aluminum alloy emissivity	$\epsilon_{aluminum}$	0.82	-	Kauder 2005
7075 aluminum alloy absorptance	$\alpha_{aluminum}$	0.68	-	Kauder 2005
7075 aluminum alloy Specific heat	$c_{aluminum}$	0.91	$\frac{J}{g \cdot K}$	[WB6]
7075 aluminum alloy density	$\rho_{aluminum}$	$2.81 \cdot 10^{6}$	$\frac{g}{m^3}$	[WB6]
7075 aluminum alloy Thermal conductivity	$k_{aluminum}$	205	$\frac{W}{K \cdot m}$	[WB6]
Solar cell absorptance	α_{solar_cell}	0.92	-	[Spectrolab, 2010]
Solar cell emissivity	ϵ_{solar_cell}	0.85	-	[Spectrolab, 2010]
Solar cell efficiency	η	0.283	-	Edmondson 2006
Solar panel packaging factor	F_{pg}	1.8	-	[WB2]
Solar cell Thermal conductivity	k_{solar_cell}	148	$\frac{W}{K \cdot m}$	Armstrong 2010
PV cell Specific heat	c_{solar_cell}	0.67	$\frac{J}{g \cdot K}$	Armstrong 2010
Solar cell density	ρ_{solar_cell}	$2.33 \cdot 10^{6}$	$\frac{g}{m^3}$	Armstrong 2010
Thermal conductivity regolith	$k_{regolith}$	$9.3 \cdot 10^{-3}$ (compacted regolith by the platform)	$\frac{W}{K \cdot m}$	Vasavada 1999
Regolith depth	$L_{regolith}$	0.02	m	Langseth 1976
FR4 thermal conductivity	K_{FR4}	0.25	$\frac{W}{K \cdot m}$	Vanek 2014
FR4 Specific heat	c_{FR4}	0.84	$\frac{J}{g \cdot K}$	Vanek 2014
FR4 density	ρ_{FR4}	$1.85 \cdot 10^{6}$	$\frac{g}{m^3}$	[Mangroli et al., 2011]
PTFE Thermal conductivity	K_{PTFE}	0.25	$\frac{W}{K \cdot m}$	[Dupon, 1996]

Table 8.2: Parameters used in the Thermal Mathematical Model

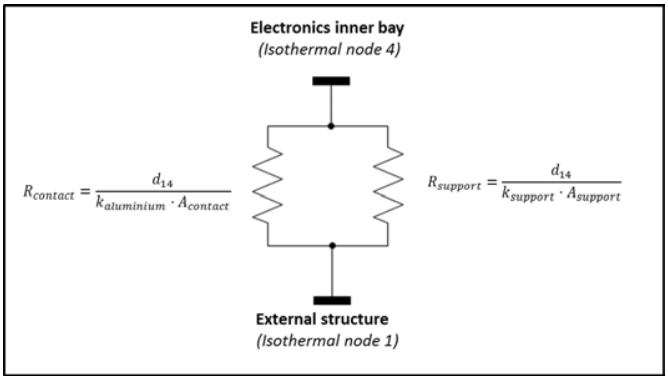

Figure 8.2: Thermal switch model

8.3 Thermal design solutions and model results

The operational strategy considered in order to handle the extremely low temperatures during the lunar nights is hibernation of the tetrahedral platform (the OBC and main batteries located in the penetrator remains operative). The surface platform will be able to obtain scientific data during the entire lunar day and during the first days of the lunar night. As later explained in chapter 9, the penetrator's subsystems remains operational, in a low consumption mode, during all the night thanks to the comfortable temperature beneath the lunar surface (around -23°C). A night energy harvesting system permits to obtain energy to charge the main batteries and perform punctual scientific measurements during the night. The adopted thermal design will permit to efficiently use the energy harvested, during the lunar day and also during the night, to heat up the inner bay of the tetrahedral platform to reach the operational temperature range and perform punctual scientific measurements during the cold nights.

The platform elements disposition has been designed in order to optimize the thermal regulation of the node. With the objective to increase as much as possible the operational time of the node during the lunar nights the thermal design includes the following concepts:

1. All the platform elements are able to survive in a non-operational mode from -40 °C to -373°C without major damages. This implies special considerations in all the electronics, electrical and mechanics elements of the node (e.g. mechanical expansions and contractions of all the node elements).

2. A highly thermally isolated electronic bay situated in the inner part of the surface platform will be the key element of the thermal design. The inner

Figure 8.3: SMA based thermal switch (7mm in height and 111 mm in diameter).

bay will be in contact with the external structure of the tetrahedral platform just at the base. A Multi-Layer Insulation (MLI) sheet covers the complete inner bay except of its base. In the base a thermal switch will be in charge of controlling the heat transfer by the thermal conduction between the inner bay and the external structure. This automatic reconfigurable hardware based on SMA technology will regulate the temperature of the electronics bay as a function of the external temperature on the Moon surface. The thermal switch (figure 8.3) will isolate the electronics bay during the cold nights and will put it in thermal contact with the Moon surface during the hot days. The thermal switch is completely passive (0 W) and its total mass is below 120g. The thermal switch operation is based on an SMA fiber in counterforce with a spring. When heated above its temperature transition the SMA will apply a force higher than the spring, generating a rotational movement that would put in thermal contact the top part of the switch with the bottom part. In this way the heat could go thru the thermal switch. Below the temperature of transition of the SMA material, the spring will make the switch open, avoiding a good thermal contact between the up and bottom parts of the thermal switch, thus isolating the inner bay of the platform.

3. Active heaters will be used to heat-up the inner bay to warm it up to -90°C (183,15K). The -90°C limitation is imposed by the minimum operational temperature range of the electronics. The node includes 8 housekeeping temperature sensors that monitor the temperature of the different subsystems to achieve a closed loop thermal control.

4. As described in chapter 7 the electronics situated in the inner bay is embedded in a thermal conductive epoxy. This will be not helpful only for shock protection; additionally this epoxy permits to homogenize the temperature of the inner bay.

The heat generated by the heaters and the own electronics power dissipation will be diffused by the epoxy. Moreover, the heat capacity of the inner bay block is increased. In return the use of this epoxy would mean an important mass penalty for the platform (around 400 grams).

5. A MLI (Multi Layer Insulation) blanket composed of 40 goldized Kapton layers covering the inner bay epoxy block reduce the heat losses by radiation between the inner bay and the external platform structure.

6. The external aluminum structure will be used as radiators to radiate the heat to the outer space during the hot days. During the lunar days the thermal switch keeps the inner bay in thermal contact with the external structure. Coating paints will be used to regulate the emissivity of the structure in order to ensure that the node does not heat over +150°C (the upper limit temperature imposed by the electronics and batteries). Additionally the heat loss to the planet surface by the node base has to be considered.

Using the mathematical model including all the thermal design consideration listed above an iterative design procedure was accomplished with the objective of optimize the thermal design. The final results obtained are described below.

Figure 8.4 presents the model results for the temperature evolution of the thermal nodes of the platform (as defined in figure 8.1) considering the aftbody platform is inactive (0 W dissipation in the electronics bay). The model results correspond to 600 hours (25 days) starting the 5/1/1972 with the platform located in the Moon equator.

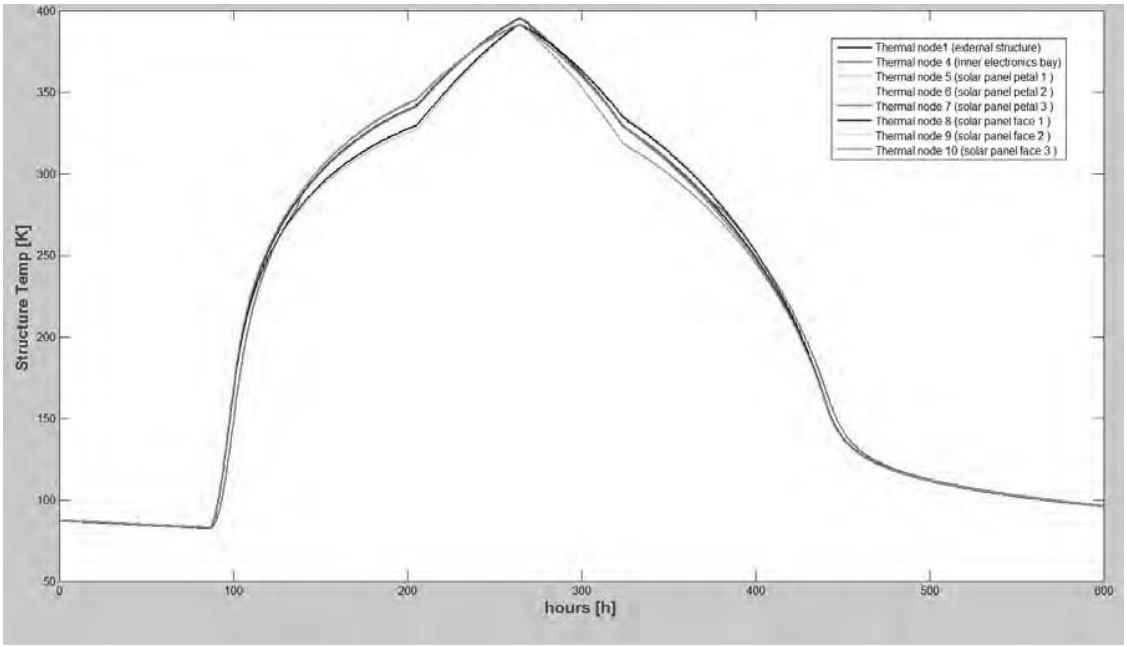

Figure 8.4: Thermal nodes temperature evolution during approximately 1 lunar day considering 0W dissipation.

As expected the node structure follows the temperature profile of the Moon surface. As there is not power dissipation within the electronics bay, its temperature remains stable at the same temperature than the external structure. The temperature variations between the different solar cells (nodes 5,6,7,8,9 and 10) depend directly on the sun position w.r.t the platform orientation. If the sun illuminates the solar cell its temperature will increase significantly, and consequently, solar cells in shadow will decrease its temperature. The area illuminated in each moment for each solar cell directly depends on the platform orientation with respect to the Sun and the solar incident angle. The solar incident angle is obtained from the mathematical model developed in chapter 6.4.2 and the platform orientation (ϑ) w.r.t the lunar equator is an input for the mathematical model. With these two parameters it is possible use geometrical relations to discretize the solar area illuminated. These geometrical relations have been introduced in the TMM. As the thermal conductivity of the solar cells with the external structure is driven by the low thermal conductivity of the FR4 material that supports the solar cells, the temperature changes can be appreciated in the figure for the different solar cells as they become illuminated or non-illuminated. In figures 8.4, 8.5 and 8.6 a sharpen transition in the temperature evolution of the

nodes can be appreciated in the hotter part of the lunar day. The temperature, that increases smoothly, presents a slope change symmetrically near the sun zenith. This effect is a direct consequence of the geometrical disposition of the tetrahedral platform. As the sun elevation increases there is a point, near the zenith, where the sun starts to illuminate the platform's surfaces that were in the shadow. In that point the temperature increases drastically as depicted in the figure. Correspondingly, when the sun reduces its elevation, an area previously illuminated enters in shadow. It must be note that the lack of atmosphere prevents the indirect illumination of the shadowed surfaces, which virtually pass from complete shadow to be illuminated by the sun, and generates the sharp transition appreciated in the TMM. This effect is even accentuated considering the geometrical discretization that has been used for the platform modelling.

Figure 8.5 presents the model results considering the surface platform is active and with a power consumption of 200mW continuously (note this is just an example aimed to show the TMM performance and does not represent a real scenario where it would not be possible to maintain a constant 200 mW power consumption in the electronics bay during 25 days). The model results correspond to 600 hours (25 days) starting the 5/1/1972 with the platform located in the Moon equator.

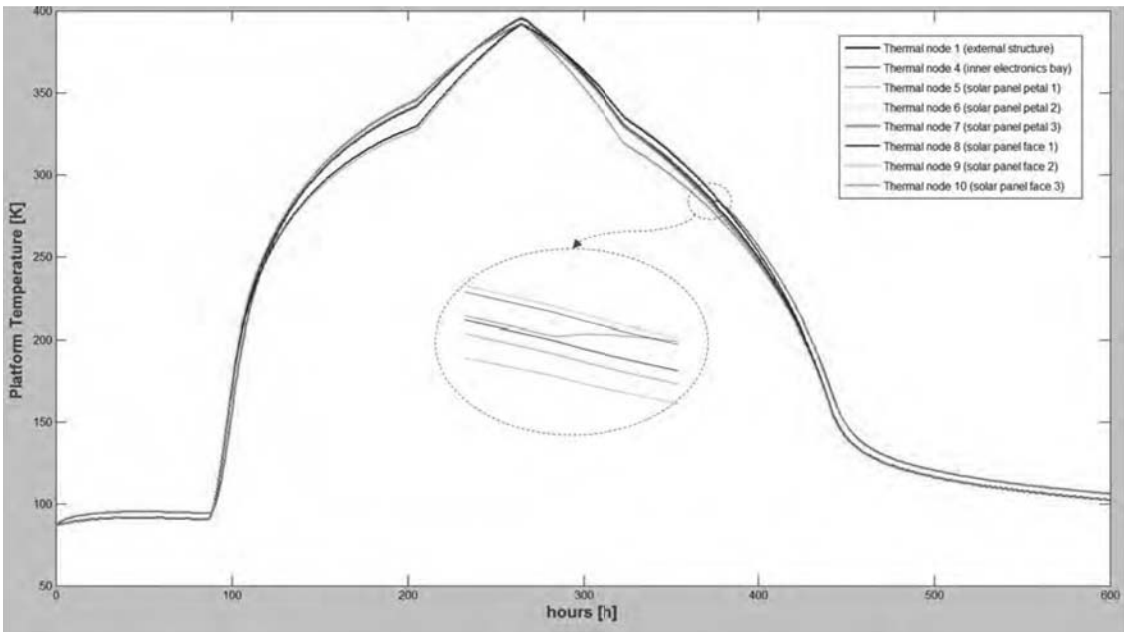

Figure 8.5: Thermal nodes temperature evolution during approximately 1 lunar day considering 0.2 W continuous power dissipation in the inner electronics bay.

As it can be appreciated the inner electronics bay (red line) is always around 4 degrees up w.r.t the rest of the structure during the night. During the day, the sun is heating up the external elements of the structure and therefore they are hotter than the inner bay that just is dissipating 200mW. The effect of the thermal switch can be clearly seen in figure 8.5 (zoom detail). As the platform get colder during the lunar evening the SMA material installed in the thermal switch relaxes, consequently opening the thermal switch and reducing the thermal heat transfer between the inner electronics bay and the external structure. As a consequence of this, and considering the 200 mW continuous power dissipation within the inner bay, its temperature increases up to the equilibrium state, nearly 4 degrees up w.r.t the external structure node.

Figure 8.6 presents the model results considering there is need of performing scientific measurements during the night. In order to perform scientific measurements during the night, it is required to heat up the inner bay up to -90°C, that is considered the minimum operational temperature of the platform. As shown in figure 8.6, it is required as a minimum 2W during 10 hours to increase the inner electronics bay temperature to -90°C (193.15K). This is possible thanks to the thermal isolation provided by the thermal switch as previously described. The model results correspond to 600 hours (25 days) starting the 5/1/1972 with the platform located in the Moon equator.

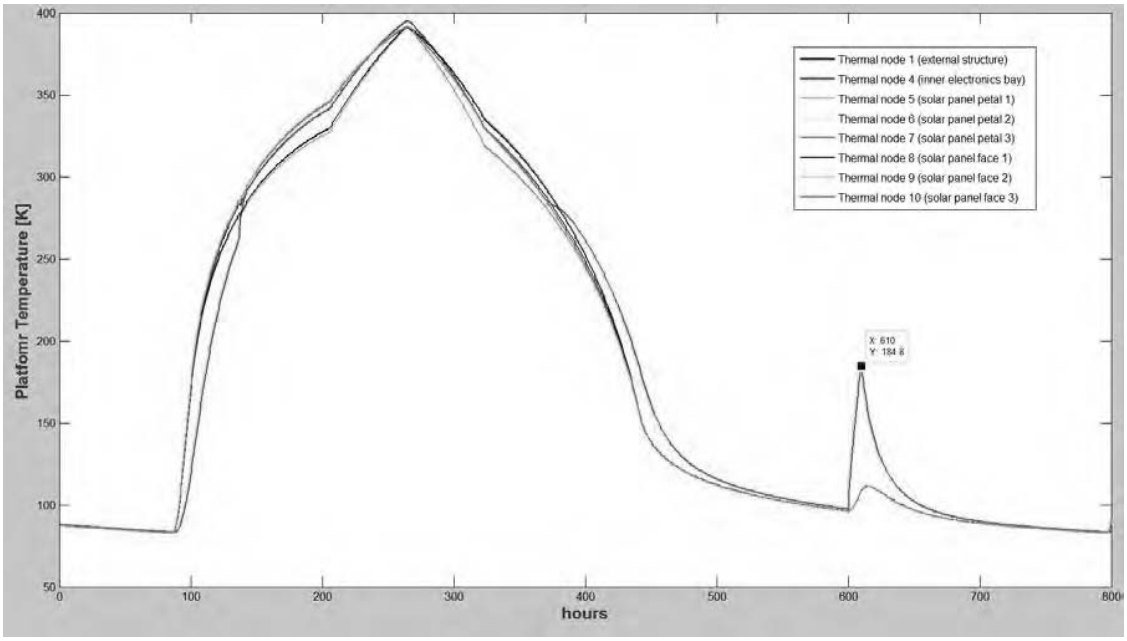

Figure 8.6: Thermal nodes temperature evolution during approximately 1 lunar day considering 2 W power dissipation during 10 hours in the inner electronics bay for a punctual measurement during the lunar night.

Chapter 9

Energy management and innovative concepts for energy harvesting.

9.1 Energy harvesting for space exploration

Reviewing the state of the art of similar space exploration platforms to the one herein proposed (refer to chapter 4 and comparative table 4.1), we can immediately realise that just a few proposals (as MetNet mission), considered solar panels for energy harvesting, and none of them considers energy harvesting systems during the night. The main reason is the complexity to fix the technical requirements mandatory for harvesting efficiently energy over the planet surface within a small and low weight platform.

In this chapter, different techniques for energy harvesting over the Moon surface, compatible with the platform conceived, are proposed. The use of these techniques will permit to extend the mission lifetime, thus permitting a long term WSN monitoring scenario that drastically increase the scientific mission returns, making the mission concept proposed a serious alternative to traditional mission concepts as big rovers or landers.

Energy harvesting has become of growing interest in the last years and the number of research reports has kept increasing for the last decade ([Harb, 2011]). The concept idea is to include in the device to be powered a subsystem able to harvest small amounts of energy from the environment and use the generated energy to maintain the system powered without the need of wires, fuel or maintenance. The increasing use of WSN made the need of improve these harvesting techniques and make them suitable to power the autonomous nodes in a WSN, with a power consumption normally below the $100\mu W$. In these commercial systems the combination of the harvesting techniques with a rechargeable battery or super capacitor makes feasible the energy autonomy of the WSN during its operational lifetime.

The sources of energy for harvesting used in the state of the art of energy harvesting techniques are very diverse: mechanical energy from vibration or motion, electromagnetic, thermal, momentum generated by radioactive reactions, pressure gradients, magnetic, liquids flow, solar, light or biological.

In the field of space exploration, and as commented in section 1.2, the Radioisotope Thermoelectric Generators (RTGs) or fuel tanks are commonly used as primary energy source. Usually, as auxiliary energy source, solar energy harvesting using solar cells are the more common harvesting technique used in conventional space exploration. For small exploration platforms, as those described in the state of the art in chapter 4 , the most common solution proposed is the use of batteries as primary energy source. Hence, the batteries are charged before the separation of the platform from the transport vehicle and used during the timeframe mission. Once the batteries are completely depleted the mission ends, even if the systems are completely operational. Obviously, following this approximation the mission lifetime is highly reduced and, even with low power consumption considerations, the mission lifetime

usually cannot overpass one year (in some cases just a few hours).

In this work we propose to completely substitute the non-renewable energy sources with energy harvesting techniques aimed to power the nodes, continuously recharging the batteries and extending the lifespan of the mission during years.

The energy harvesting for space exploration WSNs presents additional problems to those ones presented in commercial WSNs for terrestrial applications. Even though using low power consumption technologies as those proposed in this thesis, the energy requirements of each of the nodes of the WSN in an extraterrestrial environment are much higher than those equivalents in a terrestrial application. The main reasons are:

- The extreme environmental conditions in which the proposed WSN node shall work (temperature operation range, radiation, dust, etc.). Active thermal regulation shall be considered for operation in extremely low temperatures.
- Complex payloads and mechanisms with elevated punctual power consumptions.
- Additionally, the WSN deployed over an outer space planet shall work during the mission lifespan without maintenance, what implies redundancy and high reliability electronics components what usually implies higher power consumption.

Finally, we have to consider an efficient energy conditioning for its final used in the platform. If the energy source is dependent of environmental conditions energy storage shall be considered. Energy storage using batteries is a well fitted solution. It is important to ensure proper working voltage and current levels in order to ensure an efficient battery charging and discharging processes. Other possibility, also proposed in this thesis, is the use of the energy harvested directly for its final use, for example thermal energy in order to maintain warm certain elements of the platform as later explained. This is the most efficient method as there is not energy transformation involved.

In the following chapters, an analysis of the power consumption requirements of the platforms and the energy management philosophy is introduced. Afterwards, energy harvesting solutions proposed are described.

9.2 Energy management and energy consumption mathematical model

To reduce the power consumption of the exploration platform is not only possible by reducing the individual power consumption of its subsystems; a smart energy

management will play an important role in this objective.

From the point of view of energy management we can consider two general operational modes:

- Continuous operation: if the energy harvesting system is able to obtain and storage the energy required for continuous operation (mean power consumption of the platform is lower than the mean power harvested). The energy management is reduced to sequence the platform operational activities in such a way the batteries are not depleted in any moment. This operational mode is not feasible in the Moon scenario, were during the long nights the main power harvesting technique is not available (solar energy).

- Discontinuous operation: in this case, the node mean power consumption is higher than the average harvested power, thus the node shall operate intermittently.

The discontinuous operational mode can be addressed just following a predetermined sequence of activities. One of those activities could be enter in a hibernation state with the objective of reduce to a minimun the power consumption. In the Moon scenario, and considering the platform herein proposed, this would mean that during the lunar day the node will be near to a continuous operation mode. During the night the node shall be able to perform previously scheduled punctual activities and enter in an hiberation state. This would permit at least to obtain some punctual environmental measurements during the long nights that could be of main importance for certain scientific objectives.

In order to permit the platform to optimize its operational time, including night environmental monitoring, the platform shall be able of planning its activities in function not only of the energy available, but also in function of the future energy available. In chapter 10 a high level control architecture is proposed for this platform.

Therefore, the energy management of the platform is based in a discontinuous operational mode with the following approach:

1. Two set of batteries store the energy harvested: (i) the surface platform batteries will be operative during the lunar days and they will be used to power the scientific payload and the radio interface system; (ii) The principal batteries, located in the penetrator body and beneath the planet surface, will be able to provide energy continuously; generally to the OBC and sporadically to heat up and power the tetrahedron platform for night operation.

2. The OBC will plan the operation sequence of the platform considering the energy available and the expected harvested energy in the following hours or days.

3. In case the energy available is not enough to perform the activities planned or even if there is not enough energy to re-planning, the node will enter in a ultra-low power consumption mode waiting for energy availability.

This energy management approach is based in a nominal node platform; in case of an operational malfunction of any of the subsystems, redundant operational modes are described in section 5.5.

Subsystem	**Nominal power consumption [mW]**	**Idle power consumption [mW]**	**Nominal operation time [ms]**	**Energy [mJ]**
Temperature sensors (x3)	2.175* (P_T)	0	34 (τ_T)	0.07395*
Irradiance sensor (x9)	0**	0	72 (τ_I)	0**
TID measurement	57 (P_{TID})	0	18 (τ_{TID})	1.026
SEUs measurement	21(P_{SEU})	0	$3 \cdot 10^4$(τ_{SEU})	630
DDS measurement	8*(P_{DDS})	0	80 (τ_{DDS})	0.64*
DDS calibration	9000***(P_{CAL})	0	3000 τ_{CAL})	27000***
Housekeeping (x8)	5.8*(P_{HSK})	0	90 τ_{HSK})	0.522*
Acquisition electronics	110(P_{ACQ})	0	Depends on planning (τ_{ACQ})	Depends on planning
OBC general operations	100(P_{OBC})	4.558 (PI_{OBC})	Depends on planning (τ_{OBC})	Depends on planning
OBC planning operation	200 during planning algorithm implementation (PI_{PLN})	0	(PI_{PLN})	TBD
Comms module	800(PI_{COM})	0	Depends on planning (τ_{COM})	Depends on planning
Power module	75 (batteries in discharging mode; not charging mode power consumtion considered) (PI_{PWR})	7.5(PI_{PWR})	Depends on planning (τ_{PWR})	Power losses due to normal power operation. Depends on planning.
Heaters	5000(PI_{HTR})	0	Depends on planning (τ_{HTR})	Depends on planning

* Not considering the acquisition electronics power consumption considered in the Acquisition electronics subsystem
** The photodiodes are passive (the light incident generates the photocurrent used for illumination measurement). The acquisition electronics is not considered.
*** Nominal at 25°C. Operation time changes in function of the environmental temperature

Table 9.1: Platform subsystems power consumption estimation

The mathematical environmental models herein developed and described in section 6.4.2 (solar irradiance model), 6.5.2 (surface temperature model) and 8.2 (node platform thermal model) will help the planning algorithm to predict the energy that could be harvested. However, the algorithm will require the energy consumption model of the platform to compute the optimal sequence of activities in function of the power available, the future power available and the consumption of each potential task to be performed.

Table 9.1 presents the estimated power consumption of each subsystem of the platform that will be required to define the energy consumption model. Deployment mechanism power consumption is not considered in table 9.1 because it is operated

once at the beginning of operation activities using the external solar panels, which are no longer used during the mission. For details on solar panels deployment system refer to section 5.2.4. The power consumption estimations presented in table 9.1 are nominal power consumption values obtained theoretically and experimentally. The experimental power consumption values were obtained from the prototype subsystems developed and described in chapter 10.5. In order to consider a more realistic scenario we shall derate the values estimated considering aging factors, temperature variation and reliability coefficients. Herein a general derating factor (η) of 0.5 is considered, although a specific derating factor analysis (theoretical and experimental) shall be performed for each subsystem (the analysis shall be perform considering the space qualified design of the subsystems herein proposed).

Task	**Equation**
Surface Temperature measurement	$T_{TMP} = (\tau_T \cdot P_T + P_{ACQ} \cdot \tau_T + P_{PWR} \cdot \tau_T) \cdot \eta$
Irradiance measurement	$E_I = (\tau_I \cdot P_I + P_{ACQ} \cdot \tau_I + P_{PWR} \cdot \tau_I) \cdot \eta$
TID measurement	$E_{TID} = (\tau_{TID} \cdot P_{TID} + P_{ACQ} \cdot \tau_{TID} + P_{PWR} \cdot \tau_{TID}) \cdot \eta$
SEU measurement	$E_{SEU} = (\tau_{SEU} \cdot P_{SEU} + P_{ACQ} \cdot \tau_{SEU} + P_{PWR} \cdot \tau_{SEU}) \cdot \eta$
Tetrahedral platform active heating	$E_{HTR} = (\tau_{HTR} \cdot P_{HTR} + P_{PWR} \cdot \tau_{HTR}) \cdot \eta$ $= m_{inner\_bay} \cdot c_{inner\_bay} \cdot \frac{T_{end} - T_{start}}{\tau_{HTR}}$
DDS calibration	$E_{CAL} = (\tau_{CAL} \cdot P_{CAL} + P_{ACQ} \cdot \tau_{CAL} + P_{PWR} \cdot \tau_{CAL}) \cdot \eta$
DDS measurement	$E_{DDS} = (\tau_{DDS} \cdot P_{DDS} + P_{ACQ} \cdot \tau_{DDS} + P_{PWR} \cdot \tau_{DDS}) \cdot \eta$
Hibernation	$E_{SLP} = (\tau_{SLP} \cdot PI_{OBC} + \tau_{SLP} \cdot PI_{PWR}) \cdot \eta$
Housekeeping measurement	$E_{HSK} = (\tau_{HSK} \cdot P_{HSK} + P_{HSK} \cdot \tau_{HSK} + P_{PWR} \cdot \tau_{HSK}) \cdot \eta$
Radio interface communication	$E_{COM} = (\tau_{COM} \cdot P_{COM} + P_{PWR} \cdot \tau_{COM}) \cdot \eta$
Planning	$E_{PLN} = (\tau_{PLN} \cdot P_{PLN} + P_{PWR} \cdot \tau_{PLN}) \cdot \eta$

Table 9.2: Energy consumption mathematical model equations

The energy consumption equations have been established in function of each task. A task is herein defined as a set of operations in which each one requires the use of a subset of the different subsystems presented in table 9.1. Table 9.2 resumes the equations that define the energy consumption of the platform.

9.3 Solutions proposed for energy harvesting

The energy harvesting techniques proposed are in direct relation with the platform configuration (section 5.1) and the deployment technique (chapter 7). As depicted in figure 9.1 three different techniques are conceived.

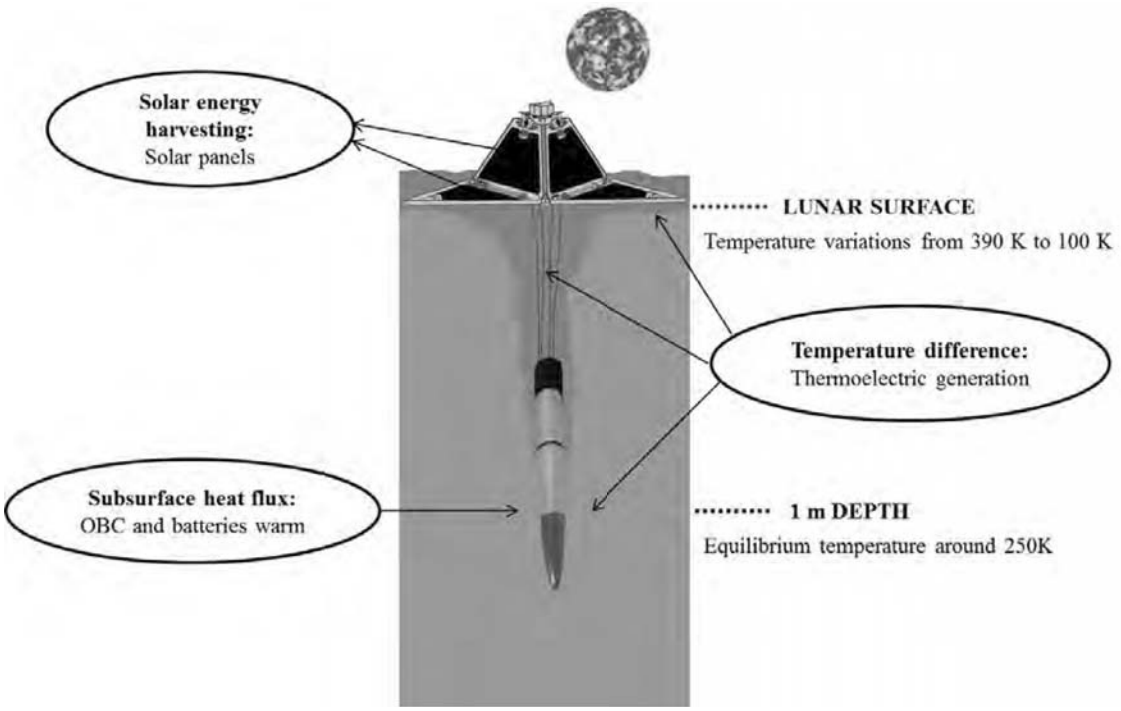

Figure 9.1: Overview of the harvesting techniques conceived for the platform

Solar energy using solar cells is foreseen as the major energy source. The long (and obviously always sunny) days over the Moon surface will provide a great amount of energy for the small platform (refer to the work-out values of $\frac{W}{m^2}$ in figure 6.10). The faces and petals of the tetrahedron platform are covered with solar cells, thus providing the means to transform the solar irradiance in electrical energy, that will be stored in the primary and auxiliary batteries of the platform. However, this energy stored will be lost when the temperatures over the Moon surface descend during the long and cold nights. Even the most advanced Lithium batteries under development at NASA auspices could not go below -60°C ([Bugga et al., 2007]). In the configuration conceived the batteries would start to be inoperative to maintain a nominal function of the electronics subsystems around -40°C. Herein it is proposed, as second method for energy harvesting, to use the heat flux of the subsurface to maintain the batteries at a constant temperature around -23°C.

Finally the third method for energy harvesting is to use the temperature difference between the surface and the subsurface to, using a Thermoelectric Generator, generate a small quantity of energy in form of electrical current that will charge the subsurface batteries during the cold nights.

9.3.1 Energy harvesting for space exploration

The Moon is a small planetary body, and there is good reason to believe that it has lost most of its initial heat during its 4.6-b.y. history. Most of the present heat flux is probably generated by radioisotopes (mainly 40K, 232Th, 235U, and 238U) present in the interior to a depth of about 300 km ([Heiken et al., 1991] after [Langseth et al., 1976]). This heat flow was measured experimentally during the Apollo missions 15 and 17 and the equilibrium temperature of the lunar regolith measured was about 254 K at the Apollo 15 landing site whose latitude is 26.13°N, and about 258 K at the Apollo 17 landing site at latitude of 20.19°N ([Ran and Wang, 2014]). Figure 9.2 shows the temperature increase in function of the depth using the revised data obtained during the Apollo missions ([Langseth et al., 1976]).

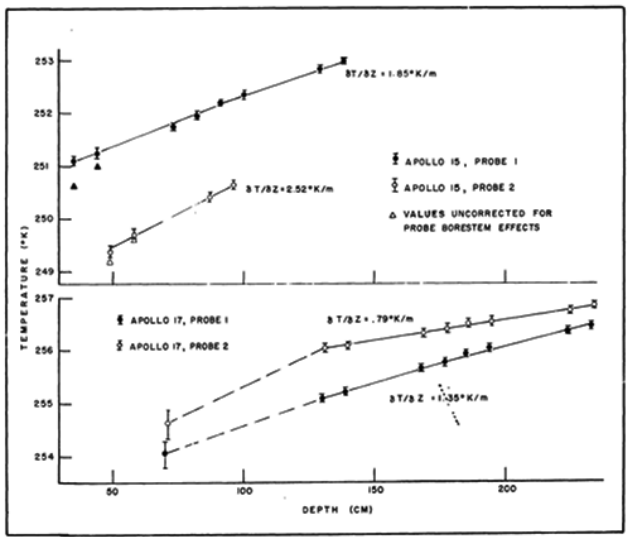

Figure 9.2: Mean substrate temperature at the four probes from the Apollo missions in function of depth (extracted from [Langseth et al., 1976]).

Following the results obtained from [Ran and Wang, 2014] and the measurements obtained during the Apollo missions ([Langseth et al., 1976]) it can be stablished, for mean latitudes, an equilibrium temperature of approximately 250 K at a depth of 1 m. Actually as shown in figure figure 9.2, at a depth of 200 cm this temperature is already reached.

This constant temperature will be used to maintain the OBC and the batteries at a constant temperature within their operative range of the batteries. As described in chapter 7 the estimated depth reached by the penetrator part of the platform will be between 0.3 to 1.2 meters, pending on factors as penetration angle and materials

present in the lunar regolith. As shown in figure 9.2, even in the worst case estimation, it would be possible to use the thermal heat of the Moon´s subsurface to maintain the batteries and the OBC operative during the lunar nights.

9.3.2 Thermoelectric generator

Innovative custom Thermoelectric Generator design

During the cold nights, the energy stored in the batteries located within the penetrator will permit the OBC to be operative. As previously described, the node will be in a hibernation state most of the time and perform sporadic measurements in function of the available energy. With the objective of increasing the number of measurements during the nights, and in this way increase the scientific data return of the mission, an alternative energy source during the night shall be considered. Herein it is proposed the use of the temperature difference between the lunar surface and the lunar sub-surface during the nights, in order to harvest a small but constant amount of energy that will permit to increase the platform activities during the lunar nights.

Electrical energy can be obtained from thermal energy by thermoelectric or pyroelectric transducers. The main difference is that the pyroelectric transducer uses the temperature variations in time to generate an electrical power while thermoelectric principle is based on temperature variation in space.

Thermoelectric Generators (TEG) are commercially available as slim devices (3-5 mm in height) with a large surface area for heat exchange as shown in figure 9.3. These optimized devices are able to obtain several watts of power with an efficiency typically around 5%. Practical devices are made of multiple pairs of p-type and n-type semiconductor legs (thermocouples). The Seebeck effect ([Shakouri, 2011]) is the principle of working of TEG. For each material, the cooling effect is gauged by the Peltier coefficient Π that relates the heat carried by the charges to the electrical current through $Q = \Pi \cdot I$. The power generation is measured by the Seebeck coefficient α, which relates the voltage generated to the temperature difference through $V = n \cdot (\alpha_1 \cdot (T_h - T_c) + \alpha_2 \cdot (T_h - T_c)^2)$. Using several elements electrically in series and thermally in parallel the operating voltage is increased, while reducing its electric current. Such an arrangement minimizes parasitic losses in the series electrical resistance of the wires and interconnects. The thermocouples are connected in series using an electrical shunt thermally in contact with a ceramic substrate that is used as insulator. Both ceramic surfaces in each side of the TEG can be put in thermal contact with the hot and cold sources (heat exchangers are frequently used to increase the heat exchange efficiency).

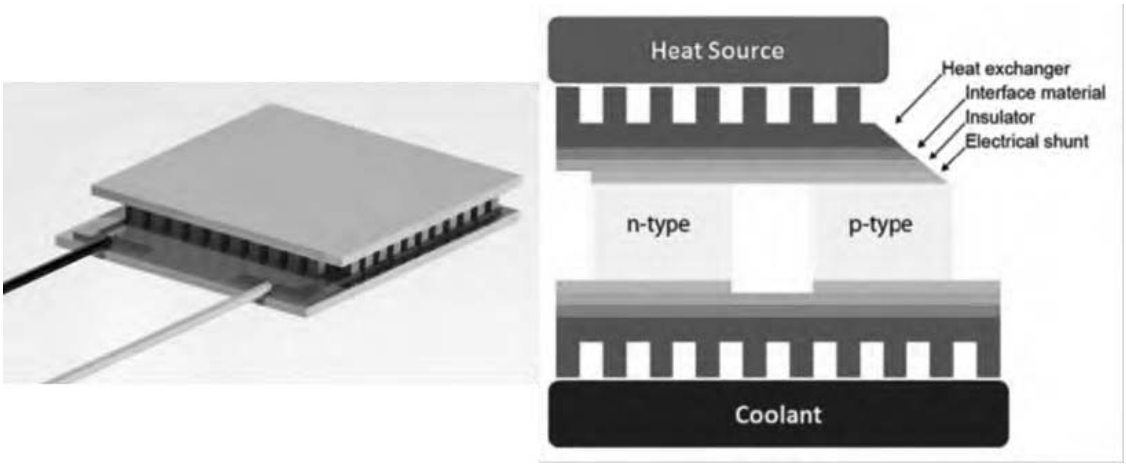

Figure 9.3: Commercial thermoelectric generator system from Marlow Industries ([Marlow Industries, 2015], model XLT6-4-01LS) (left) and schematic section of a TEG (right), extracted from [LeBlanc, 2014].

Commercially available TEG cannot be used in the proposed platform directly. The heat and cold sources are separated several hundred of centimeters. A traditional way to solve this problem is the use of heat pipes to transfer the heat from the heat source to the cold side. Usually this heat pipes use liquids to improve the heat transfer efficiency. The use of such devices would represent an important challenge at very low temperatures (100K) and also they would increase the mass and complexity of the platform. Also we should consider a reliability reduction because of the difficulty of protect the heat pipe system from the high level shock during the landing.

Another approach proposed by [Lorenz, 2003], is to use the penetrator body to conduct the heat and use commercial TEG with heatsinks to capture some energy flowing through the subsurface due to diurnal heating by Sunlight. This interesting approach was found not compatible for the platform proposed as the penetrator body will be situated several cm below the surface where the heat flow is drastically reduced (figure 9.3). Additionally the concept proposed by [Lorenz, 2003], uses the near surface heat change during the diurnal cycle, while in the application herein proposed the interest is to obtain energy during the night and far from the surface. Another important drawback of using this technique is that commercial TEG use ceramic plates that are fragile and not suitable for hard landing applications.

The TEG proposed in this thesis is based in a simple bundle of wires. Robust, extremely cheap and flexible, this TEG can extract small amounts of energy continuously during the lunar night thus charging the batteries for punctual

experiments during the cold nights.

In the TEG construction herein proposed the length of the two dissimilar semiconductors will increase drastically with respect to the commercial TEG devices, thus changing the TEG construction completely. As the minimum distance required to obtain the maximum temperature difference is 200 mm (refer to section 9.3.1) the following design approaches have been followed:

- The P and N semiconductors bars are substituted by two dissimilar metal wires. Even though the semiconductors present larger Seebeck coefficients than metals, the concept proposed requires wires to cover the distance between the hot side and cold side. Several wires of two dissimilar metal conductors will be connected in series and parallel following a custom configuration. The wire metals selected shall be able to support elevated tensile forces and be available commercially as wires. The selection of the TEG materials shall be based in the following considerations:
  - New semiconductor elements have been developed for the TEG industry, increasing the Seebeck coefficient of metals two order of magnitude and new developments promises even higher values ([LeBlanc, 2014]). Unfortunately, these semiconductors cannot be fabricated easily in the form of thin and robust wires. This is the main reason why commercial thermocouples used for remote temperature monitoring are always metallic.
  - Low resistivity of the materials selected will improve the TEG efficiency.
  - The operation temperature of the TEG drastically affects the Seebeck coefficient. The thermocouple materials used in the TEG proposed shall be compatible with low temperature application (100 K).The materials selected for the TEG are iron (99.5% Fe) and Constantan (45% Nickel-55% Copper alloy). This combination of metals is used in the industry for temperature measurement and is referred as type "J"thermocouple. Iron and constantan thermocouples are suited for vacuum operation maintaining a reasonable Seebeck coefficient below 90K and both metals have good conductivity characteristics.
- The wires are packaged in a bundle as described in the figure 9.4. This packaging will provide the stiffness to the wirings set and would avoid short-circuits. Up to 38 thermocouples in a bundle can be packed in this way. The wires have a diameter of 2.5 mm and are coated to avoid short-circuits between wires. The complete bundle, including the external PTFE cover, has an external diameter of 2.23 cm, is 200mm long and its total mass is near 700 gr.

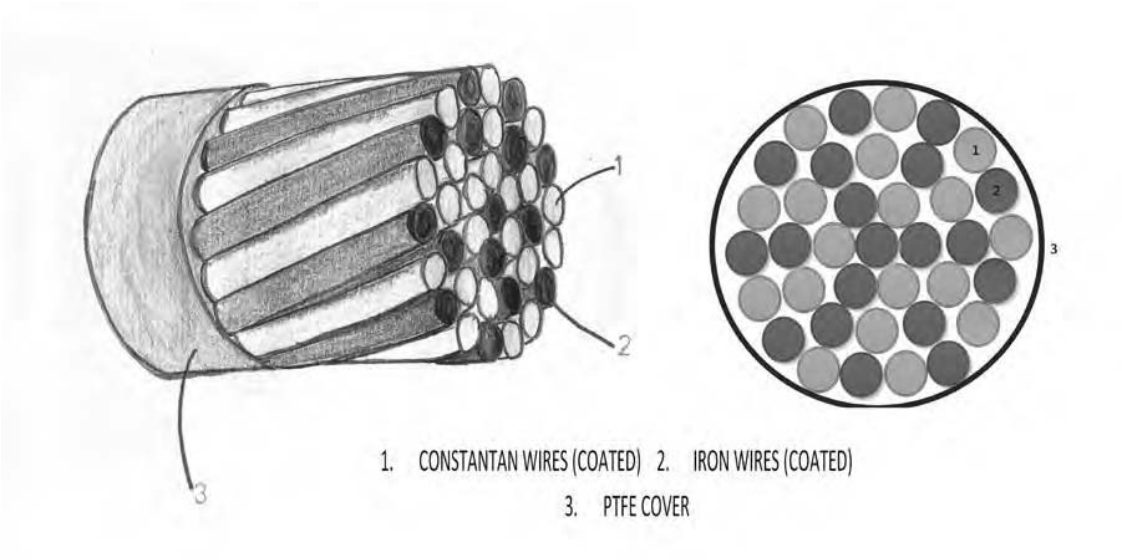

Figure 9.4: Proposed metal wires bundle sketch

- The dissimilar metal wires are connected in series using copper straps that are embedded in an electrically insolating and high thermal conductivity epoxy (e.g. EP37-3FLFAO, [Master-Bond-Inc., 2015]). The fragile ceramic substrate is herein substituted by the high thermal conductive epoxy that will protect the electrical contact from the high level shocks during the landing impact. Additionally the epoxy could be embedded directly into an aluminum structure, thus providing the thermal contact with the heat sources directly. An elevated number of metal wires connected in series would imply an elevated TEG internal resistance what would mean a very poor efficiency. In the following section a detail analysis of the internal resistivity of the TEG proposed is accomplished.

- The TEG proposed is a low voltage and high current output electrical source. This low voltage output cannot be directly used for batteries charging. Additionally we have to consider that the efficiency of the TEG will depend on the load resistor at the output of the TEG (a thermoelectric module generates maximum power when the module resistance matches the load resistance, as following described). Moreover, the batteries impedance will vary depending on the State of Charge. Considering the MP144350 model of lithium-ion batteries for space application ([Saft, 2009]) the internal impedance (RL) of the batteries

can be modeled in function of the SOC in the following way:

$$R_L = \frac{5 - SOC}{100}[\Omega] \tag{9.1}$$

In order to optimize the energy provided for charging the batteries, a DC/DC converter and a Maximum Power Point Tracking (MPPT) system shall be used. Several high gain DC/DC converters and MPPT architectures are proposed in the literature specifically designed for batteries charging using low voltage output TEGs (e.g. [Huleihel et al., 2012], [Laird and Lu, 2013] or [Kinsella et al., 2014]). The OBC, implemented in a FPGA, can easily include a parallel logic block necessary for the MPPT control.

- Finally we have to consider that in the application herein proposed, the hot and cold sides are interchanged during the day and night lunar cycle: the buried penetrator side will remain at a constant temperature of around -23°C as previously introduced. The temperature surface will vary depending on the selenographic latitude and longitude and the date as described in section 6.5.2. Thus the current flow of the thermocouples will vary its polarity along the lunar day. As during the day the solar cells will provide the energy necessary for the node operation and batteries recharging the TEG will be not used

Thermoelectric Generator mathematical model

A mathematical model is required to predict the power generated by the custom TEG design. This model will be used by the OBC during the planning procedure to estimate the power generated by the TEG in the following hours or days. Therefore, as in the mathematical models described previously, the model shall reduce as much as possible the OBC processing effort (power consumption reduction) without compromise the results accuracy.

Departing from the TEG equations described in the literature ([Shakouri, 2011], [Dughaish, 2002], [Gaowei et al., 2010], [Montecucco et al., 2014] and [Cardarelli, 2008]) and considering the peculiarities of the TEG proposed in this thesis a new mathematical model has been derived.
The heat flux in a thermocouple can be expressed as:

$$\dot{Q} = k \cdot (T_1 - T_2) \tag{9.2}$$

Where the thermal conductivity of the thermocouple can be obtained from the respective conductivities of each of the two materials which form the thermocouple:

$$k = n \cdot \left(\frac{(\lambda_n \cdot A_n)}{l} + \frac{(\lambda_p \cdot A_p)}{l} \right) \tag{9.3}$$

In this equation l is the length of the metal wires (considering both wires have the same length) and A_n and A_p are the cross section area of each wire. Herein the index n refers to the material with the most negative Seebeck coefficient. Finally, λ_n and λ_p correspond to the thermal conductivities of each material. The parameter n is the number of thermocouples connected in series. The temperature difference across the TEG generates an open circuit potential related with the Seebeck coefficient ([V/K]) of the thermocouple. A quadratic expression based in the Seebeck coefficient of the iron-constantan at 125K is herein used as conservative approximation.

$$V = n \cdot \left(\alpha_1 \cdot (T_h - T_c) + \alpha_2 \cdot (T_h - T_c)^2\right) \tag{9.4}$$

As the arrange of thermocouples are connected in series the TEG open circuit potential shall be the summation of all the potentials generated by each individual thermocouple. α_1 and α_2 are the thermocouple Seebeck coefficients ([V/K]) at 125K.

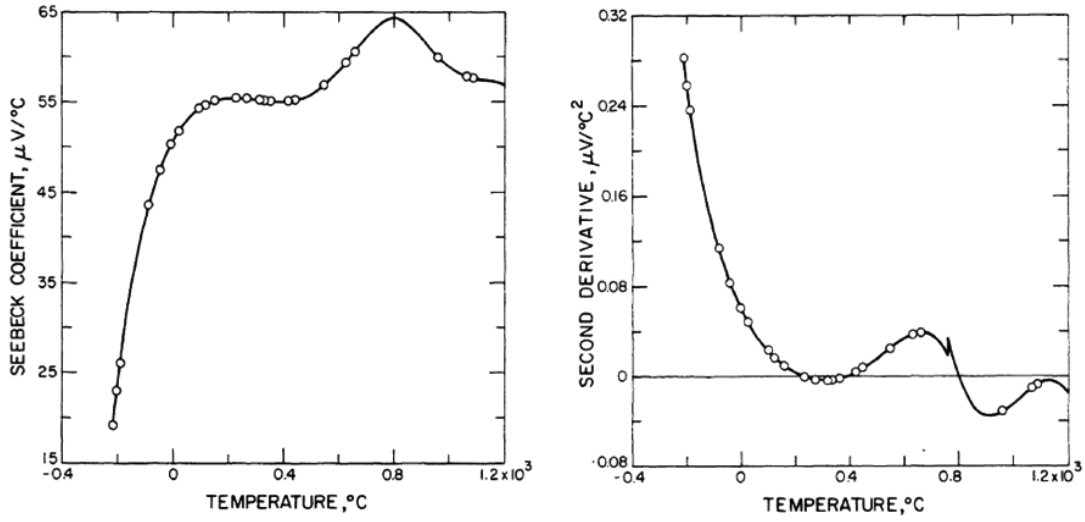

Figure 9.5: First and second derivative Seebeck coefficients for type J thermocouples in function of the temperature (extracted from [Powell et al., 1974])

In steady state conditions, the heat transfer thru the wires for n thermocouples connected in series can be obtained from the following relations:

$$\dot{Q}_h = n \cdot \left[\alpha \cdot I \cdot T_h + k(T_h - T_c) - \frac{1}{2} \cdot I^2 \cdot R\right] \tag{9.5}$$

$$\dot{Q}_h = n \cdot \left[\alpha \cdot I \cdot T_h + k(T_h - T_c) + \frac{1}{2} \cdot I^2 \cdot R\right] \tag{9.6}$$

Where the h, and c indexes refer to the hot a cold unions of the thermocouple respectively. In this way T_c and T_h are the cold and hot temperatures in each junction of the thermocouples array. The TEG equations can be simplified for the TEG herein proposed if the temperature of the thermocouples end junctions is considered not variant in function of the heat extracted as consequence of the metal connections between the hot and the cold sides. In the TEG construction proposed this is a good approximation as the heat extracted from the hot side to the cold side is below 100 mW. Considering the good thermal conductivity of the TEG construction with respect to the environment in both parts (good thermal conductivity epoxy with a metal frame), the temperature difference between the thermocouple joints and the hot and cold environment respectively can be neglected. In a commercial TEG, this is not a valid assumption because of the poor thermal conductance of the ceramic elements used in the commercial TEG arrangement (figure 9.3).

It is important to distinguish between the open circuit potential and the TEG output potential when the TEG is connected to an impedance load. The effective voltage output of the TEG is reduced as consequence of the thermocouple internal impedance and the current flowing thru the circuit.

There is need to precisely determinate the resistance of the thermocouple and the load resistance. These two values will be directly related with the efficiency and current provided by the TEG. The thermocouple resistance is the main parameter to be optimized for the TEG construction proposed. The long wires connected in series imply a high thermocouple internal resistance that has to be minimized as much as possible.

The resistance of n thermocouples connected in series can be calculated as:

$$R_T = (R_{contact} \cdot n) + n \cdot l \cdot \left(\frac{\varphi_n}{A_n} + \frac{\varphi_p}{A_p} \right) \tag{9.7}$$

Where φ_n and φ_p are the resistivity of the two metals used and $R_{contact}$ is the contact impedance of the copper straps that connects electrically in series the two materials that forms each thermocouple. Soldering these junctions using lead-tin will reduce their impedance without affecting the TEG performance. Considering the previous equation, we can reduce the total thermocouple impedance in the following way:

- Select materials with a high conductivity.

- Increase the wires diameter as much as possible. Herein a tradeoff between the total diameter of the bundle and the diameter of each wire has to be considered. The physical arrange previously described permits a compact bundle of wires up to 2.5 mm in diameter.

- Reduce the length of the wires. A minimum length of 200 mm shall be considered to use the maximum temperature difference between the surface temperature and the stabilized inner temperature (figure 9.2).

Considering n thermocouples connected in series the effective voltage, current, power and efficiency can be calculated as follows:

$$I_L = \frac{n\cdot(\alpha_1\cdot(T_h - T_c) + \alpha_2\cdot(T_h - T_c)^2)}{R_T + R_L} \tag{9.8}$$

$$\tag{9.9}$$

$$P_L = I_L^2\cdot R_L \tag{9.10}$$

$$\tag{9.11}$$

$$\eta = \frac{P_l}{Q_h} = \frac{I_L^2\cdot R_L}{n\cdot\left[\alpha\cdot I\cdot T_h + k(T_h - T_c) - \frac{1}{2}\cdot I^2\cdot R\right]} \tag{9.12}$$

The maximum efficiency of the TEG designed can be obtained when the load impedance matches the thermocouple impedance.

With the mathematical model developed a TEG was designed in order to optimize the power output characteristics, reducing as much as possible the total mass of the TEG. In table 9.3 it is summarized the main parameters of the TEG proposed:

Parameter	Unit	Value	Notes
Material n	N/A	Constantan (45Ni-55Cu)	Thermocouple type J
Material p	N/A	Fe(95%)	
A_n	mm^2	4.9087	Design
A_p	mm^2	4.9087	Design
n	N/A	38	Number of wires in series.
α_1	$\mu V/K$	33.5	Thermocouple type J at 125K. (Powell 1974)
α_2	$\mu V/K$	0.186	Thermocouple type J at 125K. (Powell 1974)
φ_n	$\mu\Omega \cdot cm$	48.9	Cardarelli 2008
φ_p	$\mu\Omega \cdot cm$	7.9	Cardarelli 2008
λ_n	$W/K \cdot m$	19.5	Cardarelli 2008
λ_p	$W/K \cdot m$	80	Cardarelli 2008
l	m	0.2	Thermocouples length
$R_{contact}$	Ω	0.01	10 $m\Omega$ for soldered junctions
$\eta_{DC/DC}$	%	90	Laird 2013

Table 9.3: TEG for the lunar platform exploration characteristics

Using the parameters listed in the table 9.3 and the mathematical model previously described, the TEG proposed has been evaluated and results are presented in table 9.4. The following operating conditions are considered:

- Steady state during the lunar night with $T_h = 250.15K$ and $T_c = 100K$.

- RL adapted by a MPPT system and a DC/DC converter.

Parameter	Unit	Value	Notes
$V_{opencircuit}$	[mV]	354	Open circuit
V_{out}	[mV]	177	Considering $R_{LOAD} = R_{TEG}$
I_L	[mA]	141	Considering $R_{LOAD} = R_{TEG}$
P_L	[mW]	25.01	Considering $R_{LOAD} = R_{TEG}$
η_{TEG}	%	0.37	Considering $R_{LOAD} = R_{TEG}$
Mass (thermocouples)	Kg	0.6256	

Table 9.4: TEG designed output characteristics for steady state condition ($T_h = 250,15K$ and $T_c = 100K$ and $R_L = R_{TEG}$)

Using the lunar temperature surface mathematical model developed and described in section 6.5.2 in combination with the model previously described, we can obtain the power generated from the TEG during one lunar cycle (figure 9.6). As shown in figure 9.6, the total energy harvested during one lunar night is above 19 kJ (considering conservative Seebeck coefficients at 125K and conversion electronics with an efficiency of 90%). This energy will permit to compensate the OBC sporadically consumption and use the energy stored in the principal battery and harvested during the day to heat up the aftbody and perform punctual measurements during the night.

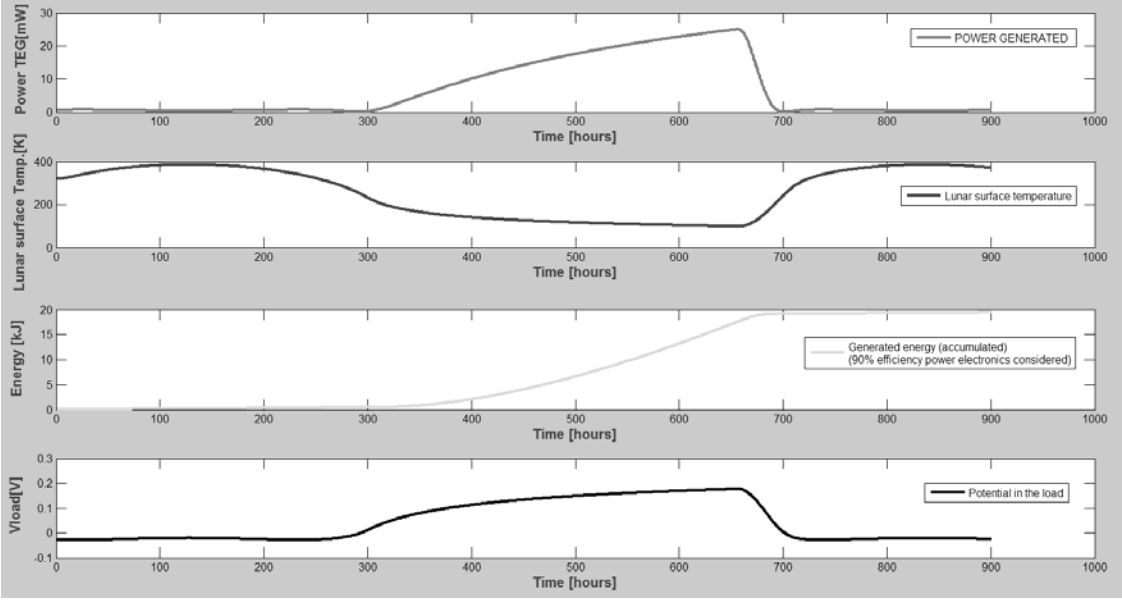

Figure 9.6: TEG performance during one lunar cycle

9.3.3 Solar energy harvesting

Solar panels design

The proposed platform harvests the great part of the energy from the Sun using solar cells. Solar panels cover the outer surface of the platform. The tetrahedral platform permits to locate solar cells in each of its three faces, thus harvesting energy from any of them independently of the platform orientation and the Sun position in the lunar sky.

As depicted in figure 5.1 and figure 7.3 the aftbody integrates three different sets of solar panels:

1. Solar panels in the outer side of the solar petals. These panels are aimed to provide the required energy to the platform to open the solar petals using the release mechanism described in section 5.2.4. Once deployed, these panels will be no longer used for energy harvesting as they will be facing the planet surface.

2. Solar panels located in the inner part of the solar petals. Once the solar petals are deployed these panels will be directly facing the sky to harvest the solar energy during the lunar day.

3. Solar panels located in each face of the tetrahedral platform. These panels will be exposed to the lunar environment when the solar petals were deployed.

The solar cell selection is of major importance to optimize the panel performance. In the last decades several new photovoltaic (PV) technologies have evolved to obtain nowadays efficiencies above the 30%. The solar energy is the main power source in the satellite market, thus PV technologies for space are mature technologies with a large heritage. The solar cells required for the platform herein proposed share the same requirements that the satellite market in terms of radiation, operational temperature range, high efficiency and reliability. However, the platform proposed poses new requirements to the solar panels as high shock, ultra-low temperature survival and dust contamination between others.

The solar panels construction conceived for the platform proposed is based in the following design considerations.

- The solar panels are mounted directly on top of flexible PCBs which incorporates the solar cells interconnections, circuitry and protection diodes. In this way the solar panels are attached to the aluminum metal frames of the platform structure. In the case of the solar petals, the PCBs that support the solar panels have solar cells installed in both PCB sides, enabling solar harvesting when the solar panels are non-deployed and deployed as previously described.

- The solar cells selected are flexible solar cells. High efficiency flexible solar panels are currently in an advance TRL for space application, and in the following years will be commonly used in numerous missions ([Beernink et al., 2007], [Law et al., 2006], [Trautz et al., 2013] and [King et al., 2006]). These high efficiency solar cells have the advantage of be low mass and more tolerant to vibration and shock than the traditional rigid approximation. A 28% efficiency is supposed for this solar cells based on [Edmondson et al., 2006].

- The flex solar cells are mounted following a sandwich approach. Flex polyimide PCB works as subtract for the solar cells mounted on top. A polymer, transparent to the wavelengths of interest, is deposited on top of the solar cell. This polymer will integrate the dust removal technology as later explained. The solar panels are structurally supported by the aluminum structure of the petals. As explained in section 7.2.3 solid sublimating material permits the cohesion of the different elements protecting the solar cells during the landing impact.

- Dust removal technology is proposed in order to reduce the dust accumulated over the solar panels, extending in this way the mission life. The dust removal technology proposed for this platform is based on the electric curtain concept

developed by NASA in 1967 ([Tatom et al., 1967]), and later developed, improved and refined during the following years by numerous researchers. Its working principle is based on a series of parallel electrodes connected to an AC source that generates a traveling wave acting as a contactless conveyor. Particles are repelled by the electrodes used to produce the field and travel along or against the direction of the wave, depending on their polarity as explained in [Calle et al., 2008]. This technique is particularly suitable for the platform proposed as it can be integrated easily in the sandwich structure previously introduced. Additionally, during the lunar days there is power in excess to perform punctual cleaning procedures in order to maintain the solar cells clean from dust.

Solar energy harvesting mathematical model

A mathematical model is required to predict the power generated by the solar cells in function of the solar irradiance received in each solar panel of the platform. This model will be used by the OBC during the planning to estimate the power generated by the solar cells in the following hours or days. Therefore the model shall reduce as much as possible the OBC processing effort (power consumption reduction) without compromise the results accuracy.

The solar cells produce electricity from Sun with a certain efficiency that is directly dependent on the technology and external factors as the temperature. The solar cell efficiency can be obtained with the following mathematical relation:

$$\eta = \frac{(V \cdot C)_{max}}{I \cdot A} \tag{9.13}$$

Where $(V \cdot C)_{max}$ is the maximum power produced (as product of potential and current) by the solar cell or panel at 25°C, I is the solar irradiance in W/m^2 necessary to obtain the maximum power output of the cell and A is the solar cell area illuminated.

From this efficiency parameter it is possible to estimate the power generated by the different solar panels in function of the solar irradiance energy I with the following relation:

$$W = \eta \cdot P_F \cdot I \cdot A \tag{9.14}$$

The parameter P_F (with values between 0 and 1), is the packaging factor used to derive the effective cell area in the panel accounting the area loss between cells due to wiring or empty spaces required for thermal contraction and expansions of the solar panel.

The solar cell area illuminated in each moment directly depends on the platform orientation with respect to the Sun and the solar incident angle. The solar incident angle is obtained from the mathematical model developed in chapter 6.4.2 and the platform orientation (ϑ) w.r.t the lunar equator is an input for the mathematical model. With these two parameters it is possible to use geometrical relations to discretize the solar area illuminated.

The model generated provides the power generated in each solar panel in function of the date, solar irradiance, solar incident angle, selenographic latitude and longitude and platform orientation (ϑ) w.r.t the lunar equator:

$$P_{solar\_panel}\,[W] = f(t, I, a, \lambda_d, \varphi_d, \vartheta) \tag{9.15}$$

The construction parameters of the solar cell are shown in table 9.5.

Parameter	Unit	Value	Notes
Petal solar panel area	m^2	0.01151	70% of area available effective for solar panels
Faced solar panel area	m^2	0.009222	
η	-	0.28	From Law 2006
PF	-	0.84	From Law 2006

Table 9.5: Solar panels parameters construction

Figure 9.7 presents the energy results obtained using the model developed for 1 lunar day (January 2016), with the face 1 of the platform oriented with respect to the lunar equator and been the platform located in the lunar equator (0°latitude, 0°longitude).

As it can be appreciated in the figure, the power generated per each cell depends on the Sun angular incidence. In the example selected, the solar cells located in petal 1 and face 1 are directly facing the Sunrise, thus generating power during the first part of the day. When the Sun is at the zenith all the solar cells generates power at their respective maximum. As the Sun advances to the Sunset, the solar cells located in petal 1 and face 1 start progressively to enter in the dark area and are the rest of the solar cells which continue providing power to the platform node until the Sunset.

The total power generated in the equator has a maximum peak of 19.37 W (solar at zenith). In this calculations we have not consider the electronics efficiency that will reduce around a 10% to 15% the power generated. Additionally, as explained in section 6.4.2 and shown in figures 6.10 and 6.11, the solar irradiance decrease as function of the latitude. Using the model generated it is possible to plot the maximum power harvested during the zenith in function of the selenographic latitude (figure 9.8).

As it can be appreciated in figure 9.8, the maximum power harvested is drastically reduced as the incident angle reached by the Sun is reduced in function of the

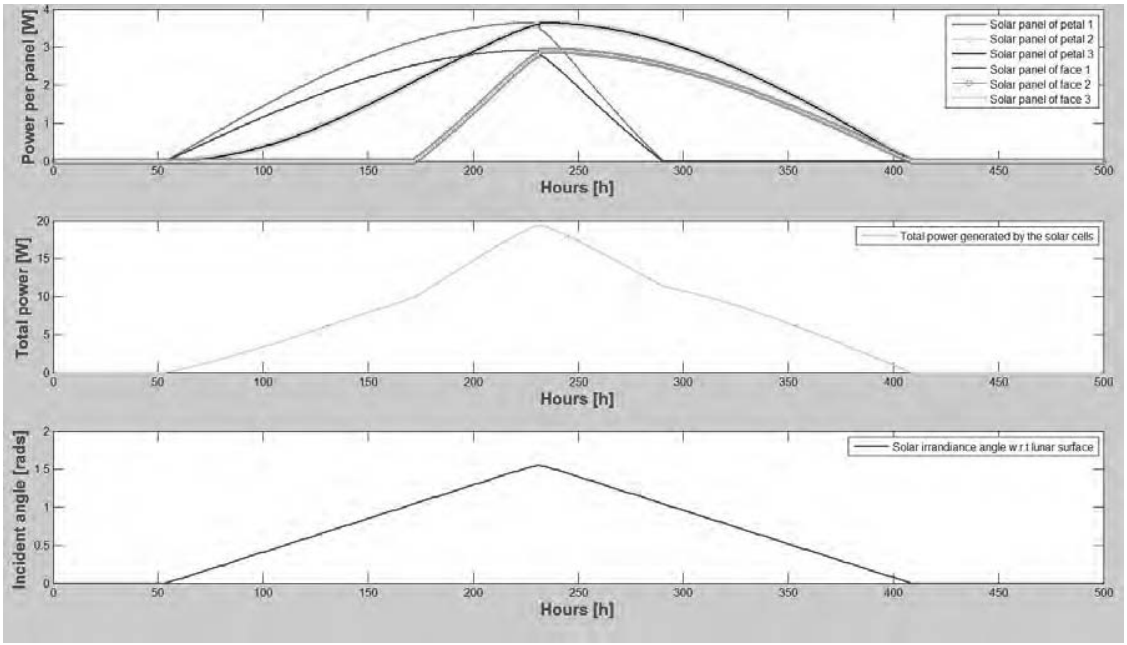

Figure 9.7: Solar power generated per solar panel (top), total power generated by all the solar panels (centre) and solar incident angle (bottom). Data obtained for January 2016, 0°latitude,0°longitude and solar panel 1 facing the lunar equator.

latitude. In figure 9.8, the different slopes in the maximum power harvested, as the latitude increases, are due to the geometrical disposition of the different solar panels in funciton of the decreasing incident solar angle.

An immediate conclusion obtained from figure 9.8 is that the platform proposed cannot be used for poles exploration as the power obtained from the solar panels would be near to cero during the winter .

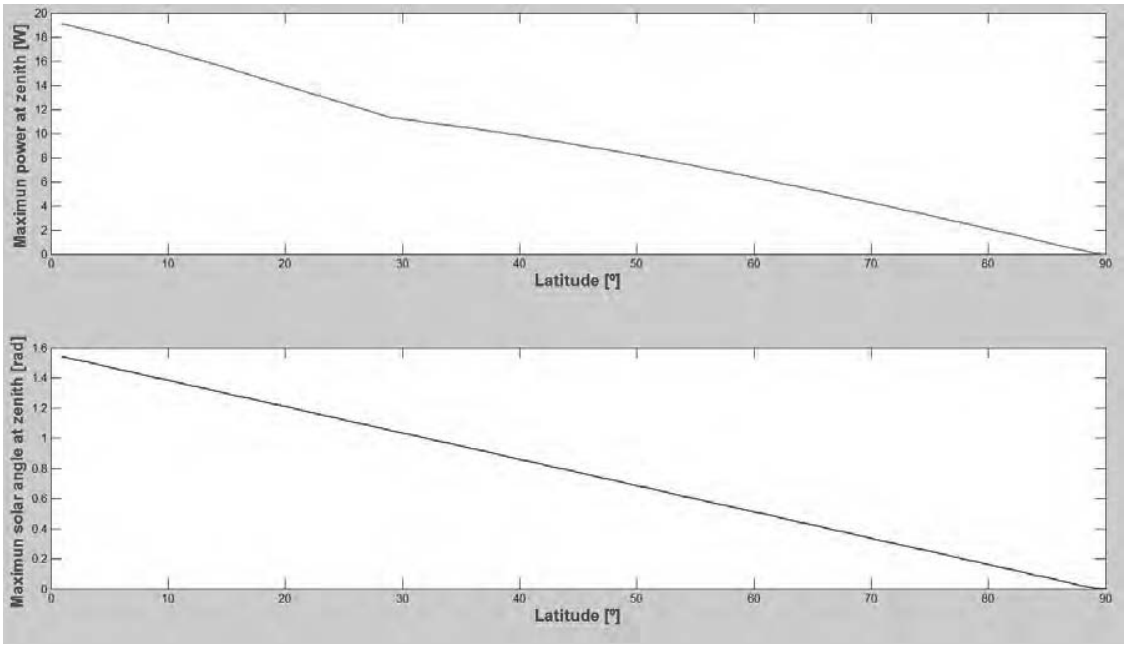

Figure 9.8: Maximum solar power harvested for January 2006 in function of the increasing latitude towards North Pole (top); and maximum solar angle of the Sun in function of the latitude (bottom)

Chapter 10

High level control architecture

10.1 Control architecture introduction

The exploration platform herein conceived is based on a complete autonomous behavior. During a great part of surface operation time the platforms that conforms the WSN will be unable to communicate with the orbiting satellite, the only link between the nodes and the GS (Ground Segment). GS comprises all the Earth stations and operation centers that are in charge of the network communications systems with a satellite or spacecraft.

The line-of-sight (LoS) duration of the link satellite with the platforms, in the case of the Moon scenario, is around 18 minutes duration every 2 hours and 20 minutes for an orbital inclination of 0°(as described in the Mission Design Report of SWIPE, [Crosnier et al., 2013a]). Also, we have to consider that for the period of the lunar nights the reduced power availability could avoid platform communications with the orbiting satellite during a great part of the night duration. The reduced link time shall be prioritized for data uploading reducing the downloading data as much as possible.

One approximation, commonly followed in satellites control, is that the GS implements all the planning and control activities. Therefore, the planning sequence of commands is calculated in Earth and transmitted to the orbiting satellite that will execute them as received. This low autonomy of the satellite is feasible while the time lack between the satellite and the GS is just of few seconds and the non-line-of-sight duration is highly reduced (several GS stations distributed around the globe could reach a virtual 100% satellite coverage during the orbit).

This control paradigm changes drastically for planetary surface exploration. As previously described. the reduced LoS duration and the high lack time between the GS and the SS (Space Segment) require another spacecraft control approximation. In this case the SS will take the responsibility of planning its own optimized tasks sequence, execute them and even implement automatic recovery routines in case of failure conditions as described in figure 10.1.

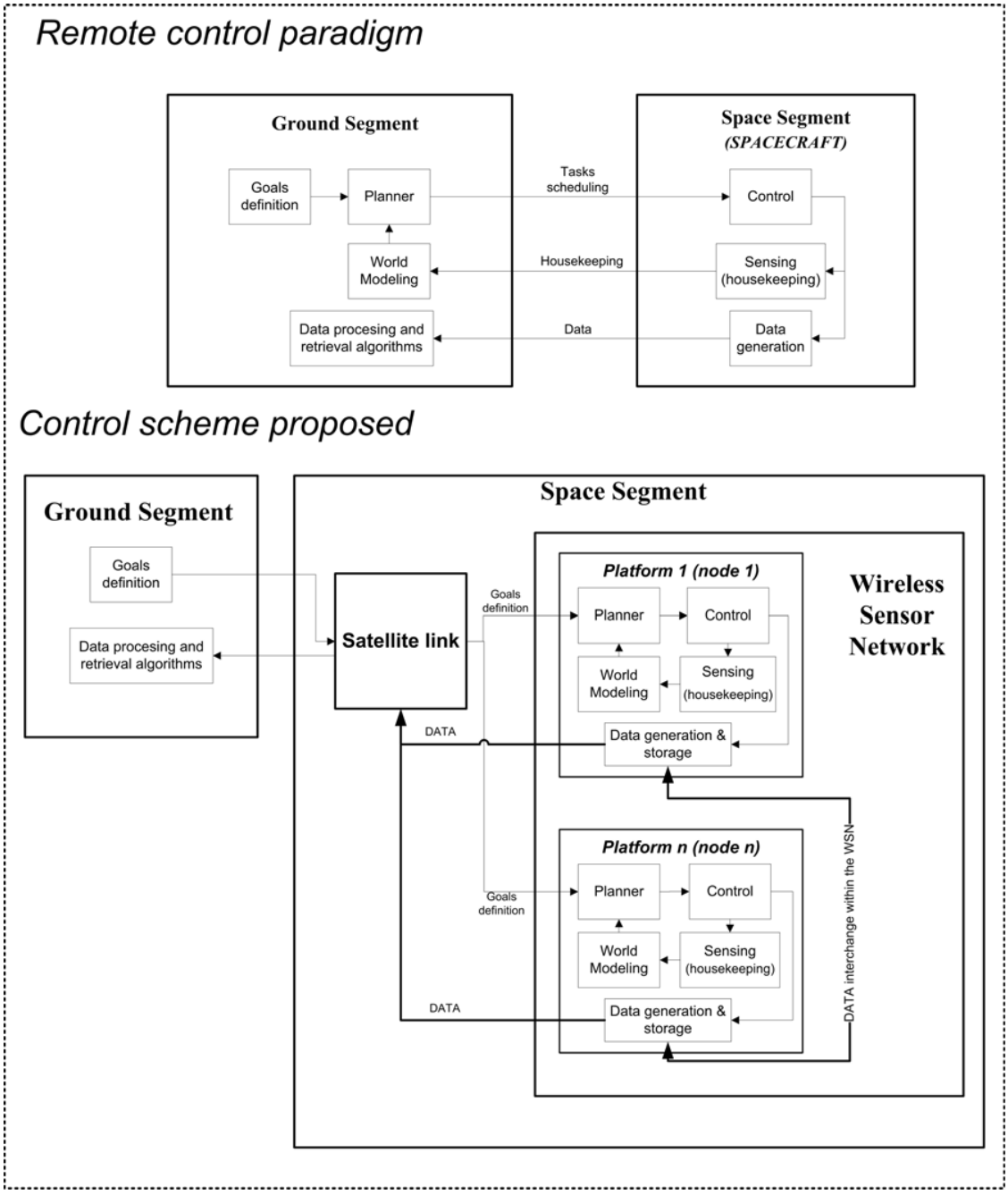

Figure 10.1: Traditional remote control and proposed control scheme.

Therefore, the high level control architecture herein proposed shall be able of achieving a complete autonomous and reliable operation of each WSN node, with the objective of reaching predefined or dynamic objectives and also reacting to failures or unpredicted situations considering the changing environment.

Different high level control architectures in robotics have been proposed around the last 40 years. The control architecture paradigm has been traditionally discomposed in how the sense, planning and actuation activities are performed. The traditional approach during the first years of robotic history is to use a "sense-plan-act"scheme, where initially the robot used a world model to plan its activities before to implement them. Brooks ([Brooks, 1991]) introduced other approach, following a "sense-act"architecture where the robot would have special-purpose task-achieving subroutines (often called behaviors) to solve specific problems in a reactive fashion. From here numerous authors proposed a hybrid approach based on a "plan-sense-act". As described in [Bonasso et al., 1997], this approach generates a control architecture with a lowest layer of reactivity, a topmost layer of traditional AI (Artificial Intelligence) planning and a middle layer which transformed the state-space representation of plans into the continuous actions of the robot.

The "plan-sense-act"approach will be used for the definition of the high level control architecture proposed in this thesis.

Figure 10.2 sketches the conceived architecture approach where the planning and checker module would represent the planning top layer of the architecture, the sequencer and the world model estimator would constitute the middle layer and the control layer would be the lowest reactivity layer.

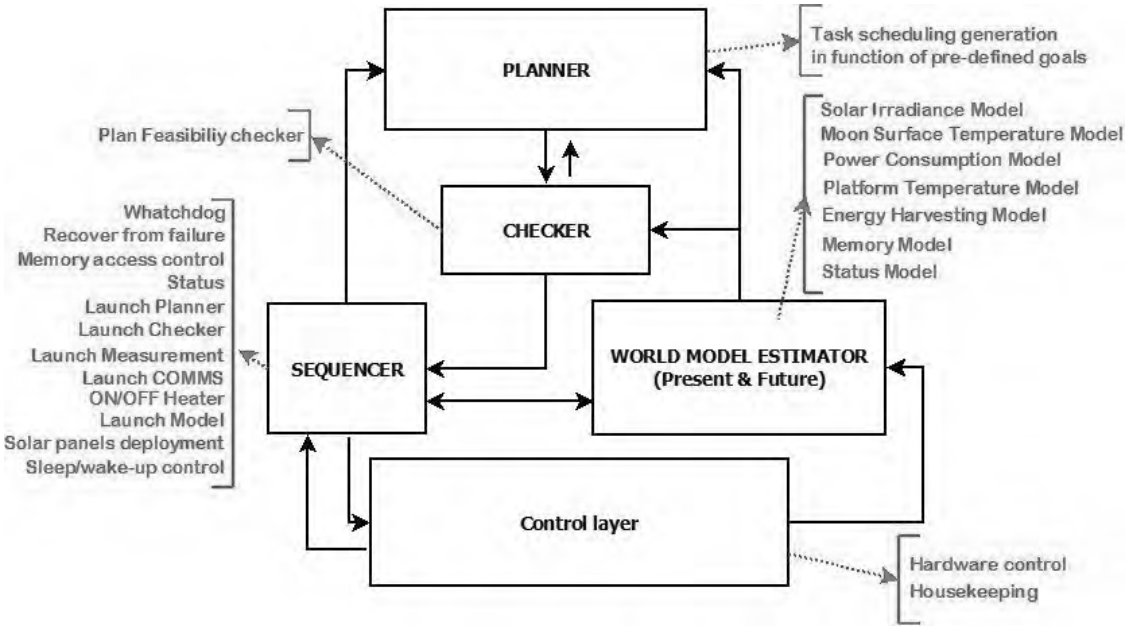

Figure 10.2: High level control architecture proposal.

An important remark is that, as described in section 5.5, the platform designed has two distributed OBCs. A main OBC located in the penetrator body, under the planet surface, and an auxiliary OBC located in the tetrahedral platform at the surface. Both OBC shall share the architecture above described, in the case of malfunction of the main OBC, the auxiliary OBC shall be able to command the node appropriately. The architecture handles this redundant situation thanks to a subroutine implemented in the payload's FPGA and in the OBC sequencer as described in the following subsections. In the following subsections each block depicted in figure 10.2 is described.

10.2 The sequencer

The sequencer is the core element of the proposed architecture and coordinates the control activities of the platform. As part of the middle layer, the sequencer launches as required the modelling, planning or acting procedures.

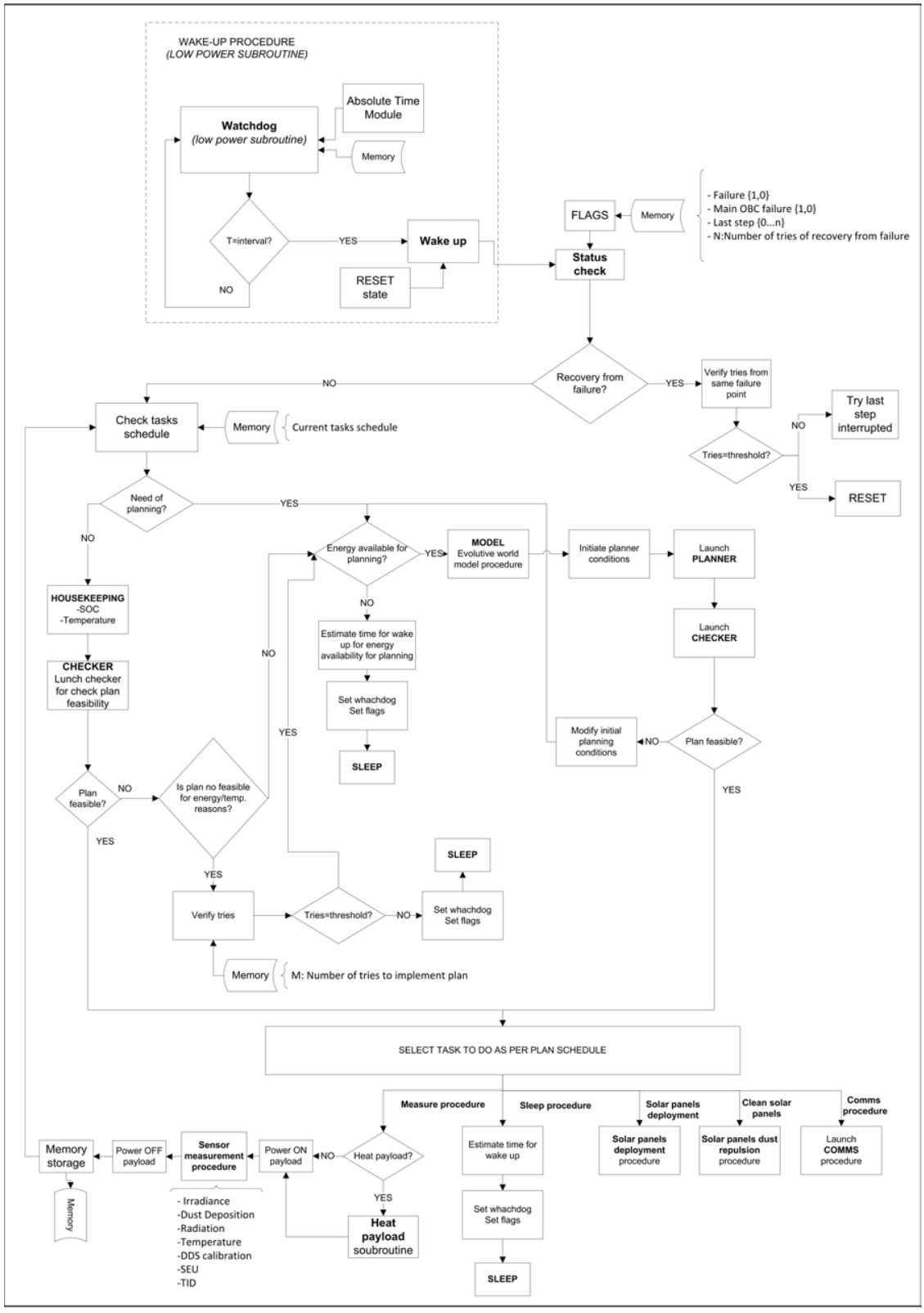
WAKE-UP PROCEDURE
(LOW POWER SUBROUTINE)
Watchdog
(low power subroutine)
Absolute Time Module
Memory
T=interval?
YES
NO
Wake up
RESET state
FLAGS
Memory
- Failure {1,0}
- Main OBC failure {1,0}
- Last step {0...n}
- N:Number of tries of recovery from failure
Status check
Recovery from failure?
NO
YES
Verify tries from same failure point
Tries=threshold?
NO
YES
Try last step interrupted
RESET
Check tasks schedule
Memory
Current tasks schedule
Need of planning?
YES
NO
Energy available for planning?
YES
NO
MODEL
Evolutive world model procedure
Initiate planner conditions
Launch PLANNER
Launch CHECKER
Plan feasible?
NO
YES
Modify initial planning conditions
HOUSEKEEPING
-SOC
-Temperature
CHECKER
Lunch checker for check plan feasibility
Estimate time for wake up for energy availability for planning
Set whachdog
Set flags
SLEEP
Plan feasible?
NO
YES
Is plan no feasible for energy/temp. reasons?
YES
NO
Verify tries
Tries=threshold?
NO
YES
SLEEP
Set whachdog
Set flags
Memory
M: Number of tries to implement plan
SELECT TASK TO DO AS PER PLAN SCHEDULE
Measure procedure
Sleep procedure
Solar panels deployment
Clean solar panels
Comms procedure
Memory storage
Power OFF payload
Sensor measurement procedure
Power ON payload
NO
Heat payload?
YES
Heat payload soubroutine
- Irradiance
-Dust Deposition
-Radiation
-Temperature
-DDS calibration
-SEU
-TID
Memory
Estimate time for wake up
Set whachdog
Set flags
SLEEP
Solar panels deployment procedure
Solar panels dust repulsion procedure
Launch COMMS procedure

Figure 10.3 depicts the proposed sequencer flowchart. The sequencer is based on a fail-safe state machine. The system has to be able to recover from unexpected malfunctions or endless loops. The control system uses two different approaches to recover from unexpected situations:

- Hardware approach: as described in section 5.6, the OBC is reset by an external device if the processor embedded in the FPGA does not generate a control signal every 5 seconds. In this way, if the microprocessor collapses, the external device resets the FPGA, forcing to reboot the firmware of the OBC from an external non-programmable memory. The application memory is also reset.

- Software approach. If during the execution of the different procedures launched by the sequencer the time response of those procedures exceeds a predetermined safe time, the sequencer will be re-started. If the sequencer fails to implement a procedure three times, then it will force a hardware reset.

The sequencer has been defined as a very simplistic state machine that request more complex procedures of the abstraction layer (planner and checker), launches modelling procedures or commands the control layer to start specific control actions following the output obtained from the planner.

As shown in figure 10.3, the sequencer departs from a low power sleep subroutine. The great part of the time the platform will be in an ultra-low power consumption mode. In this mode all the electronics subsystems of the platform would be switch off except for:

- Power subsystems.

- Payload's FPGA (in a low power consumption mode, refer to section 5.6).

- OBC (in a low power consumption mode, refer to section 5.6).

During the low power consumption mode the OBC activity is limited to verify if the absolute timer (integrated in the OBC) indicates that the period of sleep time has concluded. The sleep time was stablished before to enter into the sleep routine. If the timer indicates that it is time to wake up, the first action of the OBC is to check its status. The following flags stablish the control status of the sequencer:

- Failure flag (1,0). If the sequencer was not able to finish a determinate procedure this flag is set to one.

- Last step (0...n). The different procedures are identified with a numerical index. This flag indicates the last procedure launched by the sequencer before to enter in the sleep routine.

- N (0...3). This parameter indicates the number of tries to finish a determinate routine.

- M(0...3). This parameter indicates the number of tries to implement a plan that could not be finished because the energy available or the external temperature was not adequate.

- Main OBC failure (0,1). This flag is set to 1 if the redundant OBC is developing the tasks of the main OBC as explained later.

If the sequencer is recovering from an interrupted procedure, it will check if the number of tries are above three, in this case a hard reset is forced. In case the number of tries tries of recovering are below three attempts, the sequencer will command the last step interrupted.

If the failure flag is set to 0, a nominal operation of the sequencer is executed. The sequencer shall check the schedule and determinate if there is need of planning (no new tasks scheduled). If there is not new tasks in the plan a new schedule shall be obtained from the planner. The planning sequence is as follows:

1. The world model estimator is executed.

2. With the model obtained the planner is launched considering initial planning conditions (temporal time, objectives and parameters that determinate if the objectives are met).

3. The output of the planner is verified using the checker module. If the plan is not feasible, the initial conditions are modified following a defined procedure (relax the objectives or reducing the horizon time for example) and the planner is started again.

If there was established a previous plan, then the sequencer will check the plan feasibility. If the plan is not feasible due to energy or temperature reasons, then the sequencer will go to sleep (previously setting the sleep time and the flags). This procedure is repeated three times, if the plan could not be executed due to energy or temperature the third time, then a new plan shall be obtained from the planning layer.

If the plan is feasible, the sequencer commands the control layer to execute the following tasks as per planning sequence.

In parallel, the sequencer of the redundant OBC is periodically polling the main OBC as explained in section 5.5. Figure 10.4 describes the parallel subroutines executed in the redundant and main OBC related to this polling procedure.

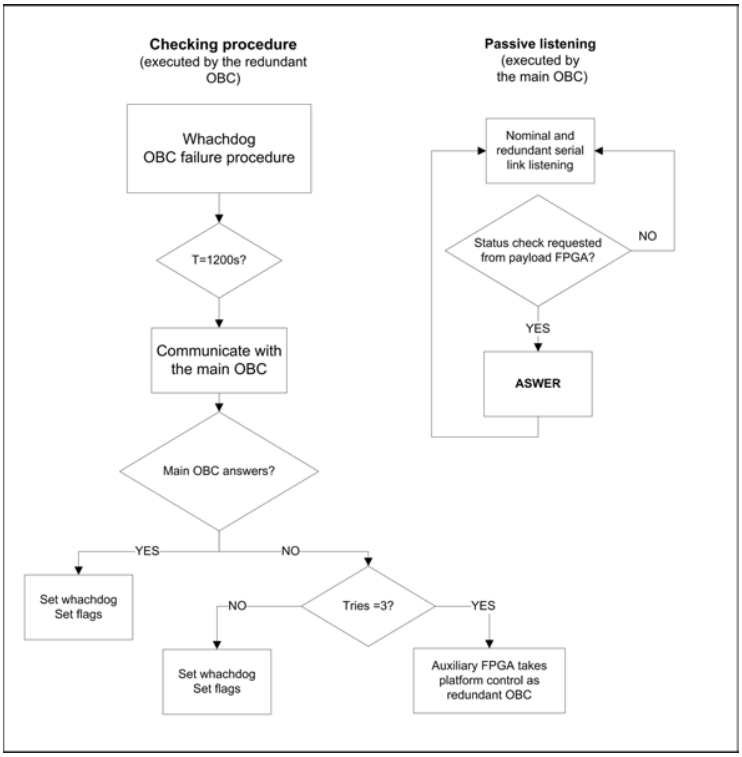

Figure 10.4: OBC status checking subroutines between the redundant OBC and main OBC.

10.3 World model estimator

The world model estimator is a set of mathematical functions that are able to determinate the future evolution of the platform environment. Provided a temporal horizon (Δt), the mathematical models generated are able to estimate an output value of the requested parameter with a time resolution of 1 hour.

The objective of the developed world model estimator is to provide a realistic estimation of the environmental boundary conditions. With this information the deliberative layer would be able to obtain the most optimal plan for the autonomous platform.

The different mathematical models developed have been described previously along the different thesis chapters. All of them have been designed in order to simplify as much as possible the processing effort (power consumption reduction) maintaining the required resolution for their respective objectives. Following, a brief overview of the different models developed is presented:

Irradiance.
The solar irradiance model is described in detail in section 6.4.2. This model provides the total solar irradiance $[W/m^2]$ and the solar incidence angle [rad]:

$$Irradiance(t)\left[\frac{W}{m^2}\right] = f(selen.latitude, selen.longitude, date, \Delta t) \tag{10.1}$$

$$\tag{10.2}$$

$$Incidence\ angle(t)[rad] = f(selen.latitude, selen.longitude, date, \Delta t) \tag{10.3}$$

The model requires the selenographic coordinates of the platform and the current date to provide the solar irradiance evolution for the temporal horizon (Δt).

Moon surface temperature.
The Moon surface temperature model is described in detail in section 6.5.2. The model provides the temperature in Kelvins of the Moon surface considering the incident irradiance (obtained using the irradiance model), the date and the temporal horizon:

$$Moon\ surface\ temperature(t)[K] = f(Irradiance(t), date, \Delta t) \tag{10.4}$$

Platform power consumption.
The platform power consumption will depend on the tasks executed by the platform. In section 9.2 the equations that relate the power consumption for each operation are provided (table 9.2). In this way, the power consumption of the platform [W], can be estimated in function of the tasks scheduling and the temporal horizon.

$$Power\ consumption(t)[W] = f(tasks\ scheduling, \Delta t) \tag{10.5}$$

Platform temperature.
A thermal mathematical model has been developed and described in detail in section 8.2. Thermal mathematical models are intrinsically complex and power demanding models. In order to reduce the complexity of the mathematical model without compromising the resolution objectives the platform was sub-divided in different isothermal nodes (refer to figure 8.1).

$$\begin{aligned} &Isothermal\ node\ n\ temp.(t)[K] = f(Irradiance(t), solar\ incidence\ angle(t) \\ &orientation(\vartheta), Moon\ surface\ temperature(t), Power\ consumption(t), date, \Delta t) \end{aligned} \tag{10.6}$$

This mathematical model provides the temperature evolution of each isothermal node in function of the irradiance, solar incidence angle,platform orientation and Moon surface temperature which most of them are obtained using the mathematical

models previously described.

Energy harvesting.
The energy that the platform is able to harvest is a main parameter to plan the platform activity. With the objective of estimating the energy that the platform is able to harvest from the planet surface, two different mathematical models have been developed:

A solar power harvested model provides the Watts obtained during each hour from the different solar panels of the platform in function of the irradiance, solar incidence angle, date and platform orientation with respect to the lunar equator. This model is presented in detail in section 9.3.3.

$$Solar\ power\ harvested(t)[W] = f(Irradiance, incidence\ angle, date, orientation, \Delta t) \tag{10.7}$$

Also, during the lunar nights it is possible to harvest thermoelectrical energy using the Thermoelectric Generator designed and presented in section 9.3.2. The model is able to provide the power harvested every hour in function of the Moon surface temperature and the initial date.

$$Thermoelectric\ energy\ harvested(t)[W] = f(Moon\ surface\ temperature(t), date, \Delta t) \tag{10.8}$$

10.4 The planning layer: Automated planning and checker

The use of optimization techniques to solve space-operations planning and scheduling problems requires, as a minimum, the following steps ([Chien et al., 1998]):

1. Use a declarative model to represent spacecraft and mission constrains, including explicit models of spacecraft subsystems and resource capacity.

2. Define and implement a Control Architecture.

3. Implement an optimization algorithm to search solutions. Solutions are defined as projected evolution of actions and states that begins in the current state and satisfies goals posed to the system.

The explicit models of spacecraft subsystems and resource capacity are presented in section 10.3 and the Control Architecture in section 10.2. In this section a brief introduction of the requirements for the planning and checker algorithm are presented.

The proposed architecture does not impose a specific declarative model or planning algorithm. The final selection of the planning algorithm shall be done in function of the specific mission constrains and development group expertise. Although some restrictions shall be considered:

- Power consumption. The selected algorithm shall reduce the power consumption of the OBC to a minimum. Unlike mobile robots, the proposed platform does not require fast responsivity to external events. The time availability to plan the activities and perform them is in the range of several minutes or even hours.

- The system shall plan, schedule and execute hard constraints, which the system must satisfy, and soft constraints or preferences, which the system must optimize:

  - Satisfy:
    * Ensure integrity and operability of the platform.
    * Manage the energy available in order to plan the switch-on, switch-off and hibernation of the platform and their related subsystems, ensuring a continuous operation of the main OBC.
    * Maintain housekeeping data updated in order to adequate the planning to the current status of the platform.
  - Optimize
    * Maximize the payload science return in function of constrains and resources availability.
    * Maximize the data communication within the WSN and the satellite link in function of constrains and resources.
    * Data analysis and prioritization: Analyze the extracted features to assess the scientific value of the data and to generate new science goals. Opportunistic goals may be added to the plan as long as resources and other operational constraints are still met and all higher priority goals can be achieved ([Castano et al., 2007]). Depending on the mission, different opportunistic goals for the platform proposed in this thesis can be defined, as for example detail monitoring of an eclipse.

- The planning algorithm shall be able to accept new goals. The GS can generate new goals in function of conclusions extracted from the previous data analyzed in ground or in order to solve a deviation or malfunction of the planner. The new goals shall be defined following the declarative model used by the planning algorithm and transmitted to the platform thru the orbiting satellite.

- Collaborative algorithm. The predefined or dynamic goals could include cooperative goals between the nodes of the WSN. The planning algorithm shall permit certain collaborative functions in order to achieve a common goal in the WSN. For example, synchronize the measurement of a certain environmental phenomenon by all the nodes of the platform.

- The algorithm shall contemplate closed planning horizons. Batch approximation shall be considered. Time is divided up into a number of planning horizons, each of which lasts for a significant period of time. When near the end of the current horizon, it is projected what the state will be at the end of the execution of the current plan ([Chien et al., 2000]).

Figure 10.5 presents an overall overview of the planning algorithm:

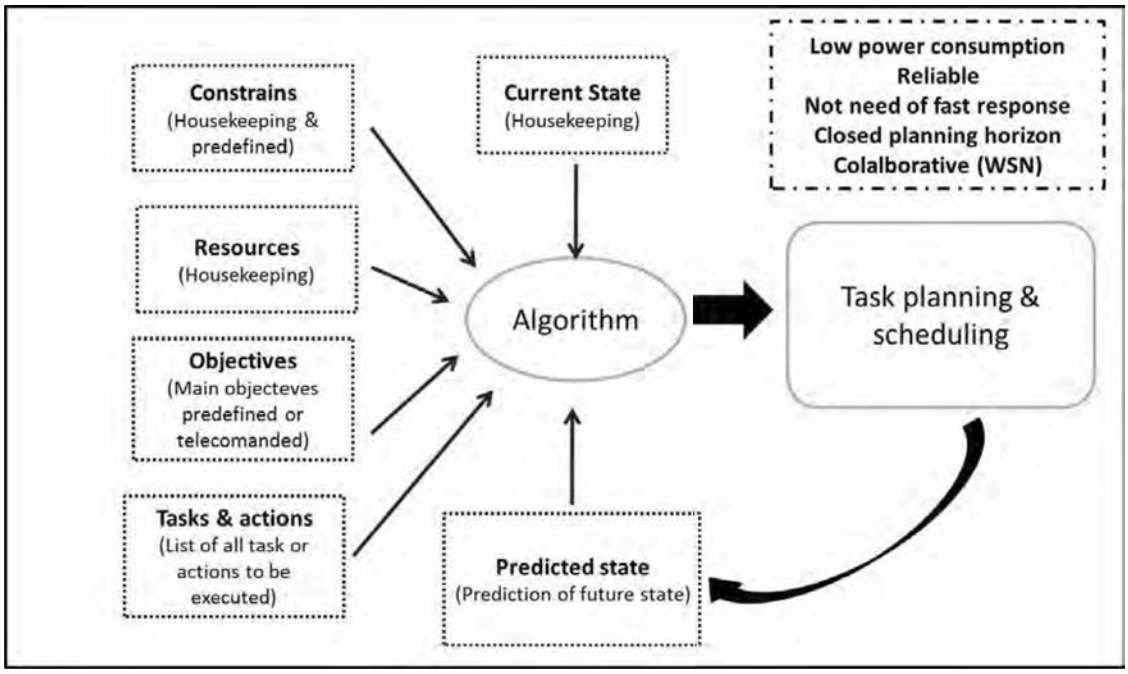

Figure 10.5: Planning algorithm scheme overview.

Finally a checker shall be defined. The combinatory of all the possible states and events do not allow the programmers to have an exhaustive representation of those states and transitions in order to prove a priori the correctness of the behaviour ([Blanquart et al., 2004]). Two initial approaches can be followed:

1. Extensive simulation testing to increase the statistical confidence of the autonomous system correct behaviour.
2. Safety dynamic supervisor to ensure that catastrophic failures are avoided.

The second option is herein selected (without detriment of a preliminary exhaustive simulation testing in the laboratory prior to the mission launch). Plan verification consists of checking, that a generated plan satisfies certain properties. [Bensalem et al., 2014] presents and exhaustive literature review of different validation and verification approaches.

10.5 The control layer

The control layer is aimed to interface directly with the hardware. The control layer, commanded by the sequencer, performs the exact sequence of hardware operations aimed to perform a specific action or monitor sensor values. A list of the different hardware operations of the control layer is presented in the following table.

Hardware operation	**Hardware subsystems involved**
Surface Temperature measurement	-Acquisition electronics: Analog to digital chain commanding (including ADC interface) -Power module: switch on and off the related sensor/electronics. -Memory access.
Surface Temperature measurement	-Acquisition electronics: Analog to digital chain commanding (including ADC interface) -Power module: switch on and off the related sensor/electronics. -Memory access.
Irradiance measurement	-Acquisition electronics: Analog to digital chain commanding (including ADC interface) -Power module: switch on and off the related sensor/electronics. -Memory access.
TID measurement	-Acquisition electronics: Analog to digital chain commanding (including ADC interface) -Power module: switch on and off the related sensor/electronics. -Memory access.
SEU measurement	-Acquisition electronics: Analog to digital chain commanding (including ADC interface) -Power module: switch on and off the related sensor/electronics. -Memory access.
Tetrahedral platform active heating	-Power module: Power ON/OFF of the corresponding heater
DDS calibration	-Acquisition electronics: Analog to digital chain commanding (including ADC interface) -Power module: switch on and off the related sensor/electronics. -Memory access.
DDS measurement	-Acquisition electronics: Analog to digital chain commanding (including ADC interface) -Power module: switch on and off the related sensor/electronics. -Memory access.
Hibernation/Sleep	-Power module: switch off/on the different electronics modules to enter in a low power consumption state. -Memory access.
Housekeeping measurement	-Acquisition electronics: Analog to digital chain commanding (including ADC interface) -Power module: switch on and off the related sensor/electronics. -Memory access.
Radio interface communication	-Power module: switch on and off the radio interface module -Radio interface module: Command the communications module to send/receive data. -Memory access.
Solar panels deployment	-Power module: switch on and off the Pin Puller in function of the output received from the end of stroke sensor.

Table 10.1: Control layer hardware operations.

Chapter 11

Platform prototyping and laboratory test results

11.1 Platform prototyping introduction

Under the scope of SWIPE project it was possible to manufacture and test functional prototypes of some elements of the platform proposed in this thesis. This chapter describes the hardware elements manufactured, the tests performed and the results obtained.

Specifically the following elements were manufactured and tested:

- Tetrahedral surface platform. The distribution of subsystems within the platform is different to the distribution proposed in this thesis, however the tetrahedral platform size and functionality is the same.
- Payload.
  - Dust Deposition Sensor.
  - Irradiance Sensor.
  - Radiation sensor.
  - Surface temperature sensor.
- Thermal switch.
- Release mechanism.

In the other hand, the following technologies and concepts proposed in this thesis are not covered, included or considered within the SWIPE project:

- Platform deployment system over the planet surface: the penetrator concept and auxiliary shock absorption subsystems.
- Thermal design.
- Thermoelectric and thermal energy harvesting techniques.
- Redundant techniques herein proposed.
- OBC high level architecture and related mathematical modelling.

The design approach followed for the functional prototypes under the scope of SWIPE project was to provide a space compatible hardware; any material, EEE component, mechanical part or process has an equivalent space qualified part/material/process. It is understood as equivalent any space qualified material, EEE component, mechanical part or process that could substitute the commercial/industrial grade used in the prototype with minimum impact or changes to the design of the system. Following

this philosophy it was possible to reduce the costs of the prototype while still having its results comparable with those potentially obtained by space qualified hardware.

Figure 11.1 presents the tetrahedral platform prototype developed under the SWIPE project and its different elements:

11.2 Tetrahedral platform structure

The tetrahedral platform structure concept proposed in this thesis for the surface tetrahedral platform was manufactured and results obtained are shown in figure 11.2.

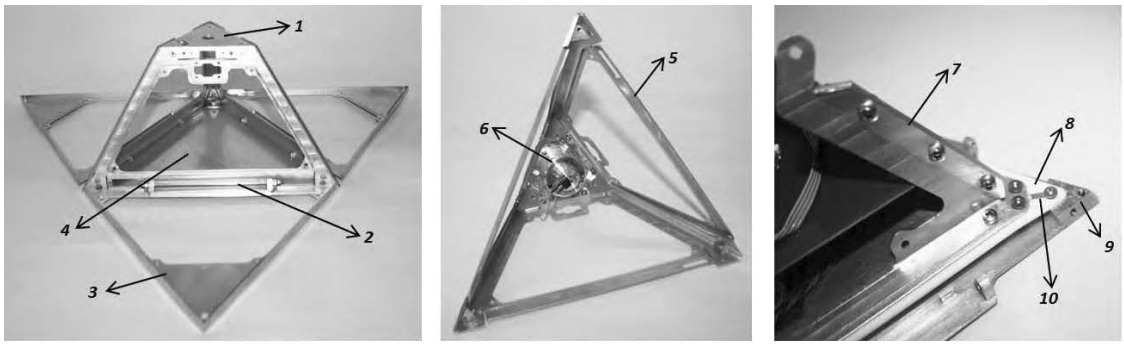

1.Upper structure 2.Hinge 3.Petal structure 4.Thermal switch bay 5.Upper structure 6.Pin Puller (release mechanism)
7. Electronics rack (inner electronics bay) 8. Low thermal conductive support for inner bay 9.Lower structure
10.Electrical bonding connecting lower and upper structure

Figure 11.2: Node structure assembled (left). Upper structure with PP assembled (center). Lower structure with electronics rack integrated (right).

The tetrahedral platform is highly reduced in volume. This fact directly implies that the volume available inside the node is highly reduced and optimized, consequently challenging the integration procedure. The integration procedure of the node was considered from the design phase. The mechanical structure was designed to be subdivided in two sub-assemblies: upper structure and lower structure (refer to figure 11.2). This subdivision was envisaged with the objective of ease the integration procedure: firstly the different subsystems are integrated in each sub-assembly and the complete node structure is finally integrated by assembling both upper and lower part. In the base of the lower structure is located the thermal switch (number 4 in the figure) and the electronics rack is attached on top of the thermal switch. An auxiliary low thermally conductive piece (number 8 in the figure) is used to provide stiffness to the electronics bay, attached to the lower part of the structure, without

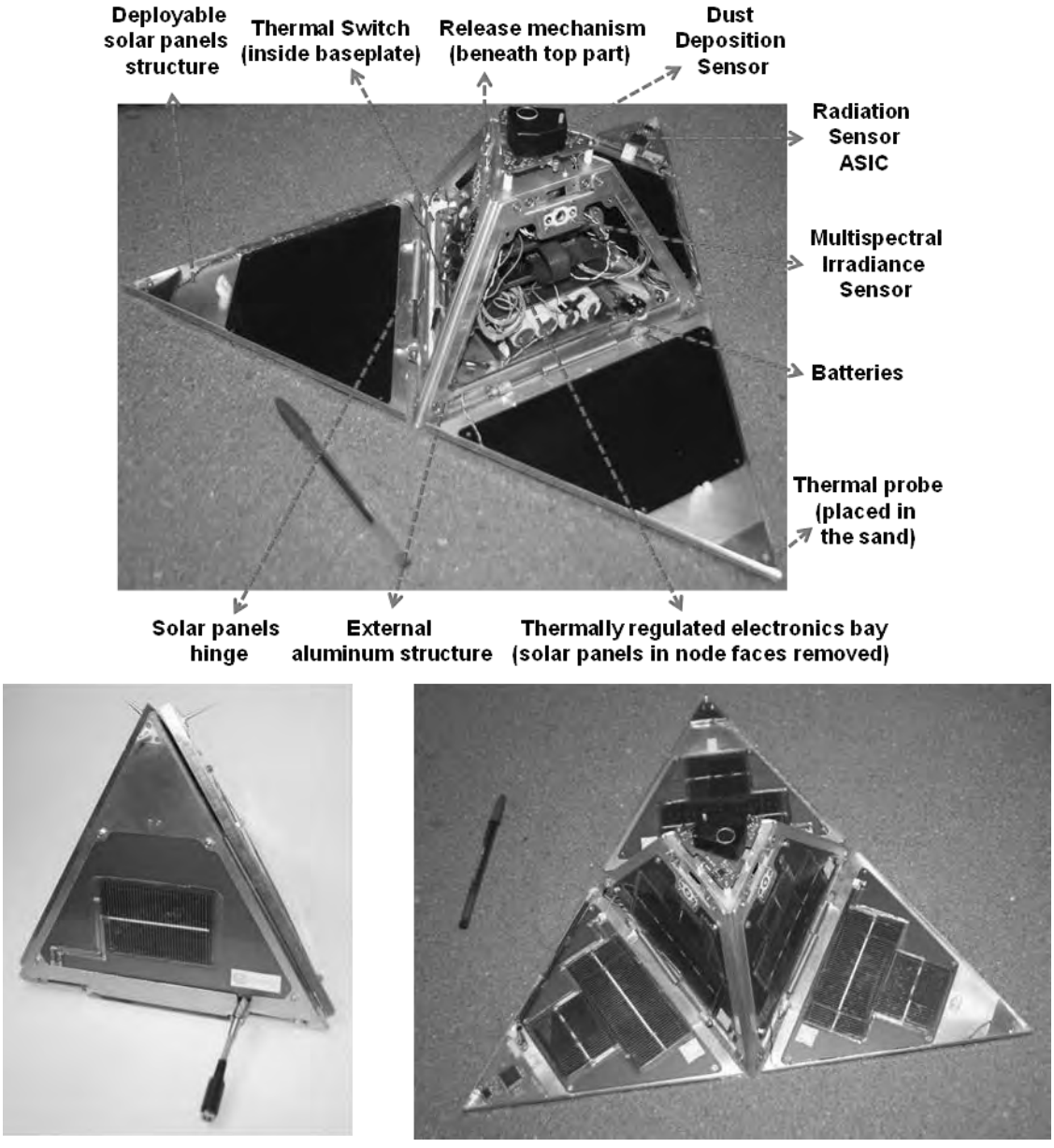

Figure 11.1: SWIPE node platform without solar panels (top); SWIPE node with solar panels closed and power cable (bottom left) and open with power cable removed (bottom right).

compromise the thermal isolation. To avoid different potential levels in the metal chassis of the structure and the electronics rack, electrical bonding consisting on thin metal pieces (number 10 in the figure) are used. This is of main importance to ensure a low impedance interconnection of all the metal elements of the structure.

The total mass of the node structure and petals structure is 520 grams.

11.3 Solar panels deployment system, functional tests and results

The release mechanism of the solar panels (detail described in section 5.2.4 and figure 5.3), was manufactured and integrated in the SWIPE platform.

Several functional test of the release mechanism was carried out as described below:

1. The release mechanism was integrated in the platform structure.
2. The petals were closed and screwed to the three arms interface metal pieces using the holding elements attached to the petals.
3. In order to simulate the terrain conditions fine sand was used as substrate for the deployment tests.
4. 10 successive deployments were performed and recorded. Figure 11.3 shows the deployment sequence.

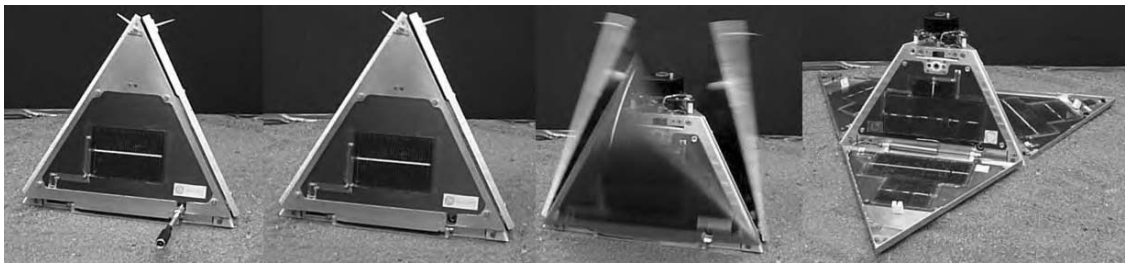

Figure 11.3: Solar panels deployment sequence.

In all the cases the results were completely successful:

- The deployment of the petals was complete.

- After a detail visual and functional inspection, any damage or malfunction was identified in the solar cells.

Low temperature tests were performed with the objective to verify the proper deployment performance at low temperatures

Figure 11.4: Low temperature tests.

Two different tests were performed:

- Independent actuation of two Pin Puller devices at -12°C (figure 11.4, right). The actuators performed properly at the nominal power consumption range. Actuation time was below 7 seconds in both cases.
- Platform deployment at -14°C (figure 11.4, left). The platform deployed the solar panels successfully in 7 seconds.

11.4 Scientific payload prototype functional tests and results

11.4.1 Dust Deposition Sensor prototype and laboratory tests results

The Dust Deposition Sensor (DDS) is a sensor-actuator system aimed to characterize the rate of dust deposited over its surface, as detailed described in section 6.2. Several DDS (including the acquisition electronics and a micro-actuator) were manufactured and integrated under the scope of the SWIPE project (figure 15). Functional, electrical and mechanical tests were performed.

Figure 11.5 shows an activation sequence of the actuator integrated in the DDS for the in-flight calibration of the sensor. As it can be seen, at ambient temperature, the micro-actuator is able to place a reflector on top of the optical window in 12 seconds. An additional test was performed at -15°C were the calibration actuator performed correctly with a nominal power consumption of 2A and with a total actuation time of 19 seconds. Table 11.1 presents the power details during both tests.

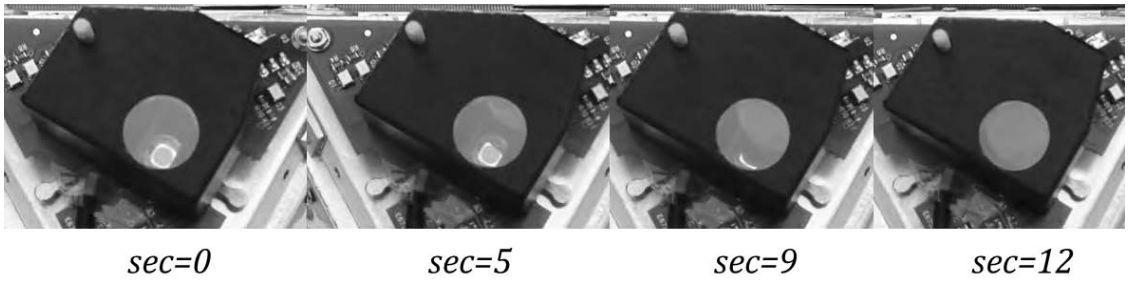

Figure 11.5: DDS actuator activation sequence at ambient temperature.

Potential [V]	**Temperature [°C]**	**Current consumption [mA]**	**Actuation time [seconds]**
+5V	+25	2000	12
+5V	-10	2000	19

Table 11.1: Power consumption DDS actuator test results.

Two tests campaigns were performed to demonstrate the performance of the designed sensor. During the first DDS test campaign a lunar dust simulant was used with the aim to demonstrate the performance of the sensor under dust samples similar to those expected to be found on the Moon surface. The objective of the second test campaign was to characterize the DDS response to samples of dust more similar to those that could be expected during the field test, which will be performed under Earth conditions.

Limited availability, high cost and toxicity of Lunar regolith simulants made impossible to test the DDS using such simulants. Instead an available commercial non-toxic lunar simulant was selected, which fulfilled the objective to test/calibrate the DDS with the best possible fidelity. A $5\mu m$ white corundum (Al_2O_3) was chosen due to its refractive index at near IR, irregular shape, commercial availability, non-toxic characteristics and sample preparation characteristics as explained below.

A 100μ m grey corundum was used during the second test campaign. Grey corundum instead white corundum was selected to be consistent with Earth's conditions. In a Moon scenario, the dust will be deposited over the optical window by electromagnetic levitation with a size not larger than 5μm ([Stubbs et al., 2006]). Meanwhile in an Earth scenario, the dust can be deposited over the optical window mainly by the wind. As the DDS is situated just only 150mm above the soil and the terrain of the Earth analogue scenario lacks any vegetation cover, the dust particles that could reach the optical window are expected to be much larger than in the case of the Moon scenario.

During the samples preparation it was required to uniformly distribute a known quantity of dust particles over the optical window surface as expected to occur during a natural deposition. Any mechanical means to dispose a low quantity of dust was discarded. It was required to use distilled water to put the dust particles in suspension. In this way it would be possible to weight a small quantity of dust and mix-up with water in order to dispose a drop of water (130μl) on to the optical window with an estimated concentration of dust.

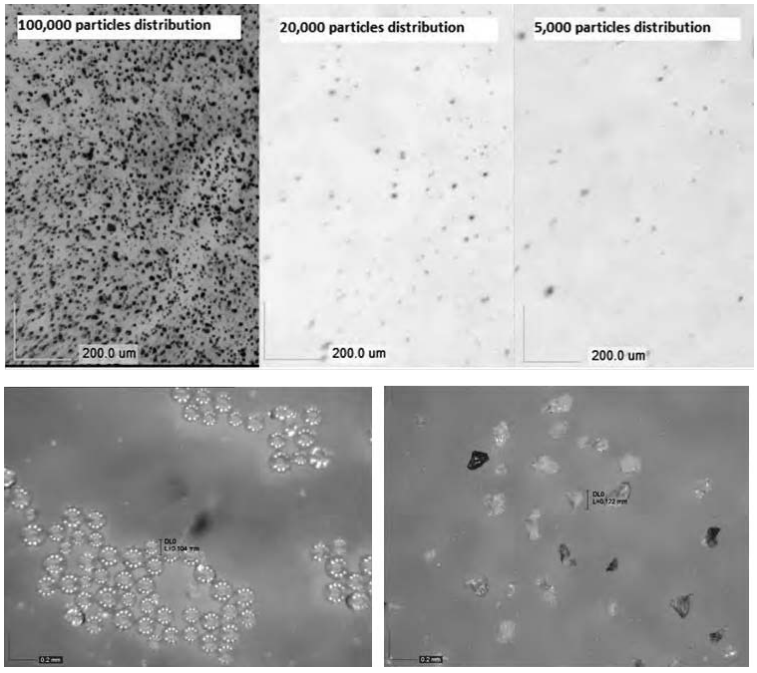

Figure 11.6: 5μm samples with a different dust particles distribution over the optical window (top); 100μm Corundum sample (bottom right); and 100μm glass microspheres sample (bottom left).

The technique followed to prepare the samples of dust deposited over the optical window (figure 11.6), is as follows: (i) Knowing the mean diameter of the particles and its density it is possible to estimate the number of particles in a known mass of Corundum. (ii) This known mass can be mixed-up in water using an orbital shaker. (iii) Using a micropipette a known quantity of water with dust in suspension is deposited over the optical window. (iv) The sample is dried in an oven at 85°C. (v) The number of particles and its uniform distribution is verified using a microscope. An experimental error of 20-25% must be considered due to (i) inherent normal distribution of the particles size (ranging from $1\mu m$ to $15\mu m$ for the $5\mu m$ particles and from 90μ m to $110\mu m$ in the case of the $100\mu m$ particles), (ii) mixing distribution during sample preparation and (iii) the error of the optical counting of particles via a microscope.

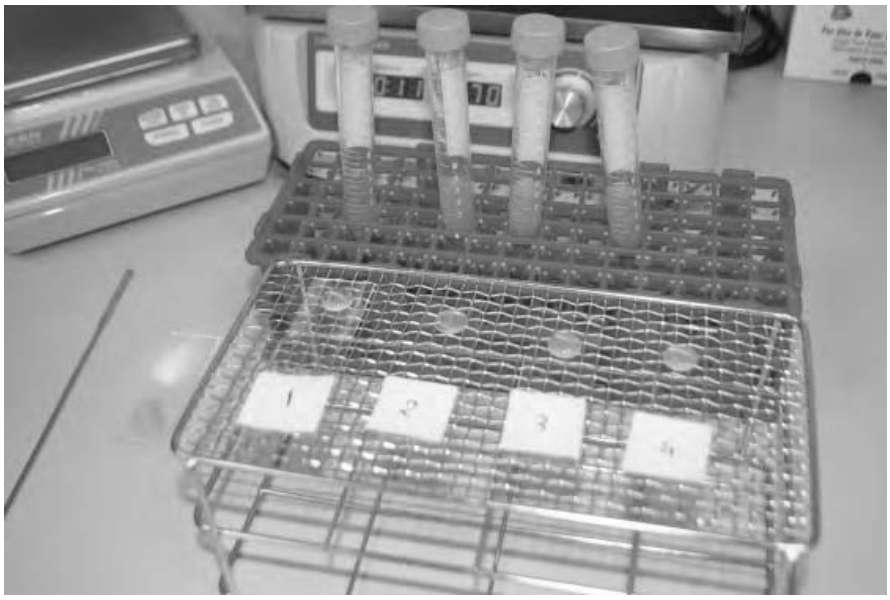

Figure 11.7: $100\mu m$ Corundum dust particles suspension and samples prepared for dry in the oven at 85°C.

As explained in section 6.3, the DDS principle of working is the scattering of the emitted light by the deposited particles in the optical window. This scattering is directly affected by the dust particle geometrical shape. The dust over the Moon surface is highly irregular with sharp edges due to the lack of meteorological erosion. Whereas, in an Earth scenario the dust particles are subjected to continuous environmental erosion that leads to less sharp particles with smooth edges. With the objective to quantify this effect on the DDS, a third type of particles was used during

	$5\mu m$ **Corundum**	$100\mu m$ **Corundum**	$100\mu m$ SiO_2 **microspheres**
Resolution $\left[\frac{particles}{cm^2}\right]$	750	12	150
Accuracy $\left[\frac{particles}{cm^2}\right]$	3800	21	350
Dynamic range $\left[\frac{particles}{cm^2}\right]$	$3.8 \cdot 10^3$-$1 \cdot 10^7$	21-$2.5 \cdot 10^4$	350-$3 \cdot 10^4$

Table 11.2: Summary of results obtained during the two DDS laboratory test campaigns.

the second test campaign. Silica glass (70% SiO_2, 15% Na_2O) microspheres with an average diameter of $100\mu m$ were employed, as shown in teh top picture of figure 11.6. The transmittance of these particles is expected not to be lower than 75% at near IR. With these characteristics the voltage output of the DDS is expected to be much lower than a similar number of corundum particles of the same size. Several samples with different concentration were prepared, optically verified via a microscope and measured with the DDS. The results are summarized in table 11.2.

As expected, the sensor accuracy with corundum particles of $5\mu m$ is around two orders of magnitude lower than with corundum particles of $100\mu m$. This is consistent with the working principle of the DDS, where bigger sharp particles would scatter more efficiently the light pulses compared to smaller particles. It has to also be taken into account that the grey corundum particles have a lower near IR transmittance index than the white corundum particles, thus reflecting more efficiently the IR light pulses. It is important to mention that as low as 21 $particles/cm^2$ of $100\mu m$ and 3800 $particles/cm^2$ of $5\mu m$ were measured with the DDS, thus demonstrating the good performance of the sensor.

Figure 11.6 shows a uniform distribution of particles in the corundum samples, however the Silica glass samples could not be distributed uniformly on the optical window. Silica glass particles tended to group during the evaporation process as shown in figure 11.6. This has to be considered because it affects directly the scattering pattern, reducing the scattering effect of the whole sample compared to uniformly distributed particles. Although a precise relationship associated with this effect could not be established, it could clearly be observed that the spherical glass particles affect the performance of the DDS reducing its accuracy by approximately one order of magnitude.

We can conclude from the obtained results that the DDS is a low power consumption and low mass sensor able to detect low quantities of dust with a four orders of magnitude dynamic range. This sensor is optimized for the small sharp particles expected to be found over the Moon surface.

Several samples with different particle concentration were prepared and measured

using the DDS and acquisition electronics. An OBC simulator installed in a PC was used to store the data obtained. It is important to remark that the measures were obtained in dark conditions (closed cabinet) to avoid ambient light disturbances. Minimum square regression was used to obtain a calibration equation using the data obtained from the $100\mu m$ corundum samples:

$$Dust\ Deposited\left[\frac{particles}{cm^2}\right] = \frac{\left(7288.8\cdot\left(\frac{x\cdot 5}{4095}-0.117\right)^{1.8459}\right)}{1.32732} \tag{11.1}$$

*Where X is the 12 bits value read from the ADC coded in decimal.

In future developments, this sensor could be improved including different emitters at different wavelengths. This could allow obtaining information about the dust deposition size distribution that would be a valuable scientific return. However, such a modification would imply an overhead in power, mass and complexity of the retrieval algorithm.

11.4.2 Irradiance sensor prototype and laboratory test results

Multiple irradiance sensors were manufactured under the scope of SWIPE project and integrated in the tetrahedral platform as shown in figure 11.8.

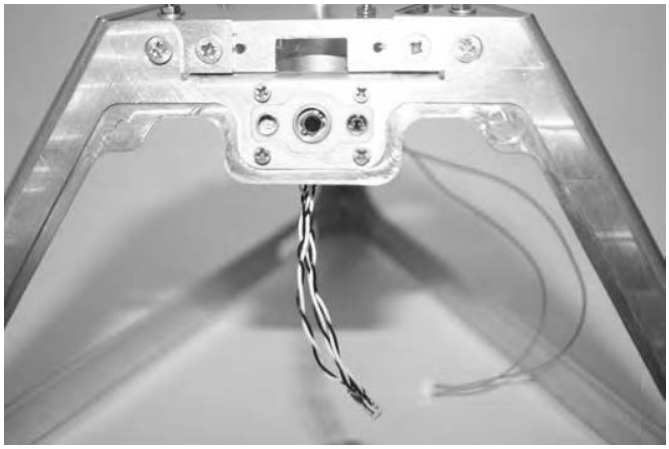

Figure 11.8: Assembled irradiance sensor.

The irradiance sensor has been calibrated experimentally using commercial calibrated photodiodes of similar spectral response than the photodiodes selected for the irradiance sensor. In an optical test bench, different reference emitters were used to provide the same reference to the calibrated photodiodes and to the photodiodes under calibration. Both output curves of the reference photodiodes were used to

calibrate the SWIPE photodiodes. A pointer laser and millimetre positioners were used to position both sensors at the same location from the reference emitters. The measurements were performed in darkness to avoid ambient light disturbances.

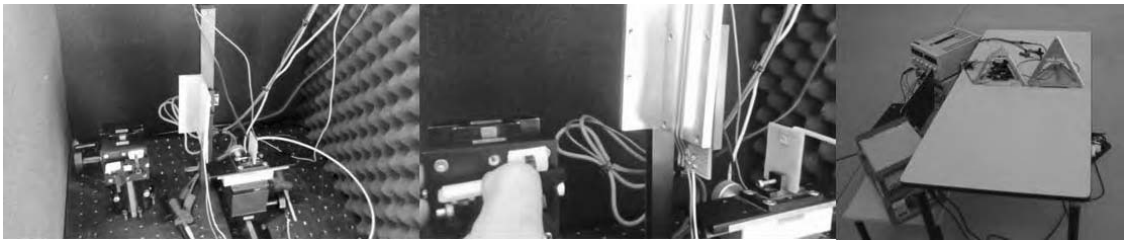

Figure 11.9: Optical test bench (left and center) and measurements at ambient light (right).

The gain of the proximity electronics included in the acquisition electronics PCB was initially designed for the expected irradiance over the Moon surface. The gain of the irradiance photodiodes was modified considering the expected irradiance in the field test in order to optimize the dynamic range of the sensor. The expected irradiance in the field test was obtained from [Maturilli et al., 2014].

Using the data obtained the following calibration equations were obtained for each spectral band of the irradiance sensor (in the following equations X is the 12 bits value read from the ADC coded in decimal):

UV:

$$P_{UV}\left[\frac{mW}{cm^2}\right] = \left(14.511 \cdot \left(\frac{x \cdot 5}{4095}\right)\right) + 0.1293 \tag{11.2}$$

IR:

$$P_{IR}\left[\frac{\mu W}{cm^2}\right] = \left(1.8096 \cdot \left(\frac{x \cdot 5 \cdot 1000}{4095}\right)\right) - 0.6783 \tag{11.3}$$

VIS:

$$P_{VIS}\left[\frac{\mu W}{cm^2}\right] = \left(2.741 \cdot \left(\frac{x \cdot 5 \cdot 1000}{4095}\right)\right) + 58.871 \tag{11.4}$$

11.4.3 Surface temperature sensor prototype and laboratory test results

Three thermal sensors responsible of measuring the upper surface temperature of the Moon are detailed described in section 6.5.3. Several sensors as those proposed in this thesis were manufactured under the SWIPE project. The sensors measure the temperature by conducting means. The temperature sensor is attached to a high thermal conductivity and low thermal inertia material (aluminium) that is used as a probe for measuring the temperature (refer to figure 11.10). It is important to remark that the position of these sensors under the scope of SWIPE project is different to the proposed in this thesis:

- SWIPE project contemplates to locate the sensors at the end of the deployable walls. In this way it is possible to use the force of the deploying panels to introduce the solar probes into the lunar soil.

- This thesis locates the soil temperature probes at the base of the platform (refer to figure 5.1). As the platforms are deployed using a penetrator approach, the soil probes will be introduced in the lunar soil during the platform landing.

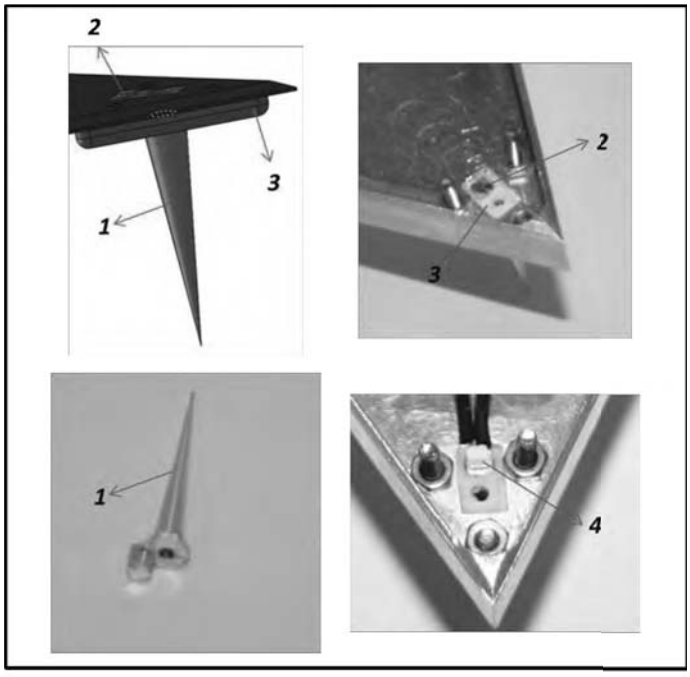

Figure 11.10: Temperature probe prototype details

The temperature sensor was experimentally calibrated using boiling distilled water and melting ice (using altitude corrections). This two absolute temperature references were used to obtain two points of calibration.

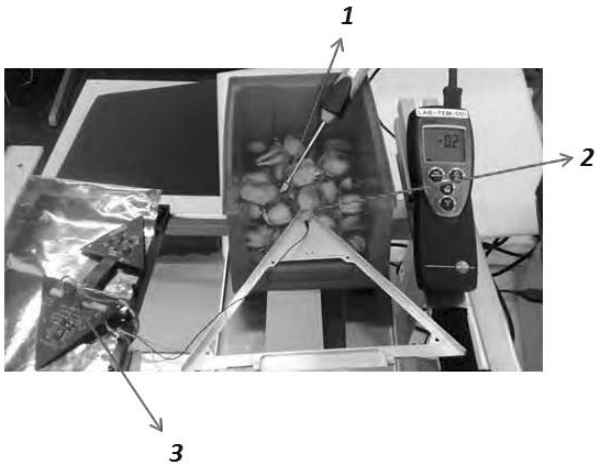

1.Reference temperature sensor 2. Soil temperature sensor
3. Acquisition electronics

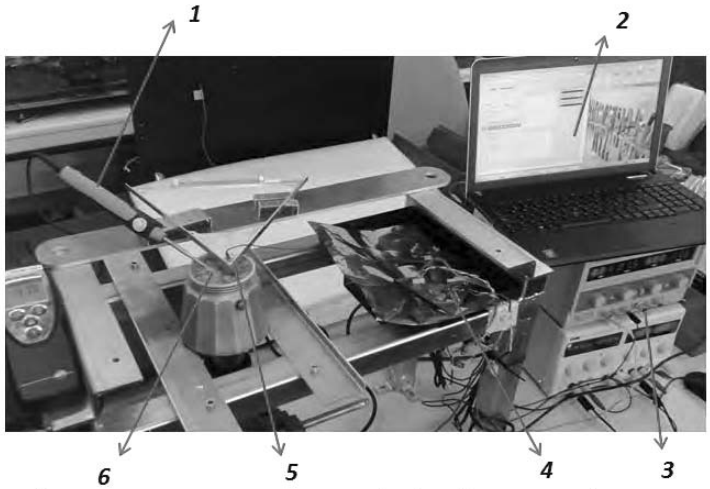

1.Reference temperature sensor 2.OBC simulator (PC supported) 3.Power source
4. Acquisition electronics 5. Soil temperature sensor 6.Boiling water

Figure 11.11: Calibration of temperature sensor. 0°C top and 100°C bottom.

As shown in figure 11.11 a petal of the structure with a temperature probe installed was used for the calibration campaign. The SWIPE acquisition electronics with an OBC simulator, installed in a PC using LabView, was used to obtain the output

value in each case. The probe was immersed in water with melting ice as shown in figure 11.11 (top) and in boiling distiller water as shown in figure 11.11 (bottom). For temperatures above 0 °C (the code in decimal for 0 °C is 2244). This equation has been corrected using experimental data (in the following equations X is the 12 bits value read from the ADC coded in decimal):

$$T\,[C] = \left(255.52 \cdot \left(\frac{x \cdot 5}{4095}\right)\right) - 700.05 \tag{11.5}$$

For temperatures below 0°C :

$$T\,[C] = \left(250.51 \cdot \left(\frac{x \cdot 5}{4095}\right)\right) - 686.17 \tag{11.6}$$

11.4.4 Acquisition electronics prototype

The acquisition PCB was manufactured, electronics components assembled and electrical verification tests performed.

External power supplies were used to provide power to the acquisition PCB and to verify the proper operational behavior of all the blocks within the PCB. In this process, it was found that the Op-amp AD8629 footprint did not properly fit the device package, so an external re-cabling was required. Once this modification was carried-out, the acquisition electronics worked as expected and the FPGA was programmed using the firmware developed by the microelectronics group of Arquimea Ingeniería. After firmware performance verification the irradiance sensors, the temperature sensor and the Dust Deposition Sensor were connected to the acquisition electronics PCB. With the objective to simulate the OBC commanding, an ¨OBC simulator˝was programmed using Labview by the software group of Arquimea Ingeniería. Following this approach, it was possible to debug completely the behavior of the FPGA, correcting the FPGA's firmware until the expected behavior of the acquisition PCB was obtained.

11.5 Thermal switch prototype functional tests and results

The thermal switch was manufactured under the scope of the SWIPE project and tested taking the opportunity of a thermal vacuum test campaign of Arquimea Ingeniería S.L.U. As it can be appreciated in figure 11.13, the thermal switch was attached to the base plate of the thermal vacuum chamber. To ensure proper thermal conductivity low outgassing thermal filler was placed between the bottom plate of the thermal switch and the base plate of the thermal chamber.

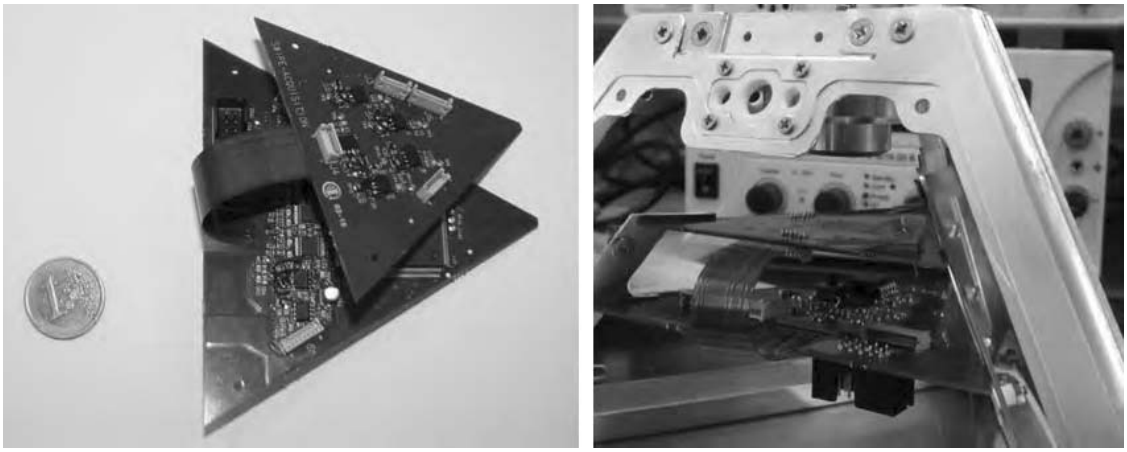

Figure 11.12: Acquisition electronics PCB (left) and acquisition electronics integrated in the SWIPE structure (right).

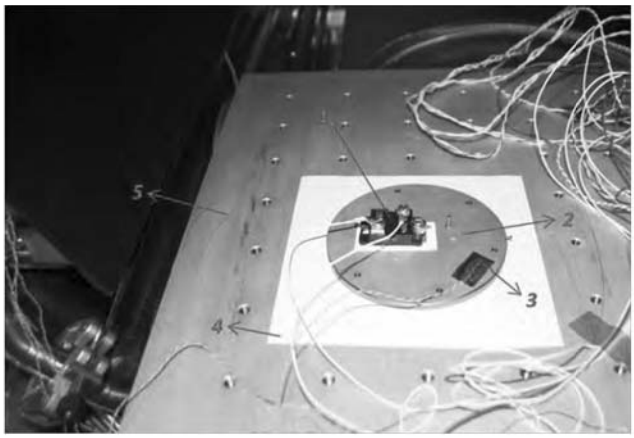

1.Resistive heater 2.Thermal switch 3.Thermocouple sensor 4. Low outgassing thermally conductive filler
5. Vacuum chamber metal plate (controlled in temperature)

Figure 11.13: Thermal switch test set-up.

A heater (power resistor) was used to heat up the upper plate of the switch. A temperature sensor (thermocouple) was attached to the top plate (spaced to the heater). The base plate of the thermal chamber was monitored in temperature and it is considered, for this test purposes, as an infinite thermal mass that does not

increase its temperature with the power generated by the heater and transmitted thru the thermal switch to its base.

With this simple set-up, it was possible to simulate the boundary conditions of the thermal switch and analyze its behavior.

With the base plate of the vacuum chamber stabilized at around -20°C (dwell time three hours), the heater was turned on, dissipating 10W constantly. Figure 11.14 presents the temperature of the top plate in function of the time. In red it is represented the data values with the thermal switch closed, and in blue the data values when the thermal switch was open. Least square regression was used in both data sets of values (black line). As it can be seen, the temperature increased constantly from -20°to around 14 °C when the slope drastically changed. This slope change (around 30%) was due to the thermal switch actuation: when the thermal witch actuated the heat dissipated to the vacuum chamber increased, thus reducing the increasing temperature slope.

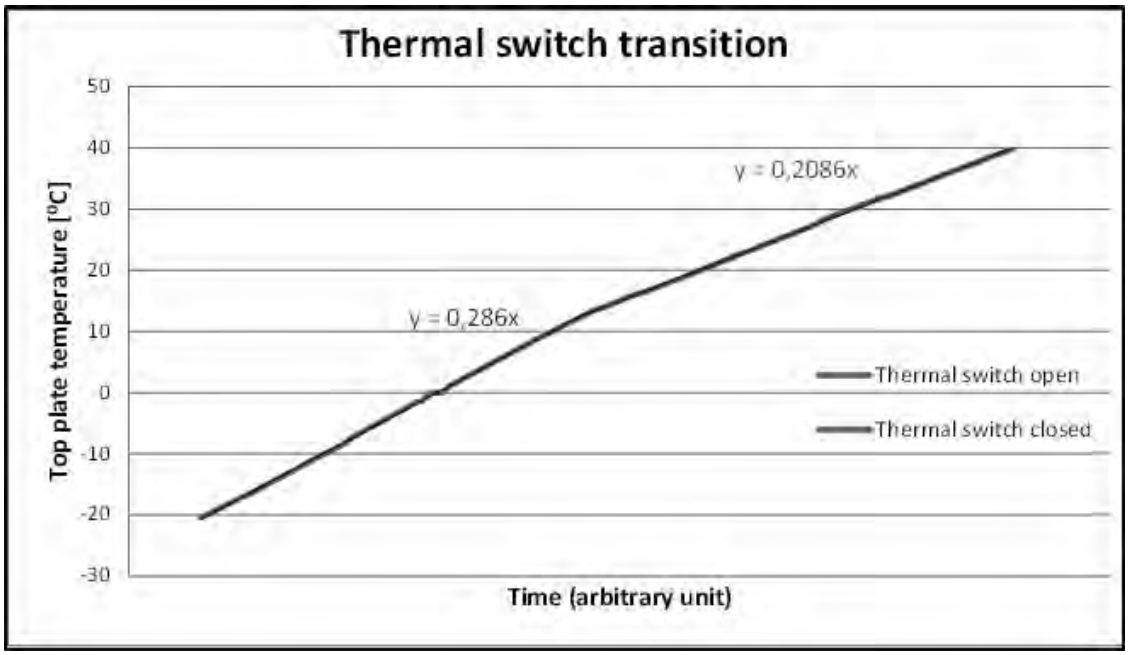

Figure 11.14: Thermal vacuum test results.

The experiment verified the proper functional behavior of the thermal switch: clearly it closed when the temperature of the top plate was above the temperature transition of the SMA material. Although, it is important to consider the following:

1. The test was aimed to verify the functional behavior of the thermal switch, not to characterize its thermal conductance. More complex experiments are required for further characterization of the thermal switch.

2. Even though the experiment was not aimed to characterize the thermal conductance of the thermal switch, it could be quantitatively verified that:

   (a) The thermal isolation was really good.

   (b) The thermal conductance was not as good as expected. The thermal contact of the thermal switch has to be improved; simple changes as change the materials used in the thermal switch contact surfaces and increasing the force of the SMA (a configuration using longer SMA or several fibres in series) would increase drastically the thermal conductance.

Chapter 12

Conclusions and future research

12.1 Conclusions

This thesis stablishes the technological basis for the implementation of a fixed scientific monitoring infrastructure over a planet surface. The concept proposed is aimed to provide a reliable and cost effective system for the continuous surface monitoring of the inner rocky planets of our Solar System.

Beyond the traditional rovers or landers, the concept proposed is composed by tents of self-powered and low mass autonomous platforms with the capability of perform a variety of different scientific measurements. Those small fixed platforms are capable to sense, process, share between them and finally transmit data to a orbiter for further transmission to Earth using an ad-hoc Wireless Sensor Network. The conceived system is able to operate autonomously during years, harvesting the required energy from the planet surface environment. Such a concept deployed over a planet surface would represent the first fixed infrastructure over an extraterrestrial rocky body.

The dissertation comprises the conceived mission approach for the Moon scenario, platform overall design and provides reliable technical solutions for the different critical aspects of the concept proposed. Even though, it was not possible to deal in depth detail with all the technologies involved in this thesis, a compressive study is presented focusing in those aspects not completely covered in other previously proposed missions or concepts.

The platform conceived is a low mass dual body presented in chapter 5. The platform can be subdivided in two different bodies: (i) a tetrahedron body highly optimized both in mass (2000g) and volume (tetrahedron envelope of 200x200 mm of base and 200 mm of height) that will remain over the planet surface; (ii) a penetrator body (3260 g) of 300 mm in height, 100 mm in diameter and with the shape of a ballistic missile aimed to go between 0.3 and 1.2 meters below the subsurface of the planet. The deployment method selected is penetration (hard-landing), simplifying drastically the descent system required, thus reducing the related costs (chapter 7).

The set of solutions proposed and the exploited synergies between the different subsystems makes the platform conceived to go beyond the state of the art (chapter 4) with respect to similar platforms:

1. The system concept proposed enhances the science return increasing significantly the mission lifetime thanks to a reliable system able to operate during years harvesting energy over the planet surface (chapter 9).

2. Day and night energy harvesting systems in combination with a smart thermal regulation (chapter 8) enhance the power efficiency of the platform and enables the node to be operative during the cold nights. A robust, extremely cheap and

flexible TEG that can extract small amounts of energy continuously during the lunar night has been proposed.

3. The cost of the platform is highly optimized thanks to its low mass and because Radioisotope Thermoelectric Generators are not used.

4. The platform includes reliable solutions to support the high shock levels associated with a hard landing (section 7.2.3). In this way the mass of the vehicles and fuel required to deploy the platform is significantly reduced, enabling the deployment of a larger number of platforms in each mission.

5. A highly integrated, low power and reduced mass payload (chapter 6) has been designed and developed. Each platform of the WSN can be configured with different sets of instruments, thus increasing significantly the scientific objectives of the whole mission. Novel dust deposition and radiation sensors have been designed. The test campaign demonstrated an excellent performance of the Dust Deposition Sensor for planetary exploration.

6. The autonomous behavior of the platform is obtained thanks to a control architecture that permits the platform plan and schedule the tasks in order to increase the science return adapting itself to the changing environment (chapter 10).

7. High reliability based on exploiting the synergies and redundancy possibilities between the subsystems of each platform and between the different platforms of the WSN.

8. The platform can be adapted to different mission scenarios, without significantly redesigning their functionality. This permits to potentially use the presented platform concept for different mission objectives as other moons, asteroids or planets.

Missions compatible with the concept proposed could take opportunity of the previously commented advantages from the platform conceived in this thesis. Certain missions would not be compatible with the exploration concept proposed. Between others, we can define two main points to be evaluated when deciding if a certain type of mission is compatible with the platform conceived in this thesis:

- The conceived platforms, as presented in this thesis, are not compatible with Polar Regions or craters exploration. Significant modifications have to be considered to adapt the platforms proposed for the exploration of those dark and cold regions. Basically the modifications required suppose a significant increase in the mass and volume of the platforms and also in a lifetime reduction.

- Even though different set of sensors can be installed in each platform of the WSN, increasing the number of parameters monitored over the planet surface, it must be noted the complexity limitation (mainly in mass and volume) of the scientific payload that can be installed in these platforms. Highly complex instruments with demanding mass, volume and energy requirements are not compatible with the platform proposed.

Some of the solutions herein proposed have been developed under the scope of a FP-7 project. The results obtained after the laboratory tests of the functional prototypes of the subsystems developed demonstrate the significant potential of the solution proposed, as the Dust Deposition Sensor, tetrahedral configuration or low shock solar panels deployment mechanism.

12.2 Future research

The proposed concept represents a reliable alternative for space exploration. However, from the concept presented in this dissertation to the final Flight Model there is a long way to travel.

From the concept herein proposed and with the adequate support, it would be possible to consider a phase A of an exploration mission, involving expert research groups and companies in the different fields required to consolidate the mission concept and the platform design.

Additionally it is important to note that the dissertation presented in this document is highly ambitious and cover a large different number of design areas and technologies. As it was not possible under the scope of this thesis develop in detail some of the solutions proposed, there are several areas susceptible of further research:

- The TEG concept proposed is susceptible to new improvements, particularly in relation to the metal material selection, TEG construction and electronics related.
- The sublimating material proposed in this thesis requires an extensive research and testing.
- A specific planning algorithm and checker algorithm have not been developed under the scope of this thesis. The custom development of the planning and checker algorithms will be required for future developments of the platform.
- The mathematical models do not contemplate the topography of the Moon. New improvement at this respect will permit to adapt the design of the platform to new scenarios.

- Further work is required to improve the performance of the thermal switch that demonstrated a great potential and proper functional behavior in vacuum but with a reduced thermal conductivity when closed.

Bibliography

[Albee et al., 2000] Albee, A., Battel, S., Brace, R., Burdick, G., Casani, J., Lavell, J., Leising, C., MacPherson, D., Burr, P., and Dipprey, D. (2000). Report on the loss of the mars polar lander and deep space 2 missions. *NASA STI/Recon Technical Report N*, page 61967.

[Alvarez et al., 2011] Alvarez, F., Collado, M., Nava, N., and Cabas, R. (2011). Qualification results of the qualification model of a rotary actuator based on shape memory alloy for operation in mars. In *14th European Space Mechanisms & Tribology Symposium (ESMATS), Constance, Germany*.

[Alvarez et al., 2014] Alvarez, F., Millen, D., Rivera, C., Benito, C., Lopez, J., Fernandez, D., and Moreno, L. (2014). New approaches in low power and mass payload for wireless sensor networks (wsns) for lunar surface exploration. In *SENSORS, 2014 IEEE*, pages 726–729. IEEE.

[Alvarez et al., 2015] Alvarez, F., Rodrigues, P., Sinogas, P., Oliveira, A., Vladimirova, T., Zhai, X., Liberati, F., Oddi, G., Pietrabissa, A., Crosnier, M., Rivera, C., Millen, D., and Moreno, L. (2015). Low power lightweight micro-meteorological station for wireless sensor network based space exploration. In *66th International Astronautical Congress (IAC)*. IAC.

[Armstrong and Hurley, 2010] Armstrong, S. and Hurley, W. (2010). A thermal model for photovoltaic panels under varying atmospheric conditions. *Applied Thermal Engineering*, 30(11):1488–1495.

[Ashby et al., 2000] Ashby, M. F., Evans, T., Fleck, N. A., Hutchinson, J., Wadley, H., and Gibson, L. (2000). *Metal Foams: A Design Guide: A Design Guide*. Elsevier.

[Badescu, 2012] Badescu, V. (2012). *Moon: Prospective Energy and Material Resources*. Springer Science & Business Media.

[Ball et al., 2007] Ball, A., Garry, J., Lorenz, R., and Kerzhanovich, V. (2007). *Planetary landers and entry probes*. Cambridge University Press.

[Barth et al., 2003] Barth, J. L., Dyer, C., and Stassinopoulos, E. (2003). Space, atmospheric, and terrestrial radiation environments. *Nuclear Science, IEEE Transactions on*, 50(3):466–482.

[Bastin, 1973] Bastin, J. (1973). The lunar surface layer. *Reports on Progress in Physics*, 36(3):289.

[Bauch et al., 2009] Bauch, K., Hiesinger, H., and Helbert, J. (2009). Estimation of lunar surface temperatures: A numerical model. In *EGU General Assembly Conference Abstracts*, volume 11, page 10395.

[Beernink et al., 2007] Beernink, K., Guha, S., Yang, J., Banerjee, A., Lord, K., DeMaggio, G., Liu, F., Pietka, G., Johnson, T., Reinhout, M., et al. (2007). Lightweight, flexible solar cells on stainless steel foil and polymer for space and stratospheric applications. *NASA/CP*, 214494:54–66.

[Bensalem et al., 2014] Bensalem, S., Havelund, K., and Orlandini, A. (2014). Verification and validation meet planning and scheduling. *International Journal on Software Tools for Technology Transfer*, 16(1):1–12.

[Bhandari, 2008] Bhandari, N. (2008). Planetary exploration: scientific importance and future prospects. *Current Science*, 94(2):185–200.

[Blanquart et al., 2004] Blanquart, J., Fleury, S., Hernerk, M., Honvault, C., Ingrand, F., Poncet, J., Powell, D., Strady-Lécubin, N., and Thévenod, P. (2004). Software safety supervision on-board autonomous spacecraft. In *Proceedings of the 2nd European Congress Embedded Real Time Software (ERTSâ€™04)*.

[Bonasso et al., 1997] Bonasso, R. P., Kortenkamp, D., and Whitney, T. (1997). Using a robot control architecture to automate space shuttle operations. In *AAAI/IAAI*, pages 949–956.

[Brooks, 1991] Brooks, R. A. (1991). Intelligence without representation. *Artificial intelligence*, 47(1):139–159.

[Brown and Davidson, 2010] Brown, M. and Davidson, A. (2010). The use of cyclododecane to protect delicate fossils during transportation. *Journal of Vertebrate Paleontology*, 30(1):300–303.

[Bugga et al., 2007] Bugga, R., Smart, M., Whitacre, J., and West, W. (2007). Lithium ion batteries for space applications. In *Aerospace Conference, 2007 IEEE*, pages 1–7. IEEE.

[Burdick and Fiorini, 2003] Burdick, J. and Fiorini, P. (2003). Minimalist jumping robots for celestial exploration. *The International Journal of Robotics Research*, 22(7-8):653–674.

[Calle et al., 2008] Calle, C., McFall, J., Buhler, C., Snyder, S., Arens, E., Chen, A., Ritz, M., Clements, J., Fortier, C., and Trigwell, S. (2008). Dust particle removal by electrostatic and dielectrophoretic forces with applications to nasa exploration missions. In *Proc. ESA Annual Meeting on Electrostatics*, pages 1–14.

[Canning et al., 1981] Canning, T. N., Barns, C. E., Murphy, J. P., Gin, B., and King, R. W. (1981). High acceleration cable deployment system. US Patent 4,271,761.

[Cardarelli, 2008] Cardarelli, F. (2008). *Materials handbook: a concise desktop reference*. Springer Science & Business Media.

[Castano et al., 2007] Castano, R., Estlin, T., Anderson, R. C., Gaines, D. M., Castano, A., Bornstein, B., Chouinard, C., and Judd, M. (2007). Oasis: Onboard autonomous science investigation system for opportunistic rover science. *Journal of Field Robotics*, 24(5):379–397.

[Chien et al., 1998] Chien, S., Smith, B., Rabideau, G., Muscettola, N., and Rajan, K. (1998). Automated planning and scheduling for goal-based autonomous spacecraft. *IEEE Intelligent Systems*, (5):50–55.

[Chien et al., 2000] Chien, S. A., Knight, R., Stechert, A., Sherwood, R., and Rabideau, G. (2000). Using iterative repair to improve the responsiveness of planning and scheduling. In *AIPS*, pages 300–307.

[Christie et al., 2008] Christie, R. J., Plachta, D. W., and Hasan, M. M. (2008). Transient thermal model and analysis of the lunar surface and regolith for cryogenic fluid storage. *NASA TM-215300*.

[Collinson et al., 2008] Collinson, G., Consortium, U. P., et al. (2008). Planetary penetrators-the vanguard for the future exploration of the solar system. *Journal of the British Interplanetary Society*, 61:198–202.

[Crosnier et al., 2013a] Crosnier, M., Boutry, P., Alberty, E., Rofrigues, P., and Oliveira, A. (2013a). Mission design report. Technical Report D2.1, Seventh Framework Programme Space Theme, Grant No. 312826.

[Crosnier et al., 2013b] Crosnier, M., Boutry, P., Rofrigues, P., and Oliveira, A. (2013b). Deployment strategies tailoring to swipe scenarios. Technical Report D2.3, Seventh Framework Programme Space Theme, Grant No. 312826, 2013.

[Dahl, 2006] Dahl, M. (2006). Final environmental impact statement for the mars science laboratory mission. Technical report, National Aeronautics and Space Administration.

[Doengi et al., 1998] Doengi, F., Burnage, S., Cottard, H., and Roumeas, R. (1998). Lander shock-alleviation techniques. *ESA bulletin*, 93:2.

[Dubowsky et al., 2006] Dubowsky, S., Iagnemma, K., and Boston, P. (2006). Microbots for large-scale planetary surface and subsurface exploration.

[Dughaish, 2002] Dughaish, Z. (2002). Lead telluride as a thermoelectric material for thermoelectric power generation. *Physica B: Condensed Matter*, 322(1):205–223.

[Dupon, 1996] Dupon (1996). Teflon ptfe. dupon. properties handbook. H-37051-3.

[ECSS, 2011] ECSS (2011). Derating - eee components, space product assurance.

[Edmondson et al., 2006] Edmondson, K. M., Law, D., Glenn, G., Paredes, A., King, R., and Karam, N. (2006). Flexible iii-v multijunction solar blanket. In *Photovoltaic Energy Conversion, Conference Record of the 2006 IEEE 4th World Conference on*, volume 2, pages 1935–1938. IEEE.

[Finckenor, 2006] Finckenor, M. M. (2006). The materials on international space station experiment (misse): First results from msfc investigations. In *44th AIAA Aerospace Sciences Meeting and Exhibit*, pages 9–12.

[Fortescue et al., 2011] Fortescue, P., Swinerd, G., and Stark, J. (2011). *Spacecraft systems engineering*. John Wiley & Sons.

[Furlong and Wahlquist, 1999] Furlong, R. R. and Wahlquist, E. J. (1999). Us space missions using radioisotope power systems. *Nuclear news*, 42:26–35.

[Gaier, 2005] Gaier, J. R. (2005). The effects of lunar dust on eva systems during the apollo missions. *NASA/TM*, 213610:2005.

[Gaisler, 2008] Gaisler, A. (2008). Sparc v8 32-bit processor leon3/leon3-ft companioncore data sheet.

[Gaisler, 2010] Gaisler, A. (2010). Aeroflex gaisler sparc v8 32-bit processor leon3 / leon3-ft companion core data sheet.

[Gaisler and Catovic, 2006] Gaisler, J. and Catovic, E. (2006). Multi-core processor based on leon3-ft ip core (leon3-ft-mp). In *DASIA 2006-Data Systems in Aerospace*, volume 630, page 76.

[Galimov, 2005] Galimov, E. (2005). Luna-glob project in the context of the past and present lunar exploration in russia. *Journal of earth system science*, 114(6):801–806.

[Gao et al., 2007] Gao, Y., Ellery, A., Jaddou, M., Vincent, J., and Eckersley, S. (2007). Planetary micro-penetrator concept study with biomimetric drill and sampler design. *Aerospace and Electronic Systems, IEEE Transactions on*, 43(3):875–885.

[Gao et al., 2008] Gao, Y., Phipps, A., Taylor, M., Crawford, I. A., Ball, A. J., Wilson, L., Parker, D., Sweeting, M., da Silva Curiel, A., Davies, P., et al. (2008). Lunar science with affordable small spacecraft technologies: Moonlite and moonraker. *Planetary and Space Science*, 56(3):368–377.

[Gaowei et al., 2010] Gaowei, L., Jiemin, Z., and Xuezhang, H. (2010). Output characteristics analysis of thermoelectric generator based on accurate numerical model. In *Power and Energy Engineering Conference (APPEEC), 2010 Asia-Pacific*, pages 1–4. IEEE.

[Gat, 1997] Gat, E. (1997). Esl: A language for supporting robust plan execution in embedded autonomous agents. In *Aerospace Conference, 1997. Proceedings., IEEE*, volume 1, pages 319–324. IEEE.

[GmbH, 2013] GmbH, S. (2013). Broadband sic based uv photodiode datasheet.

[Gowen et al., 2011] Gowen, R., Smith, A., Fortes, A. D., Barber, S., Brown, P., Church, P., Collinson, G., Coates, A. J., Collins, G., Crawford, I. A., et al. (2011). Penetrators for in situ subsurface investigations of europa. *Advances in Space Research*, 48(4):725–742.

[Gowen et al., 2007] Gowen, R., Smith, A., Griffiths, A., Coates, A., Ball, A., Barber, S., Hagermann, A., Sheridan, S., Crawford, I., Church, P., et al. (2007). Kinetic penetrators for exploration of solar system bodies. In *Fifth International Planetary Probes Workshop (IPPW-5), Bordeaux, France*, pages 23–29.

[Gowen et al., 2008] Gowen, R., Smith, A., Winter, B., Theobald, C., Rees, K., Ball, A. J., Hagermann, A., Sheridan, S., Brown, P., Oddy, T., et al. (2008). An update on moonlite. In *Proceedings of 59th International Astronautical Congress*, volume 7, pages 4359–4369.

[Grün and Horányi, 2013] Grün, E. and Horányi, M. (2013). A new look at apollo 17 leam data: Nighttime dust activity in 1976. *Planetary and Space Science*, 89:2–14.

[Halekas et al., 2001] Halekas, J., Mitchell, D., Lin, R., Frey, S., Hood, L., Acuña, M., and Binder, A. (2001). Mapping of crustal magnetic anomalies on the lunar near side by the lunar prospector electron reflectometer. *Journal of Geophysical Research: Planets (1991–2012)*, 106(E11):27841–27852.

[Harb, 2011] Harb, A. (2011). Energy harvesting: State-of-the-art. *Renewable Energy*, 36(10):2641–2654.

[Harri et al., 2015] Harri, A.-M., Aleksashkin, S., Arruego, I., Schmidt, W., Genzer, M., Vazquez, L., and Haukka, H. (2015). Mars metnet mission status. In *EGU General Assembly Conference Abstracts*, volume 17, page 13336.

[Harri et al., 2013] Harri, A.-M., Aleksashkin, S., Guerrero, H., Schmidt, W., Genzer, M., Vazquez, L., and Haukka, H. (2013). Mars metnet precursor mission status. *Evolution*, 2:2.

[Harri et al., 2007] Harri, A.-M., Leinonen, J., Merikallio, S., Paton, M., Haukka, H., and Polkko, J. (2007). Metnet-in situ observational network and orbital platform to investigate the martian environment. *Reports of the Finnish Meteorological Institute Space Research, 2007, No. 3, 30 pages*, 1:1.

[Harri et al., 2012] Harri, A.-M., Schmidt, W., Guerrero, H., and Vázquez, L. (2012). Future plans for metnet lander mars missions. In *EGU General Assembly Conference Abstracts*, volume 14, page 8224.

[Hayne, 2011] Hayne, P. O. (2011). An explicit finite difference formulation of the 1-d heat diffusion equation.

[Heiken et al., 1991] Heiken, G., Vaniman, D., and French, B. M. (1991). *Lunar sourcebook: A user's guide to the Moon*. CUP Archive.

[Hood et al., 2001] Hood, L., Zakharian, A., Halekas, J., Mitchell, D., Lin, R., Acuna, M., and Binder, A. (2001). Initial mapping and interpretation of lunar crustal magnetic anomalies using lunar prospector magnetometer data. *Journal of Geophysical Research: Planets (1991–2012)*, 106(E11):27825–27839.

[Hopf et al., 2010] Hopf, T., Kumar, S., Karl, W., and Pike, W. (2010). Shock protection of penetrator-based instrumentation via a sublimation approach. *Advances in Space Research*, 45(3):460–467.

[Hufenbach et al., 2014] Hufenbach, B., Reiter, T., and Sourgens, E. (2014). Esa strategic planning for space exploration. *Space Policy*, 30(3):174–177.

[Huleihel et al., 2012] Huleihel, Y., Cervera, A., and Ben-Yaakov, S. (2012). A high gain dc-dc converter for energy harvesting of thermal waste by thermoelectric generators. In *Electrical & Electronics Engineers in Israel (IEEEI), 2012 IEEE 27th Convention of*, pages 1–5. IEEE.

[IST, 2014] IST (2014). Platinum temperature sensors. $BTP_E1.0$.

[Kauder, 2005] Kauder, L. (2005). Spacecraft thermal control coatings references. *NASA, Goddard space flight center*.

[Kawaguchi et al., 2010] Kawaguchi, J., Yamada, T., and Kuninaka, H. (2010). HayabusaâЄ™s reentry and recovery of its capsule. In *Proceedings of 61st International Astronautical Congress. Prague: International Astronautical Federation*.

[King et al., 2006] King, R. R., Fetzer, C. M., Law, D. C., Edmondson, K. M., Yoon, H., Kinsey, G. S., Krut, D. D., Ermer, J. H., Hebert, P., Cavicchi, B. T., et al. (2006). Advanced iii-v multijunction cells for space. In *Photovoltaic Energy Conversion, Conference Record of the 2006 IEEE 4th World Conference on*, volume 2, pages 1757–1762. IEEE.

[Kinsella et al., 2014] Kinsella, C., OâЄ™Shaughnessy, S., Deasy, M., Duffy, M., and Robinson, A. (2014). Battery charging considerations in small scale electricity generation from a thermoelectric module. *Applied Energy*, 114:80–90.

[Kubota and Tomiki, 0015] Kubota, T. and Tomiki, A. (20015). Asteroid surface exploration rovers developed for hayabusa2 mission. In *66th International Astronautical Congress, IAC-15*.

[Laird and Lu, 2013] Laird, I. and Lu, D. D.-C. (2013). High step-up dc/dc topology and mppt algorithm for use with a thermoelectric generator. *Power Electronics, IEEE Transactions on*, 28(7):3147–3157.

[Langevin and Arnold, 1977] Langevin, Y. and Arnold, J. (1977). The evolution of the lunar regolith. *Annual Review of Earth and Planetary Sciences*, 5:449–489.

[Langseth et al., 1976] Langseth, M. G., Keihm, S. J., and Peters, K. (1976). Revised lunar heat-flow values. In *Lunar and Planetary Science Conference Proceedings*, volume 7, pages 3143–3171.

[Law et al., 2006] Law, D. C., Edmondson, K., Siddiqi, N., Paredes, A., King, R., Glenn, G., Labios, E., Hadd, M., Isshiki, T., and Karam, N. (2006). Lightweight, flexible, high-efficiency iii-v multijunction cells. In *Photovoltaic Energy Conversion,*

Conference Record of the 2006 IEEE 4th World Conference on, volume 2, pages 1879–1882. IEEE.

[Lazansky, 2012] Lazansky, C. (2012). Refinement of a low-shock separation system. In *Proc. of the 41st Aerospace Mechanisms Symposium, JPL, Pasadena, CA*, pages 329–343.

[LeBlanc, 2014] LeBlanc, S. (2014). Thermoelectric generators: Linking material properties and systems engineering for waste heat recovery applications. *Sustainable Materials and Technologies*, 1:26–35.

[Li et al., 2008] Li, X., Wang, S., Zheng, Y., and Cheng, A. (2008). Estimation of solar illumination on the moon: A theoretical model. *Planetary and Space Science*, 56(7):947–950.

[Li et al.,] Li, X., Zheng, Y., Li, Q., Zhang, D., Liao, Y., Wang, S., Lang, L., and Fu, S. Estimation of the surface temperature of flat areas on the moon.

[Li et al., 2010] Li, Y., Wang, Z., and Jiang, J. (2010). Simulations on the influence of lunar surface temperature profiles on ce-1 lunar microwave sounder brightness temperature. *Science China Earth Sciences*, 53(9):1379–1391.

[López-Soto et al., 2014] López-Soto, J., González-Gutiérreza, D., Ilstad, J., Cirillo, M., and Korndörfer, F. (2014). Use of ihp's 0.25 μm bicmos process in the development of european lvds devices.

[Lorenz, 2003] Lorenz, R. D. (2003). Subsurface ambient thermoelectric power for moles and penetrators. In *IEEE aerospace conference, Big Sky, MT*. Citeseer.

[Lorenz et al., 2000] Lorenz, R. D., Moersch, J. E., Stone, J. A., Morgan, A. R., and Smrekar, S. E. (2000). Penetration tests on the ds-2 mars microprobes: penetration depth and impact accelerometry. *Planetary and Space Science*, 48(5):419–436.

[Mangroli et al., 2011] Mangroli, A., Vasoya, K., and Mesa, C. (2011). Optimizing thermal and mechanical performance in pcbs.

[Margheritis et al., 2015] Margheritis, D., Cassi, C., and Nistico, A. (2015). Exomars mission 2016 planetary protection implementation. In *66th International Astronautical Congress, Space Exploration Symposium (A3), Mars Exploration - Science, Instruments and Technologies (3B)*.

[Marlow Industries, 2015] Marlow Industries, I. (2015). Xlt6-4 technical data sheet. DOC 102-0415 REV A.

[Marshall et al., 2001] Marshall, W., Spudis, P., Regnart, H., Trayner, C., Clarkson, W., and Coates, A. (2001). The case for renewed human exploration of the moon-discussion. *Earth Moon Planets*, 87(3):169–171.

[Master-Bond-Inc., 2015] Master-Bond-Inc. (2015). Ep37-3flfao product data sheet.

[Maturilli et al., 2014] Maturilli, M., Herber, A., and König-Langlo, G. (2014). Surface radiation climatology for ny-ålesund, svalbard (78.9 n), basic observations for trend detection. *Theoretical and Applied Climatology*, 120(1-2):331–339.

[Mauney, 2006] Mauney, C. (2006). Thermal considerations for surface mount layouts. In *Texas Instruments Portable Power Supply Design, Seminar*.

[Mazur et al., 2015] Mazur, J., Zeitlin, C., Schwadron, N., Looper, M., Townsend, L., Blake, J., and Spence, H. (2015). Update on radiation dose from galactic and solar protons at the moon using the lro/crater microdosimeterswe. *Space Weather*.

[McKay et al., 1974] McKay, D., Fruland, R., and Heiken, G. (1974). Grain size and the evolution of lunar soils. In *Lunar and Planetary Science Conference Proceedings*, volume 5, pages 887–906.

[Meeus, 1991] Meeus, J. H. (1991). *Astronomical algorithms*. Willmann-Bell, Incorporated.

[Microsemi, 2015] Microsemi (2015). Microsemi rtax-s/sl and rtax-dsp radiation-tolerant fpgas datasheet. 5172169-17/02.15.

[Mizutani et al., 2003] Mizutani, H., Fujimura, A., Tanaka, S., Shiraishi, H., and Nakajima, T. (2003). Lunar-a mission: goals and status. *Advances in Space Research*, 31(11):2315–2321.

[Mizutani et al., 2005] Mizutani, H., Fujimura, A., Tanaka, S., Shiraishi, H., and Nakjima, T. (2005). Lunar-a mission: outline and current status. *Journal of earth system science*, 114(6):763–768.

[Montecucco et al., 2014] Montecucco, A., Siviter, J., and Knox, A. R. (2014). The effect of temperature mismatch on thermoelectric generators electrically connected in series and parallel. *Applied Energy*, 123:47–54.

[Montminy et al., 2008] Montminy, S., Dupuis, E., and Champliaud, H. (2008). Mechanical design of a hopper robot for planetary exploration using sma as a unique source of power. *Acta Astronautica*, 62(6):438–452.

[Murphy et al., 1981] Murphy, J. P., Reynolds, R. T., Blanchard, M., and Clanton, U. (1981). Surface penetrators for planetary exploration: science rationale and development program. *NASA TM-81251, Ames Research Center*.

[Nava et al., 2012] Nava, N., Collado, M., Alvarez, F., Cabás, R., San Juan, J., Patti, S., and Lautier, J.-M. (2012). Ultra-low-weight rotary actuator for operation on mars and pin puller mechanism based on a novel shape memory alloy technology.

[Nouvellon et al., 2012] Nouvellon, S., Berthoud, L., and Rickwood, W. (2012). Thermal design of a lunar penetrator. *parameters*, 4(7):8.

[Oddi et al., 2014a] Oddi, G., Pietrabissa, A., and Liberati, F. (2014a). Energy balancing in multi-hop wireless sensor networks: an approach based on reinforcement learning. In *Adaptive Hardware and Systems (AHS), 2014 NASA/ESA Conference on*, pages 262–269. IEEE.

[Oddi et al., 2014b] Oddi, G., Pietrabissa, A., Liberati, F., Rodrigues, P., and Alvarez, F. (2014b). Dissemination report. Technical Report D7.1, SWIPE-Seventh Framework Programme Space Theme, Grant No. 312826.

[Optoelectronics, 2015] Optoelectronics, P. (2015). Vtb process photodiode datasheet.

[O'SULLIVAN JR, 1964] O'SULLIVAN JR, W. J. (1964). Method and apparatus for shock protection.

[Pacific-Silicon-Sensor, 2010] Pacific-Silicon-Sensor (2010). Pc10-7-to5 part description.

[Paige et al., 2010] Paige, D., Foote, M., Greenhagen, B., Schofield, J., Calcutt, S., Vasavada, A., Preston, D., Taylor, F., Allen, C., Snook, K., et al. (2010). The lunar reconnaissance orbiter diviner lunar radiometer experiment. *Space Science Reviews*, 150(1-4):125–160.

[Penella and Gasulla, 2007] Penella, M. and Gasulla, M. (2007). A review of commercial energy harvesters for autonomous sensors. In *Instrumentation and Measurement Technology Conference Proceedings, 2007. IMTC 2007. IEEE*, pages 1–5. IEEE.

[Powell et al., 1974] Powell, R. L., Hall, W. J., Hyink Jr, C. H., Sparks, L. L., Burns, G. W., Scroger, M. G., and Plumb, H. H. (1974). Thermocouple reference tables based on the ipts-68. Technical report, National Bureau of Standards, Washington, DC (USA).

[Racca, 1995] Racca, G. D. (1995). Moon surface thermal characteristics for moon orbiting spacecraft thermal analysis. *Planetary and Space Science*, 43(6):835–842.

[Ran and Wang, 2014] Ran, Z. and Wang, Z. (2014). Simulations of lunar equatorial regolith temperature profile based on measurements of diviner on lunar reconnaissance orbiter. *Science China Earth Sciences*, 57(9):2232–2241.

[REM, 2009] REM, L. O. (2009). Component data sheet rft0888cc10dat0b.

[Rodrigues et al., 2014] Rodrigues, P., Oliveira, A., Alvarez, F., Cabas, R., Oddi, G., Liberati, F., Vladimirova, T., Zhai, X., Jing, H., and Crosnier, M. (2014). Space wireless sensor networks for planetary exploration: Node and network architectures. In *Adaptive Hardware and Systems (AHS), 2014 NASA/ESA Conference on*, pages 180–187. IEEE.

[Rodrigues et al., 2015] Rodrigues, P., Oliveira, A., Sinogas, P., Oddi, G., Lisi, F., Alvarez, F., Cabas, R., Vladimirova, T., Zhai, X., and Crosnier, M. (2015). Test of a routing algorithm for wireless sensor networks with application to planetary exploration applications. In *66th International Astronautical Congress*.

[Roos and Diner, 1999] Roos, D. and Diner, A. (1999). Thermal design analysis of a satellite with articulating solar panels. In *MSC Aerospace Users' Conference*, pages 1–13. Citeseer.

[Rummel et al., 2009] Rummel, J. D., Ehrenfreund, P., and Peter, N. (2009). Cospar workshop on planetary protection for outer planet satellites and small solar system bodies.

[Saft, 2009] Saft (2009). Mp 144350 rechargeable lithium-ion battery datasheet.

[Sanz et al., 2013] Sanz, D., Barrientos, A., Garzón, M., Rossi, C., Mura, M., Puccinelli, D., Puiatti, A., Graziano, M., Medina, A., Mollinedo, L., et al. (2013). Wireless sensor networks for planetary exploration: Experimental assessment of communication and deployment. *Advances in Space Research*, 52(6):1029–1046.

[Sanz et al., 2010] Sanz, D., Garzon, M., Barrientos, A., Rossi, C., Medina, A., and Puiatti, A. (2010). Robotic deployment system for space exploration. In *Proc. of The 10th International Symposium on Artificial Intelligence, Robotics and Automation in Space (iSAIRAS)*.

[Seidelmann et al., 2007] Seidelmann, P. K., Archinal, B. A., Aâ€™hearn, M. F., Conrad, A., Consolmagno, G., Hestroffer, D., Hilton, J., Krasinsky, G., Neumann, G., Oberst, J., et al. (2007). Report of the iau/iag working group on cartographic

coordinates and rotational elements: 2006. *Celestial Mechanics and Dynamical Astronomy*, 98(3):155–180.

[Shakouri, 2011] Shakouri, A. (2011). Recent developments in semiconductor thermoelectric physics and materials. *Materials Research*, 41(1):399.

[Skulinova et al., 2011] Skulinova, M., Zheng, W., Hu, Y.-R., and Soucy, Y. (2011). Micro-penetrator for canadian planetary exploration.

[Smrekar et al., 1999] Smrekar, S., Catling, D., Lorenz, R., Magalhães, J., Moersch, J., Morgan, P., Murray, B., Presley, M., Yen, A., Zent, A., et al. (1999). Deep space 2: the mars microprobe mission. *Journal of Geophysical Research E*, 104(E11):27013–27030.

[Sorloaica-Hickman et al., 2012] Sorloaica-Hickman, N., McFall, J., Nason, S., Davis, K., and Arens, E. (2012). Optimization of the photovoltaic powered systems with dust mitigation technology for future lunar and martian missions. In *Photovoltaic Specialists Conference (PVSC), 2012 38th IEEE*, pages 002815–002818. IEEE.

[Spectrolab, 2010] Spectrolab (2010). Spectrolab 28.3% ultra triple junction (utj) solar cells datasheet.

[Stubbs et al., 2006] Stubbs, T. J., Vondrak, R. R., and Farrell, W. M. (2006). A dynamic fountain model for lunar dust. *Advances in Space Research*, 37(1):59–66.

[Surkov et al., 1999] Surkov, Y. A., Moskaleva, L., Shcheglov, O., Sheretov, E., Kremnev, R., Pichkhadze, K., Akulov, Y. P., and Dolgopolov, V. (1999). Lander and scientific equipment for exploring of volatiles on the moon. *Planetary and space science*, 47(8):1051–1060.

[Tammepõld et al., 2011] Tammepõld, R., Fiorini, P., and Kruusmaa, M. (2011). Attitude control of small hopping robots for planetary exploration: theory and simulations. *ESA/ESTEC, Netherlands*, pages 1–8.

[Tatom et al., 1967] Tatom, F., Srepel, V., Johnson, R., Contaxes, N., Adams, J., Seaman, H., and Cline, B. (1967). Lunar dust degradation effects and removal/prevention concepts. *NASA Technical Report No. TR-792-7-207A*, pages 3–1.

[Thangavelautham et al., 2012] Thangavelautham, J., Strawser, D., Cheung, M. Y., and Dubowsky, S. (2012). Lithium hydride powered pem fuel cells for long-duration small mobile robotic missions. In *Robotics and Automation (ICRA), 2012 IEEE International Conference on*, pages 415–422. IEEE.

[Tobiska et al., 2000] Tobiska, W. K., Woods, T., Eparvier, F., Viereck, R., Floyd, L., Bouwer, D., Rottman, G., and White, O. (2000). The solar2000 empirical solar irradiance model and forecast tool. *Journal of Atmospheric and Solar-Terrestrial Physics*, 62(14):1233–1250.

[Trautz et al., 2013] Trautz, K., Jenkins, P., Walters, R., Scheiman, D., Hoheisel, R., Tatavarti, R., Chan, R., Miyamoto, H., Adams, J., Elarde, V., et al. (2013). High efficiency flexible solar panels. In *Photovoltaic Specialists Conference (PVSC), 2013 IEEE 39th*, pages 0115–0119. IEEE.

[Truszkowski et al., 2009] Truszkowski, W., Hallock, H., Rouff, C., Karlin, J., Rash, J., Hinchey, M., and Sterritt, R. (2009). *Autonomous and autonomic systems: with applications to NASA intelligent spacecraft operations and exploration systems*. Springer Science & Business Media.

[Vanek, 2014] Vanek, M. (2014). *System Level Analysis of Thermal Properties of Integrated Circuits*. PhD thesis, Faculty of Electrical Engineering and Communication Department of Electrical and Electronic Technology.

[Vasavada et al., 1999] Vasavada, A. R., Paige, D. A., and Wood, S. E. (1999). Near-surface temperatures on mercury and the moon and the stability of polar ice deposits. *Icarus*, 141(2):179–193.

[Williams et al., 2012] Williams, H., Ambrosi, R., Bannister, N., Samara-Ratna, P., Tinsley, T., Rice, T., Sarsfield, M., Cordingley, L., Slade, R., Deacon, T., et al. (2012). Radioisotope thermoelectric power systems: Enabling technology for european space exploration missions. In *European Planetary Science Congress 2012*, volume 1, page 379.

[Yoshimitsu et al., 1999] Yoshimitsu, T., Nakatani, I., and Kubota, T. (1999). New mobility system for small planetary body exploration. In *Robotics and Automation, 1999. Proceedings. 1999 IEEE International Conference on*, volume 2, pages 1404–1409. IEEE.

[Zhai et al., 2014] Zhai, X., Jing, H., and Vladimirova, T. (2014). Multi-sensor data fusion in wireless sensor networks for planetary exploration. In *Adaptive Hardware and Systems (AHS), 2014 NASA/ESA Conference on*, pages 188–195. IEEE.

[Ziach, 2015] Ziach, C. e. a. (2015). Mascot, the small mobile asteroid landing package on its piggyback journey to 1999ju3: Pre-launch and post-launch activities. In *66th International Astronautical Congress, IAC-15*.

WEB REFERENCES

[$WB1$] $http://www.russianspaceweb.com/luna_glob.html$

[$WB2$] $http://webserver.dmt.upm.es/\ isidoro/$

[$WB3$] $http://www.ergaerospace.com/index.html$

[$WB4$] $http://www.astronomynotes.com/tables/tablesb.htm.$

[$WB5$] $http://metnet.fmi.fi/index.php?id = 51$

[$WB6$] $http://www.aerospacemetals.com/$